NASA/CR—2004-213119

Inlet Flow Valve Engine Analyses

G.A. Champagne
United Technologies Corporation, Pratt & Whitney, West Palm Beach, Florida

July 2004

The NASA STI Program Office . . . in Profile

Since its founding, NASA has been dedicated to the advancement of aeronautics and space science. The NASA Scientific and Technical Information (STI) Program Office plays a key part in helping NASA maintain this important role.

The NASA STI Program Office is operated by Langley Research Center, the Lead Center for NASA's scientific and technical information. The NASA STI Program Office provides access to the NASA STI Database, the largest collection of aeronautical and space science STI in the world. The Program Office is also NASA's institutional mechanism for disseminating the results of its research and development activities. These results are published by NASA in the NASA STI Report Series, which includes the following report types:

- TECHNICAL PUBLICATION. Reports of completed research or a major significant phase of research that present the results of NASA programs and include extensive data or theoretical analysis. Includes compilations of significant scientific and technical data and information deemed to be of continuing reference value. NASA's counterpart of peer-reviewed formal professional papers but has less stringent limitations on manuscript length and extent of graphic presentations.

- TECHNICAL MEMORANDUM. Scientific and technical findings that are preliminary or of specialized interest, e.g., quick release reports, working papers, and bibliographies that contain minimal annotation. Does not contain extensive analysis.

- CONTRACTOR REPORT. Scientific and technical findings by NASA-sponsored contractors and grantees.

- CONFERENCE PUBLICATION. Collected papers from scientific and technical conferences, symposia, seminars, or other meetings sponsored or cosponsored by NASA.

- SPECIAL PUBLICATION. Scientific, technical, or historical information from NASA programs, projects, and missions, often concerned with subjects having substantial public interest.

- TECHNICAL TRANSLATION. English-language translations of foreign scientific and technical material pertinent to NASA's mission.

Specialized services that complement the STI Program Office's diverse offerings include creating custom thesauri, building customized databases, organizing and publishing research results . . . even providing videos.

For more information about the NASA STI Program Office, see the following:

- Access the NASA STI Program Home Page at ***http://www.sti.nasa.gov***

- E-mail your question via the Internet to help@sti.nasa.gov

- Fax your question to the NASA Access Help Desk at 301–621–0134

- Telephone the NASA Access Help Desk at 301–621–0390

- Write to:
  NASA Access Help Desk
  NASA Center for AeroSpace Information
  7121 Standard Drive
  Hanover, MD 21076

NASA/CR—2004-213119

Inlet Flow Valve Engine Analyses

G.A. Champagne
United Technologies Corporation, Pratt & Whitney, West Palm Beach, Florida

Prepared under Contract NAS3–26618, Task Order 13

National Aeronautics and
Space Administration

Glenn Research Center

July 2004

Document History

This research was originally published internally as HSR035 in June 1996.

Acknowledgments

The NASA Project Manager for this study was Jerry Knip (retired) of the Aeropropulsion Analysis Office, NASA Glenn Research Center, Cleveland, Ohio. This study was performed at Pratt & Whitney in West Palm Beach, Florida, under the direction of George Champagne. Other key technical contributors at Pratt & Whitney include Michael Palmieri and Warren Boudreaux (performance analysis), George Allen (component designs), Barry West and Eric Ward (engine mechanical design), David Larson (IFV CFD analysis). Bill Speers (compression system design), Ann Guthrie (nozzle aerodynamic design), Gunther Eichhorn (nozzle mechanical design), Francis Smith (engine dynamic model and analysis), and Bob Bengtson (mission analysis).

Note that at the time of research, the NASA Lewis Research Center
was undergoing a name change to the
NASA John H. Glenn Research Center at Lewis Field.
Both names may appear in this report.

Available from

NASA Center for Aerospace Information
7121 Standard Drive
Hanover, MD 21076

National Technical Information Service
5285 Port Royal Road
Springfield, VA 22100

Available electronically at http://gltrs.grc.nasa.gov

TABLE OF CONTENTS

LIST OF FIGURES

LIST OF FIGURES (CONT'D)

LIST OF FIGURES (CONT'D)

LIST OF FIGURES (CONCL'D)

LIST OF TABLES

LIST OF TABLES (CONT'D)

SUMMARY

The objectives of this study were to evaluate the dynamic operation of Inlet Flow Valve (IFV) engines, to design components that will provide sufficient stability margins, to conduct conceptual design studies and to evaluate these IFV concepts in a Mach 2.4 HSCT.

IFV propulsion concepts contain a valve between fan stages to bring extra ambient air into the engine during takeoff operation. This flow is mixed with the normal engine flow to reduce the exhaust jet velocity and noise. Two IFV concepts were examined in this study.

- A Partial Bypass Inlet Flow Valve (PIFV) turbofan which increases the engine flow by 26 percent
- A Full Bypass Inlet Flow Valve (FIFV) turbofan which increases the engine flow by 69 percent

Conceptual designs were developed for both the PIFV STF1029 and FIFV STF1035 engines. Cross sectional layouts of these engines are presented in Figure 1 and Figure 2:

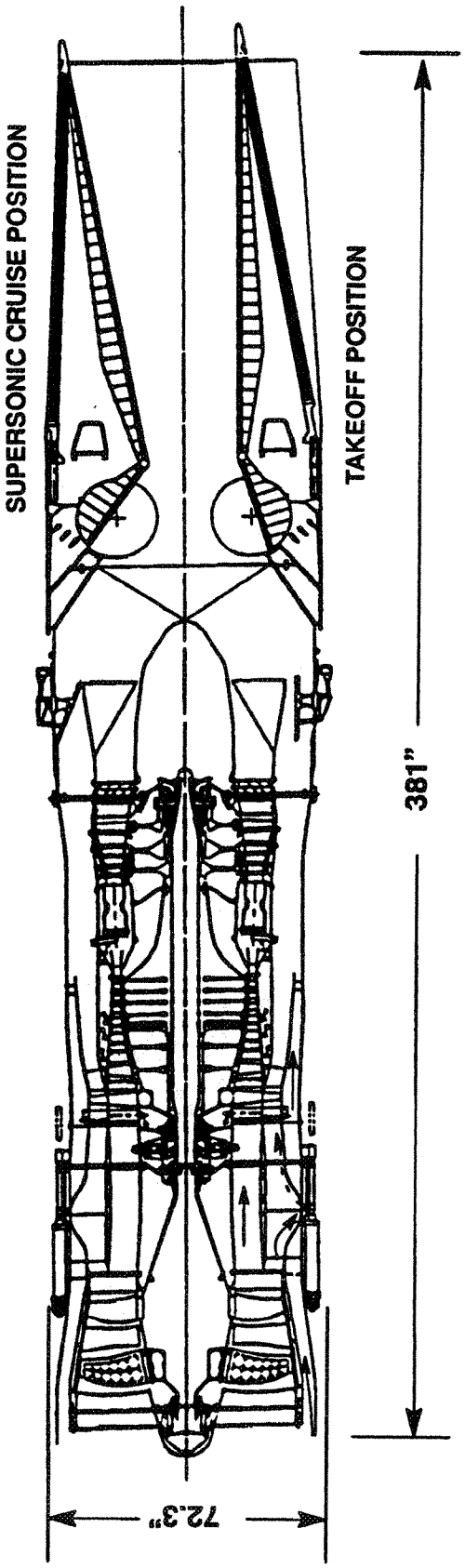

Figure 1. STF 1029 Partial Bypass Inlet Flow Valve Turbofan

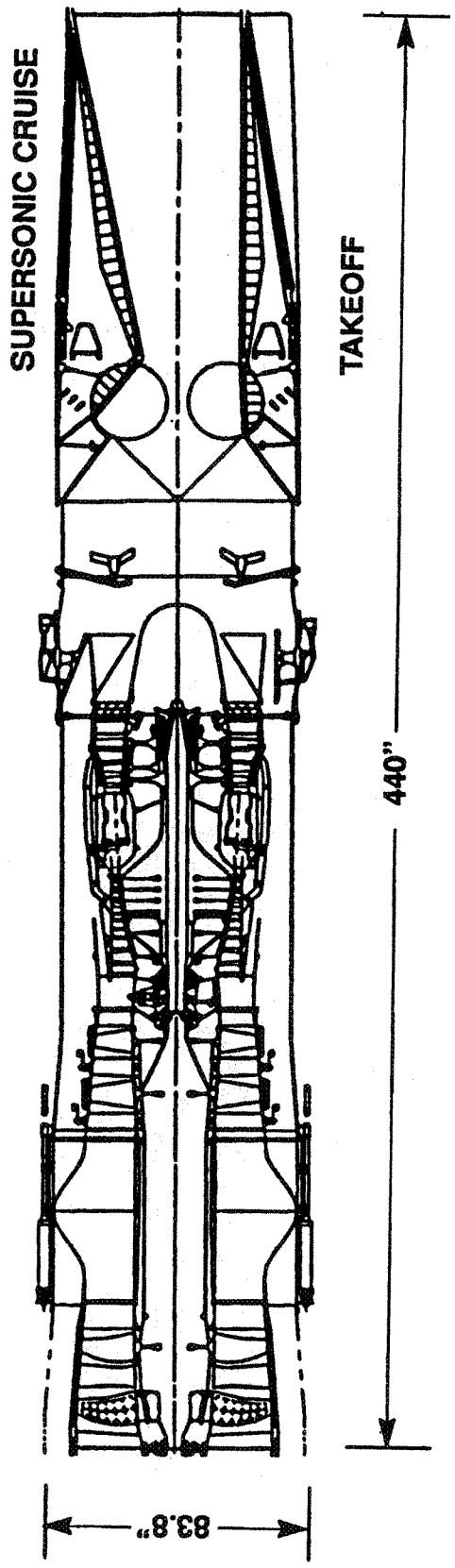

Figure 2. STF 1035 Full Bypass Inlet Flow Valve Turbofan

Table 1 summarizes the installed performance, weights and dimensions of these engines and those of a conventional mixed flow turbofan with an 85% flow entrainment mixer ejector nozzle.

Table 1. Conventional and IFV Turbofan Summary

Engine Type	MFTF	STF1029 PIFV	STF1035 FIFV
Base Engine Size, lb/sec	650	650	650
Secondary Flow Entrainment, %	85	26	69
Propulsion System Weight, Lb	11,445	12,140	12,460
Inlet Weight, Lb	6,430	6,700	7,780
Pod Weight, Lbf	17,875	18,840	20,240
Total Propulsion System Length, in	347	381	440
TSFC at Mach 2.4, lb/hr–Lb	1.30	1.28	1.291
Net Thrust at 2.4, Lbf	19,400	15,300	18,800
Net Takeoff Thrust, Lbf	46,600	35,000	44,000

Figure 3 presents the results of the P&W mission analysis study for the 309 passenger, 5000 n. mi, Boeing Mach 2.4 aircraft. This mission evaluation shows that the conventional MFTF produces the lowest takeoff gross weight (TOGW) of 750,000 pounds when the engine is sized to meet FAR Stage III noise. The full IFV STF1035 engine, which has a total weight that is 2,365 Lbs higher than that of the conventional MFTF, produces a TOGW of 859,000 Lbs. The partial IFV turbofan, STF1029, which produces a TOGW of 987,000 lbs cannot meet FAR Stage III noise without use of power cutback procedures after liftoff.

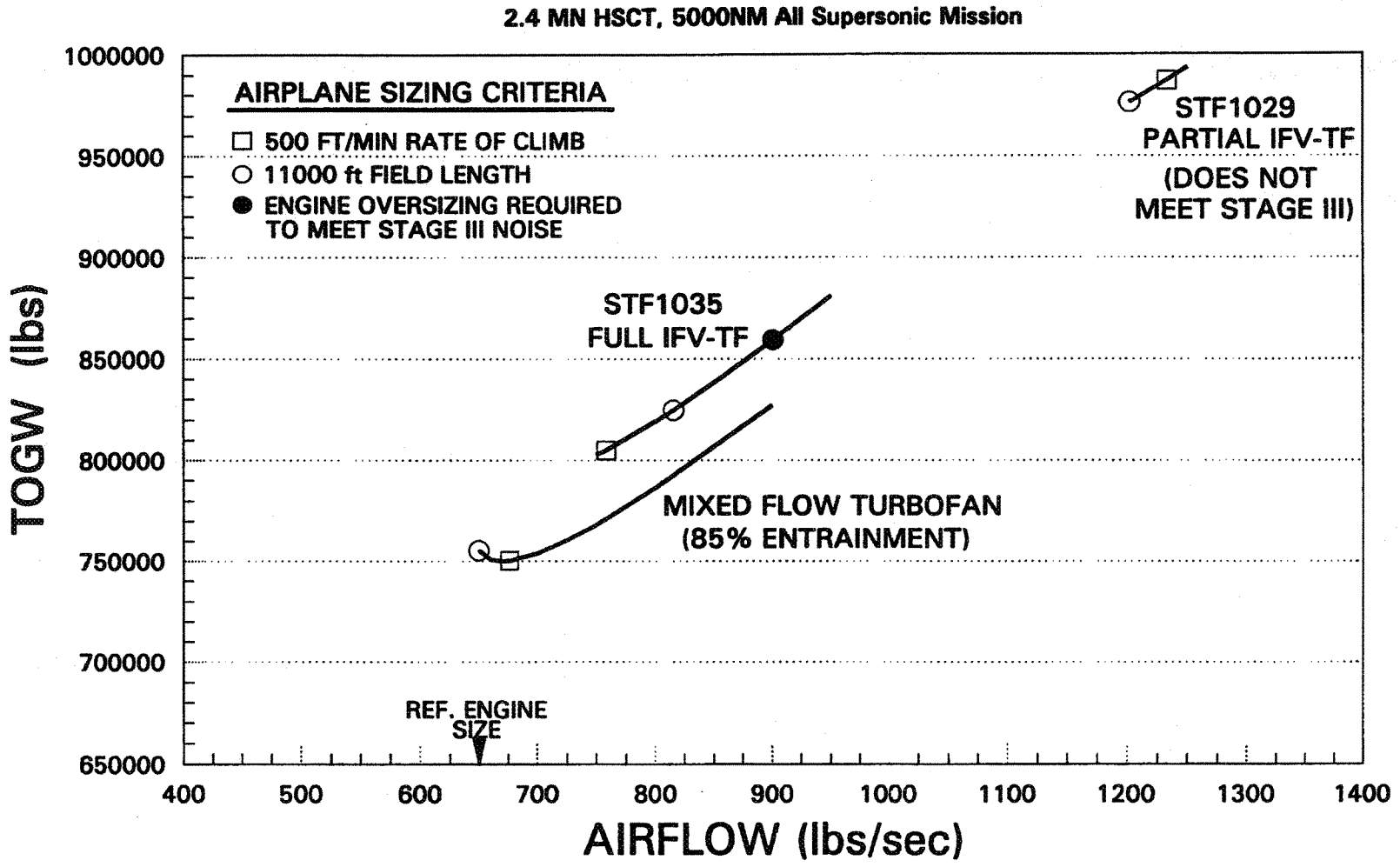

Figure 3. MFTF & IFV Powered HSCT TOGW Results

INTRODUCTION

The following studies were conducted to evaluate the Partial Bypass Inlet Flow Valve Turbofan (PIFVTF) propulsion concept:

A. An engine flowpath analysis to determine the aerodynamic designs of the engine components.

B. An engine mechanical design study to determine component sizes and weights.

C. A Computational Fluid Dynamic (CFD) analysis of the Annular Inverter Valve (AIV) to determine the flow quality in the valve during all modes of operation.

D. A compression system design study to develop performance characteristics of the fan, core driven fan stage and high pressure compressor.

E. Development of a dynamic engine model and analyses of the transient engine operation.

F. Mission analysis.

The following studies were conducted to evaluate the full bypass inlet flow valve turbofan:

G. Cycle studies to determine fan pressure ratios, bypass ratio and turbine temperature.

H. Engine flowpath analyses to evaluate two and three spool configurations.

I. An Engine Mechanical design of the STF 1035.

J. Mission Analysis.

Performance, dimensional and weight information for both the STF 1029 and STF 1035 engines were provided to NASA, Boeing and McDonnell Douglas for the system evaluation studies.

These studies are described in detail in the following sections of this report.

A. PARTIAL BYPASS IFV TURBOFAN COMPONENT AERODYNAMIC DESIGNS

Flowpath analyses were conducted for the Partial Inlet Flow Valve Turbofan (PIFVTF) propulsion concept to determine the best arrangement and numbers of stages for the engine rotating components. The PIFVTF concept, shown in Figure 1, is a two spool turbofan with an Inlet Flow Valve (IFV) between the front and rear stages of the fan. This valve is used to allow secondary air from the inlet (C) be passed into the outer portion of the rear fan during takeoff to increase the total airflow through the engine and reduce the exhaust jet velocity. At the same time, the front fan outer flow (B) is inverted in the valve and passes around the rear fan. Since this valve inverts flows B&C, it is referred to as an Annular Inverter Valve (AIV). These two flows are then mixed together in the bypass duct before being mixed with the core stream (A) in the exhaust nozzle. The engine operating mode shown in Figure 4 will be referred to as high flow operation.

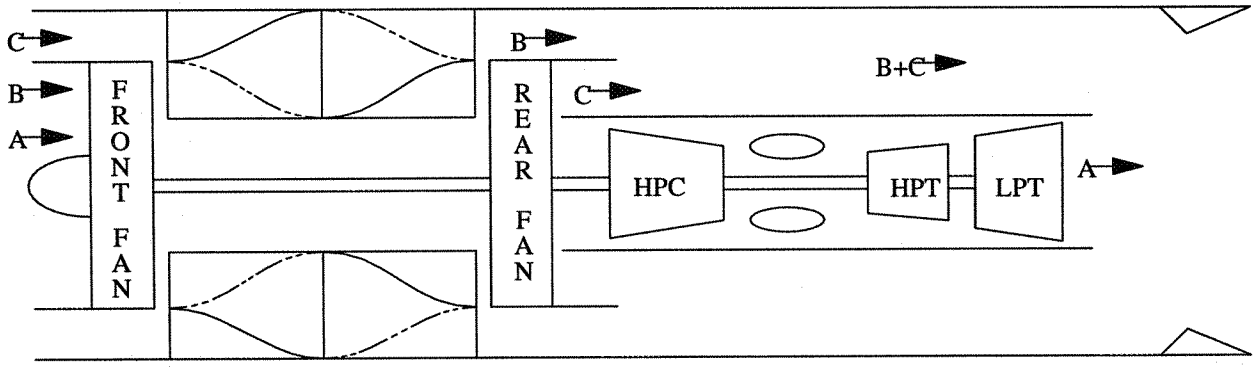

Figure 4. Partial Inlet Flow Valve Turbofan During High Flow Operation

Once the HSCT airplane is outside the area where it will cause a community noise problem, the secondary air is turned off and the valve is positioned such that the front fan outer air (B) now passes through the valve and into the outer section of the rear fan stage, as shown in Figure 5. This mode of operation is referred to as conventional or low flow operation.

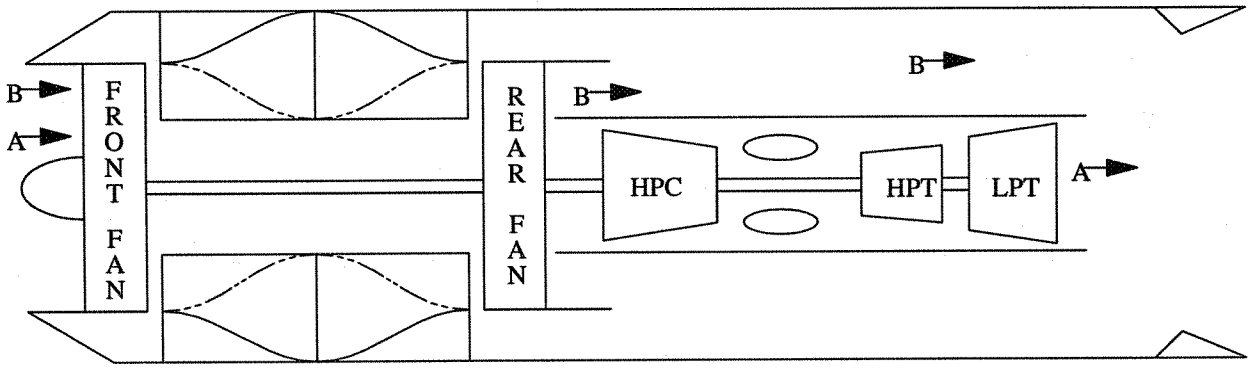

Figure 5. PIFVTF Turbofan Concept (Low Flow Operation)

The partial IFV turbofan concept evaluated in this study places the rear fan stage on the same spool as the high pressure compressor. This rear fan stage is referred to as a core driven fan stage (CDFS).

The cycle characteristics for the partial IFV turbofan engine evaluated in this study were provided to P&W by NASA Lewis. P&W then developed a steady state performance model of the engine and gave it a P&W study turbofan (STF) designation as the STF1029. Table 2 presents STF1029 cycle and uninstalled performance characteristics for high flow operation at sea level static and 689 ft–0.32 Mn sideline noise point, and for low flow operation at SLS and at the 55,000 ft–2.4 Mn supersonic cruise point.

Table 2. STF1029 Cycle Characteristics and Performance Summary

Mode of Operation	High Flow	High Flow	Low Flow	Low Flow
Mach Number	0.0	0.32	0.0	2.4
Altitude, ft	0.0	689	0.0	55,000
Δ Tambient, °F	0.0	18.0	0.0	0.0
Engine Inlet Total Temperature, °R	518.7	545.3	518.7	837.8
Primary Inlet Pressure Recovery	0.932	0.9706	0.932	0.932
Secondary Inlet Pressure Recovery	0.896	0.933	---	---
Primary Airflow, Lb/sec.	605.8	644.8	605.8	439.7
Secondary Airflow, Lb/sec.	155.6	165.6	---	---
Secondary/Primary Airflow	0.26	0.26	---	---
Total Airflow, Lb/sec.	761.4	810.4	605.8	439.7
Core Stream Airflow, Lb/sec.	360.9	383.7	340.5	229.5
Bypass Ratio	1.11	1.11	0.78	0.92
Front Fan Corrected Flow, Lb/sec.	650	650	650	455
CDFS OD Corrected Flow, Lb/sec.	173.7	173.7	161.9	150.0
CDFS ID Corrected Flow, Lb/sec.	187.8	187.5	205.6	161.9
Front Fan Pressure Ratio (FPR1)	2.39	2.39	2.02	1.59
CDFS, OD Pressure Ratio (FPR2)	1.706	1.702	1.40	1.11
Overall Fan Pressure Ratio	1.877	1.875	2.83	1.765
CDFS ID Pressure Ratio	1.201	1.201	1.225	1.18
HPC Pressure Ratio	6.99	6.98	8.21	5.95
CDFS ID + HPC Pressure Ratio	8.40	8.38	10.1	7.0
Overall Compression Ratio	19.9	19.9	20.1	11.05
Turbine Cooling Air, %	28.5	28.5	28.5	28.5
HPC Exit Temperature (TT3), °R	1306	1368	1315	1710

Table 2. STF1029 Cycle Characteristics and Performance Summary (Cont'd)				
Mode of Operation	**High Flow**	**High Flow**	**Low Flow**	**Low Flow**
Combustor Exit Temperature (TT4), °R	2676	2799	3054	3470
HPT Rotor Inlet Temperature, (TT4.1), °R				3360
HPT Expansion Ratio	4.11	4.10	3.83	3.66
LPT Expansion Ratio	1.94	1.94	1.63	1.54
Front Fan OD Bypass Flow, Lb/sec.	244.9	261.1	---	---
CDFS OD Flow, Lb/sec.	155.6	165.6	265.3	210.2
Total Bypass Flow (B+C), Lb/sec.	400.5	426.7	265.3	210.2
Bypass Flow Total Temp., °R	660	693	729	1006
Bypass Flow Total Pressure, psia	25.7	28.0	37.0	30.2
Bypass Flow Parameter ($W\sqrt{TP}$)	400.1	400.9	193.4	220.9
Static Pressure at Mixing Plane, psia	25.1	27.4	36.7	29.8
Bypass Flow Mach Number	0.182	0.182	0.113	0.130
Bypass Flow Mixing Area, in^2	2448	2448	1881	1881
Total Core Flow (A), Lb/sec.	365.6	389.1	346.5	233.6
Core Flow Total Temp., °R	1501	1576	1805	2151
Core Flow Total Pressure, psia	31.75	34.62	41.4	32.9
Core Flow Parameter ($W\sqrt{T/P}$)	446.0	446.3	355.9	329.0
Core Flow Mach Number	.599	.600	.43	.39
Core Flow Mixing Area, in^2	1015	1015	1015	1015
Total Exhaust Flow, Lb/sec.	766.1	815.8	611.8	443.8
Mixed Exhaust Temp., °R	1076	1131	1364	1636
Mixed Exhaust Pressure, psia	27.9	30.4	39.0	31.4
Mixed Flow Parameter Lb/ sec$\sqrt{}$°R/psia	900.8	902.4	579.3	571.9
Exhaust Nozzle Throat Area, in^2	1704	1708	1101	1092
Gross Thrust (Cv=.982)	34470	40500	37480	47670
Absolute Jet Velocity, fps	1448	1597	1971	---
Net Thrust, Lbf	34470	31300	37480	15900
TSFC, Lbm/hr−Lbf	.594	.737	.677	1.22

The engine design point was set at the SLS high flow point. The cycle characteristics, i.e., fan pressure ratio, CDFS pressure ratio, secondary flow, bypass ratio and combustor temperature were selected by NASA Lewis to produce an average exhaust jet velocity of 1450 ft/sec. The secondary airflow of 155.6 lb/sec. is set by the inlet corrected flow of 173.7 lb/sec which is required by the outer section of the CDFS. This 155.6 lb/sec. of secondary air increases the total engine airflow to 761.4 lb/sec.

During high flow operation the combined CDFS OD flow (C) and front fan OD flow (B) produce an average fan pressure ratio of 1.877 and a bypass ratio of 1.11 at the SLS design point.

Table 2 lists the conditions at the rear mixing plane. Column 1 shows that in the high flow mode of operation the core stream total pressure is 31.75 psia while the bypass stream total pressure is set at 25.7 psia. To achieve a static pressure of 25.1 psia at the mixing plane, the core stream Mach Number is 0.599 while the bypass stream Mach Number is 0.182. These Mach Numbers result in a core stream mixing plane area of 1015 in^2 and a bypass stream mixing area of 2448 in^2.

During high flow mode operation at the sideline noise measuring point (Table 2 – Column 2) the engine is operated at the same fan and compressor match points as at the design point. The combustor temperature is increased because of the higher engine inlet temperature. The absolute exhaust velocity is increased to 1597 ft/sec. because of the 0.32 flight Mach Number.

During low flow operation (Table 2, Columns 3 and 4), the secondary air is turned off and the engine operates as a conventional mixed flow turbofan. At the SLS condition, the overall front (FPR1) plus rear (FPR2) fan pressure ratio is 2.83 and the bypass ratio is 0.78. Since the secondary flow is turned off, the rear mixing plane area in the bypass stream is reduced to 1881 in^2.

Table 2 shows that the benefit of partial IFV concept is to increase the overall flow through the engine by 26% in order to reduce the exhaust velocity from 1971 to 1448 ft/sec. If the engines are compared at the same thrust level, the high flow operating point would have a 365 ft/sec. lower exhaust velocity.

At the 55,000 ft–Mach 2.4 operating condition (Table 2, Column 4), the STF1029 operates with an overall fan pressure ratio of 1.765 and a bypass ratio of 0.92. The HPC pressure ratio is set to achieve a compressor discharge temperature (TT3) of 1710°R. The HPT rotor inlet temperature (TT4.1) is set at its maximum value of 3360°R. The STF1029 produces an uninstalled (Cv=0.982, no boattail drag) net thrust of 15330 Lbf and a TSFC of 1.198 Lbm/hr–Lbf.

The performance data shown in Table 2 was generated by P&W during the initial engine flowpath analysis. The performance model was later updated to reflect the component performance levels and turbine cooling requirements defined by the flowpath analyses.

The final STF1029 flowpath is shown in Figure 6. The low spool consists of a 2 stage fan driven by a conventional single stage low pressure turbine (LPT). The annular flow inverter valve and intermediate case are located immediately aft of the fan. The intermediate case will support the number 2/3 bearing compartment and establish the location of the tower-shaft. Location of the intermediate case aft of the inverter valve assembly reduces the distance between the No. 2 and No. 5 bearings which support the low shaft. This, in turn, will allow a significant reduction in low shaft diameter required to achieve acceptable critical speed margin. The reduced low shaft diameter will allow the compressor disk bore diameters to be reduced a corresponding amount, resulting in a significant weight savings for the core engine.

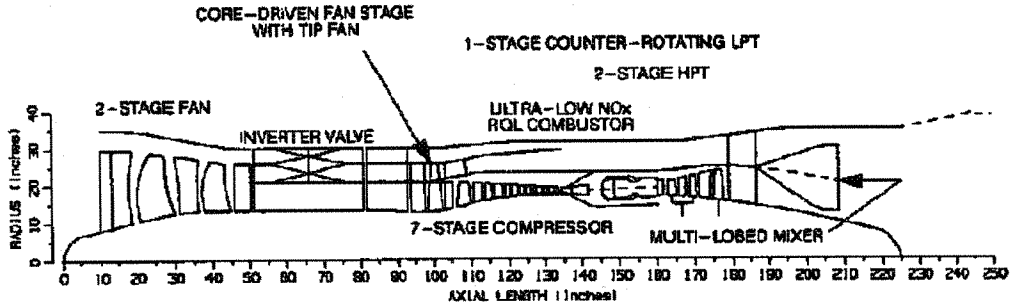

Figure 6. STF1029 Flowpath

The high spool counter–rotates with respect to the low spool and consists of a core driven fan stage (CDFS) and a 7–stage compressor driven by a 2–stage turbine. The CDFS is unique in that it incorporates a rotating splitter to maintain separate flow streams in the hub and tip (Figure 7), allowing the tip to operate at significantly different pressure ratios and corrected flows than the hub. Without the splitter, unacceptable radial flows would occur, resulting in losses in performance and operability.

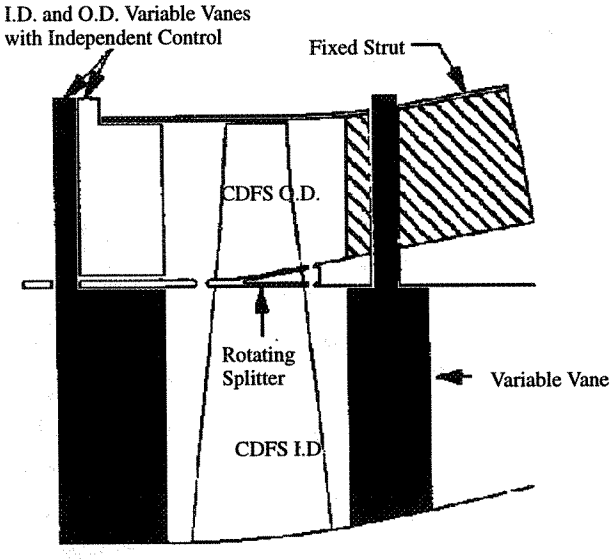

Figure 7. Schematic of the STF1029 Core Driven Fan Stage

Variable vane assemblies are located forward and aft of the CDFS to insure adequate stability throughout the required operating range. Due to the drastic differences in operating conditions between the CDFS I.D. and O.D. section, the forward variable vane assembly allows independent control of the I.D. and O.D. vane angle settings. A variable vane is located aft of the CDFS I.D. to provide proper flow conditions into the high pressure compressor. A fixed strut is located aft of the CDFS O.D. to provide axial flow into the duct.

Aero/mechanical design characteristics of the STF1029 fan are provided in Table 3 and performance characteristics at various flight points are summarized in Table 4. The fan was designed to balance efficiency and stall margin throughout the flight envelope. The highest nominal operating pressure ratio is 2.4 at a corrected airflow of 650 lbm/sec and occurs during high flow mode operation at sea–level–static (SLS) max power. During low mode SLS max power operation the fan corrected flow and speed are held constant but the pressure ratio is decreased to 2.02. Designing the fan for 25% stall margin at the 2.4 pressure ratio, hi flow operating condition resulted in poor fan efficiency during off–design low flow mode operation such as subsonic and supersonic cruise. Designing for 25% stall margin at the 2.02 pressure ratio condition did not provide acceptable stall margin during hi–flow operation. In order to provide acceptable off–design efficiency during cruise conditions, it was decided to design the fan for 25% stall margin at an intermediate pressure ratio of 2.20. This yields 15% stall margin during takeoff in hi flow mode. The validity of designing for 15% stall margin at takeoff cannot be defined until further information about inlet distortion characteristics is available.

Table 3. Summary of STF1029 Fan Aero/Mechanical Design Characteristics

Aerodynamic Design Point (ADP)	0/0K
Operating Mode	Hi Flow
Number of Stages	2
Variable Stages	IGV
Corrected Speed (rpm)	6095
Corrected Airflow (lbm/sec)	650
Pressure Ratio	2.40
Adiabatic Efficiency (%)	88.15
Stall Margin (%)	15.00
R1 Inlet Specific Flow (Lbm/sec–ft^2)	41.30
ADP Exit Mach Number	0.44
ADP Exit Swirl	90.00
ADP Corrected Tip Speed (ft/sec)	1545
Max Physical Tip Speed (ft/sec)	1585
R1 Inlet Hub/Tip Ratio	0.37
Exit Hub/Tip Ratio	0.54

Table 4. STF1029 Fan Performance Summary

Flight Condition	0.0K Hi Flow	0/0K Lo Flow	.32/689K Hi Flow	2.4/55K Lo Flow
Corrected Speed (rpm)	6095	6043	6095	4899
Corrected Airflow (lbm/sec)	650	650	650	455
Pressure Ratio	2.39	2.02	2.39	1.59
Adiabatic Efficiency, %	88.15	85.06	88.15	89.75
Physical Rotational Speed (rpm)	6095	6043	6250	6226

Aero/mechanical design characteristics for the core driven fan stage are summarized in Table 5. Both the I.D. and O.D. sections were designed near their maximum flow and pressure ratio operating conditions. For the I.D. section this occurred at the 0/0K Lo Mode condition while it occurred at 0/0K Hi Mode for the tip. The meanline designs for both sections were optimized to insure that the root and tip blade counts were consistent. The O.D. section aspect ratio was also adjusted to insure that the O.D. root chord length matched the tip chord length of the I.D. section. The entire compressor flowpath and the core engine rotational speeds were set to maintain acceptable tip speeds and stresses in the O.D. section. The final O.D. maximum tip speed is 1800 ft/sec., equal to the maximum allowable based upon the P&W/GEAE design groundrules.

Table 5. Summary of STF1029 Core Driven Fan Stage Aero/ Mechanical Design Characteristics

	HUB (I.D.)	TIP (O.D.)
Aerodynamic Design Point (ADP)	0/0K Lo Mode	0/0K Hi Flow
ADP Corrected Speed (rpm)	6581	7229
ADP Corrected Airflow (lbm/sec)	205.6	173.7
ADP Pressure Ratio	1.23	1.71
ADP Adiabatic Efficiency (%)	86.43	83.94
ADP R1 Inlet Specific Flow (lbm/sec–$ft^{2)}$	36.13	34.85
ADP Corrected Tip Speed (ft/sec)	1188	1624
Max Physical Tip Speed (ft/sec)	1215	1796

Operating conditions at several flight points are summarized in Table 6 for the CDFS hub and tip. As previously mentioned, the hub and tip can experience significantly different operating conditions, particularly during high flow mode. At this condition, the CDFS hub is fed by fan discharge air while the tip is fed by ambient air.

Table 6. Summary of Operating Conditions for the STF1029 Core Driven Fan Stage (CDFS Hub/CDFS Tip)

Flight Condition	0/0K Hi Flow	0/0K Lo Flow	0.32/0.69K Hi Flow	2.4/55K Lo
Inlet Total Pressure (psia)	32.46/13.16	27.33/27.05	35.43/14.36	28.43/28.11
Inlet Total Temperature(°F)	225.31/59.00	195.50/195.50	260.27/85.63	506.30/506.30
Corrected Speed (rpm)	6291/7229	6581/6581	6289/7227	5857/5857
Corrected Airflow (lbm/sec)	187.8/173.69	205.58/161.88	1187.51/173.70	161.89/150.00
Pressure Ratio	1.20/1.71	1.23/1.40	1.20/1.70	1.18/1.11
Adiabatic Efficiency (%)	86.80/83.94	86.43/87.74	86.80/84.03	86.84/69.60

Aero/mechanical design characteristics for the high pressure compressor are summarized in Table 7. The compressor configuration was selected from a meanline analysis which considered the impact of flowpath shape, flowpath elevation, number of stages, stage pressure ratio distribution, stator exit swirl angle distribution, airfoil aspect ratio, and number of airfoils per stage. These parameters were selected to achieve a compressor design which balanced the aerodynamic performance (efficiency and stall margin), weight, and manufacturing cost while maintaining a speed/flow relationship compatible with the core driven fan stage.

Table 7. Summary of STF1029 Compressor Aero/Mechanical Design Characteristics

Aerodynamic Design Point	0/0K
Operating Mode	Low Flow
Number of Stages	7
Variable Stages	IGV/S1/S2/S3
ADP Corrected Speed (rpm)	6366
Corrected Airflow (lbm/sec)	173.49
Pressure Ratio	8.21
Adiabatic Efficiency (%)	89.46
Stall Margin (%)	25.00
R1 Inlet Specific Flow (lbm/sec–ft^2)	33.77
ADP Exit Mach Number	0.28
ADP Exit Swirl(°)	90.00
R1 Inlet Hub/Tip Ratio	0.67
Exit Hub/Tip Ratio	0.91

Parametric studies were also conducted to define the optimum high (HPT) and low (LPT) turbine combination. During the STF1029 design effort it was determined that the area ratio between the HPT exit and the LPT inlet required to achieve the LPT operating range was too large to close couple the HPT with a vaneless LPT. This required that a significant axial distance be placed between the two turbines to control the diffusion and insure unseparated flow. Use of large axial gaps between the HPT and LPT introduced problems with leakage control and cooling/structural integrity of the rotating inner wall. Due to these considerations, the vaneless LPT was dropped from consideration. The STF1029 features a conventional vaned LPT close–coupled to a 2–stage HPT. Turbine aero/mechanical design parameters are summarized in Table 8.

Table 8. Summary of STF1029 Turbine Design Parameters

	HPT	LPT
Aerodynamic Design Point	2.4/55K	0/0K
Operating Mode	Low Flow	Hi Flow
ADP Inlet Flow Parameter (Lb/sec $p\sqrt{R}$/psia)	52.76	235.90
Max Inlet Flow Parameter (Lb/sec $p\sqrt{R}$/psia)	53.06	235.90
ADP Expansion Ratio	3.66	1.94
Max Expansion Ratio	4.11	1.94
ADP Cooled Adiabatic Efficiency (%)	89.31	91.73
ADP Rim Velocity Ratio	0.48	0.45
ADP Mean Velocity Ratio	0.57	0.56
ADP Exit Mach Number	0.46	0.62
ADP Exit Swirl (°)	32.00	8.00
Max AN^2 ($x10^8$ in^2–rpm^2)	450.00	392.15
Blade Exit Hub/Tip Ratio	0.74	0.65
Total Cooling & Leakage (%Wae)	24.1	4.41

The nozzle for the partial IFV turbofan is a conventional 2D–CD design with thrust reversing capability. An aerodynamic design was performed for this nozzle. Since no acoustic treatment is required, this nozzle was designed to provide the optimum balance between performance and weight. The nozzle throat and area requirements, dimensions and weignt are presented in Table 9.

Table 9. STF1029 2D–CD Nozzle Design Summary

Nozzle Throat Area, in^2	1088 to 1955
Nozzle Exit Area, in^2	1100 to 4520
Internal Flowpath Width, in.	61.7
External Width, in.	73.3
External Maximum Height, in.	73.3
Maximum Area, in^2	5373
Divergent Flap Length, in.	120
External Flap Length, in.	126
Nozzleweight, lb.	3125

Table 10 summarizes the STF1029 nozzle performance at the Mach 2.4/55,000 ft. cruise condition. The boattail angle at the maximum dry power condition (Power Code 50) is 3°.

Table 10. STF1029 Nozzle Performance Summary

Nozzle Expansion Ratio	24.31
Nozzle Throat Area, in^2	1131
Nozzle Exit Area (A9), in^2	3799
Equivalent Nozzle Exit Diameter (D9), in	69.55
Maximum Area (AMAX), in^2	5373
Equivalent Maximum Diameter (DMAX), in	82.71
h = (DMAX – D9) / 2 , in	6.58

Table 10. STF1029 Nozzle Performance Summary (continued)

External Flap Length (L), in	126
Boattail Angle = arc sin h/L	2.99
A9/AMAX	0.71
Boattail Drag Coefficient (CD)	.0094
Ambient Pressure (PAM), psia	1.3227
Dynamic Pressure (Q=101 Pam MN^2), psf	769.5
Boattail Drag = CD . Q . AMAX/144, Lbf	271
Internal Performance Coefficient (CV)	0.9833
Overall Nozzle Performance Coefficient (CFG)	0.9777

Table 10 shows that the internal nozzle gross thrust coefficient (CV) is equal to 0.9833. When the boattail drag is included the overall nozzle performance coefficient (CFG) is 0.9777.

B. PARTIAL BYPASS IFV TURBOFAN MECHANICAL DESIGN

A mechanical design of the STF1029 engine was conducted using materials and structural concepts projected to be available in the year 2000. These concepts and materials are consistent with those used for other propulsion systems being studied for the next generation HSCT. Table 11 provides a summary of the materials used in the STF1029 design.

Table 11. Engine Component Materials

Material	Engine Component
Polymer Matrix Composites	Inlet Case
PMC/Titanium	Fan: IGV/Vane
Ti Honeycomb/Kevlar	Blade Containment
Advanced Titanium	Fan: Blades, Stage 2 Disk, IGV, CDFS Blades, Compressor: Blades 1–3, Disk 1–3 Fan, Intermediate and Bypass Duct
Advanced Nickel	Compressor: Blades 4–7, Disks 4–7, Vanes 4–7, TEC, Turbine Disks 1–3
TiMMC	Fan Stage 1 Disk, CDFS Disk
Single Crystal Nickel	Turbine: Blades/Vanes
Ceramic Matrix Composites	TEGV, Combustor Rich Zone Liner
TiAl	Compressor Case, Turbine Outer Case, Diffuser, Combustor Case
Hastelloy	Combustor Lean Zone Floatwall Liner

HSCT propulsion systems operate at near maximum cycle temperatures and component rotational speeds throughout supersonic cruise, resulting in steady–state operation at the worst combination of stress and temperature for the majority of the engine life. Engine design limits are summarized in Table 12. Component material selection and operating temperatures were established by the steady–state supersonic cruise flight condition. The engine cold section, defined as the entire compression system, was designed for 18,000 hours of supersonic cruise operation. Based on a typical Mach 2.4 HSCT flight profile this results in a total life of 35,100 hours with 9,000 Type 1 cycles. The engine hot section, the turbine system, was designed for half the life of the cold section.

Table 12. Engine Design Limits

Design Parameter	Design Limit
Engine Inlet Temperature ($TT2_{max}$)	380°F
Compressor Exit Temperature ($TT3_{max}$)	1250°F
HPT Rotor Inlet Temperature ($TT4.1_{max}$)	2900°F
Low Rotor Speed ($N1_{max}$)	6226 rpm
High Rotor Speed ($N2_{max}$)	7984 rpm
HPT AN^2_{max}	450 x 10^8 in^2–rpm^2
LPT AN^2_{max}	392 x 10^8 in^2–rpm^2

Figure 8 shows the mechanical design layout that was developed for the STF1029. The following sections describe the mechanical designs of the individual components.

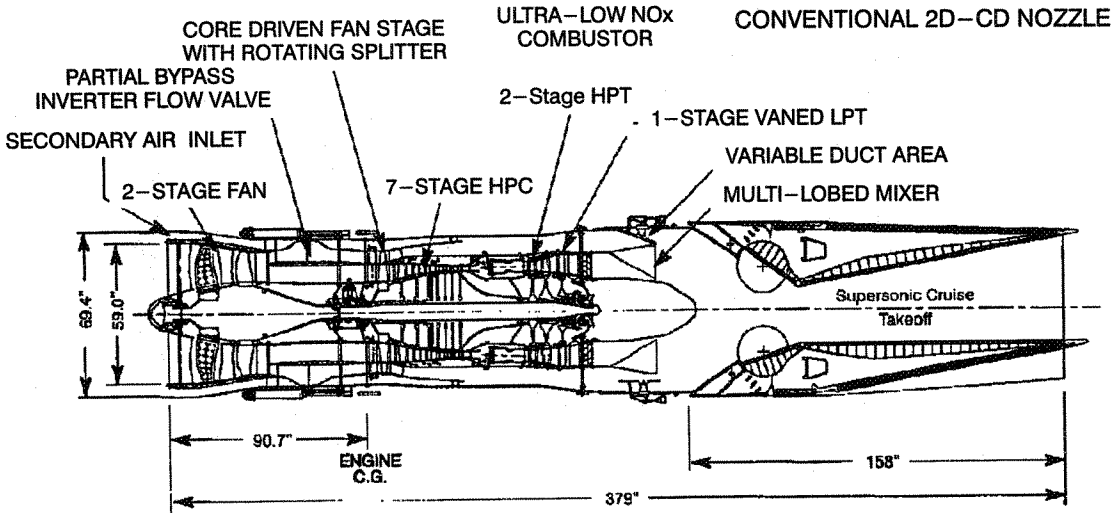

Figure 8. Features and Dimensions of the STF1029 PIFVTF

The forward fan, illustrated in Figure 9, is a two stage design. Both stages employ swept, low aspect ratio airfoils. The first stage blades are large enough and the weight savings are significant enough to employ a hollow airfoil design. The blades are manufactured in halves and the inside surfaces are machined before the blade halves are bonded together. The assembled first stage blades are mechanically attached via dovetail attachments. The second stage's blades are bonded to their rotor. Both stages utilize compact bore disks. The first stage disk is made of Titanium metal matrix composite (TiMMC). An advanced titanium alloy is used for the second stage. Casing treatment is used over the fan blade tips to increase stall margin. A Kevlar barrier is also located above the fan blades to provide containment in the event of a blade loss. Forward of the fan, a variable inlet guide vane is utilized to insure stability throughout the operating range.

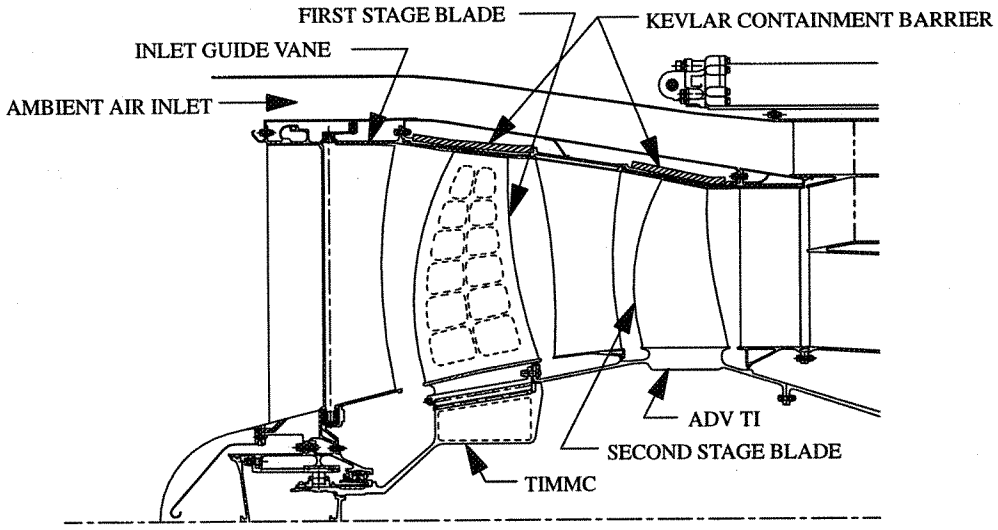

Figure 9. STF1029 Front Fan

The inverter flow valve, Figure 10, is located aft of the forward fan. It consists of two components, a forward, static section and an aft rotating section. The annular inverter valve is designed with eight passages for both the front fan OD flow (B) and the secondary flow (C). At the entrance of the valve these passages are concentric as shown in Figure 10. The passage shapes change in the valve so that at the center of the valve the passages are side by side. The aft rotating section of the valve has the same geometry as the front half. By rotating the aft section 22.5° about the engine centerline the flow inversion is produced.

The aft section of the valve is driven by two redundant actuators via a roller and track arrangement. Integral with the forward section is the fan exit splitter and a bypass duct for the fan inner air (A). This inner duct also acts as a major engine structure, and provides support for the rotating section of the valve.

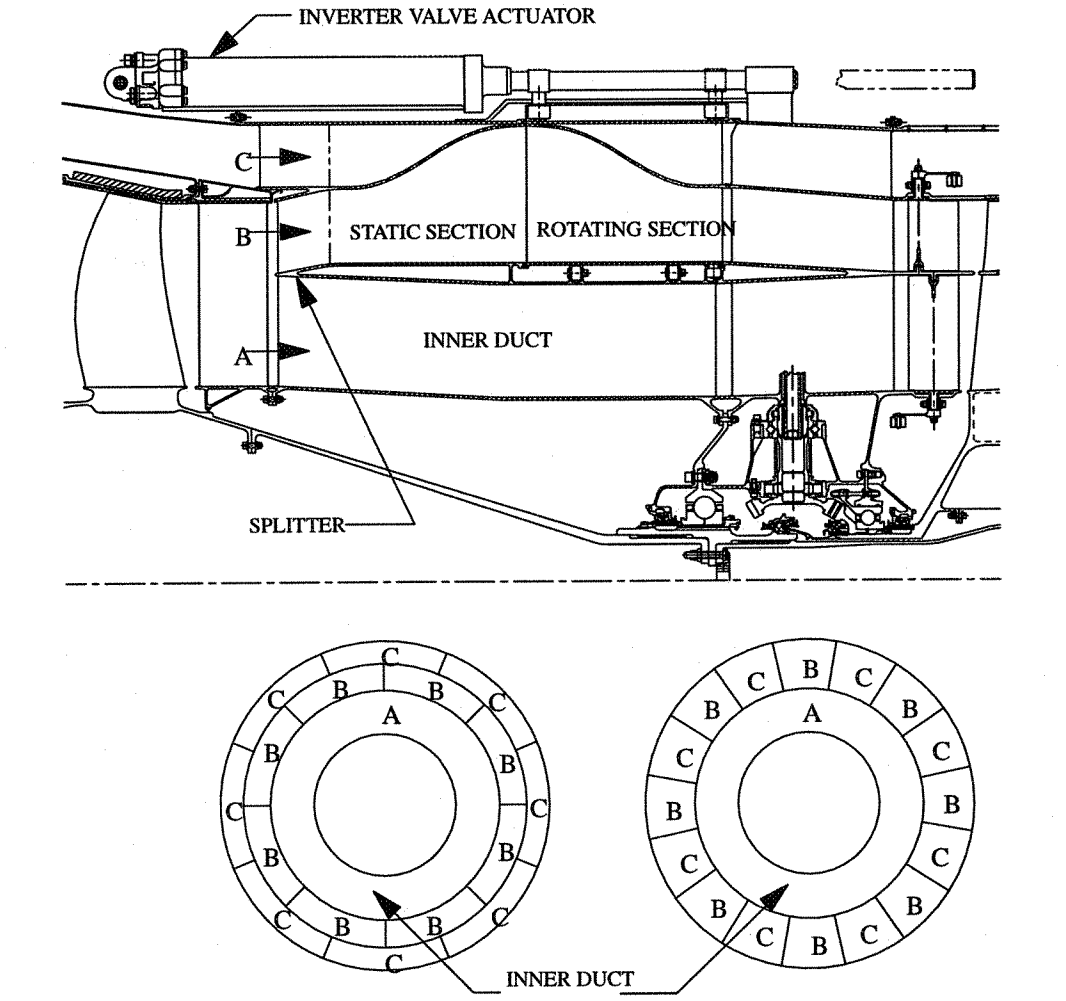

Figure 10. Inverter Flow Valve Design

The core driven fan stage (CDFS), shown in Figure 11, incorporates a rotating splitter and a compact bore disk made of TiMMC. Both the inner and outer flowpaths have their own set of inlet guide vanes, which are independently controlled to insure stability. The tip section of the CDFS is fed by the inverter flow valve inner section. This flow then passes through a fixed vane and into the bypass duct. The root flow of the core driven fan stage is supplied by the inner duct shown in Figure 7. This flow then proceeds into the high pressure compressor.

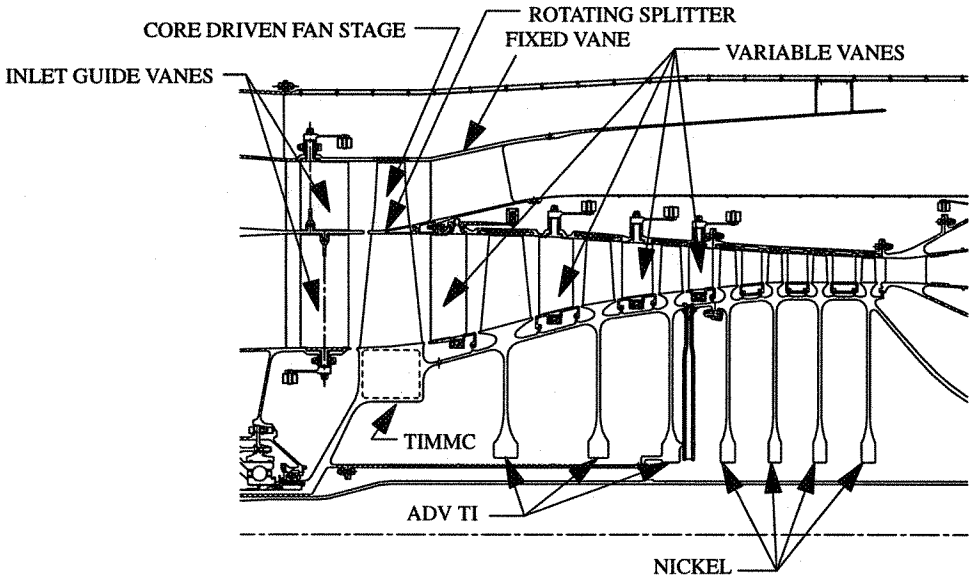

Figure 11. CDFS and Compressor Design

The seven stage compressor employs conventionally shaped monolithic disks. The first three stages use titanium, while the remaining four stages are nickel alloy. Integrally Bladed Rotor (IBR) construction is used, and a bolted flange is located at the Ti/Ni interface between stages three and four. Variable guide vanes are placed before each of the first four compressor stages. The remaining stages have fixed geometry vanes. To increase performance, a smooth abradable rub strip is incorporated into the double wall case over all seven compressor stages. The variable vanes are individually inserted into the split case and held in place by an ID shroud. The fixed vanes are fabricated in segments and circumferentially inserted into the case. A split case design was incorporated into the compressor because the stages are bonded together to form a drum rotor. Brush seals provided an interstage seal between static and rotating structure and an abrasive coating is applied to the rotor allowing small clearances to be obtained.

The conceptual design of the RQL combustor is shown in Figure 12. Variable geometry is required to reduce NOx emissions throughout the flight envelope. Variations in air loading is accomplished by translating cowls on the swirlers concentric with the fuel injectors. Swirler area variation is achieved by a cam and linkage mechanism located aft of the diffusers. Wheeler vortex generators are located inside the case to reduce diffusion losses.

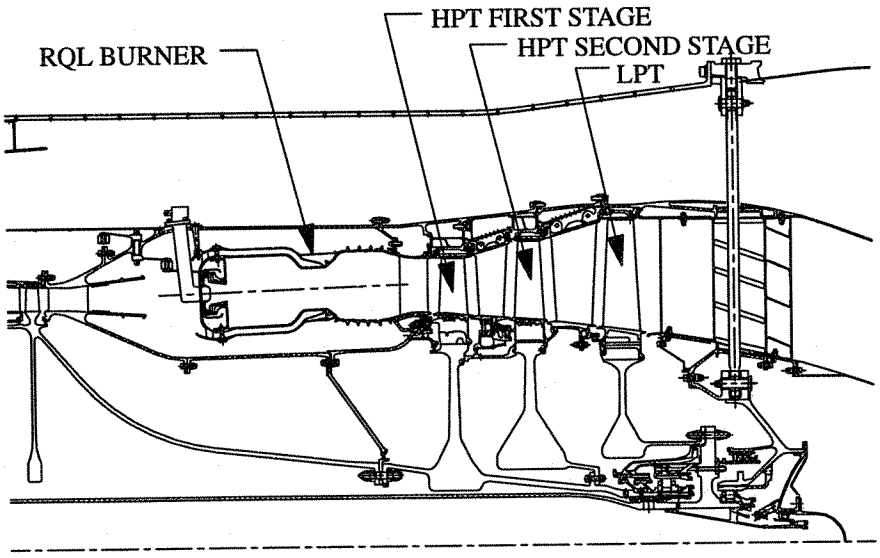

Figure 12. STF1029 Burner and Turbine Design

The high (HPT) and low (LPT) designs are shown in Figure 12. The turbine disks are conventionally shaped monolithic advanced nickel alloy. The disk stress and temperature profiles are shown in Table 13. The blades are individually removable and are held by dove tail attachments. The first vane is CMC and is film cooled. The turbine blades and other vanes are an advanced single crystal nickel. The HPT is cooled with compressor discharge air, while the LPT is cooled with compressor interstage bleed air.

Table 13. Disk Stress/Temperature Profile

STAGE	BORE TEMP °F	RIM TEMP °F	BORE STRESS KSI	RIM STRESS KSI
Fan 1	562	422	—	—
Fan 2	550	495	63.0	60.0
CDFS	570	534	61.3	58.3
HPC 1	570	614	61.3	56.4
HPC 2	585	729	60.8	54.0
HPC 3	620	840	60.0	55.5
HPC 4	905	946	102.0	95.9
HPC 5	971	1050	102.0	94.9
HPC 6	1038	1152	101.0	93.5
HPC 7	1104	1248	101.0	89.8
HPT 1	1170	1250	116.0	92.7
HPT 2	1180	1270	116.8	95.3
LPT 1	1190	1210	115.7	106.0

Before entering the exhaust nozzle, the air traveling through the bypass duct must be combined with the core air exiting the turbine. This mixing is facilitated with a multi–lobe mixer and a variable area mixing plane, which are shown in Figure 13.

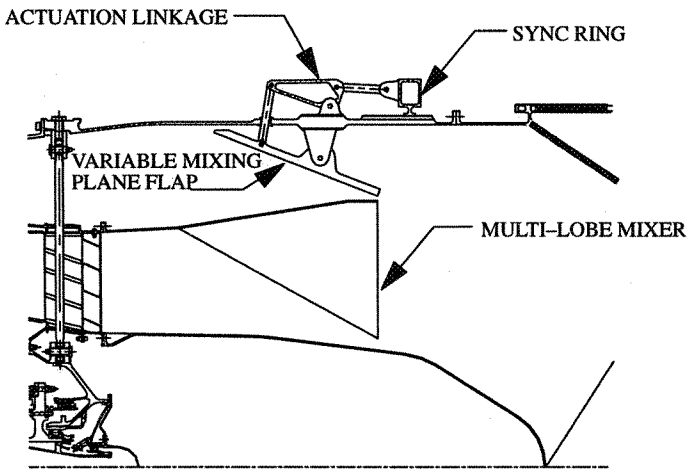

Figure 13. STF1029 Mixer

The multi–lobe mixer is an annular divider between the two flows. A series of 18 lobes proceeding around its perimeter alternately ramp inward and outward. The inward ramping lobes provide passages for the bypass air to travel inward toward the tailcone, while the outward ramping cones allow the core air to move toward the outer case. By the time the mixing plane is reached at the mixer exit, the flow is transformed from two concentric flows to a series of interleafed wedges.

The flow area for the bypass air at the mixing plane is variable between 800 and 2300 in^2. A bypass duct area of 2300 in^2 is required during high flow mode of operation. The 800 in^2 bypass area is used during reduced power low flow mode of operation. During the design of the STF1029, the mixing plane areas were reduced from the original areas shown in Table 2 in order to decrease the diameter of the exhaust system. The area control is provided by a set of articulating flaps similar to those of the nozzles on afterburning engines. These flaps are actuated via linkage and sync ring, by three actuators.

The exhaust nozzle for the STF1029 is a conventional 2D–CD design. Figure 14 shows the nozzle in the supersonic cruise (top) and takeoff (bottom) positions. In order to accommodate the large amount of flow in the bypass duct during takeoff operation, the variable mixing plane flaps are in the full open position to produce a bypass duct mixing plane area of 2300 in^2 . The exhaust nozzle throat area is opened to 1705 in^2.

The multilobe mixer and nozzle are designed to produce 80% mixing effectiveness during takeoff operation.

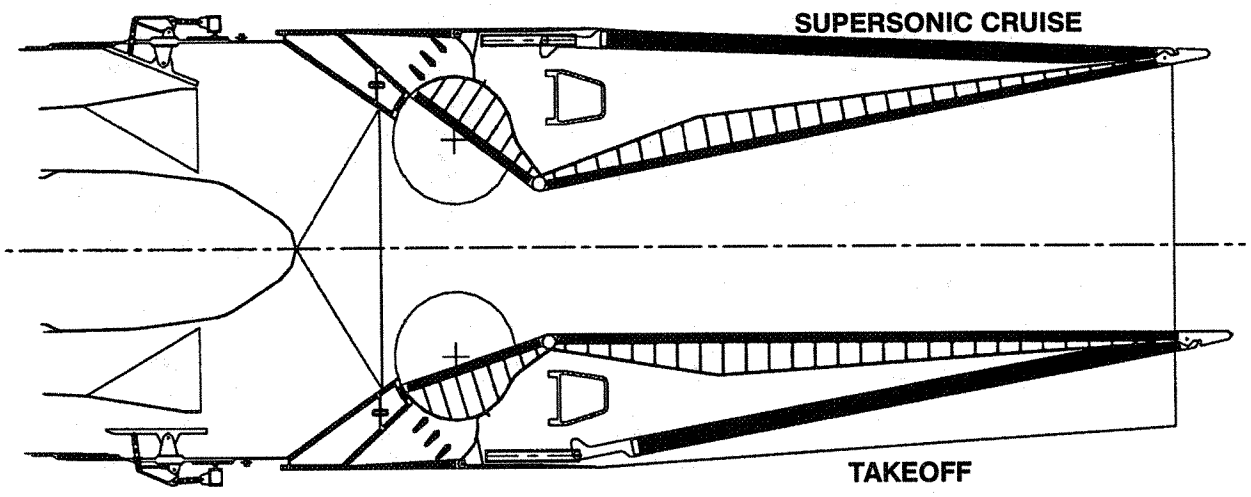

Figure 14. STF1029 2D/CD Nozzle in Supersonic Cruise and Takeoff Positions

During low flow mode of operation, the variable mixing plane flaps are in the closed position and all the bypass duct flow passes through the mixer chutes, which provide a bypass duct area of 800 in^2 at the exit of the mixer. The nozzle throat area at the Mach 2.4 cruise condition is 1100 in^2.

An afterburning version of the STF1029 engine was also examined. Figure 15 illustrates the exhaust system for the afterburning engine. The nozzle length was increased by 17 inches to provide the required combustion length to achieve an efficiency of 92 percent.

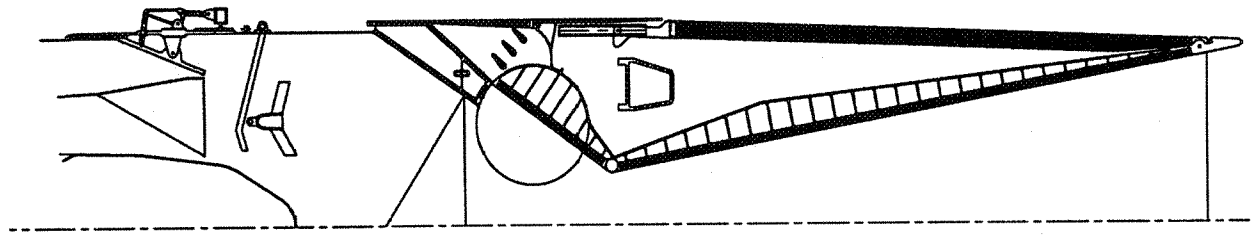

Figure 15. Exhaust System for the STF 1029 Afterburning Engine

Table 14 presents the STF1029 component weights.

Table 14. STF1029 Component Weights

COMPONENT	WEIGHT, LB
Fan Rotor, Stator, Case	1576
Flow Inverter Valve	529
Intermediate Case, Towershaft	349
CDFS and HPC Rotor, Stator, Cases	2173
Diffuser/Combustor	418
High Turbine Rotor, Stator, Case	1247
Low Turbine Rotor, Stator, Case, Shaft	706
Turbine Exhaust Case, Tailcone	356
Bearing Compartments	354
Bypass Duct	221
Variable Mixing Plane Flaps	311
Lobed Mixer	125
Controls, Accessories	650
2D–CD Nozzle	3125
Total Weight–Non Augmented	12,140
Afterburner	264
Total Weight–Augmented	12,404

C. ANNULAR INVERTER VALVE CFD ANALYSIS

A three dimensional computational fluid dynamics (3D−CFD) analysis was conducted of the STF1029 annular inverter valve (AIV) to determine the quality of the flow inside the valve and the levels of pressure drop to be expected during supersonic cruise (55,000 ft−2.4 Mn) and takeoff (689 ft−0.32 Mn) operation. Static pressure profiles were developed on all passage surfaces and boundary layer analyses were conducted to identify areas of probable flow separation. Total pressure profiles were developed at the exit of the valve in order to determine the pressure distortion to the core driven fan stage. Average total pressures were calculated at the midplane and exit of the valve in order to determine the pressure drops in the forward and aft sections of the valve.

A CFD analysis was also conducted for a transition mode operating condition in which the rear section of the valve was positioned half way between the high and low mode operating positions. In this position, the fan exit (B stream) and secondary flow (C stream) are mixed together in the aft sections of the valve.

The annular inverter valve geometry used in the STF1029 was selected based on model tests conducted by Boeing in 1972 (reference 1). Table 15 lists the valve geometry used for the STF1029 AIV. Both the inner (B) and outer (C) flowpaths have areas of 757 in^2 at the valve inlet, the valve centerline, and valve exit. Each flowpath has 8 equal area segments of 94.6 in^2. The valve length of 27.2 inches was selected to produce a valve pressure loss of 2% at the Mach 2.4 flight condition.

Table 15. Annular Inverter Valve Geometry

Total Length (L), in.	27.2
Annulus Area (A), in^2	757
$L/\sqrt{4A/\pi}$	0.88
Inner Flowpath (B)	
Inlet Inner Radius, in.	21.6
Inlet Mean Radius, in.	24.1
Inlet Outer Radius, in.	26.6
Hub Tip Ratio	0.81
Outer Flowpath (C)	
Inlet Inner Radius, in.	26.8
Inlet Mean Radius, in.	28.9
Inlet Outer Radius, in.	31.0
Hub Tip Ratio	.865
Distance Between Mean Radii (Δ Rm), in.	4.8
$L/\Delta Rm$	5.7

CFD analyses were conducted for the following cases:

(a) high flow mode of operation at 689 ft–0.32 Mn for both the secondary air outer–to–inner flowpath (Figure 16 stream C) and the front fan exhaust inner–to–outer flowpath. (Figure 16 stream B)

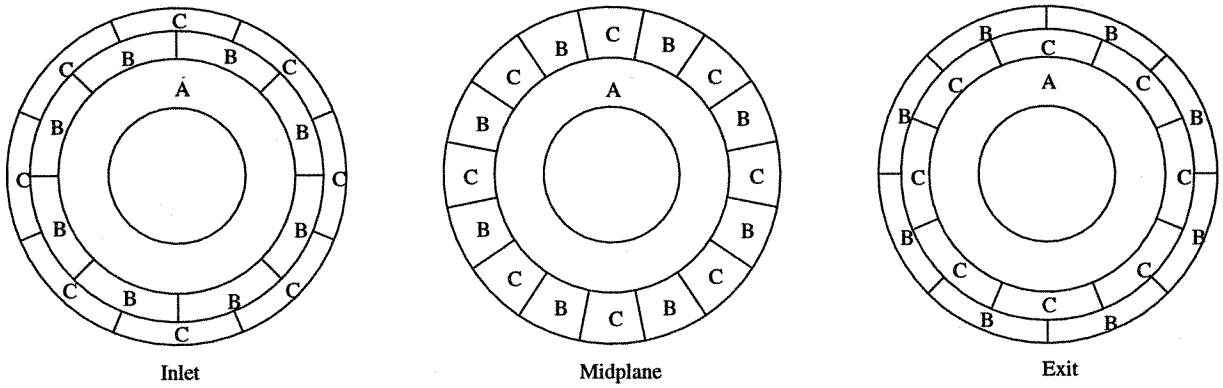

Figure 16. Flow Distribution in Valve During High Flow Mode Operation

(b) low flow mode of operation at 55,000 ft–2.4 Mn for the fan bypass air flowpath (Figure 17 stream B)

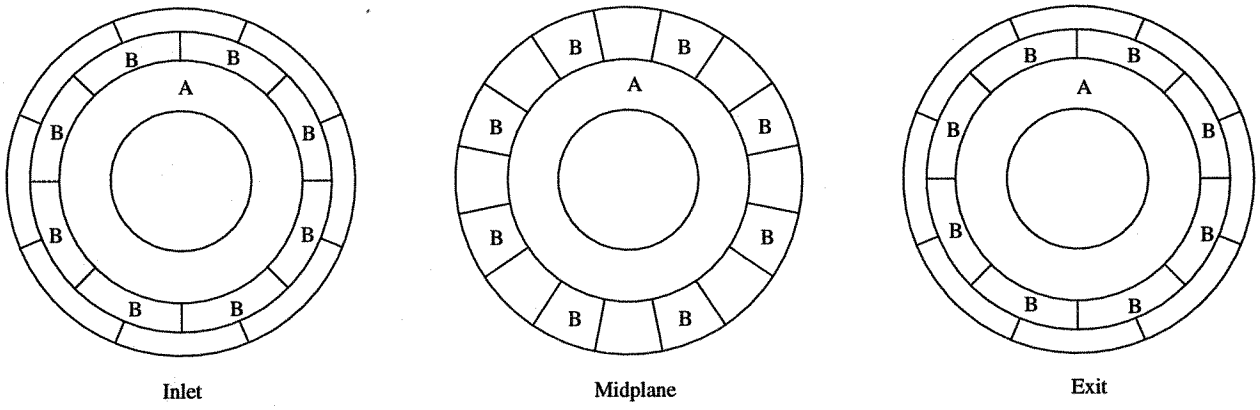

Figure 17. Flow Distribution in Valve During Low Flow Mode Operation

(c) transition mode of operation at 15,000 ft–0.7 Mn, with the rear section of the valve positioned halfway between the high and low mode positions (Figure 18).

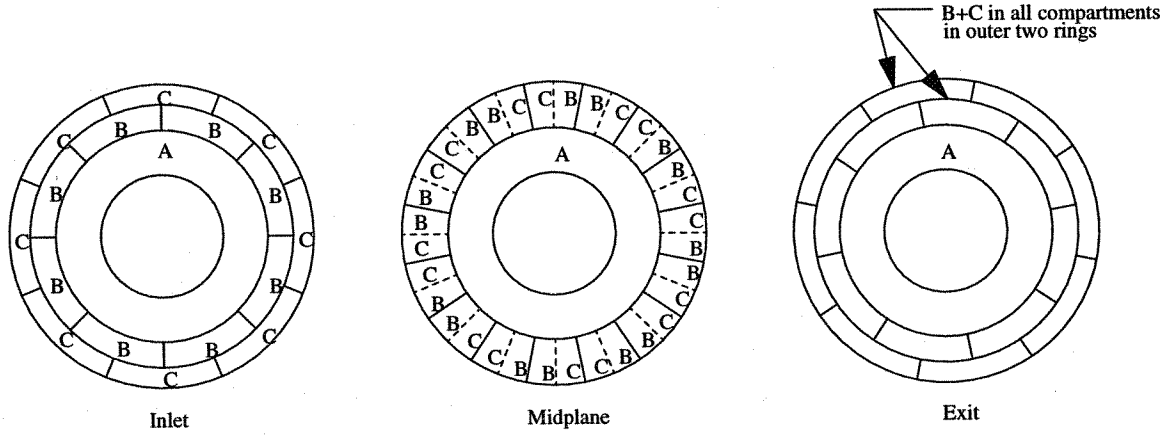

Figure 18. Transition Mode Valve Flow Pattern

Figure 19 shows the valve flowpaths that were analyzed.

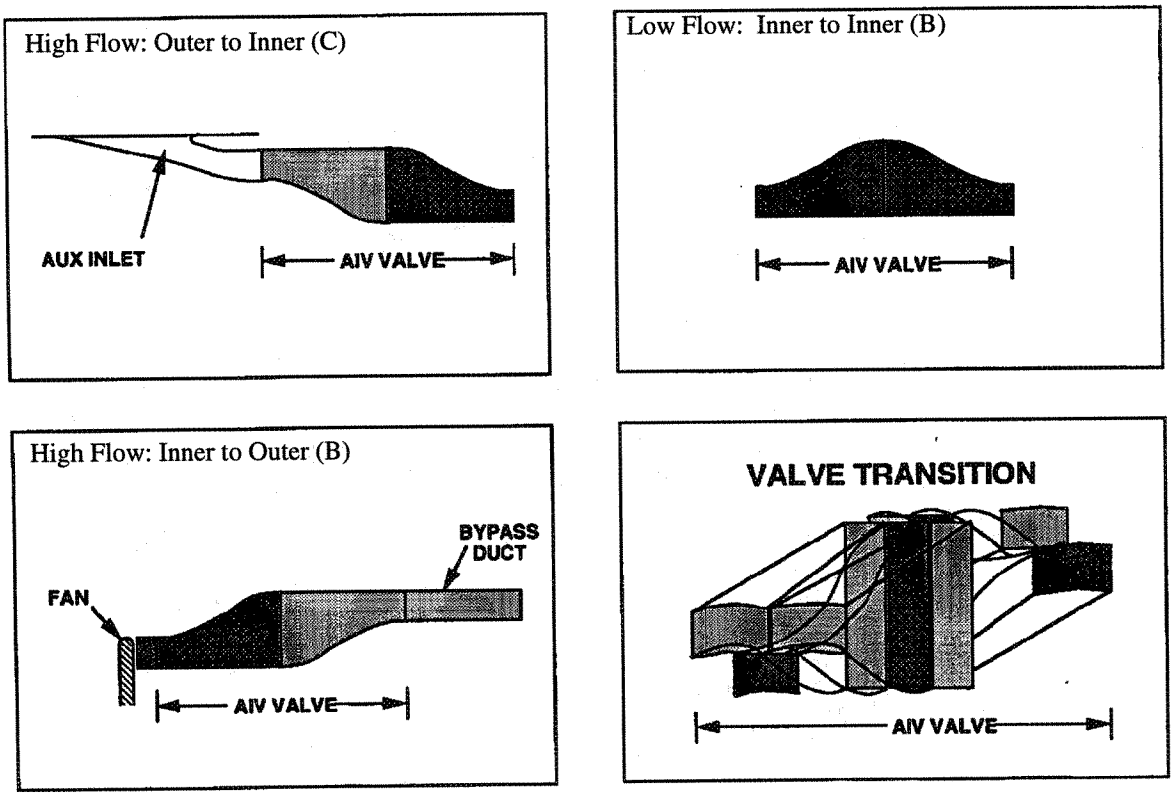

Figure 19. Valve Flowpaths for CFD Analyses

Table 16 summarizes the valve inlet boundary conditions for the three single duct flowpaths, and the predicted total pressure losses from reference 1.

Table 16. Single Duct Flowpath Inlet Conditions

Valve Flowpath	Outer to Inner	Inner to Outer	Inner to Inner
Stream	C	B	B
Engine Operating Mode	High Flow	High Flow	Low Flow
Flight Mach Number	0.32	0.32	2.4
Altitude, ft.	689	689	55,000
Power Code	Max Dry	Max Dry	Max Dry
Valve Inlet Area (A) in^2	757	757	757
Inlet Flow (W) Lb/sec.	165.6	261.1	210.2
Inlet Total Pressure (P), psia	14.95	35.79	28.65
Inlet Total Temperature (T), °R	545.3	719.9	965
Flow Parameter ($W\sqrt{T}/P$), Lb/sec$\sqrt{}$°R/psia	258.7	195.7	227.9
$W\sqrt{T}/PA$	.342	.258	.301
Inlet Mach Number	0.411	0.296	.353
Predicted $\Delta P/P$ (Reference 1)	.039	.012	.020
Predicted P_{TOUT}/P_{TIN}	.961	.988	.980

The IFV flowpath surface definition was designed based on lessons learned from Boeing's testing of similar valves (ref. 1,2) while imposing HSCT integration constraints. Eight circumferential passages was chosen as the optimal number of sections for the valve as suggested by the Boeing tests. Based on the mechanical layout of the engine, the inlet, mid, and exit planes along with the valve length were defined as boundary conditions for the initial valve design. A wall thickness of 0.150 inches in the valve was incorporated based on a preliminary structural evaluation.

By taking advantage of geometric radial symmetry for individual flowpaths over the full annulus of the valve, it was only required to model one half of both the inner–to–mid–plane and outer–to–mid plane duct. Unigraphics computer aided design (CAD) from the Boeing test data manipulation of these two designs was then mirrored and duplicated to achieve the full geometry of each single flowpath, and subsequently the full annulus of the AIV. Additionally, surface fillets were incorporated in all corners of the ducts as recommended by Boeing's previous test. Figure 20 and Figure 21 show the inner–to–mid plane and outer–to–mid–plane flowpath CFD grids, respectively.

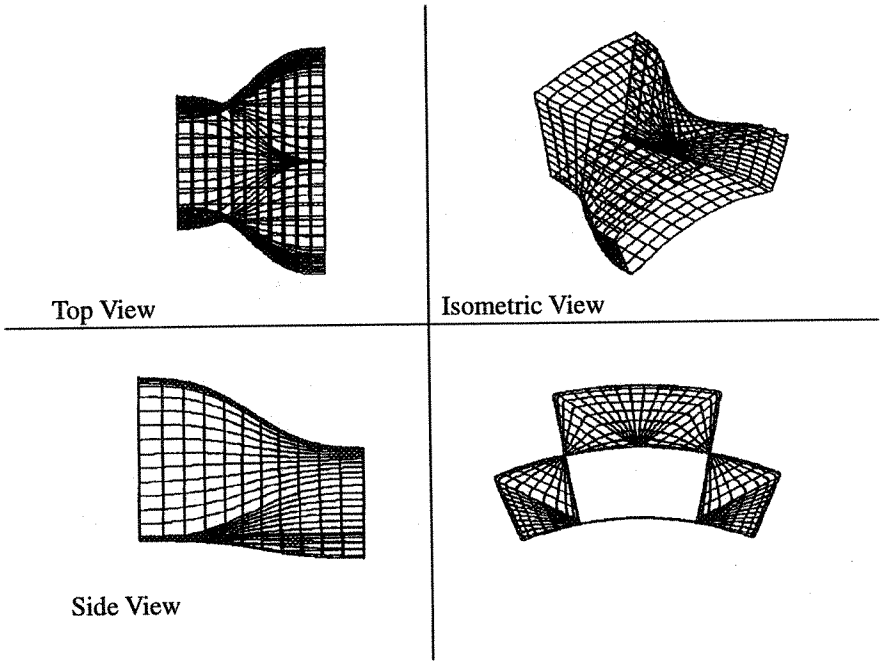

Figure 20. AIV Inner–To–Mid–Plane Flowpath and CFD Grid

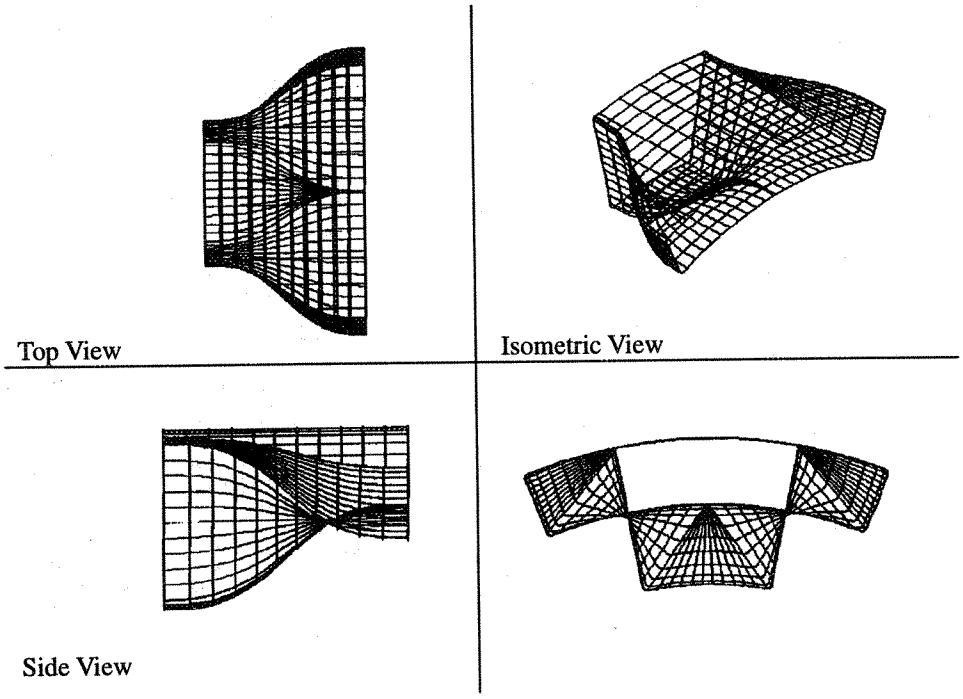

Figure 21. AIV Outer–To–Plane Flowpath and CFD Grid

Each flowpath design was achieved by attempting to minimize the surface wall gradients while maintaining zero rates of axial curvature at each of the ducts entrance, mid–plane, and exit. This progression tends to minimize separations at the valve inflow, transition (mid–valve plane), and outflow planes. This was accomplished by defining quintic B–spline surfaces within the geometrical bounds of the valve. Therefore, a balance between minimizing surface area, maintaining zero rates of curvature where required, and obtaining both inner and outer flowpaths to overlap and merge into identically shaped mid–plane boundaries, was achieved.

Ideally, one would like to maintain constant area flowpaths in the valve in order to limit duct losses to only friction and turning. Further efforts can be directed toward refining duct area distributions and rates of surface wall curvature. Our initial design resulted in a non–constant (sinusoidal) area progression throughout each half of both flowpaths. The valve did however maintain a rate of change in cross–sectional area equal to zero at each duct end and at the mid–plane. Figure 22 shows the area progressions of both flowpaths as a function of each duct's centroidal axis arc length, for one segment which has an inlet, midplane and exit area of 94.6 in^2.

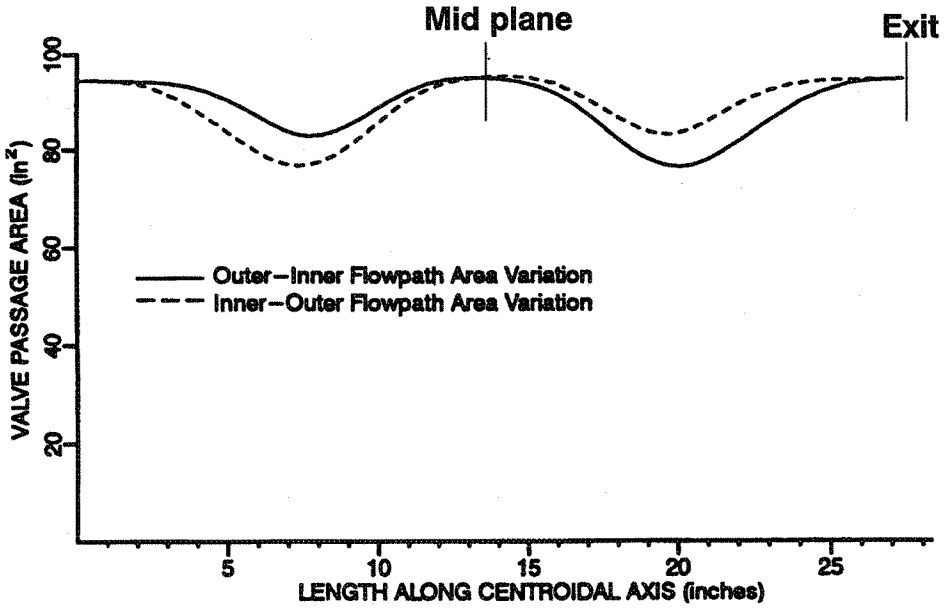

Figure 22. Area Variation Through the Annular Inverter Valve

The AIV flowpaths presented a formidable task in 3D–CFD grid generation. ICEM (Integrated Computer–aided Engineering and Manufacturing) CFD, a state–of–the–art CAD based grid generation package was utilized to develop the 3D–CFD models being analyzed. A building block approach to the CFD solutions was incorporated by taking advantage of the radial symmetry of each flowpath. This allowed for single domain models to be generated by the ICEM CFD system. Then, company–developed grid pre–processors were used to develop the final multi–block structure of the valve by translating, rotating,

and/or mirroring individual domains and linking them together to form the desired flowpath. A constant area duct of 25 inches in length (approximately 5ΔR) was added upstream and downstream of the valve geometry in order to allow any downstream influences in the flow to propagate upstream of the valve inflow and outflow planes.

The 3D–CFD was executed for all geometries using the General Aerodynamic Simulation Program (GASPv2.0) and solving the Euler (invisid) equations assuming air as a perfect gas with a constant ratio of specific heats (constant γ=1.4). Inflow boundary conditions were specified by the total conditions listed in Table 16. Outflow boundary conditions made use of Riemann invariants, which allow for the downstream characteristic waves, based on far–field freestream conditions, to propagate upstream. These boundary conditions allow for state variable profiles to develop across the valve boundaries, instead of fixing constant profiles across the boundaries.

Once each 3D–CFD solution was completed, the wall pressure profiles and gradients were analyzed for possible flow separation and to determine the pressure distortion at the valve exit and the total pressure drop through the valve.

Figure 23 and Figure 24 show the wall static pressure profiles for the outer–to–inner flowpath for the secondary air. The boundary layer analysis reveals four areas of possible flow separation, which are shown by the white/pink areas in Figures 23 and 24. The first two areas of possible separation are on the sidewalls near the valve inlet plane where there is a rapid convergence of the flowpaths. The other two areas are on the upper surface downstream of the mid–plane (Figure 23) and on the lower surface just upstream of the mid–plane (Figure 24), where the flowpaths go through a fair amount of divergence. All four areas result in adverse pressure gradients.

Figure 25 and Figure 26 show the wall static pressure profiles for the inner–to–outer flowpath for the high pressure front fan exhaust air. The boundary layer analysis reveals four areas of possible flow separation for this flowpath. These areas include the sidewalls downstream of the valve inlet plane, the upper surface upstream of the valve midplane (Figure 25) and the lower surface downstream of the valve midplane (Figure 26).

The boundary layer analysis of the inner–to–inner flowpath at the Mach 2.4 cruise condition, Figure 27 and Figure 28, reveal three areas of possible separation. The first two areas are again the symmetric compression corners on the sidewalls downstream in the valve inlet plane. The third area of concern is on the upper surface aft of the valve midplane.

These boundary layer analyses were conducted using the Analysis of Boundary Layer Equations (ABLE) code developed at United Technologies Research Center (UTRC).

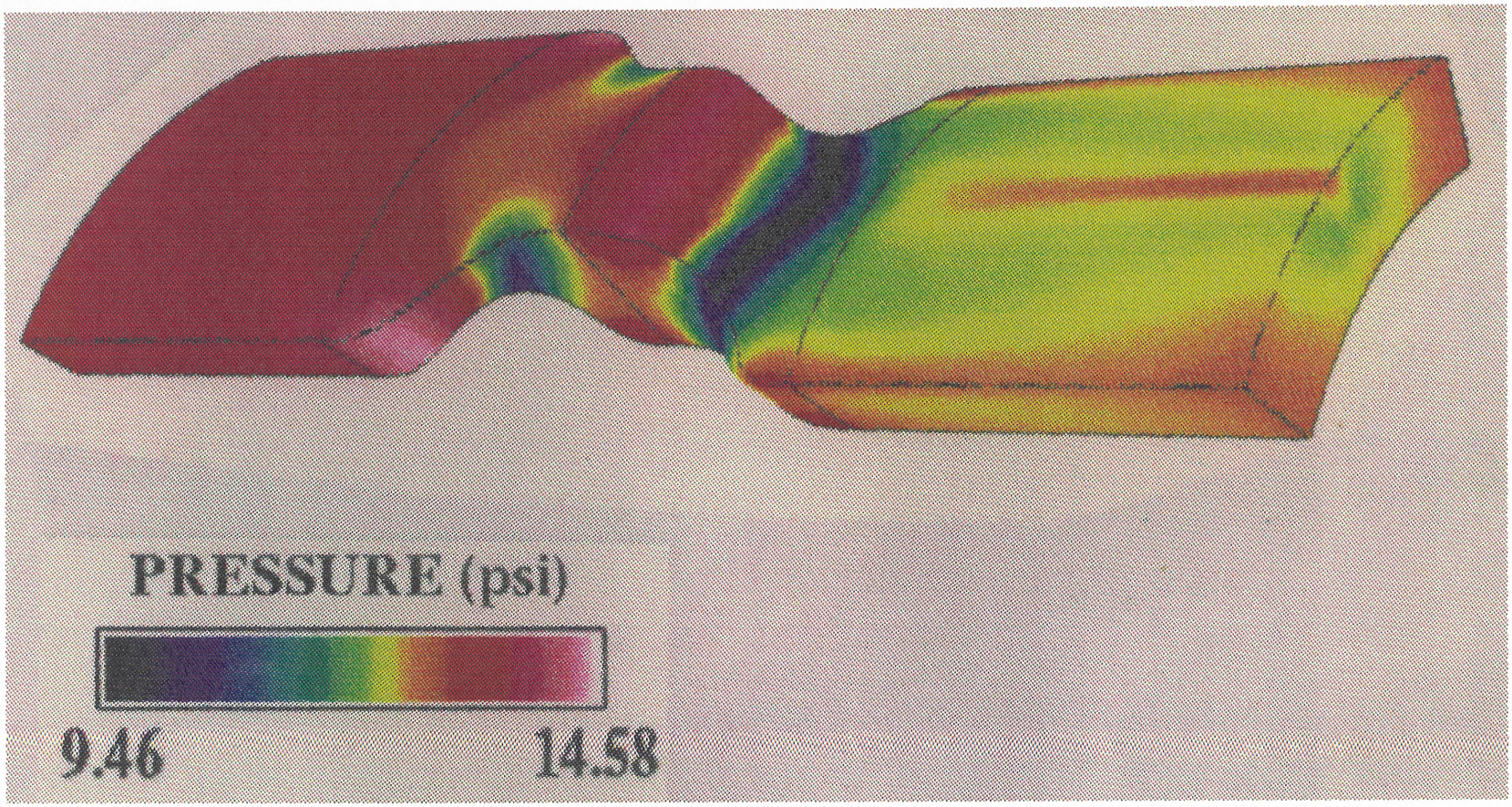

Figure 23. Wall Static Pressure Profiles for Outer–to–Inner Flowpath for Secondary Air (Top View)

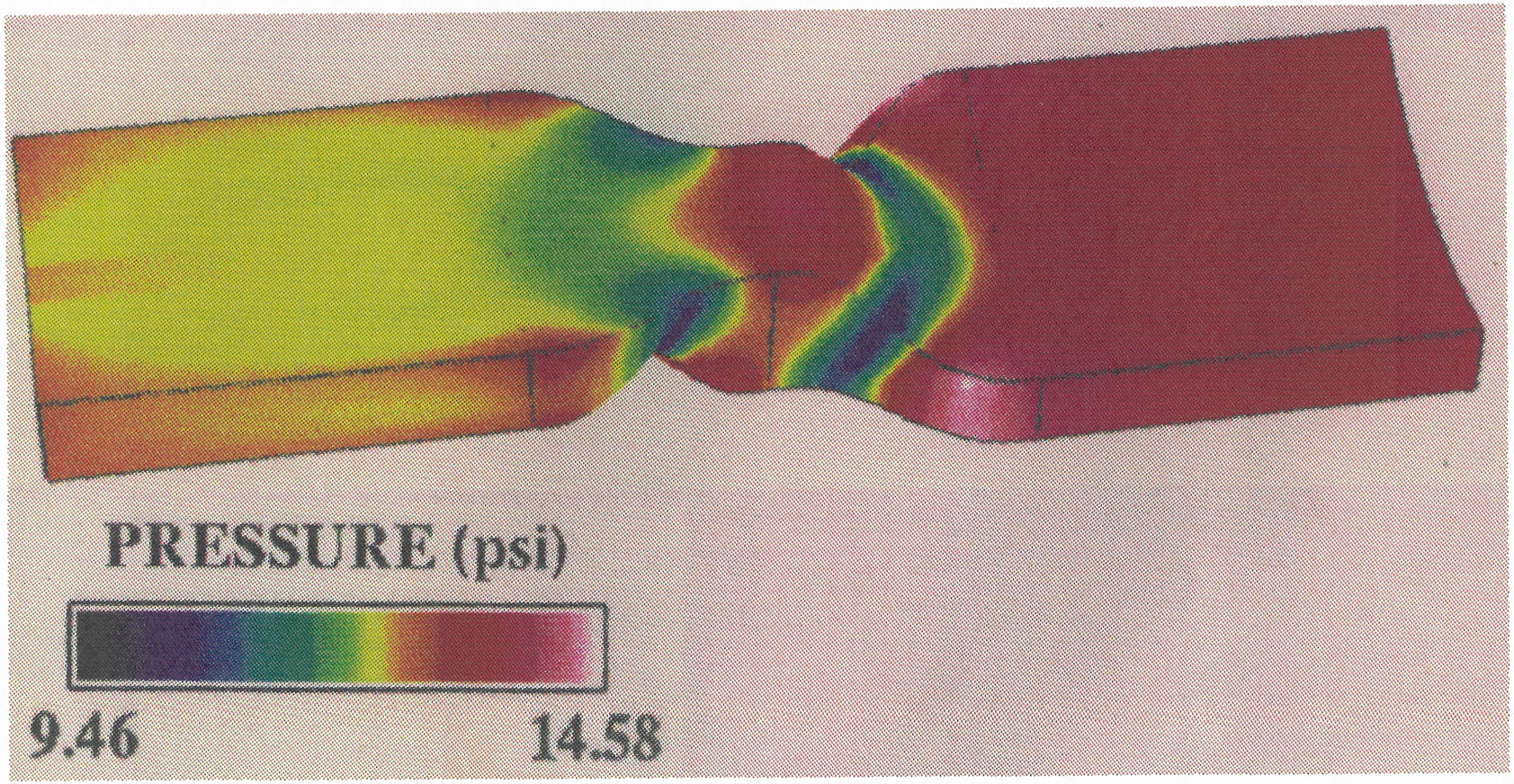

Figure 24. Wall Static Pressure Profiles for Outer–to–Inner Flowpath for Secondary Air (Bottom View)

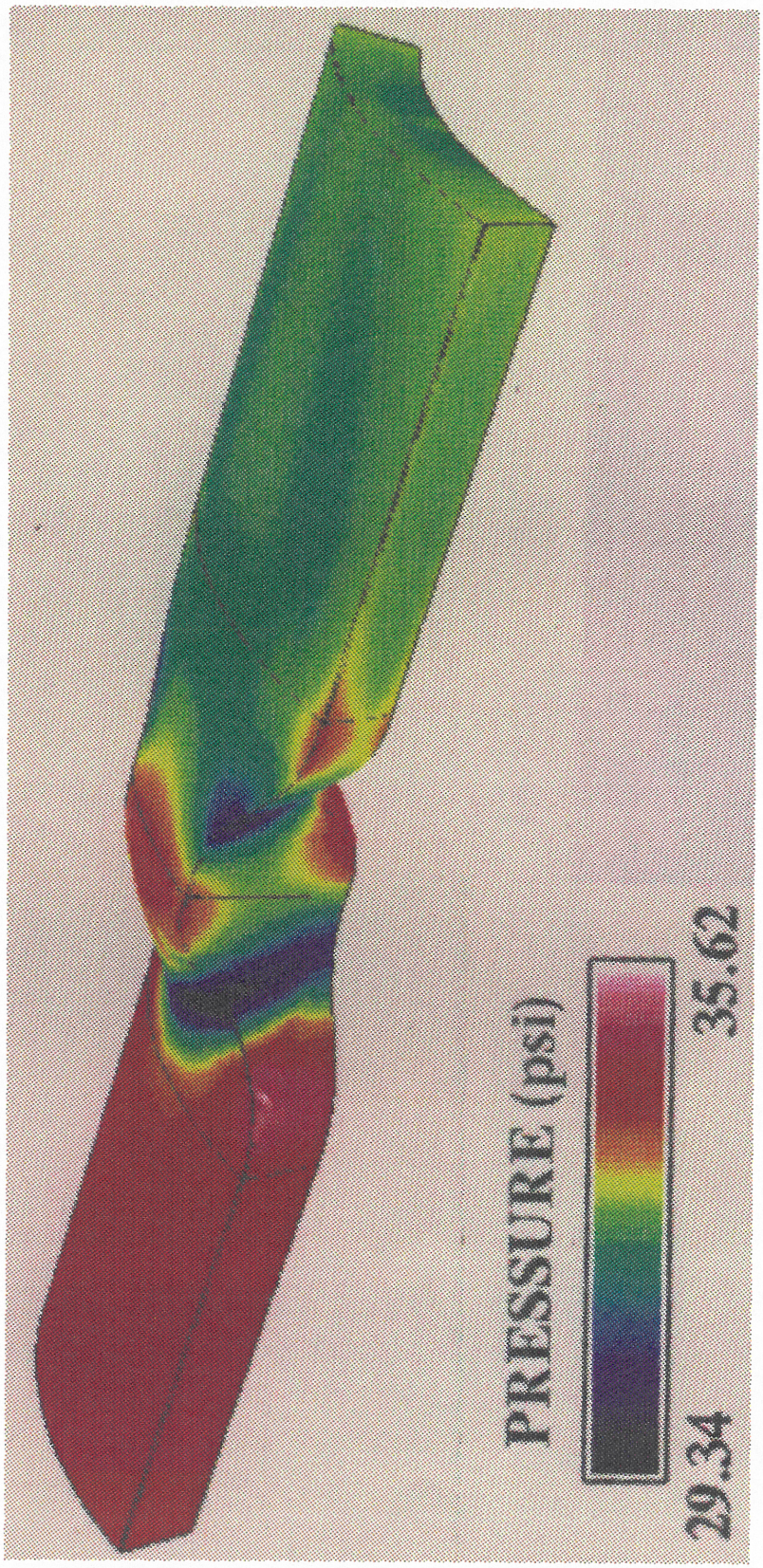

Figure 25. Wall Static Pressure Profiles for Inner–to–Outer Flowpath for High Pressure Front Fan Exhaust Air (Top View)

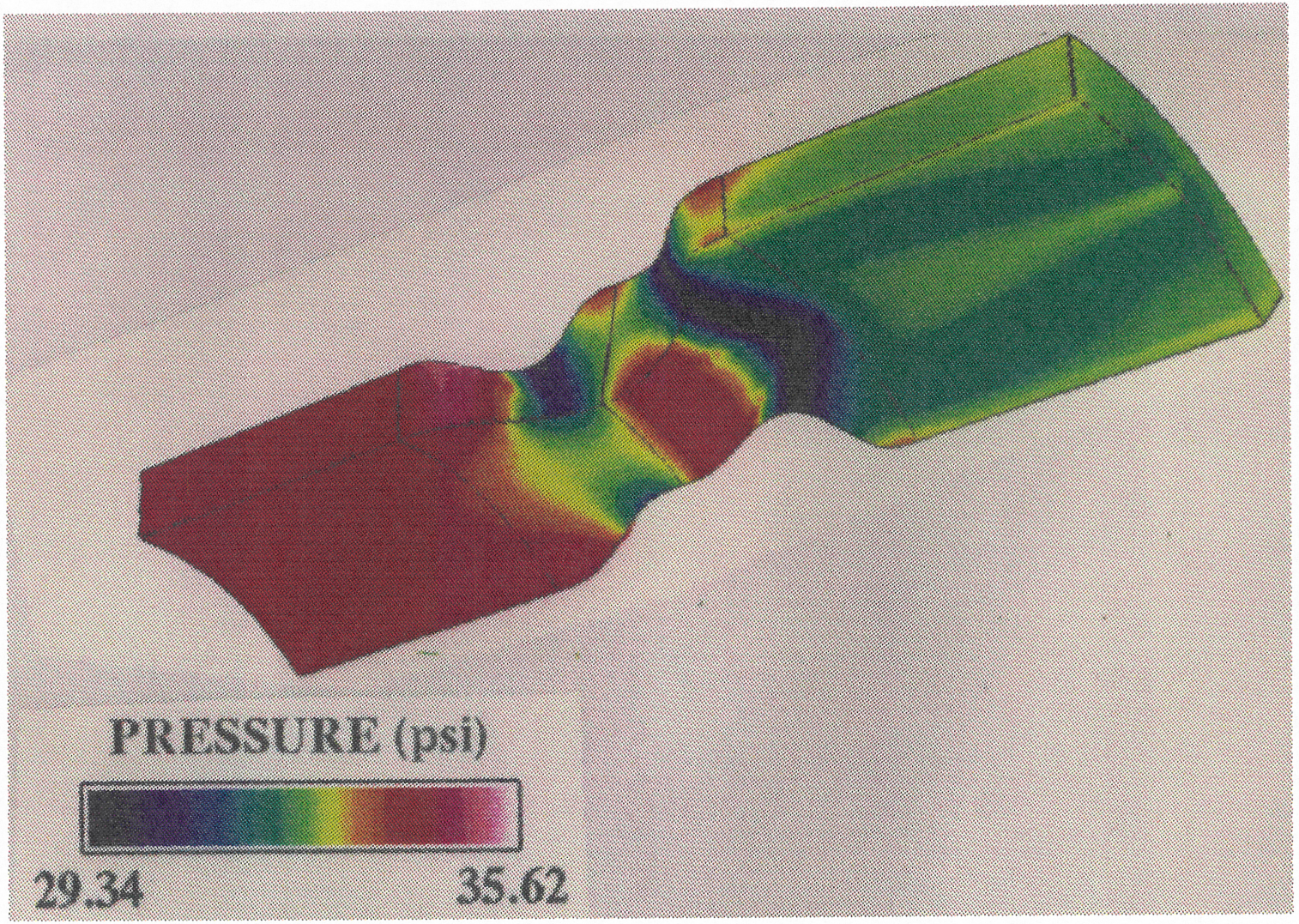

Figure 26. Wall Static Pressure Profiles for Inner–to–Outer Flowpath for High Pressure Front Fan Exhaust Air (Bottom View)

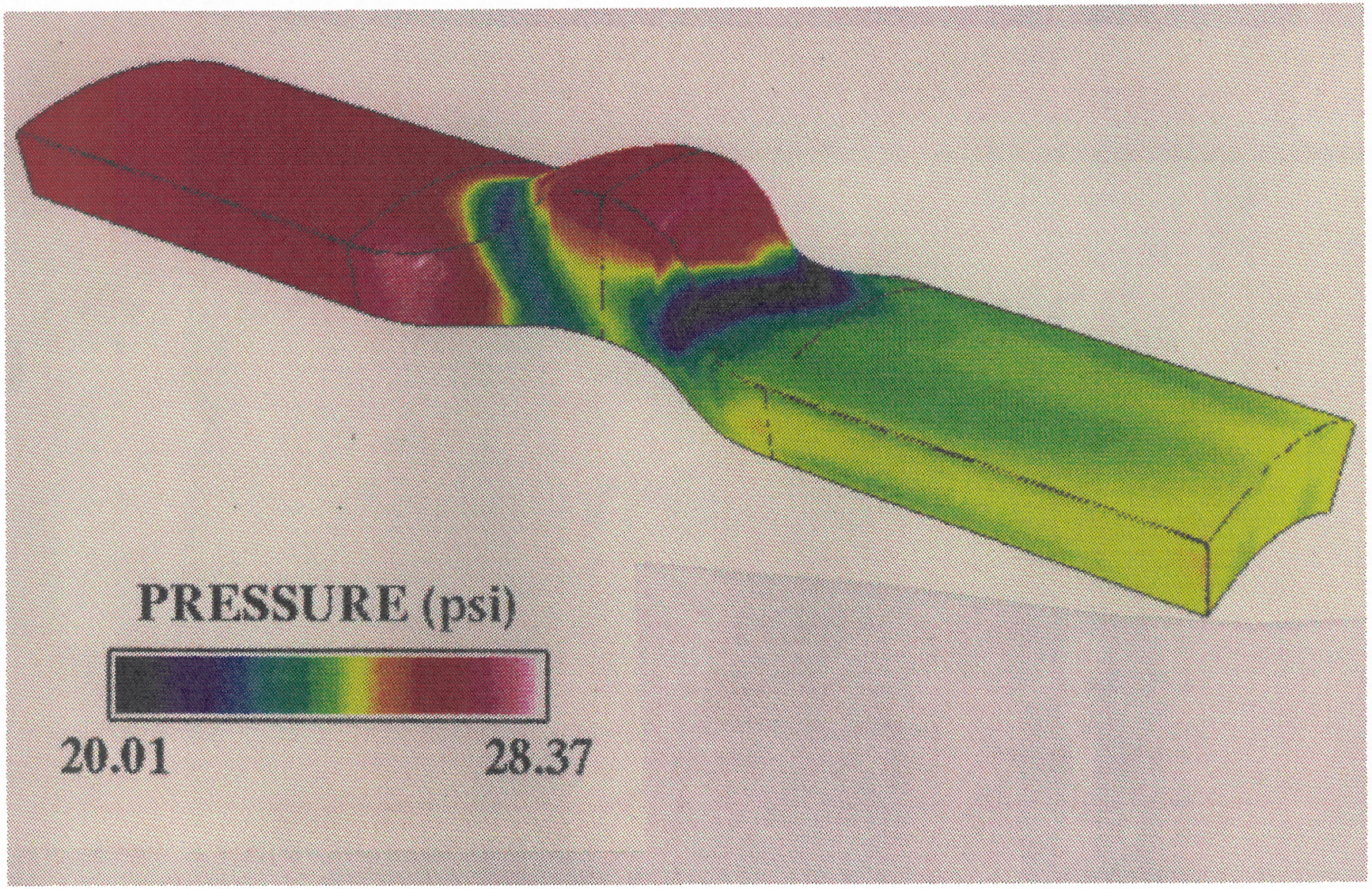

Figure 27. Wall Static pressure Profiles for Inner–to–Inner Flowpath at Mach 2.4 (Top View)

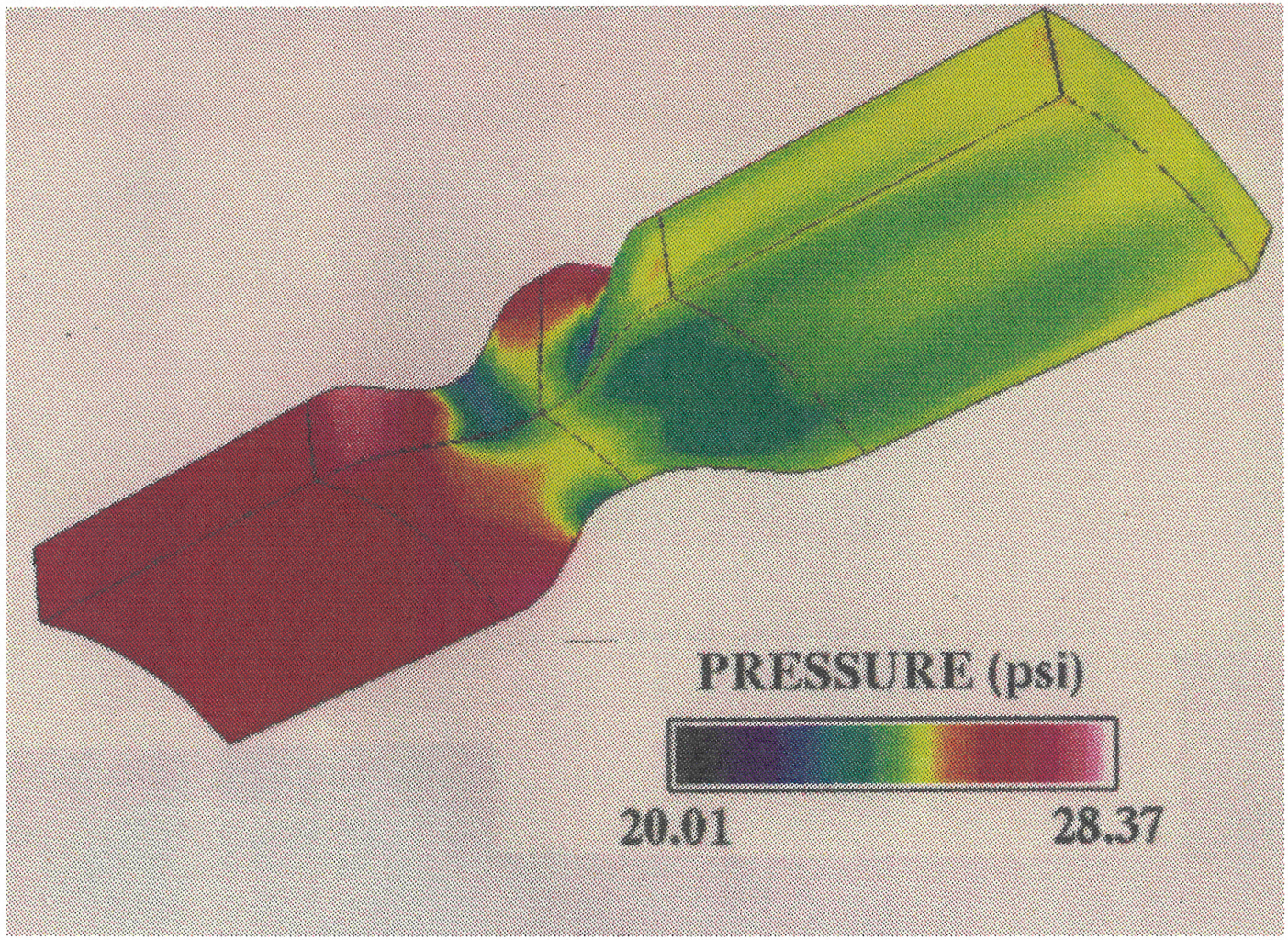

Figure 28. Wall Static Pressure Profiles for Inner to Inner Flowpath at Mach 2.4 (Bottom View)

Table 17 summarizes the total pressure recoveries for the three single duct flowpaths.

Table 17. Valve Pressure Loss Summary

Valve Flowpath	Outer/Inner	Inner/Outer	Inner/Inner
Stream	C	B	B
Valve Inlet Total Pressure (PTIN), psia	14.95	35.79	28.65
Mid Plane Average Total Pressure (PTMP), psia	14.59	35.18	28.19
Exit Plane Average Total Pressure (PTEX), psia	14.22	34.75	27.33
Pressure Recovery Inlet to Mid Plane (PTMP/PTIN)	.976	.983	.984
Pressure Recovery Mid Plane to Exit (PTEX/PTMP)	.974	.988	.970
Total Valve Pressure Recovery (PTEX/PTIN)	.951	.971	.954

Total pressure distortion patterns were also developed from the CFD analyses at the valve mid plane, the valve exit plane and at a location 13 inches downstream of the valve exit plane, which corresponds to the inlet of the rear fan. Table 18 summarizes the maximum (PTMAX) minimum (PTMIN) and average (PTAVG) total pressures at these stations for the three single flowpaths examined. The total pressure distortion coefficient (TPDC) is:

$$TPDC = \frac{(PTMAX - PTMIN)}{PTAVG}$$

Table 18. Total Pressure Distortion Summary

Valve Flowpath	Outer to Inner	Inner to Outer	Inner to Inner
Stream	C	B	B
Mid Valve PTMAX, psia	14.94	35.80	28.65
Mid Valve PTMIN, psia	13.30	31.31	25.77
Mid Valve PTAVG, psia	14.59	35.23	28.16
Mid Valve TPDC	.1125	.0707	.1022
Valve Exit PTMAX, psia	14.85	35.63	28.55
Valve Exit PTMIN, psia	12.56	32.50	24.05
Valve Exit PTAVG, psia	14.22	34.75	27.33
Valve Exit TPDC	.1612	.0900	.1651
Rear Fan Inlet PTMAX, psia	14.80	35.56	28.5
Rear Fan Inlet PTMIN, psia	12.77	32.70	24.5
Rear Fan Inlet PTAVG, psia	14.16	34.68	27.22
Rear Fan Inlet TPDC	.1431	.0826	.1481

A CFD analysis was conducted for the annular inverter valve for a transition operating condition. During this operation the rear half of the valve is moved to a position halfway between the high and low mode operating conditions, as illustrated in Table 19. In this posi-

tion, the fan exit bypass flow (B) and the secondary flow (C) come into contact with each other at the mid plane of the valve and mix together in the rear section of the valve.

The transition mode was even more complex in modeling for CFD. The required number of zones to model the transition mode was reduced from sixteen (the full annulus) to four. This is a result of the implementation of a new flow rotational boundary condition in GASP. The new boundary condition allowed for the split mid–plane of the upstream and downstream flowpaths to properly model the radial symmetry of the flow over a spatially discontinuous zonal boundary (Figure 29).

The amount of secondary flow that is entrained during this mode of operation is dependent upon the pressures of streams B and C. In order to get secondary air to flow through the valve, the static pressure of the fan discharge air, PSB at the mid plane of the valve must be less than the total pressure of the secondary air (PTC). Therefore the valve transition must take place at a low engine power setting. The transition case examined for this CFD analysis was at 15,000 ft–0.7 Mn with the engine operating at 50% of maximum dry power. Table 19 summarizes the conditions at the valve inlet and mid plane for the fan exhaust (B) and secondary air (C) streams.

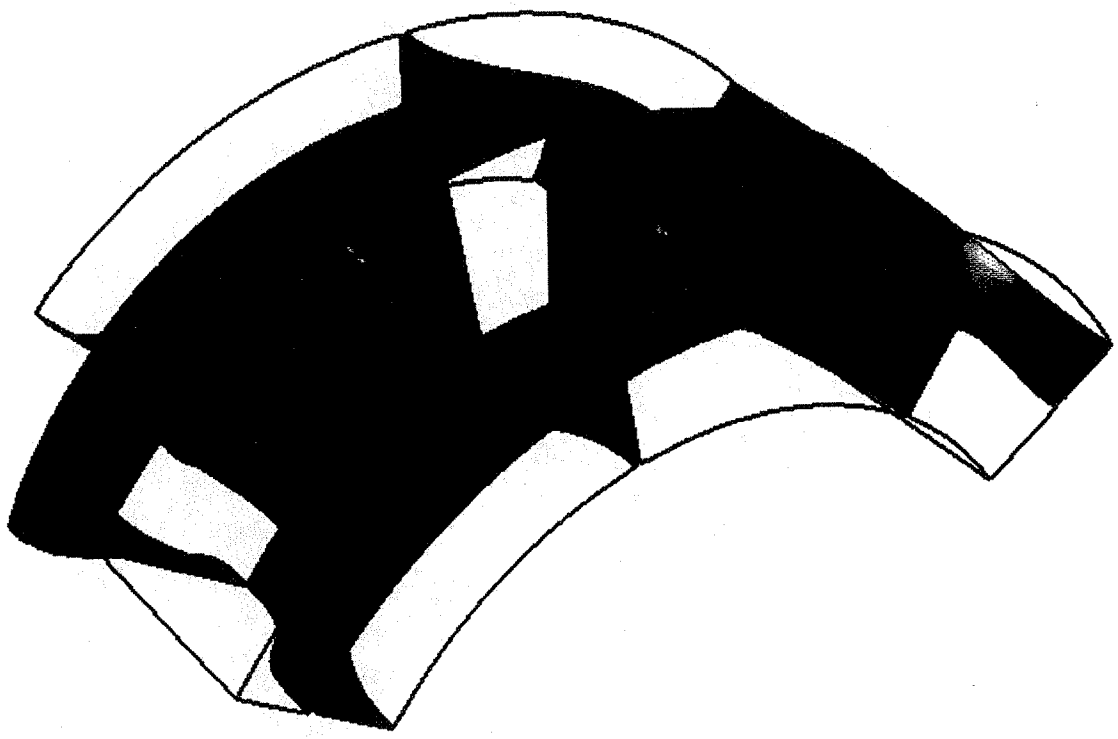

Figure 29. Annular Inverter Valve Transition Flowpath

Table 19. Predicted Transition Mode Operation

Stream	Fan Exhaust (B)	Secondary Air (C)	Average (B+C)
Flow, Lb/sec.	261.7	60.8	322.5
Valve Inlet Total Pressure, psia	19.26	11.65	17.83
Valve Inlet Total Temperature, °R	635.3	531.8	615.8
Inlet W$\sqrt{T}$/P, Lb/sec$\sqrt{}$ °R/psia	342.5	120.4	
Inlet Area, in^2	757	757	
Inlet Mach Number	0.61	.175	
Inlet Static Pressure, psia	15.0	11.4	
Front Section Pressure Recovery	.877	.955	
Valve Mid Plane Total Pressure, psia	16.89	11.13	15.80
Valve Mid Plane Static Pressure, psia	10.87	10.87	
Valve Mid Plane Mach Number	.819	.185	

Figure 30 presents the wall static pressures in the valve during the transition mode of operation. The boundary layer analysis reveals three areas of probable flow separation. These areas include the compression surfaces on the sidewalls downstream of the valve inlet plane, and the sidewall of the valve downstream of the midplane of the valve that is contacted by stream B, as illustrated in Figure 30. The main reason for this flow separation downstream of the midplane is that the static pressure in stream B at the midplane of the valve is actually higher than the static pressure in the secondary stream, and that there isn't a static pressure balance, as we had assumed.

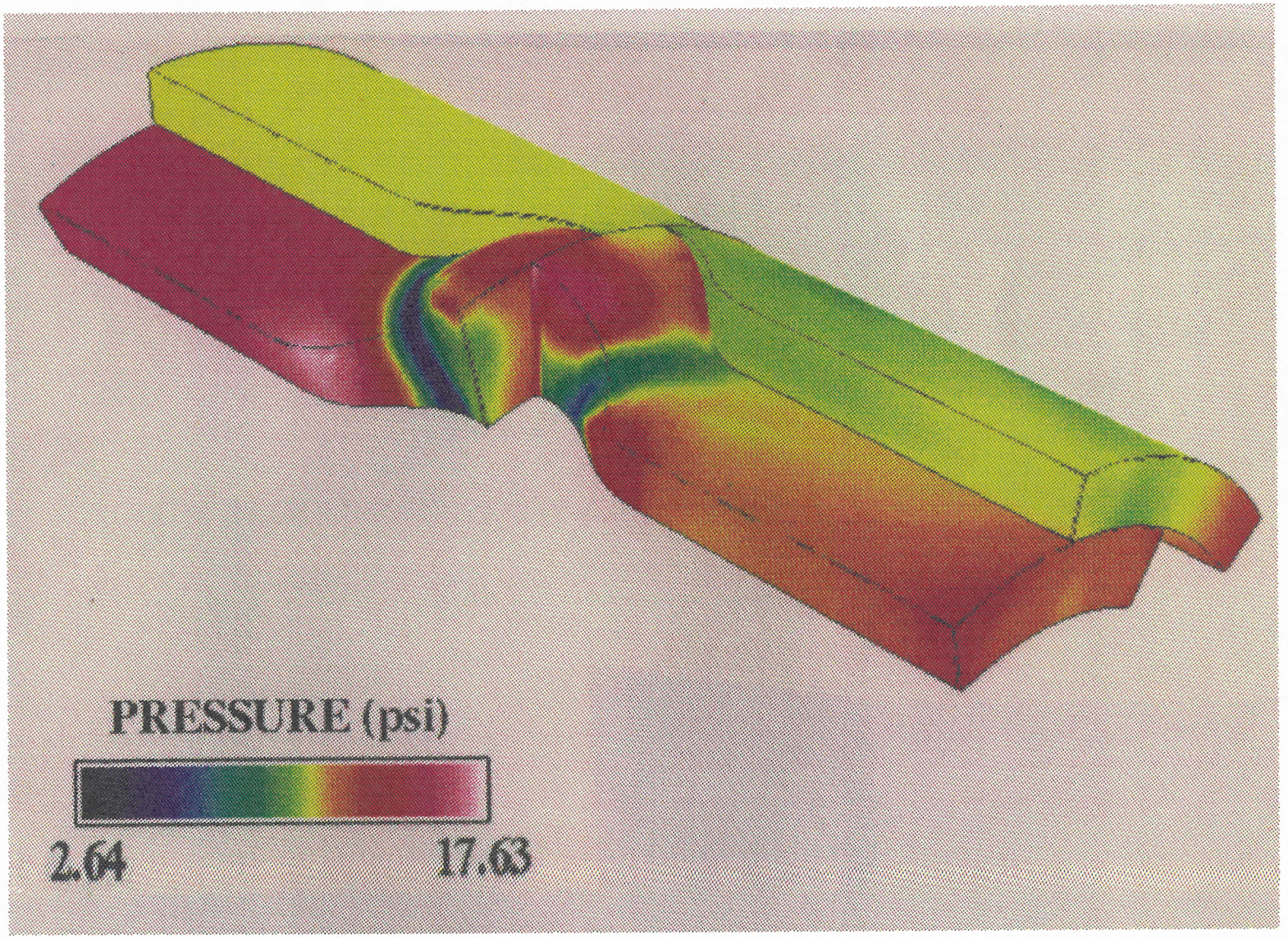

Figure 30. Static Pressure Distribution During Transition Mode Opertion

Table 20 shows the results of the CFD analysis at the entrance and mid plane of the valve.

Table 20. Transition Mode CFD Analysis Summary

Stream	Fan Exhaust (B)	Secondary Air (C)	Mixed (B+C)
Flow, Lb/sec	210	49.7	259.7
Valve Inlet Total Pressure, psia	19.26	11.65	17.80
Total Temperature, °R	635.3	531.8	615.5
Inlet W$\sqrt{T}$/P, Lb/sec $\sqrt{}$°R/psia	274.7	98.4	
Inlet Area, in^2	757	757	
Inlet Mach Number	.442	.140	
Inlet Static Pressure, psia	16.8	11.5	
Inlet to Mid Plane Pressure Recovery	.909	.947	
Mid Plane Average Total Pressure, psia	17.51	11.03	16.27
Mid Plane Max Total Pressure, psia	18.5	11.5	
Mid Plane Min Total Pressure, psia	11.0	10.5	
Mid Plane Pressure Distortion	.43	.10	
Mid Plane Static Pressure, psia	14.79	10.85	
Mid Plane Mach Number	.504	.150	

Table 20 shows that the total pressure recovery in the front half of the valve for the fan exhaust stream is 0.909 and that the mid valve pressure distortion is very high at 43%. The average static pressure in the fan exhaust stream at the valve mid plane is 14.79 psia, which is higher than the total pressure in the secondary air of 11.0 psia, which means that some flow reversal would occur at the valve mid plane.

Table 21 presents the pressure losses and total pressure distortion for the inner and outer streams at the exit of the valve during transition mode operation. The average exit total pressure from the valve is 14.87 psia. Using the mass averaged valve inlet total pressure of 17.80 psia (Table 20), the transition mode valve average pressure recovery is 0.835.

Table 21. Valve Exit Conditions from CFD Analysis

Stream	Inner	Outer	Avg
Valve Mid Plane Average Total Pressure, psia	16.27	16.27	
Valve Exit Average Total Pressure, psia	15.08	14.65	14.87
Pressure Recovery in Aft Section of Valve	.927	.900	
Valve Exit Maximum Total Pressure, psia	17.20	17.60	
Valve Exit Minimum Total Pressure, psia	11.0	9.5	
Valve Exit Total Pressure Distortion	.41	.55	
Rear Fan Inlet Average Total Pressure, psia	14.72	14.03	
Rear Fan Inlet Maximum Total Pressure, psia	16.9	17.0	
Rear Fan Inlet Minimum Total Pressure, psia	11.5	10.4	
Rear Fan Inlet Total Pressure Distortion	.37	.47	

This CFD analysis of the transition mode of operation has shown that in order to eliminate the possible flow separation downstream of the valve midplane and the possible reverse flow of stream B air into the front portion of the valve, occupied by stream C, the transition should be made at an even lower power setting to bring the total pressures of the fan exhaust air (PTB) and secondary air (PTC) closer together. Performing the transition at a lower power setting will also reduce the total pressure distortion in the valve and at the rear fan.

D. COMPRESSION SYSTEM DESIGN STUDY

Aerodynamic designs and off design performance characteristics were developed for the fan, core driven fan stage outer section and the high pressure compressor of the STF1029 partial IFV engine. The performance characteristics for these components were developed using a meanline analysis to determine speed, flow, efficiency and stall pressure ratios. Variable stator vane geometry requirements were identified to provide sufficient component stability margins during steady state and transient operation. The following sections describe the compression system designs.

Fan Design:

The STF1029 incorporates a 2 stage fan with a variable Inlet Guide Vane (IGV). This fan is designed for an inlet corrected flow (WC2) of 650 Lb/sec and a Fan Pressure Ratio (FPR) of 2.20 to achieve a Stall Margin (SM) of 27%. The first rotor is designed with an inlet flow per unit area of 40.0 Lb/sec ft^2, a hub tip ratio of 0.36 and a corrected tip speed of 1560 ft/sec, which produces a rotor inlet tip diameter of 58.9 inches and a corrected rotor speed (NC) of 6070 rpm. This design produces a polytropic efficiency of 90.6 percent and an adiabatic efficiency (η ad) of 89.5%. Table 22 summarizes the performance of this fan at the sea level static aerodynamic design point (ADP) and at other critical flight conditions. This fan was designed to achieve the best efficiency balance over the entire flight envelope while achieving a minimum of 15% stall margin.

Table 22. STF1029 Fan Performance Summary

Flight Points	WC2 (pps)	FPR	NC (rpm)	η ad (rpm)	SM (%)
SLS – Max	674	2.51	6298	87.2	16.0
SLS – Hi Mode	650	2.39	6150	88.3	17.0
SLS – ADP	650	2.20	6070	89.5	27.0
SLS – Lo Mode	650	2.08	6044	88.0	35.0
55k/2.4 – Cruise	455	1.67	5068	89.6	18.0

A 2–stage fan was required to meet stall margin requirements in high mode operation and to improve efficiency over the operating range. A single stage fan design was studied and was found to have insufficient stall margin. Individually removable blades were also specified for this engine which would have required a very innovative blade attachment design to satisfy with a low aspect ratio single stage fan design.

The following requirements and assumptions were used to define this design. The first stage fan rotor is treated as a swept blade with no midspan shroud to reduce shock and profile drag losses. The second blade is a conventional unshrouded blade. A variable inlet guide vane flap with fixed stators provide improved low speed cruise efficiency and stall margin. The maximum overflow point is WC2 = 674 pps during sea level takeoff conditions.The flowpath for the STF1029 2–stage fan design is presented in Figure 31.

The resulting fan design meets or exceeds performance and stability requirements. The fan map is shown in Figure 32. The IGV flap schedule in Figure 33 was established to improve off–design performance. The 100% corrected speed is 6070 rpm.

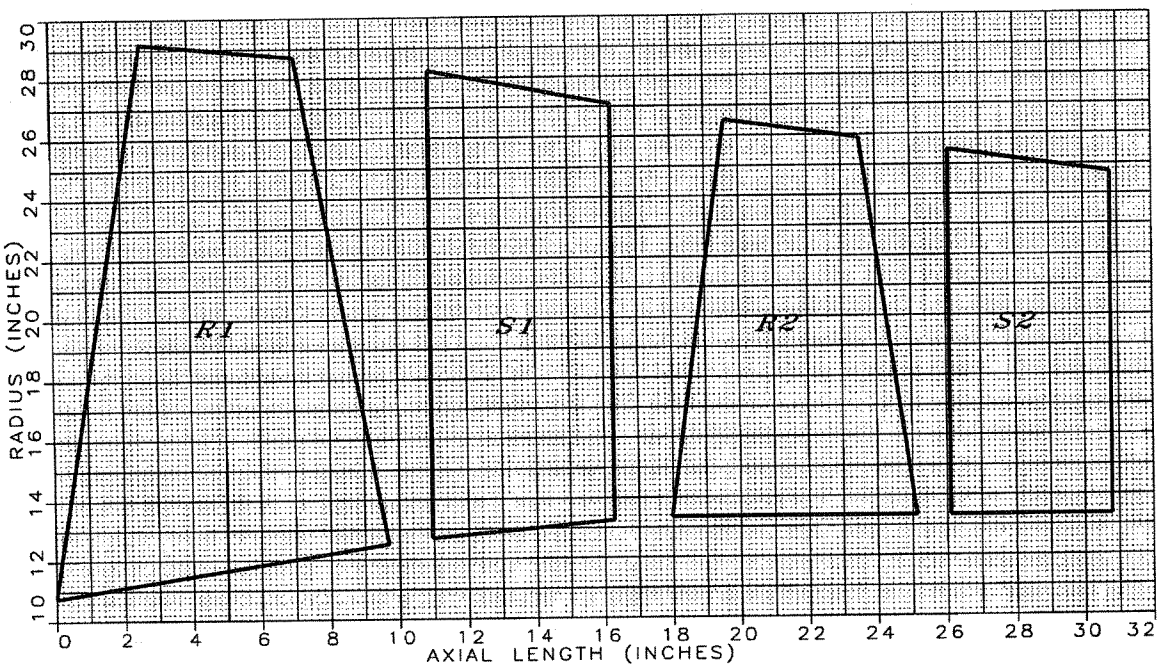

Figure 31. STF 1029 2–Stage Fan Flowpath

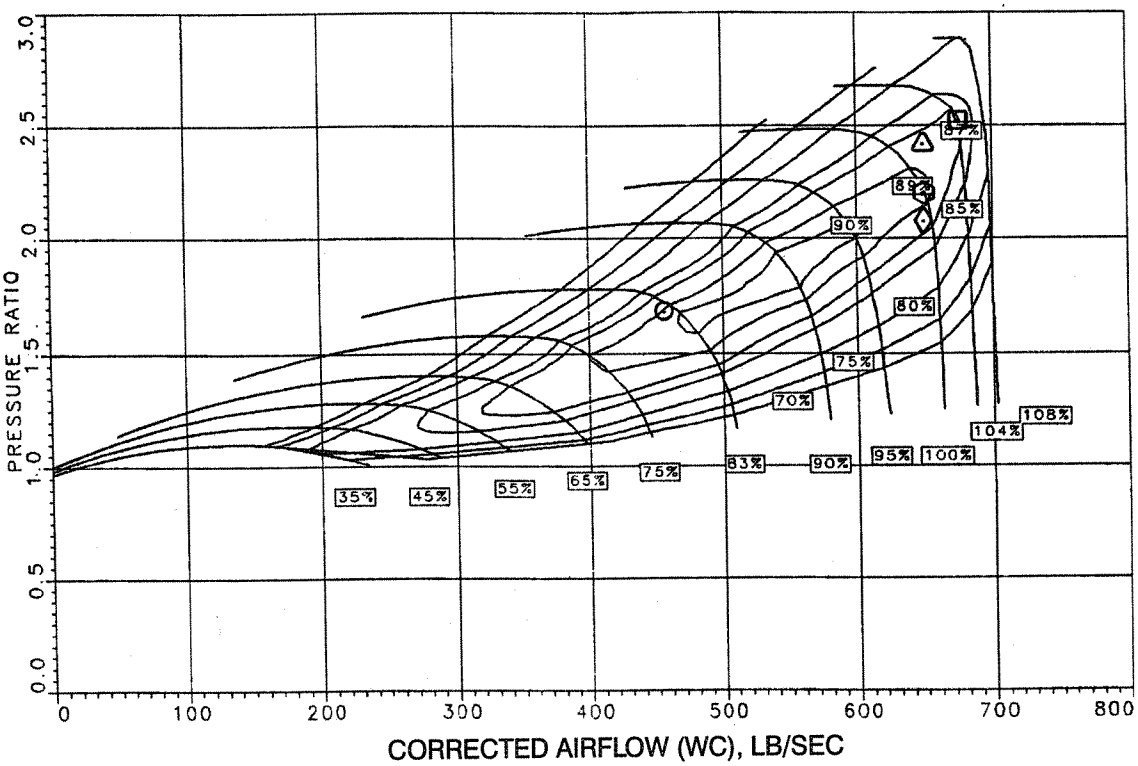

Figure 32. STF 1029 Fan Performance Characteristics

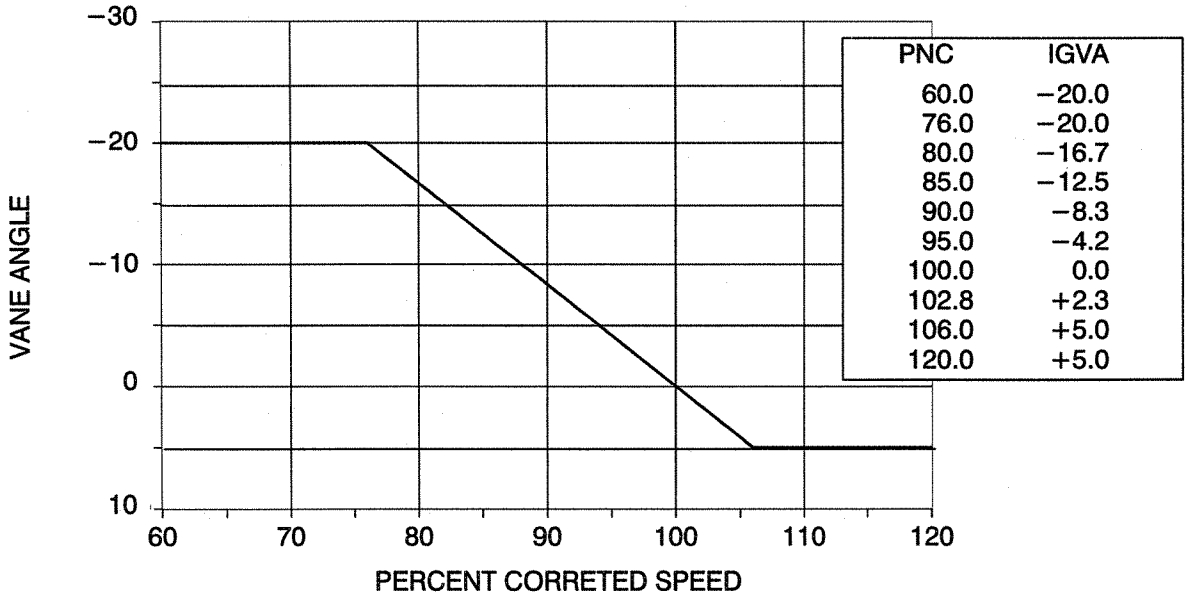

Figure 33. Fan Inlet Guide Vane Angle (IGVA) Schedule

Core Driven Fan Stage (CDFS) Design:

The CDFS outer tip fan is a single stage fan with the blade attached to the tip of the high compressor first blade through a rotating shroud that separates the tip fan and core flow streams, as illustrated in Figure 34.

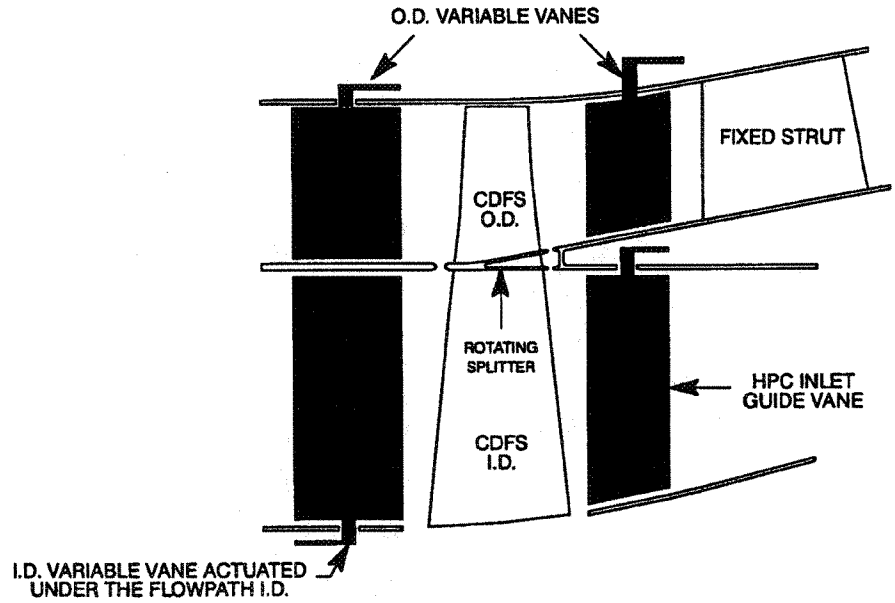

Figure 34. STF 1029 Core Driven Fan Stage

The CDFS has a variable Inlet Guide Vane (IGV), a variable vane (stator) after the CDFS and a fixed Exit Guide Vane (EGV).

Table 23 provides a summary of the CDFS tip inlet corrected flow (WC), Pressure Ratio (PR), corrected speed (NC), adiabatic efficiency (η ad) and Surge Margin (SM) at the Aerodynamic Design Point (ADP) and other operating conditions. The design point was set at the maximum flow condition (Wc=217) which is subsonic cruise for the CDFS outer tip fan. A design pressure ratio of (PR=2.04) was chosen to maximize efficiency and stall margin at the sea level static high mode and the engine maximum overflow point. The following table lists the CDFS tip fan performance at various high and low mode flight points.

The CDFS is designed at an inlet corrected specific flow of 41.5 Lb/sec−ft^2 at a corrected tip speed of 1573 ft/sec and a hub tip ratio of 0.8, which produce a rotor inlet tip diameter of 52.26 inches and a corrected rotor speed of 6900 rpm.

Table 23. STF1029 CDFS Performance Summary

Flight Points	WC (pps)	PR	IGVA degrees	NC (rpm)	NC %	η ad (%)	SM (%)
ADP	217.0	2.04	0	6900	100	85.1	7.3
Subsonic Cruise (low)	217.0	1.14	+2	6163	89.3	66.0	91.2
SLS – Max (Hi)	190.2	1.96	−23	7700	111.6	83.9	10.0
SLS – (Hi)	173.7	1.70	−29	7229	104.8	84.0	17.6
SLS – (Lo)	155.0	1.37	−36	6652	96.4	80.4	32.1
55k/2.4 – Cruise (low)	134.0	1.09	−45	6115	88.6	53.7	48.6

This partial IFV engine concept results in the CDFS operating at very low pressure ratios at the subsonic and supersonic cruise conditions as shown in Table 23.

The flowpath for the CDFS tip is presented in Figure 35. The fan blade incorporates sweep to reduce shock losses. The stators are conventional designs.

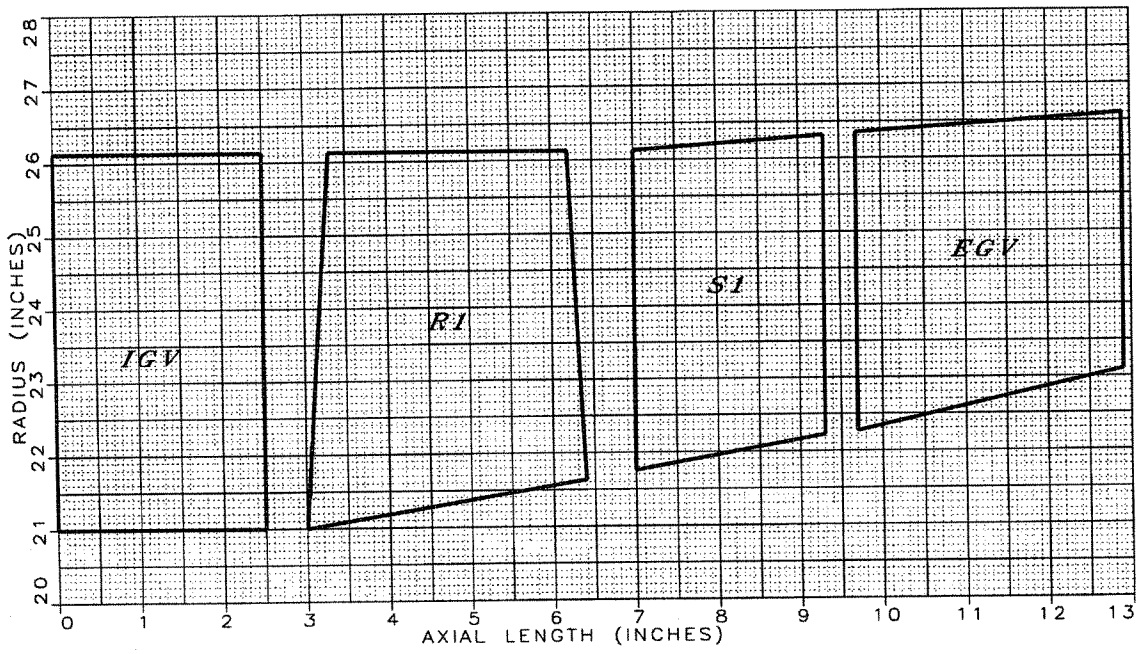

Figure 35. STF 1029 CDFS Flowpath

A variable vane row was added between the rotor and EGV to reduce the amount of turning required in the EGV and to permit stator incidence adjustment at off design conditions for improved performance and stability. The variable stator and EGV aspect ratio and solidity were adjusted to obtain reasonable design diffusion factors while holding vane count for both vane rows at 64 airfoils. The variable stator 1 is treated like it is ganged to the IGV actuation and moves 1.5 degrees for each 10 degrees of IGV movement. Although the optimized vane schedule resulted in a flat slope for stator 1 with little vane movement, the meanline model was very sensitive to stator position and required a variable vane to generate a reasonable fan map.

The IFV engine requires a considerable amount of variation in the CDFS Inlet Guide Vane (IGV) angle to achieve stable operation at all flight conditions. At subsonic cruise the IGV is opened 2 degrees, while at supersonic cruise the IGV is in the 45 degrees closed position as shown in Table 23. The CDFS efficiencies at these conditions are low because the core driven fan stage is running on a low operating line. Performance at the SLS points is also relatively poor because of the high blade tip speeds and associated shock losses.

Figure 36 through Figure 40 present the CDFS performance characteristics for IGV vane settings of +10, 0, −15, −30 and −45 degrees. Figure 41 shows the IGV and exit stator (S1) vane schedules versus corrected rotor speed. The SLS high and low mode and Mach 2.4 points are on a linear schedule with rotor speed.

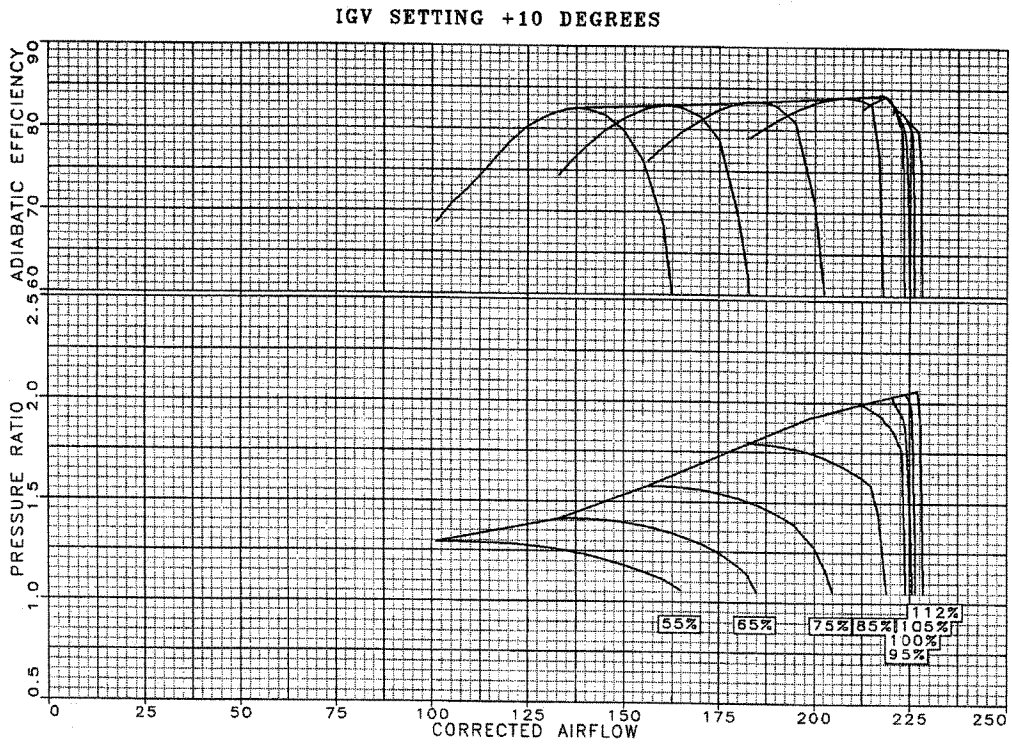

Figure 36. STF 1029 Core Driven Fan Stage Map (IGV = +10°)

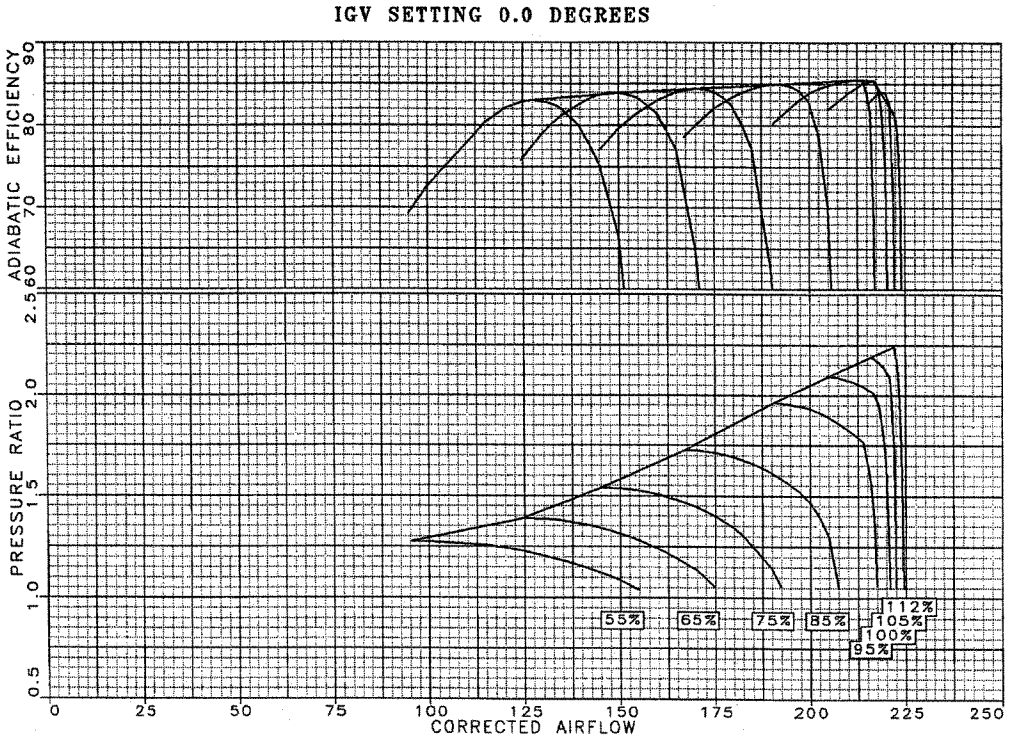

Figure 37. STF 1029 CDFS Map (IGV = 0.0)

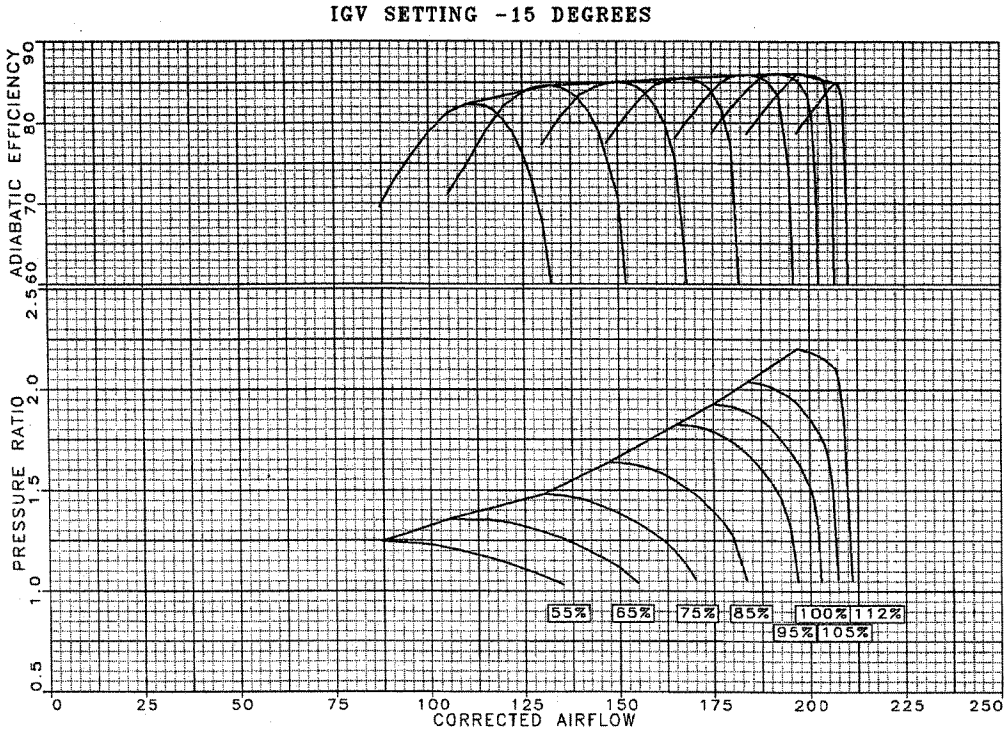

Figure 38. STF 1029 CDFS Map (IGV = 15°)

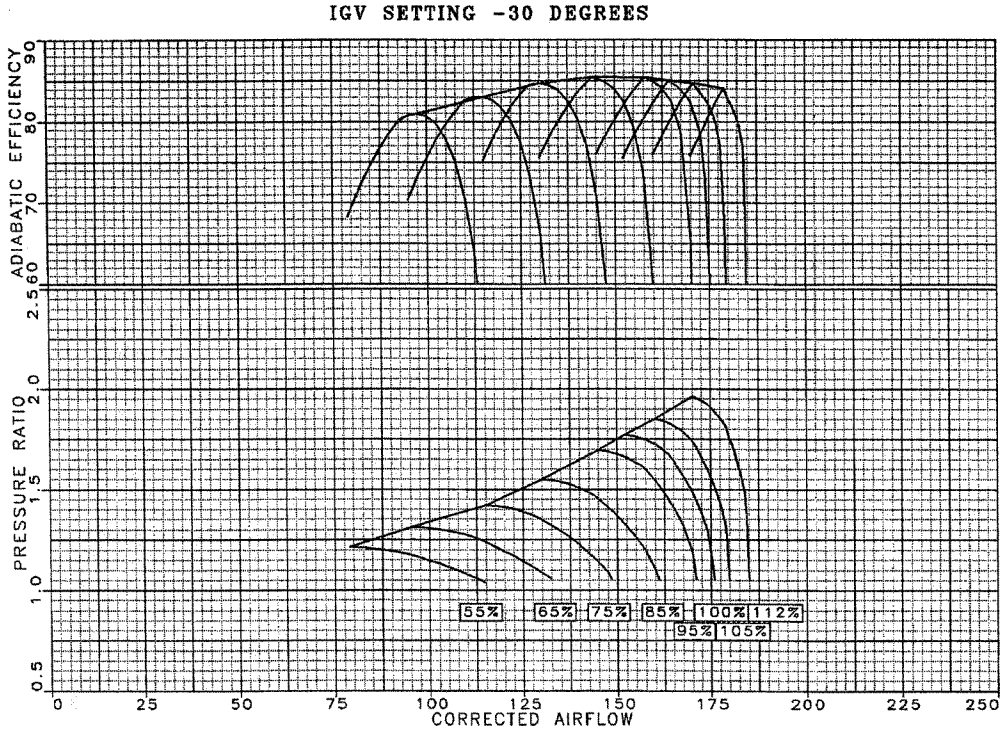

Figure 39. STF 1029 CDFS Map (IGV = 30°)

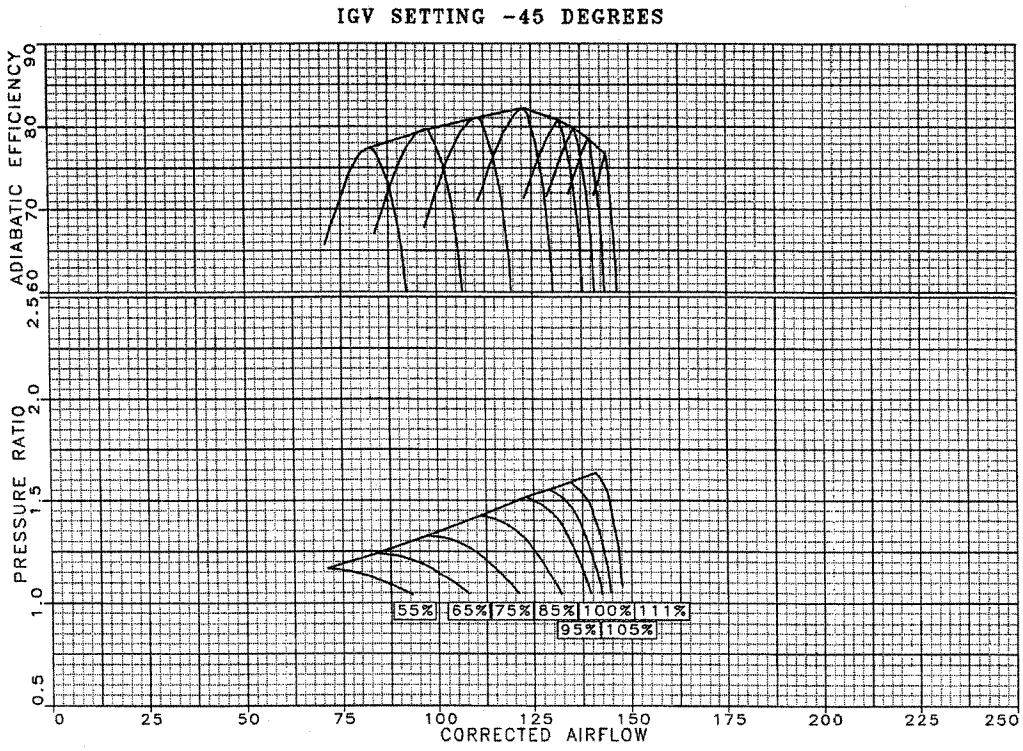

Figure 40. STF 1029 CDFS Map (IGV = −45°)

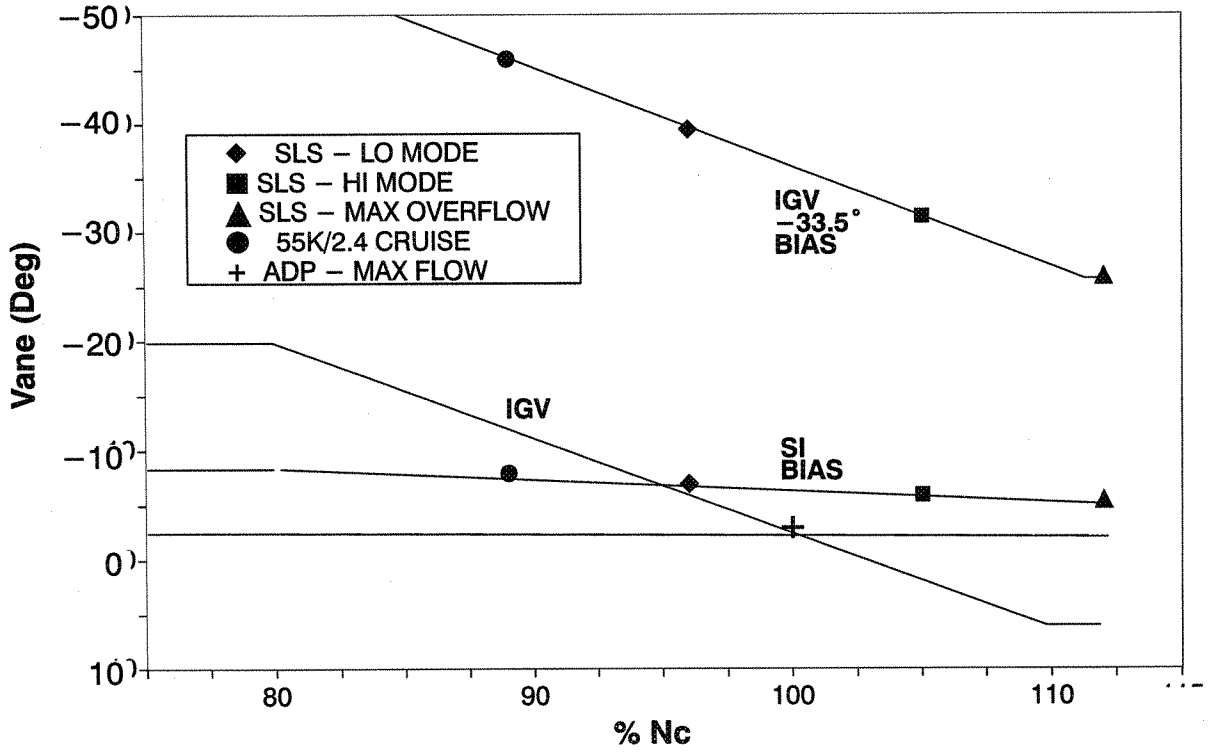

Figure 41. STF 1029 CDFS OD Vane Schedule

High Pressure Compressor Design:

The High Pressure Compressor (HPC) design is based on a single stage core driven fan Stage (CDFS) inner blade followed by a 7−stage high pressure compressor. The design requires 4 stages of variable vanes. The adiabatic design point was selected at sea level static low mode where the maximum core flow (Wc = 202.6) and pressure ratio (PR=9.40) occurs. Table 24 highlights the compressor performance at key flight points.

Table 24. STF1029 High Pressure Compressor Performance Summary

Flight Points	Wc (pps)	PR	Nc (rpm)	Eff ad (%)	SM (%)
SLS – Lo Mode	202.6	9.40	6652	88.8	25.0
SLS – Max	199.7	8.80	6553	88.6	31.0
SLS –Hi Mode	187.6	7.96	6291	88.5	36.0
55k/2.4 – Cruise	164.1	6.71	6136	88.4	36.0

The compressor design uses conventional transonic blading. Swept blades would complicate the CDFS structural design and would offer little or no benefit. Bowed vanes would be used to improve airfoil loading capability and reduce endwall losses. The HPC was designed for 25% stall margin at the ADP with inlet losses for the intermediate case and IGV set at 1.0 % at design flow. The exit Mach number was limited to 0.28 at design conditions.

Figure 42 presents the high pressure compressor flowpath. Figure 43 presents the high pressure compressor performance characteristics.

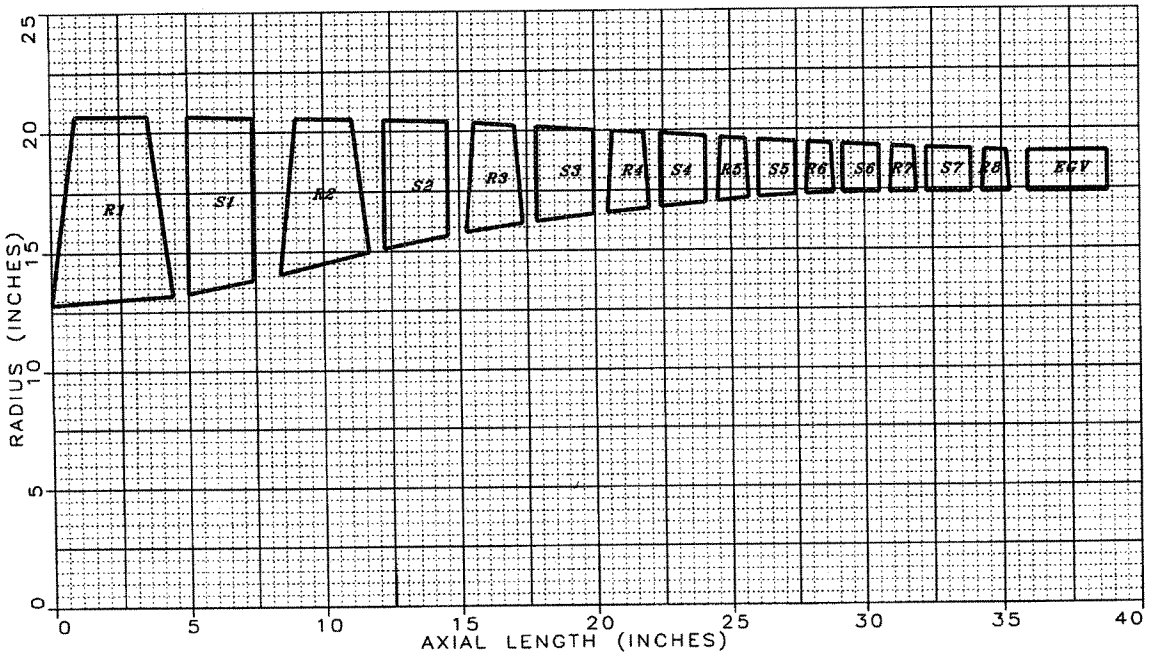

Figure 42. High Pressure Compressor Flowpath

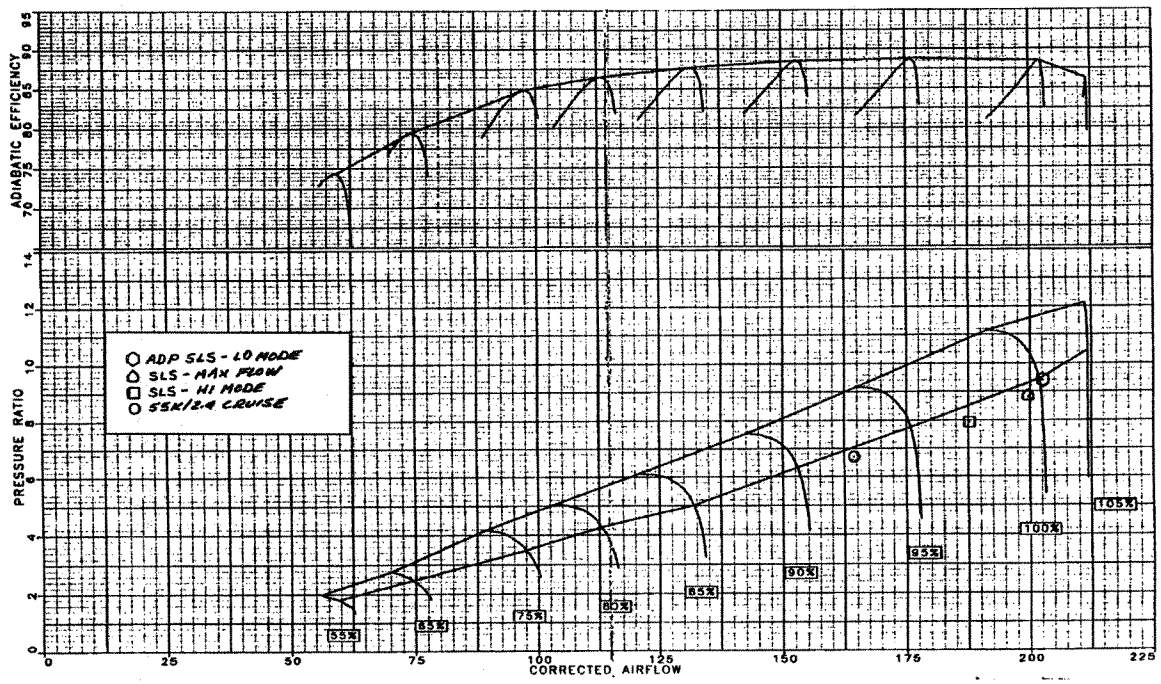

Figure 43. STF 1029 HPC Performance Characteristics

The variable vane schedules for the HPC inlet guide vane (IGV) and stators 1, 2 and 3 are presented in Figure 44.

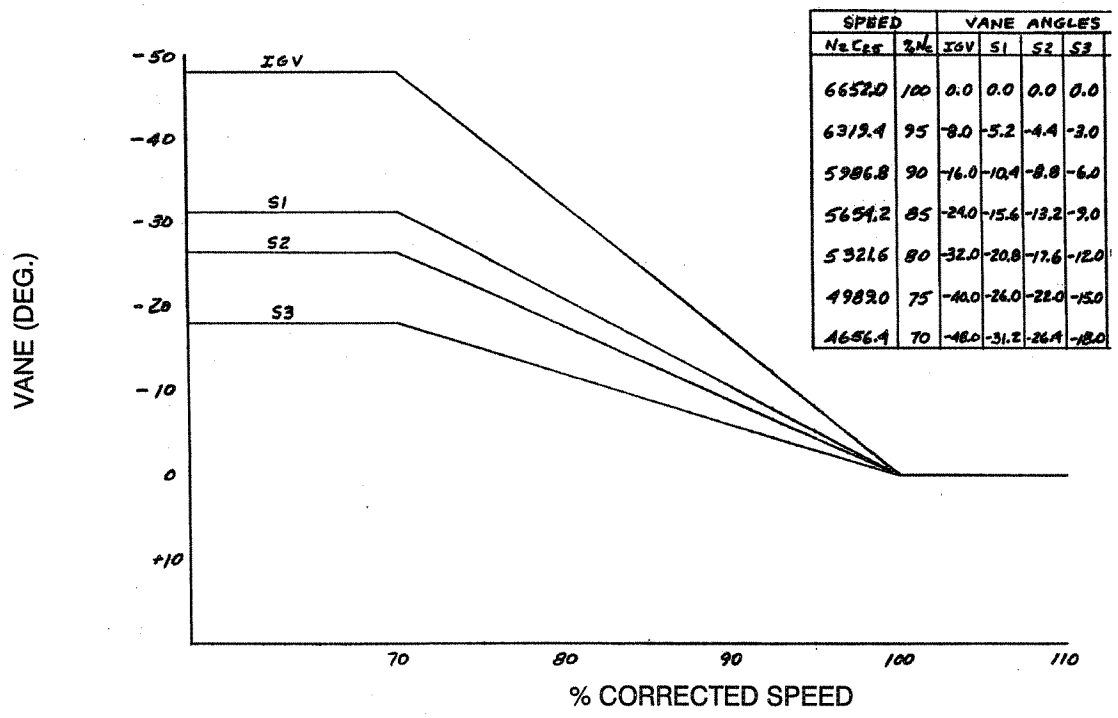

SPEED		VANE ANGLES			
N_2C_{ES}	$\%N_c$	IGV	S1	S2	S3
6652.0	100	0.0	0.0	0.0	0.0
6319.4	95	-8.0	-5.2	-4.4	-3.0
5986.8	90	-16.0	-10.4	-8.8	-6.0
5654.2	85	-24.0	-15.6	-13.2	-9.0
5321.6	80	-32.0	-20.8	-17.6	-12.0
4989.0	75	-40.0	-26.0	-22.0	-15.0
4656.4	70	-48.0	-31.2	-26.4	-18.0

Figure 44. STF 1029 HPC Vane Schedules

E. PARTIAL BYPASS IFV ENGINE DYNAMIC ANALYSES

A dynamic engine performance model was developed for the partial bypass IFV engine in order to determine the component operating characteristics and variable geometry requirements during the following transients.

a. accel and decel between idle and maximum power in low flow operating mode (SLS)

b. accel and decel between idle and maximum power in high flow operating mode (SLS).

c. low flow to high flow mode transition (sea level static)

d. high flow to low flow mode transition (15,000 ft – 0.7 Mn)

The engine dynamic model was also integrated with the NASA Large Amplitude Perturbation INlet (LAPIN) dynamic model so that inlet/engine dynamic analyses can be conducted in future studies.

Low Mode Transient Analyses:

Low flow mode transient analyses were conducted at sea level static. A five second acceleration from idle (10% power) to 95% maximum dry thrust was run as well as a five second deceleration from maximum dry power to 15% power. Table 25 presents the steady state idle and maximum power operating points. Figure 45 shows the net thrust variations with time for both the accel and decel. The exhaust nozzle area throat area is opened at idle to 1900 in^2 to reduce the idle combustor temperature.

Table 25. STF1029 Low Flow Mode Operation at Sea Level Static

Power Setting	Idle	Maximum
Net Thrust, Lbf	3760	37600
Front Fan Speed, rpm	3313	6158
Front Fan Corrected Speed, rpm	3257	6053
Front Fan Corrected Airflow, Lb/sec	292	650
Front Fan Pressure Ratio	1.14	2.10
Front Fan Surge Margin, %	58	41.5
CDFS (OD) Corrected Airflow, Lb/sec	185.8	155.4
CDFS Pressure Ratio	1.174	1.39
CDFS Surge Margin, %	43	36.5
CDFS IGV Setting, °	+10	−20
HPC Corrected Flow, Lb/sec	87.2	202.3
HPC Pressure Ratio	3.69	9.37
HPC Rotor Speed, rpm	5027	7628

Table 25. STF1029 Low Flow Mode Operation at Sea Level Static (continued)

Power Setting	Idle	Maximum
HPC Corrected Speed, rpm	4826	6641
Combustor Temperature, °R	2287	3160
Front Mixing Plane Outer Area, in^2	–	–
Front Mixing Plane Inner Area, in^2	994	994
Aft Mixing Plane Bypass Stream Area, in^2	825	825
Aft Mixing Plane Core Stream Area, in^2	1026	1026
Exhaust Nozzle Throat Area in^2	1900	1112

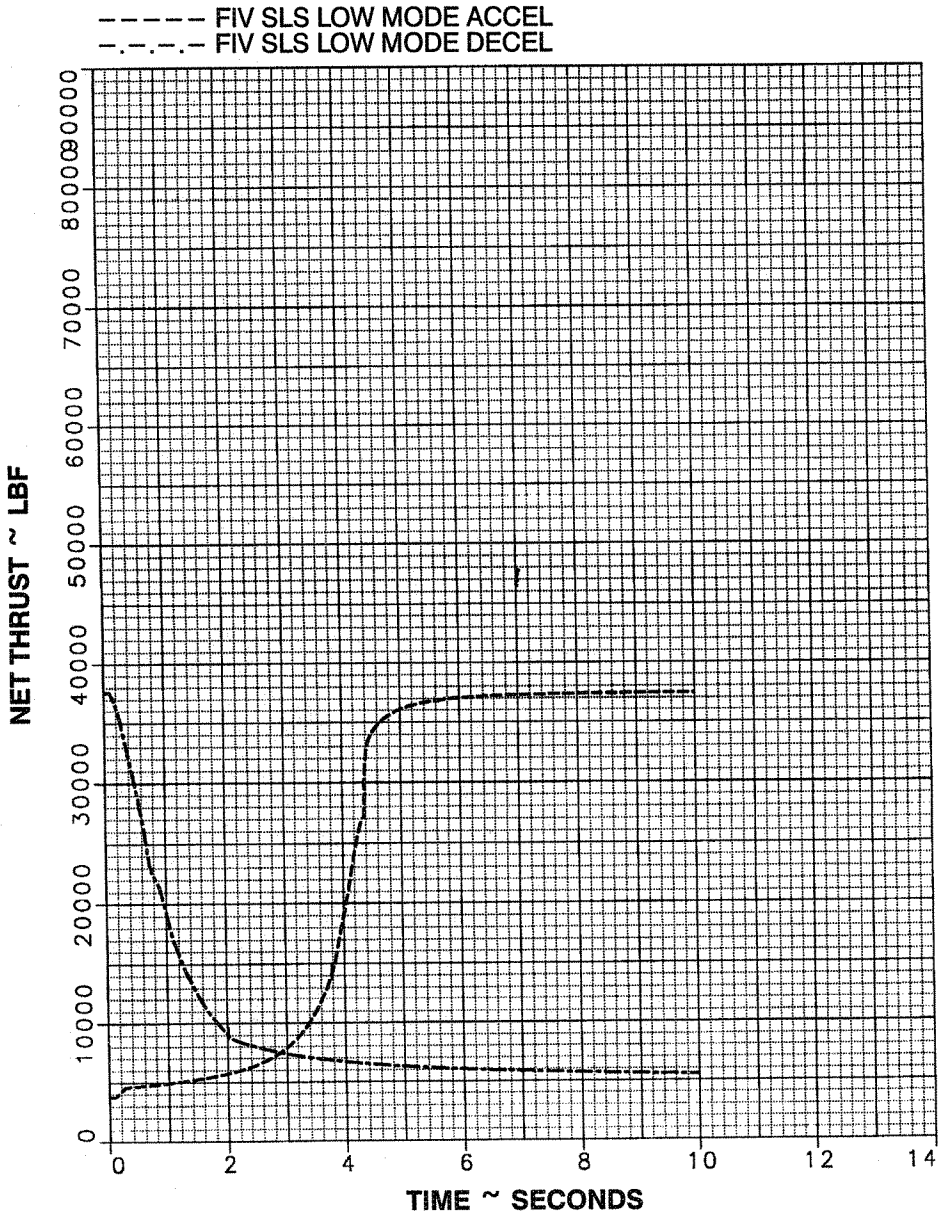

Figure 45. Low Mode Transient Thrust Lapse Rates

Figure 46 illustrates the fuel flow variation with thrust for both the accel and decel and for the steady state operating points between idle and maximum dry power.

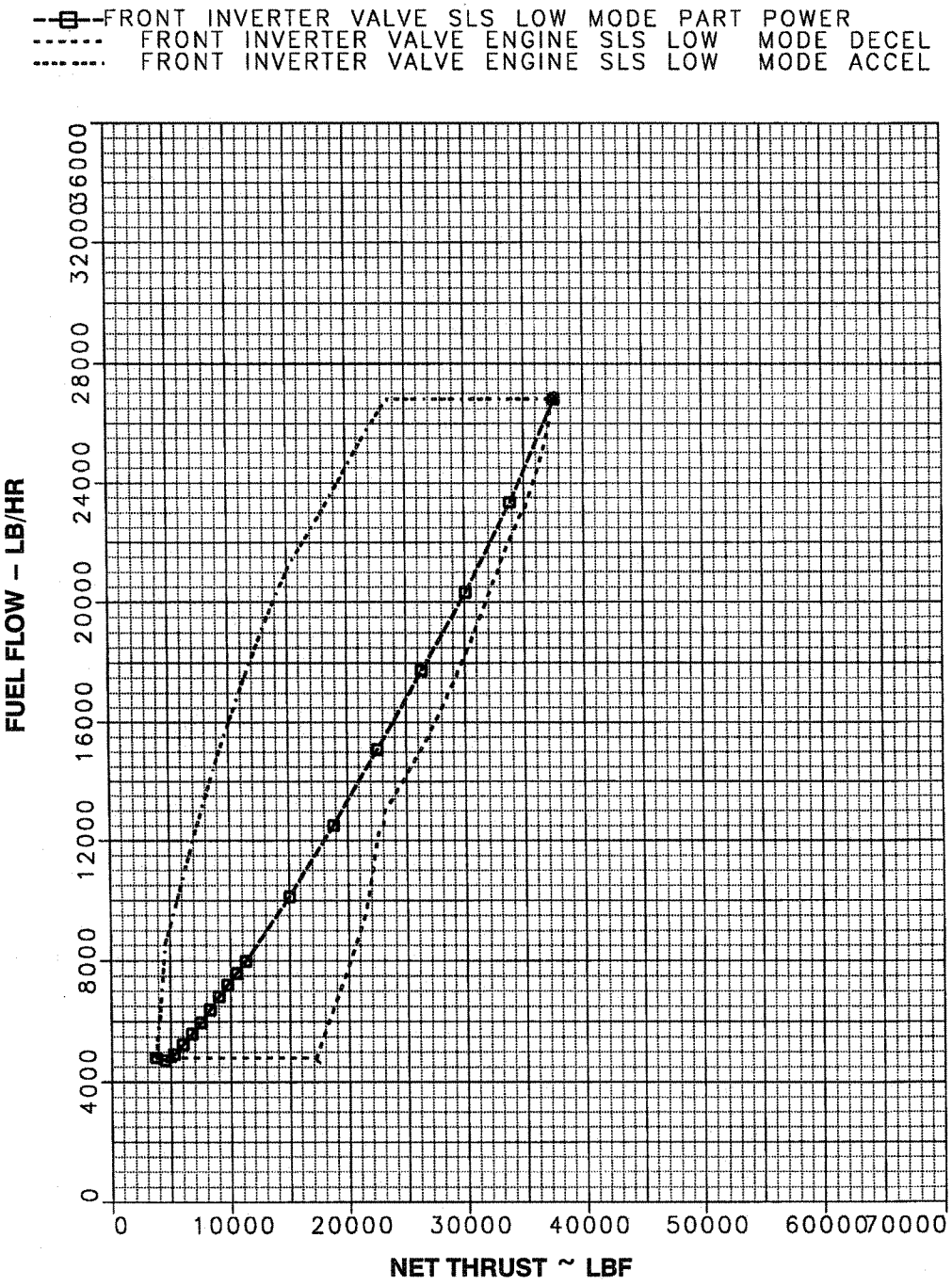

Figure 46. Low Mode Fuel Flow Lapse Rates

Figure 47 illustrates the variation in combustor exit temperature (TT4) during steady state and transient operation. The maximum transient TT4 of 3670°R is 200°F above the maximum steady state TT4 of 3470°R and is typical of the transient margin used in current engines.

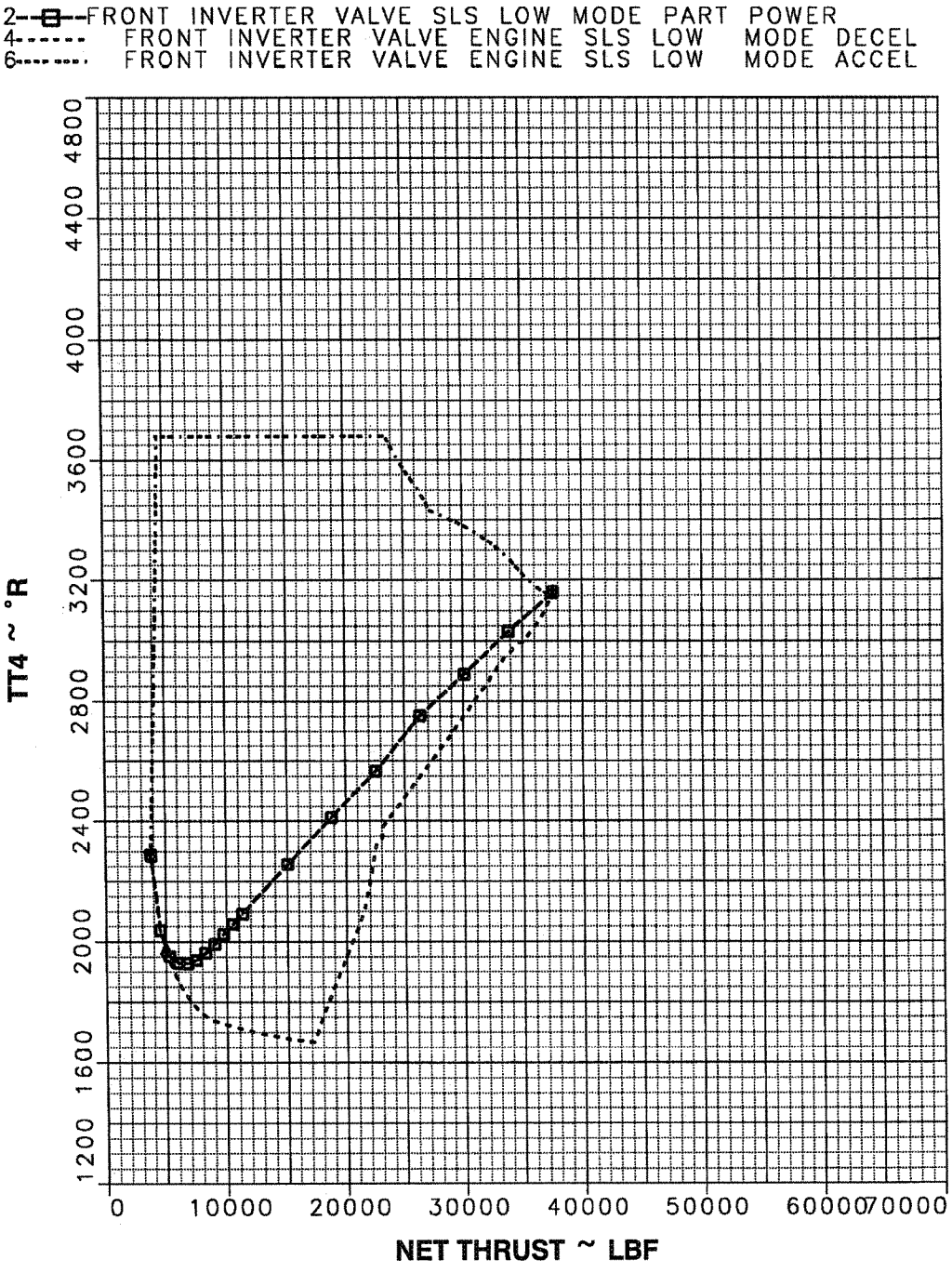

Figure 47. Low Mode Combustor Temperature Variations

Figure 48 illustrates the low mode front fan operating lines during steady state and transient operation, while Figure 49 shows the resulting fan surge margin levels. At the beginning of the accel, the front fan pressure ratio increases at constant speed from 1.14 to 1.20 and then the speed increases. The front fan operating line during the accel is higher than the steady state operating line as shown in Figure 48. The fan surge margin, Figure 49, is above 38% for the entire acceleration. During the decel, the fan operating line is below or equal to the steady state operating line.

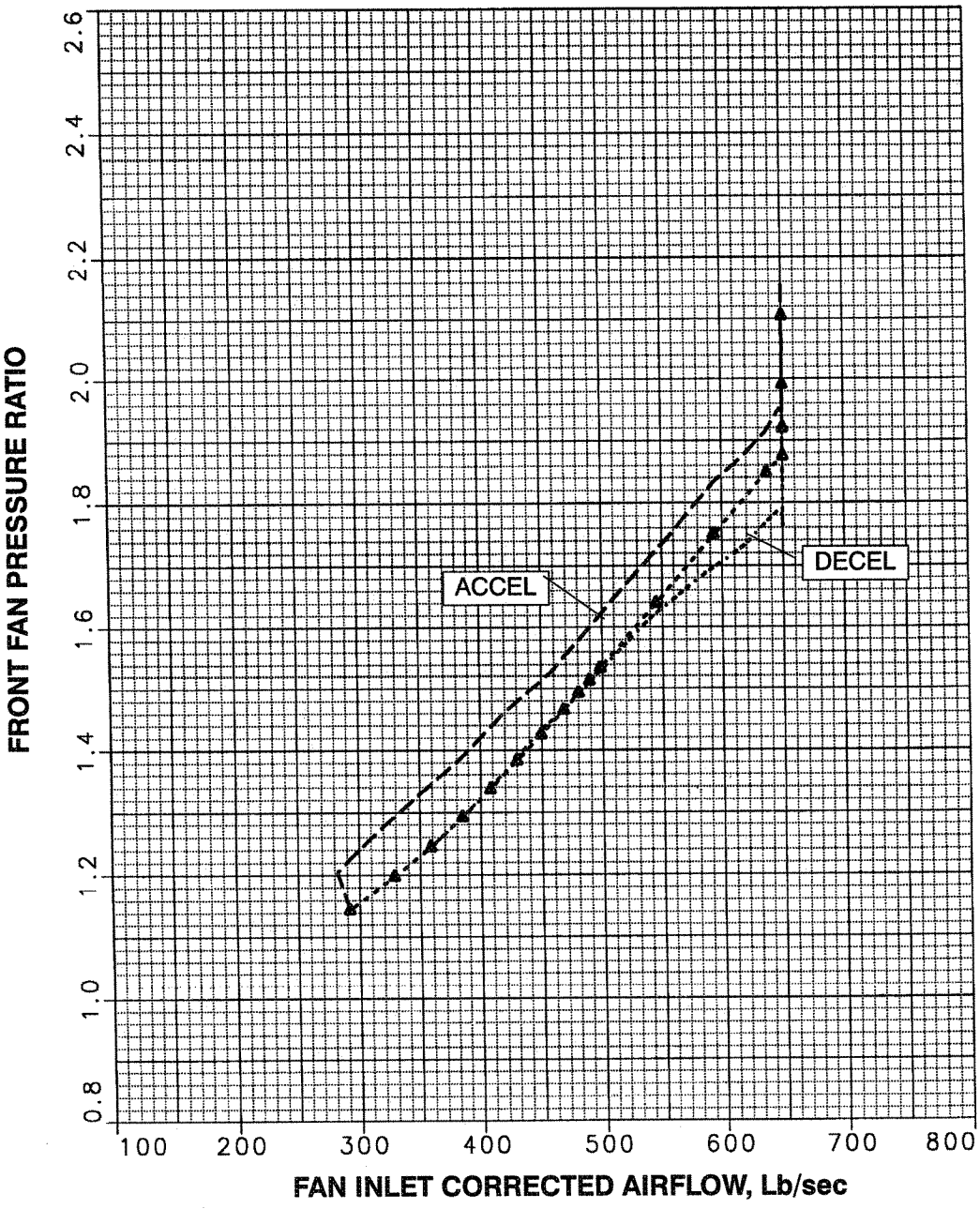

Figure 48. Low Mode Front Fan Operating Lines

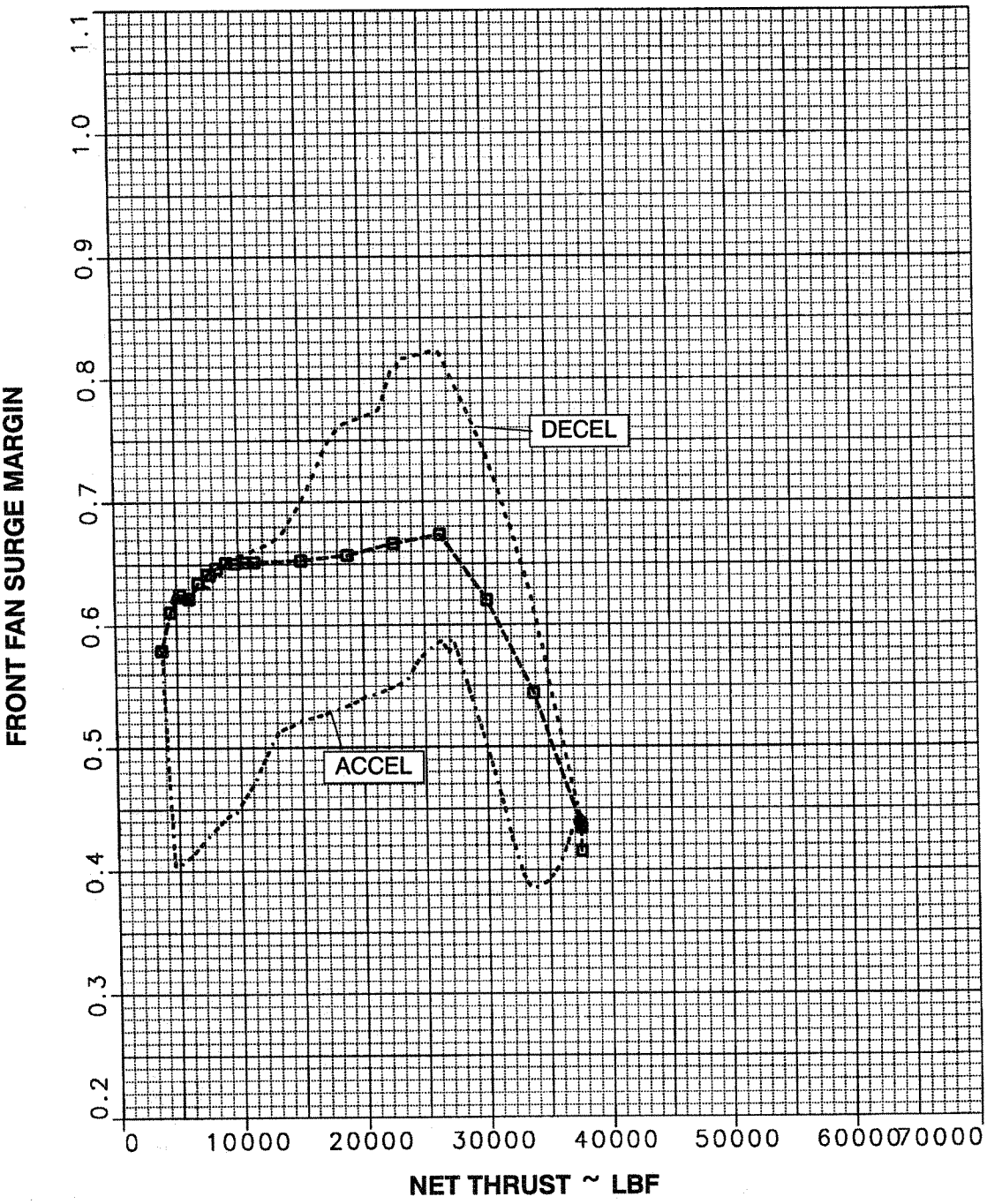

Figure 49. Low Mode Front Fan Surge Margin

The core drive fan (outer portion) operating lines during low mode transient and steady state operation are presented in Figure 50. At maximum dry power the CDFS is operating at an inlet corrected flow (WC25) of 155 lb/sec and a pressure ratio of 1.39. As power is reduced, the CDFS inlet guide vane (IGV) angle is increased as shown in Figure 51 from −20° at 100% power to +10° at 70% power. This is done to prevent the CDFS from choking. The impact of this CDFS IGV angle increase is to raise the CDFS inlet corrected

flow as power is reduced, as shown in Figure 50. At idle power, the CDFS is operating at a higher inlet corrected flow (WC25=186.5 lb/sec) than at maximum dry power.

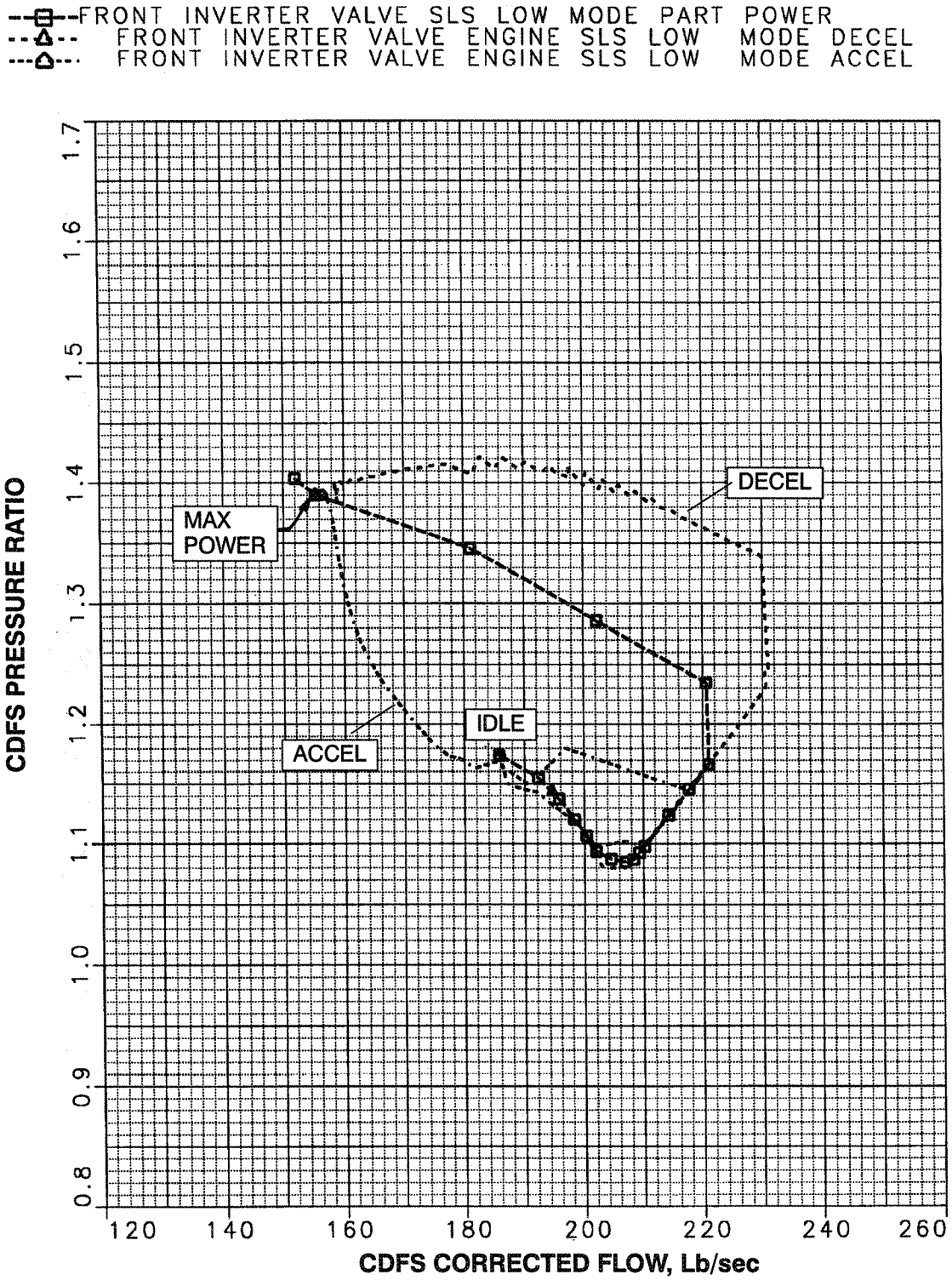

Figure 50. Low Mode CDFS Operating Lines

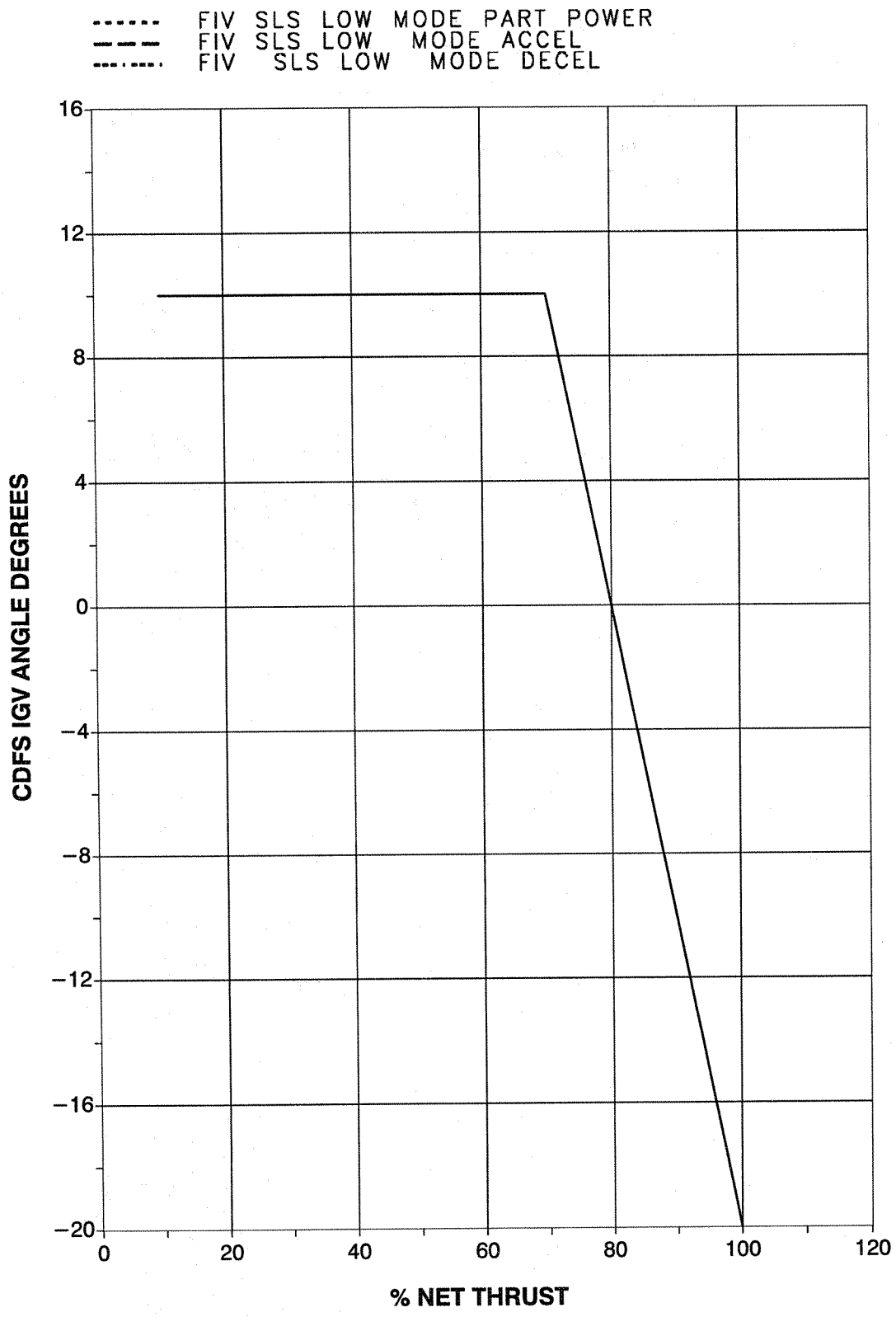

Figure 51. Low Mode CDFS Inlet Guide Vane Angle Settings

Figure 52 presents the CDFS low mode surge margin variations during transient and steady state operation.

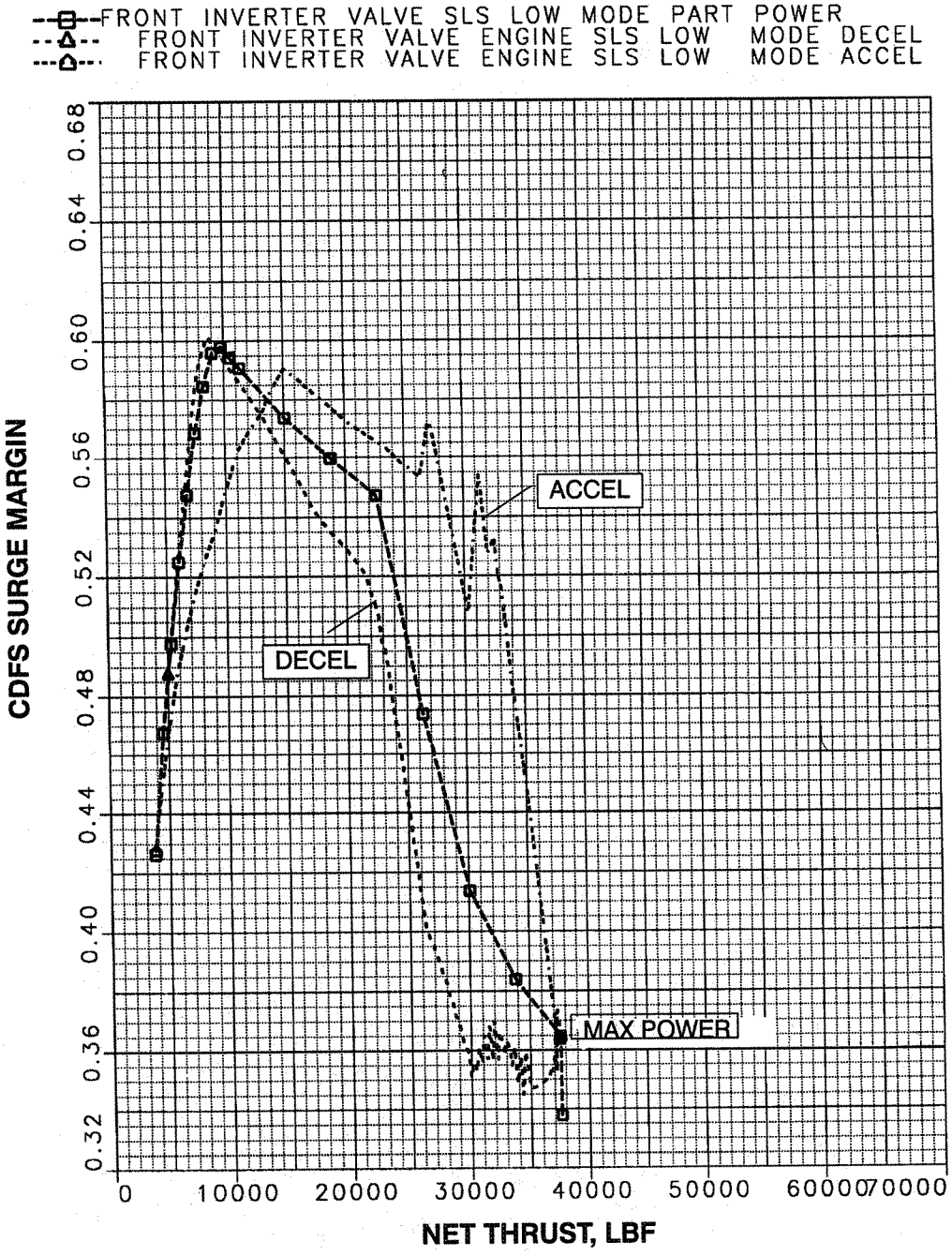

Figure 52. Low Mode CDFS Surge Margins

The high pressure compressor (HPC) operating lines during low mode steady state and transient operation are presented in Figure 53. The accel fuel schedule was set to maintain a minimum high compressor surge margin of 25%.

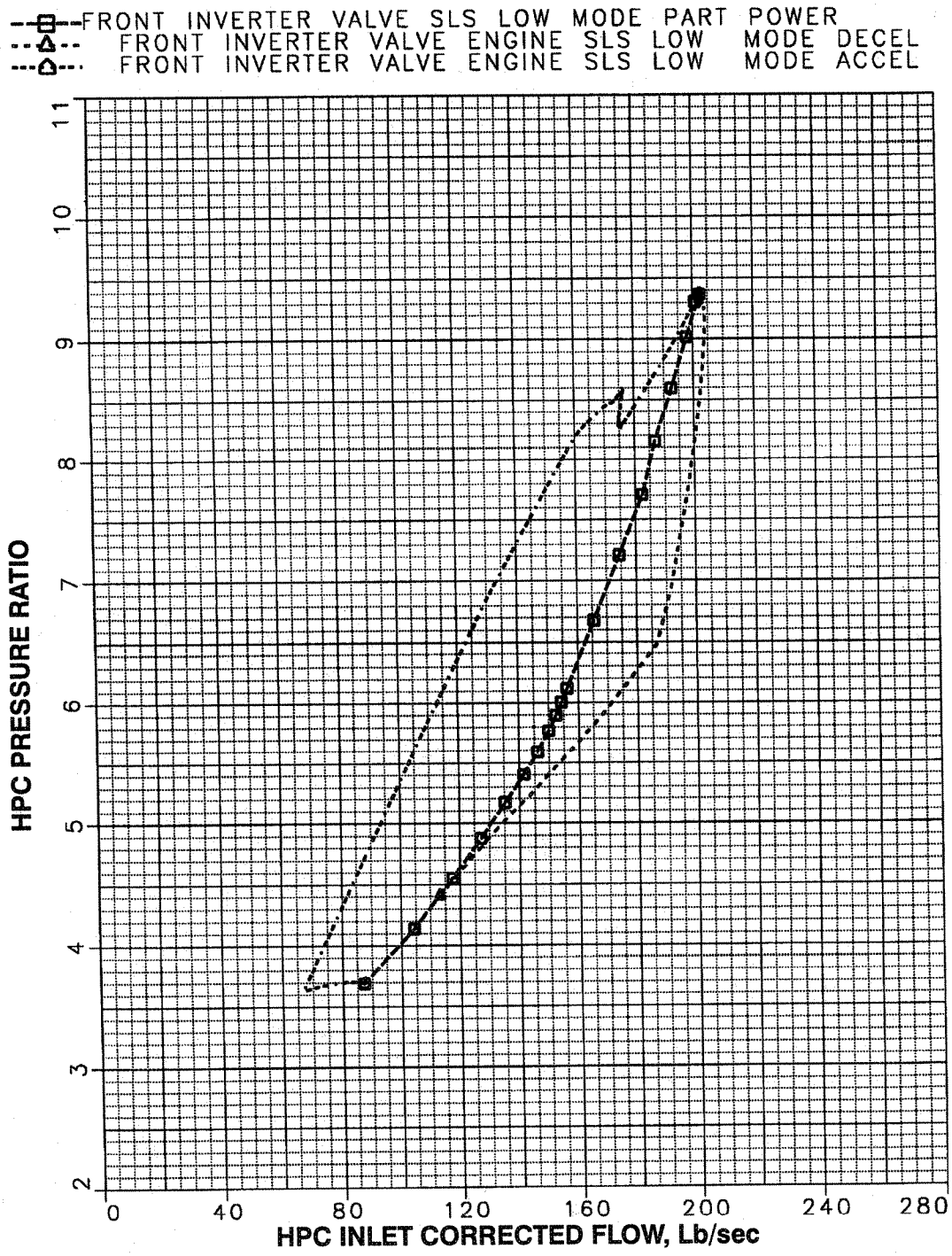

Figure 53. Low Mode HPC Operating Lines

High Flow Mode Transient Analyses:

High flow mode transient analyses were conducted at sea level static. A five second acceleration from idle (10% power) to 95% maximum dry thrust was run. A five second deceleration from maximum dry power to 15% power was also evaluated. Table 26 presents a summary of the high mode steady state idle and maximum power operating points.

Table 26. STF1029 High Flow Mode Operation at Sea Level Static

Power Setting	Idle	Maximum
Net Thrust, Lbf	3390	33900
Front Fan Speed, rpm	2643	6200
Front Fan Corrected Speed,, rpm	2598	6095
Front Fan Corrected Airflow, Lb/sec	191	650
Front Fan Pressure Ratio	1.176	2.394
Front Fan Surge Margin, %	20	21.5
CDFS (OD) Corrected Airflow, Lb/sec	107.0	175.7
CDFS Pressure Ratio	1.13	1.70
CDFS Surge Margin, %	36.5	22
CDFS IGV Setting, °	−20	−20
HPC Corrected Flow, Lb/sec	99.8	187.6
HPC Pressure Ratio	3.67	7.96
HPC Rotor Speed, rpm	5171	7354
HPC Corrected Speed, rpm	4944	6291
Combustor Temperature, °R	1731	2760
Front Mixing Plane Outer Area, in^2	399	399
Front Mixing Plane Inner Area, in^2	994	994
Aft Mixing Plane Bypass Stream Area, in^2	2178	2178
Aft Mixing Plane Core Stream Area, in^2	1026	1026
Exhaust Nozzle Throat Area in^2	1900	1751

Figure 54 presents the high mode accel and decel thrust lapse rates with time. Figure 55 and Figure 56 show the fuel flow and combustor temperature (TT4) variations with time during the accel and decel.

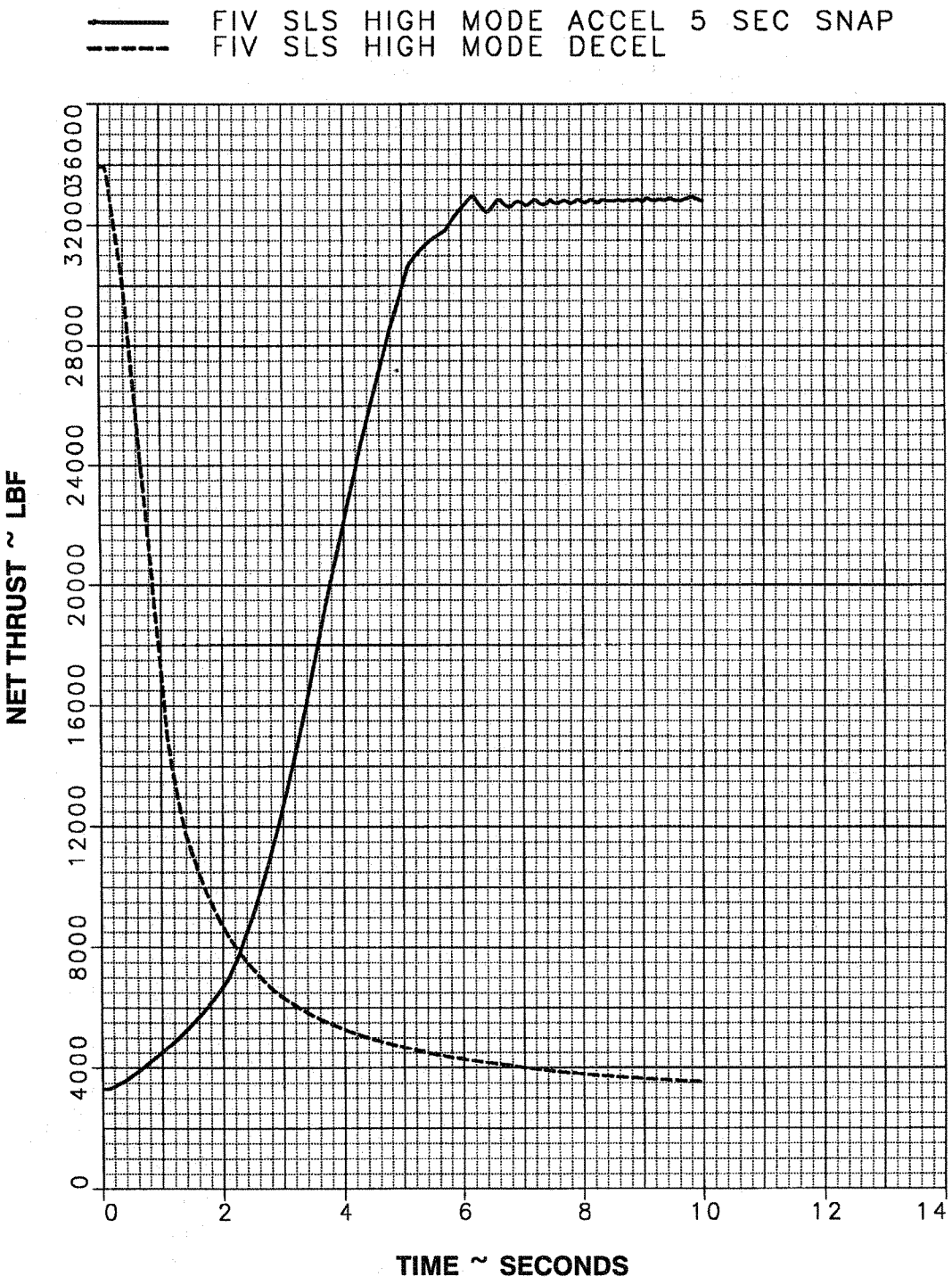

Figure 54. High Mode Transient Thrust Lapse Rates

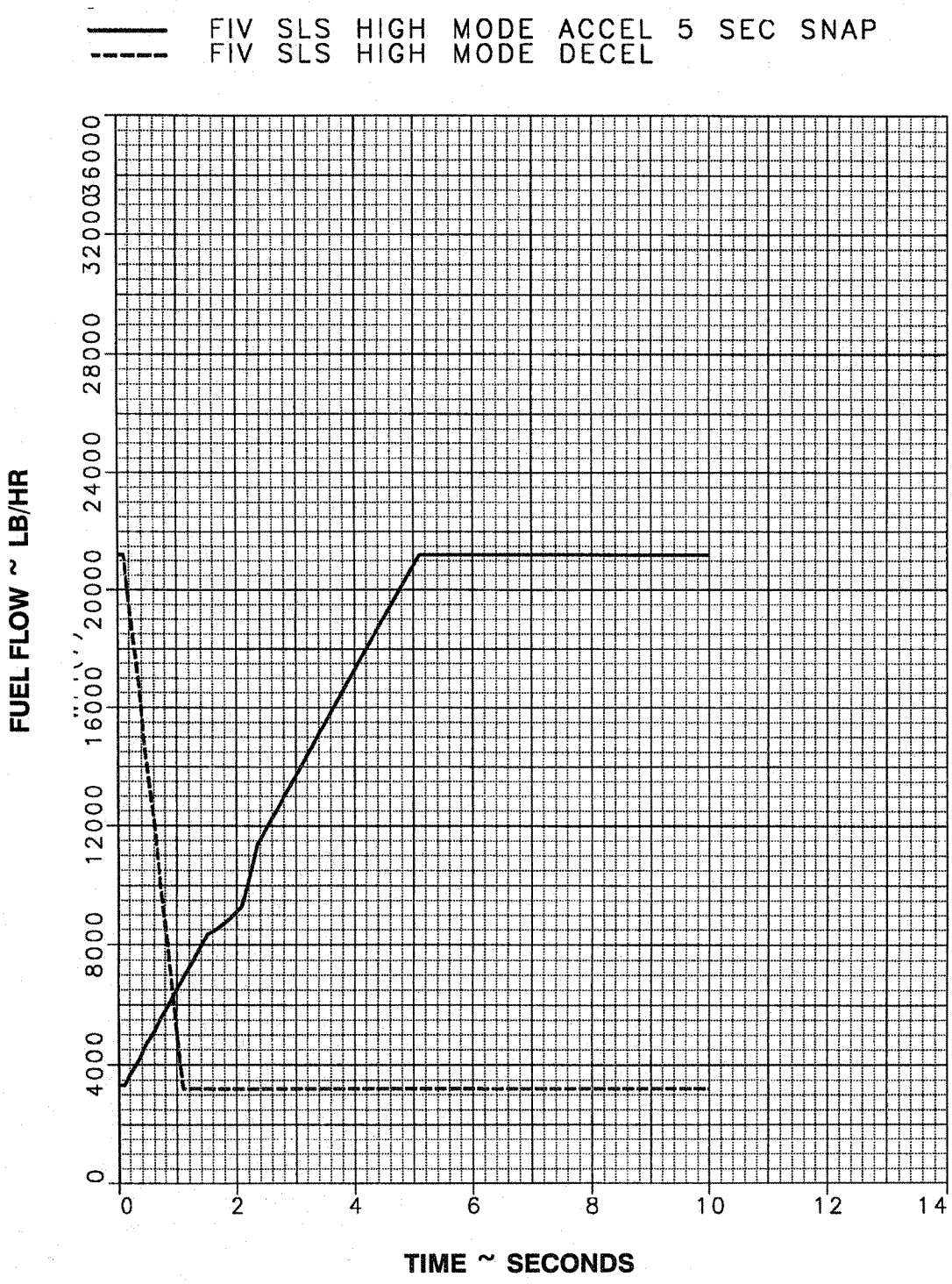

Figure 55. High Mode Transient Fuel Flow Schedules

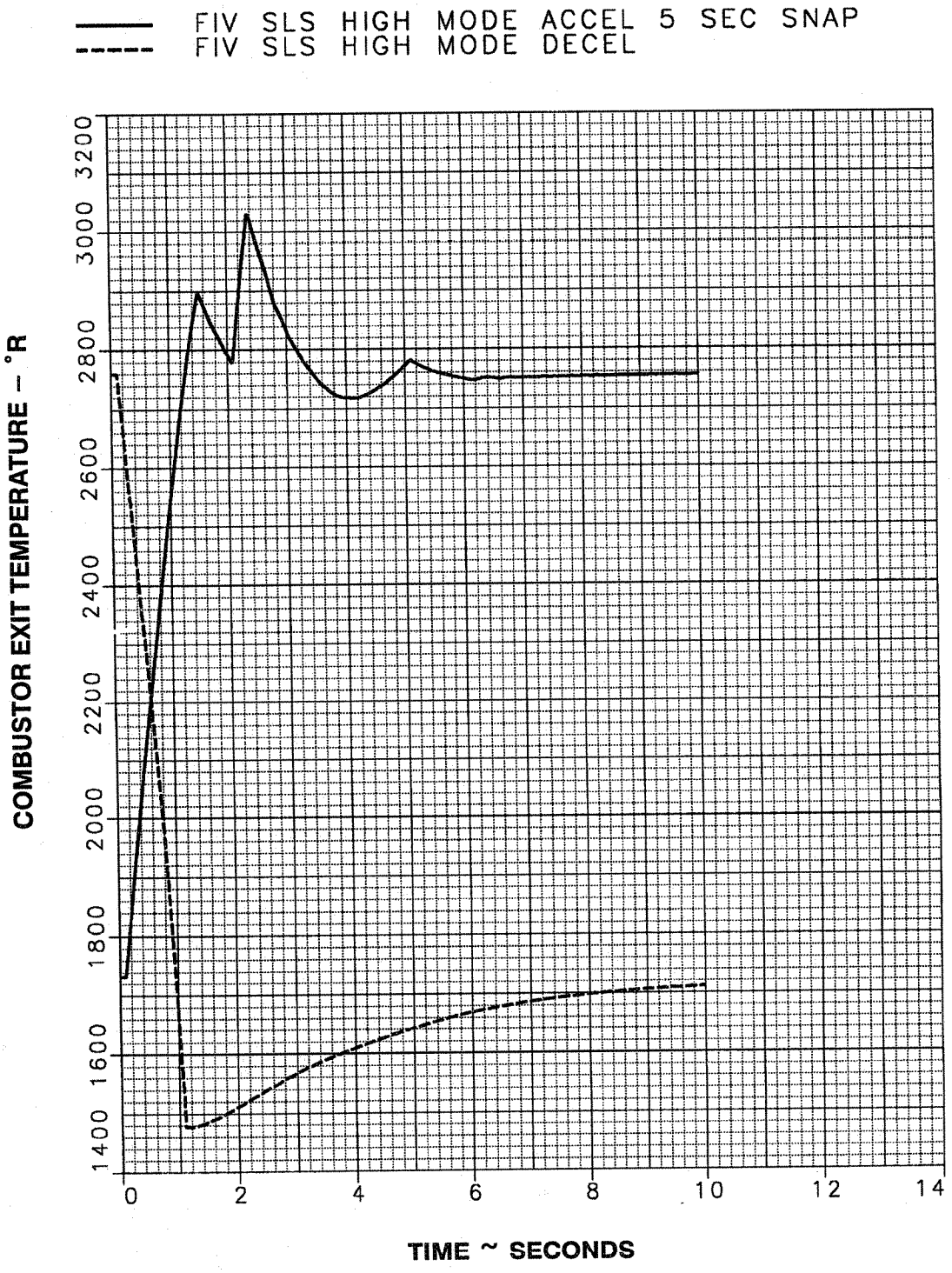

Figure 56. High Mode Combustor Temperature Variation

During the accel, the fuel flow is scheduled to reach its peak value in 5 seconds. This fuel flow schedule was selected to keep the front fan surge margin above 10% as shown in Figure 57. Figure 58 presents the fan operating lines during an accel, a decel and steady state operation.

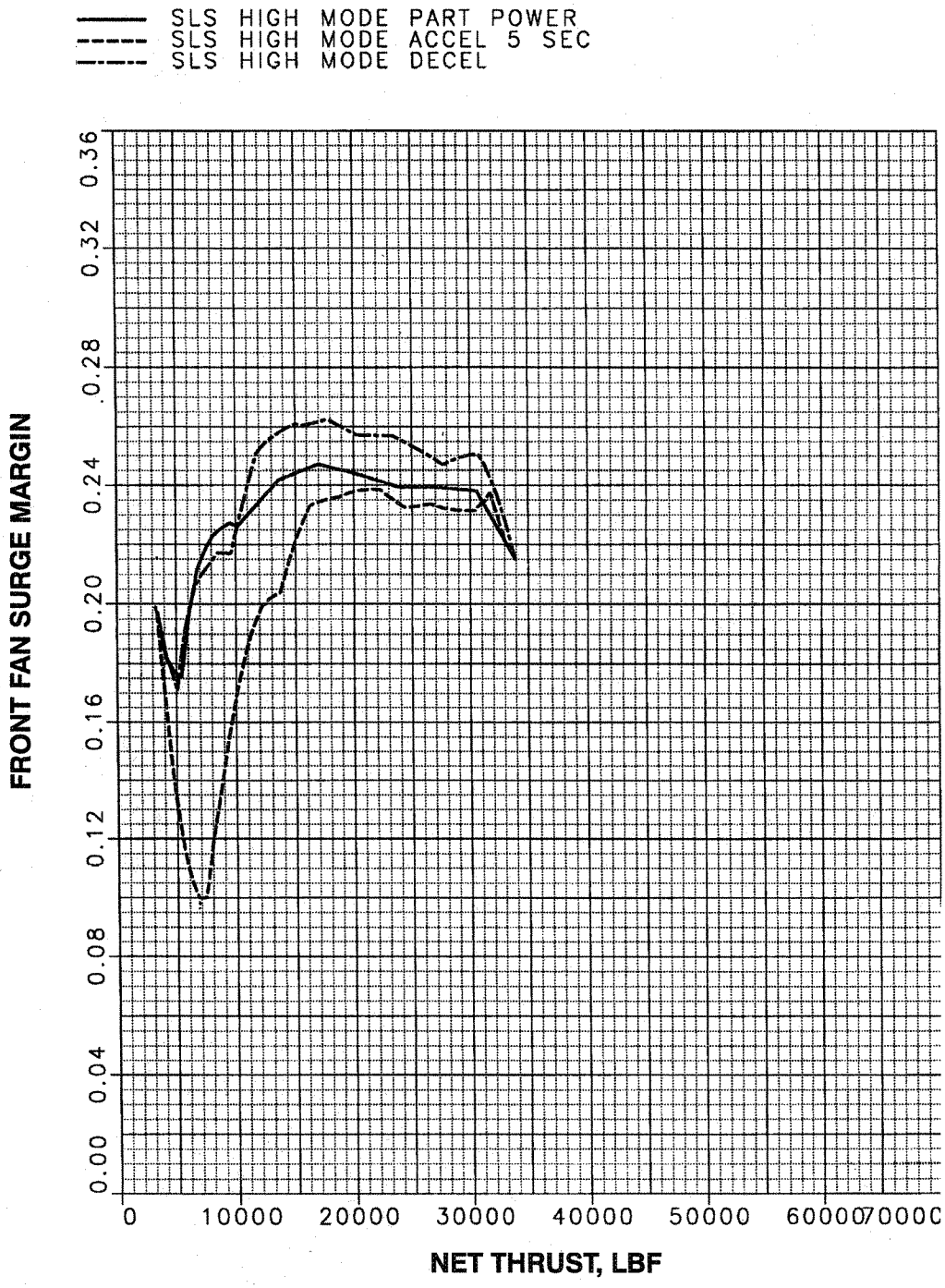

Figure 57. High Mode Front Fan Surge Margin

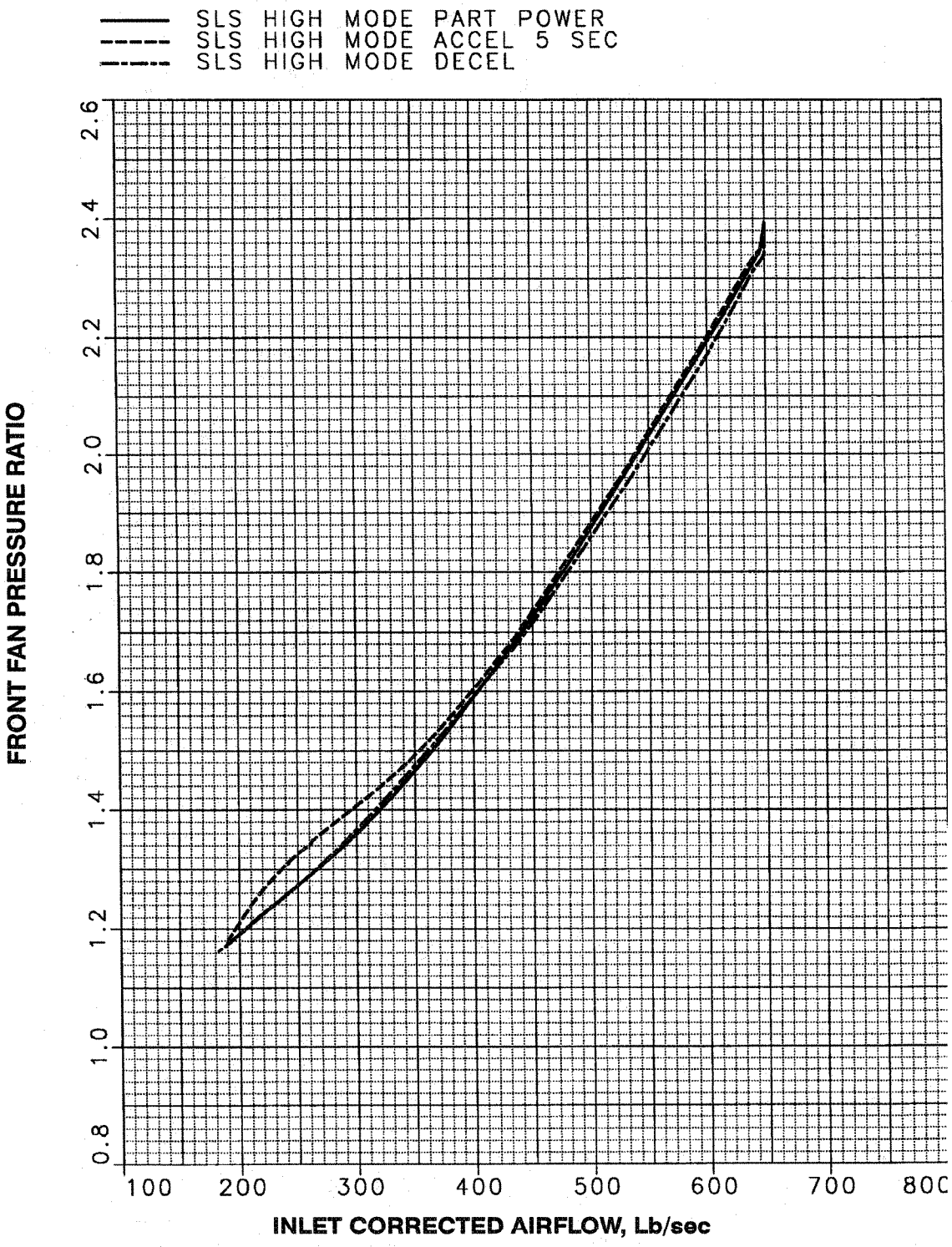

Figure 58. High Mode Front Fan Operating Lines

Figure 59 and Figure 60 present the core driven fan stage operating lines and surge margins during high mode transient and steady state operation. The surge margin varies from 36% at idle to 22% at maximum dry power. For high mode operation the CDFS inlet guide vane angle is set at −20° from maximum power to idle.

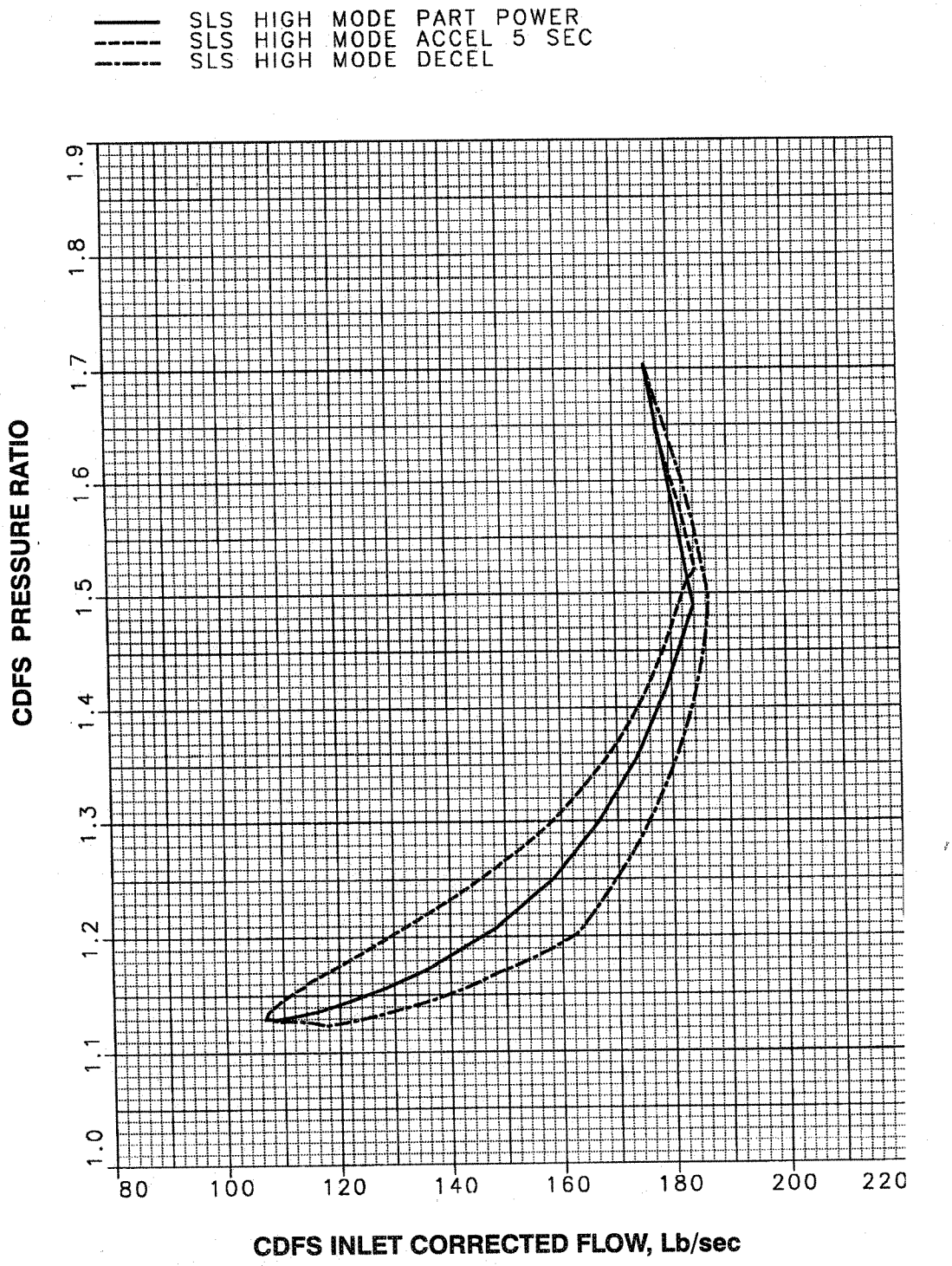

Figure 59. High Mode CDFS Operating Lines

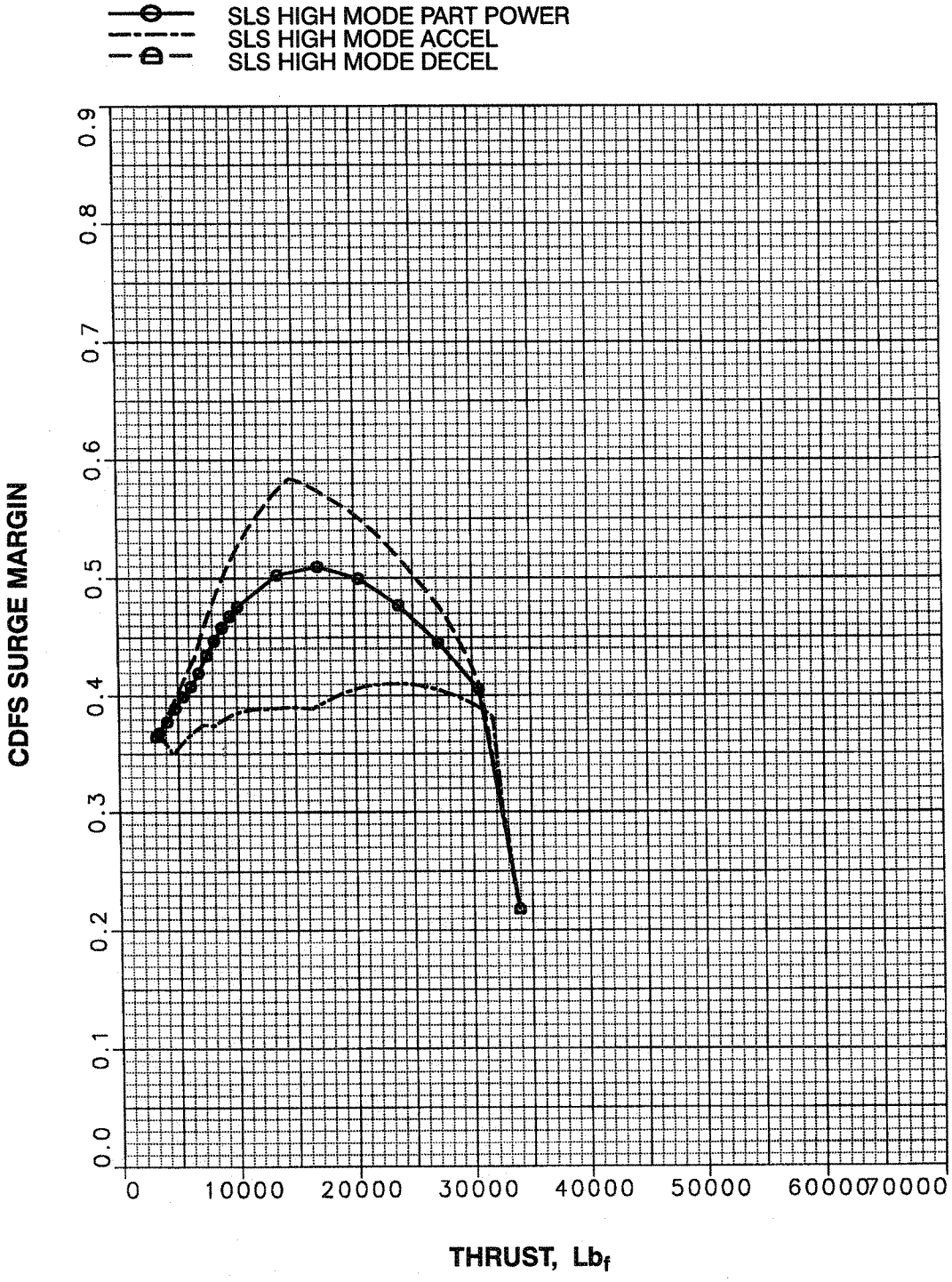

Figure 60. High Mode CDFS Surge Margin

Figure 61 presents the high pressure compressor transient and steady state operating lines. As in the low mode, the fuel flow schedule during the accel is set to maintain at least 25% surge margin in the HPC.

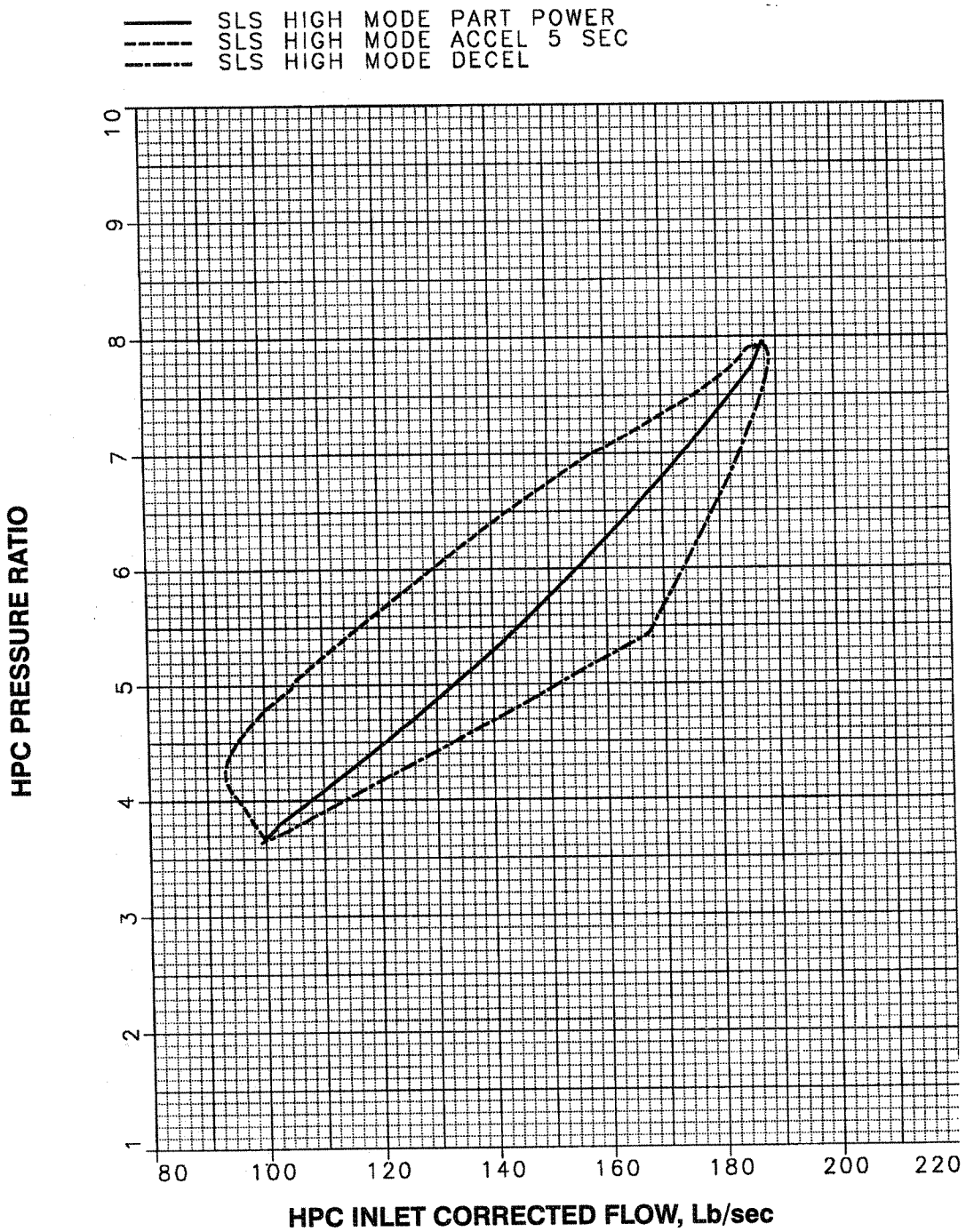

Figure 61. High Mode HPC Operating Line

Low to High Mode Transient Analysis:

The partial bypass IFV engine will be started in the conventional low flow mode of operation. For this study, the low to high mode transition transient was conducted at sea level static, with the front fan held at a constant fan rotor speed of 4150 rpm. At this rotor speed the engine produces 5640 pounds of thrust in the low mode and 7570 pounds in the high mode. Table 27 summarizes the low and high mode operating points at the beginning and end of this low power transient.

Table 27. STF1029 Low to High Mode Transition (SLS)

Operating Mode	Low FLow	High FLow
Net Thrust, Lbf	5640	7570
Front Fan Speed, rpm	4150	4150
Front Fan Corrected Speed, rpm	4080	4080
Front Fan Corrected Airflow, Lb/sec	373.6	346.2
Front Fan Pressure Ratio	1.268	1.444
Front Fan Surge Margin, %	62	24
CDFS (OD) Corrected Airflow, Lb/sec	197.1	137.4
CDFS IGV Setting, Deg.	10	−17.2
CDFS Surge Margin, %	51	52
HPC Corrected Flow, LB/sec	122.9	134.5
HPC Pressure Ratio	4.72	5.085
HPC Rotor Speed, rpm	5683	5981
HPC Corrected Speed, rpm	5367	5544
Combustor Temperature, °R	1937	1918
Front Mixing Plane Outer Area (MXD2), in^2	399	399
Front Mixing Plane Inner Area (MXD1), in^2	994	994
Aft Mixing Plane Bypass Stream Area, in^2	825	2178
Aft Mixing Plane Core Stream Area, in^2	1026	1026
Exhaust Nozzle Throat Area, in^2	1900	2258

The low to high mode transition was conducted with the valve being transitioned from the low mode to the high mode position between the 0.5 and 10.5 second points shown in the transient curves. Figure 62 and Figure 63 show the linear transition of the valve areas at the CDFS OD Inlet. In the low flow mode, at time = 0.5 seconds, all the front fan outer flow feeds the CDFS OD and there is no secondary flow. At the 10.5 second point, all the CDFS OD flow is secondary flow.

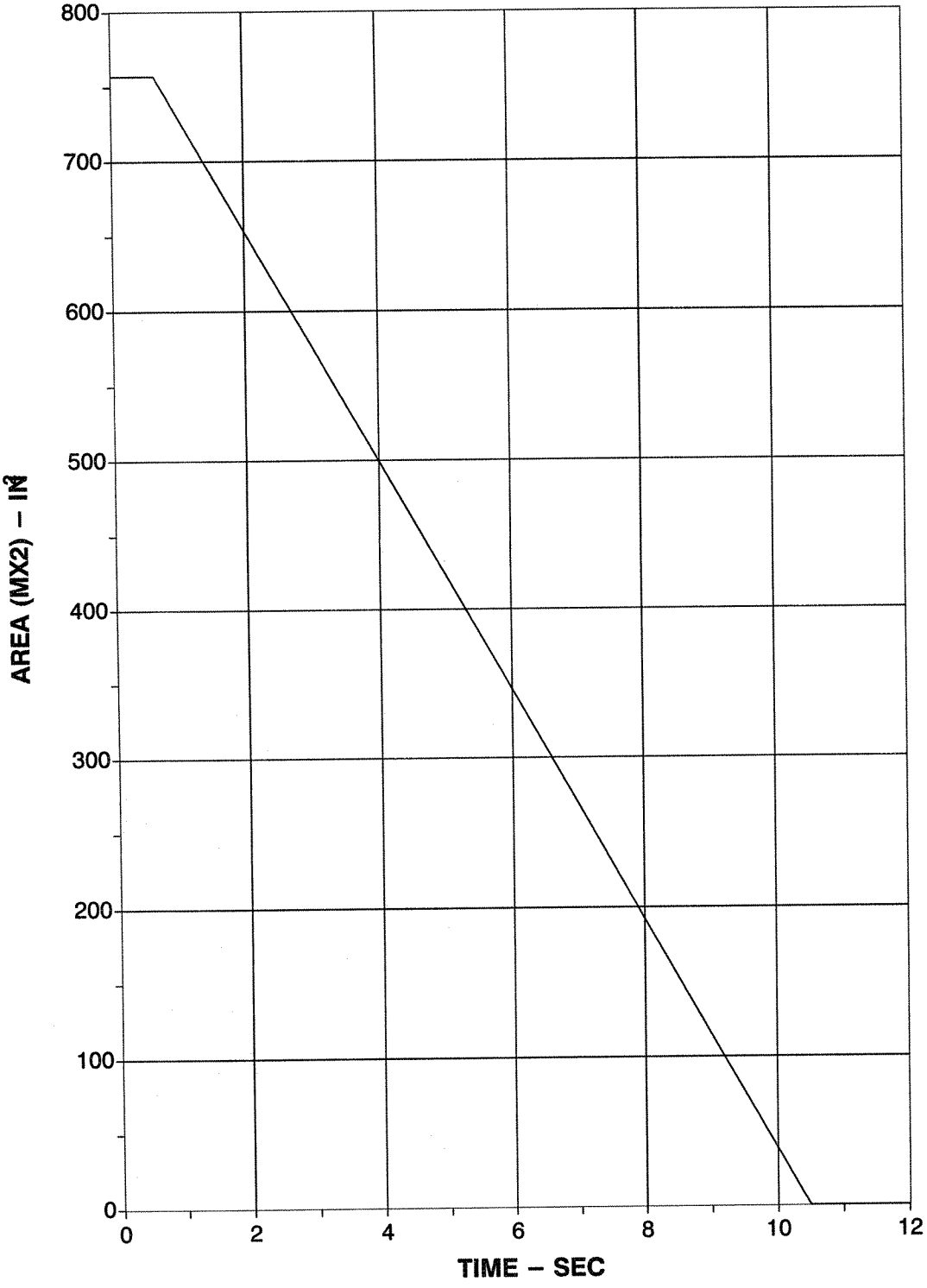

Figure 62. Valve Area at CDFS Inlet Which Feeds Front Fan OD Flow Into CDFS OD

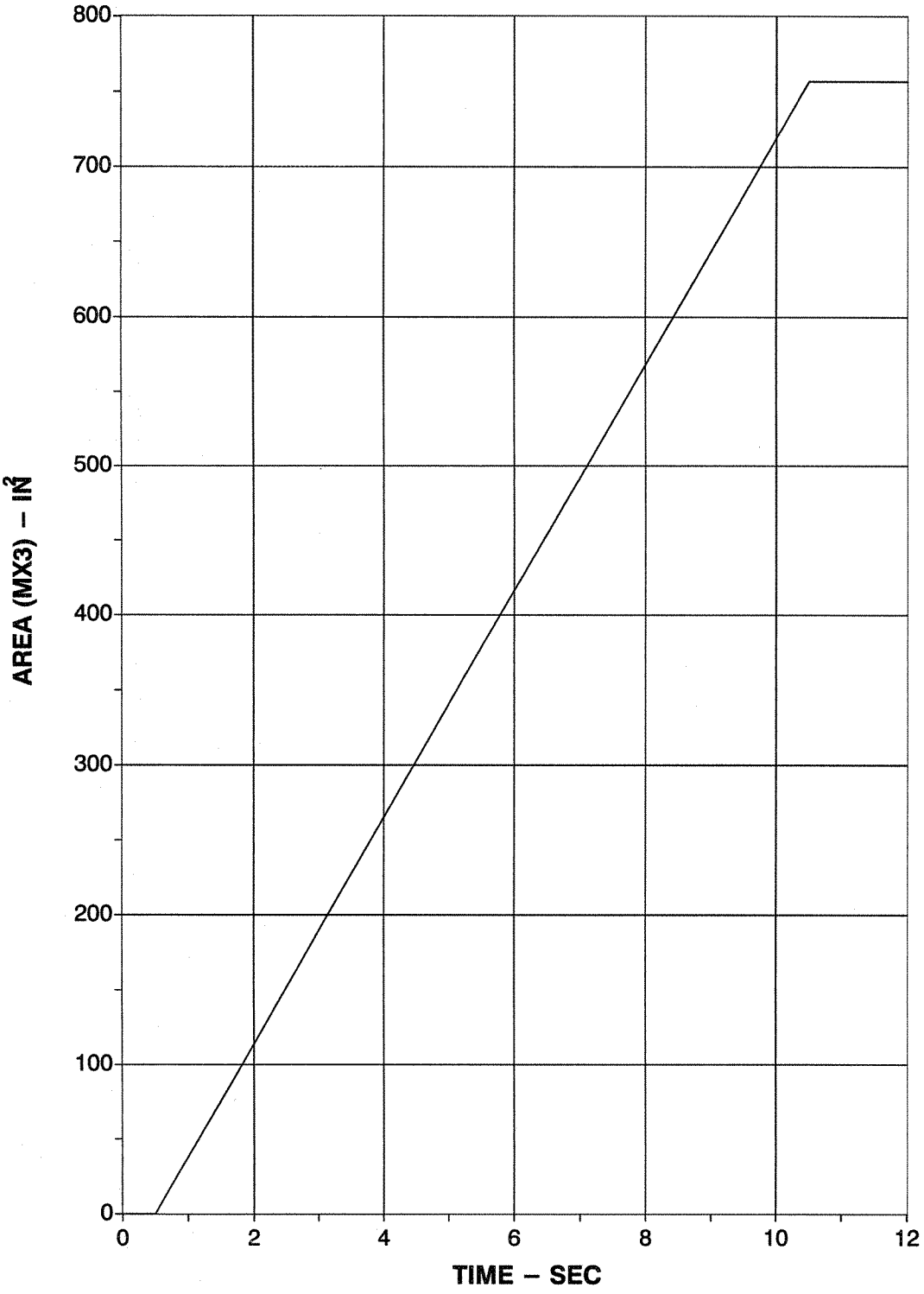

Figure 63. Valve Area at CDFS Inlet Which Feeds Secondary Flow Into CDFS OD

The amount of secondary flow that is brought into the engine is shown in Figure 64. As this flow passes through the valve, some of it feeds the core driven fan and some of it by-passes the CDFS. At the 10.5 second point, all the secondary flow goes to the core driven fan stage. The final high mode steady state operating point is achieved at the 12 second point.

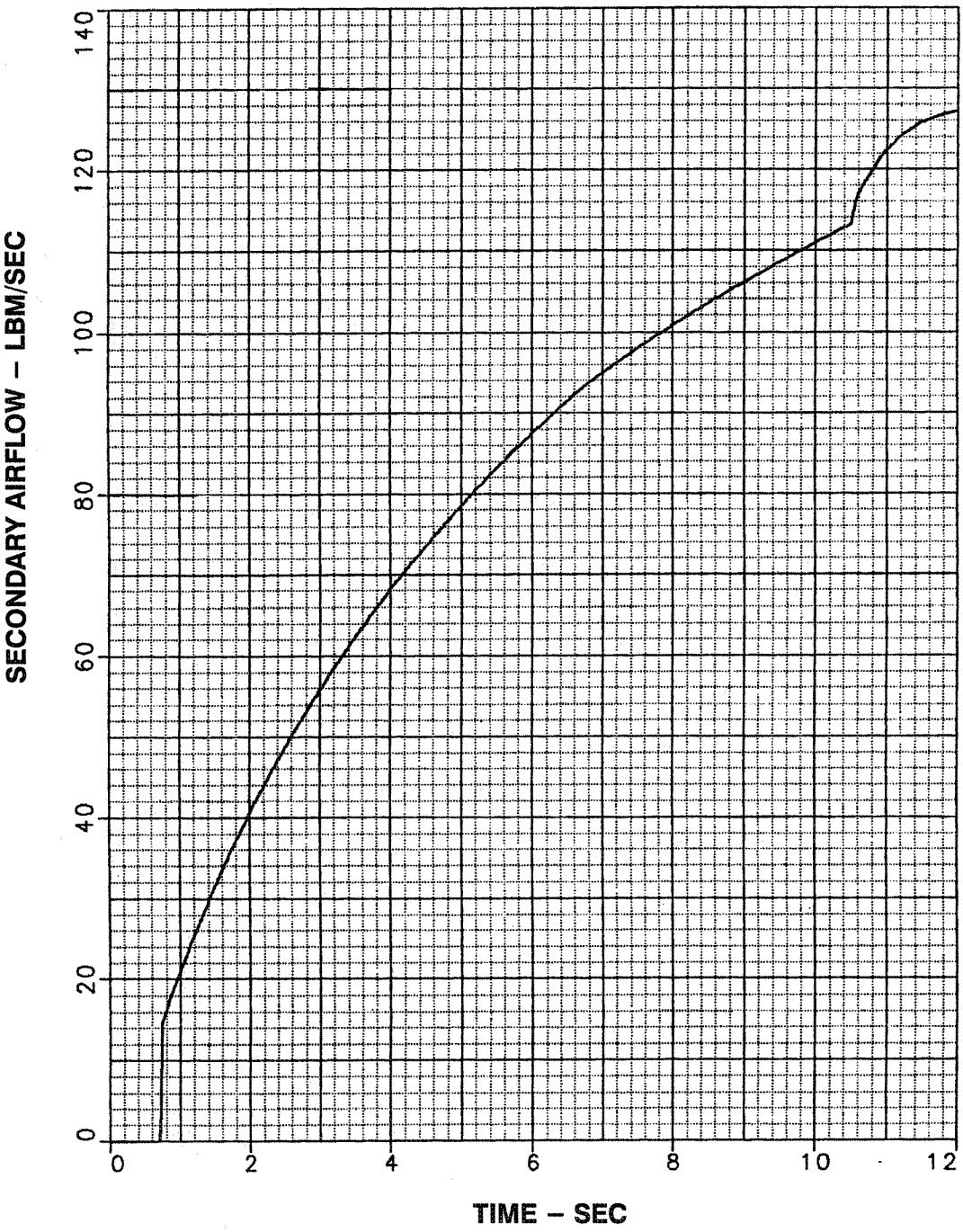

Figure 64. Secondary Airflow Variation

During this low to high mode transition the CDFS inlet guide vane angle, VGRW(CDF2); the mixing plane areas behind the core driven fan stage, AREA(MXD1) and (MXD2); the rear bypass stream mixing plane area, AREA(DCEX); and the nozzle throat area AREA(AJT) are varied to insure stable operation of the front fan, core driven fan stage and high pressure compressor.

Figure 65 shows that the CDFS inlet guide vane angle is varied from +10 degrees to −17.2 degrees.

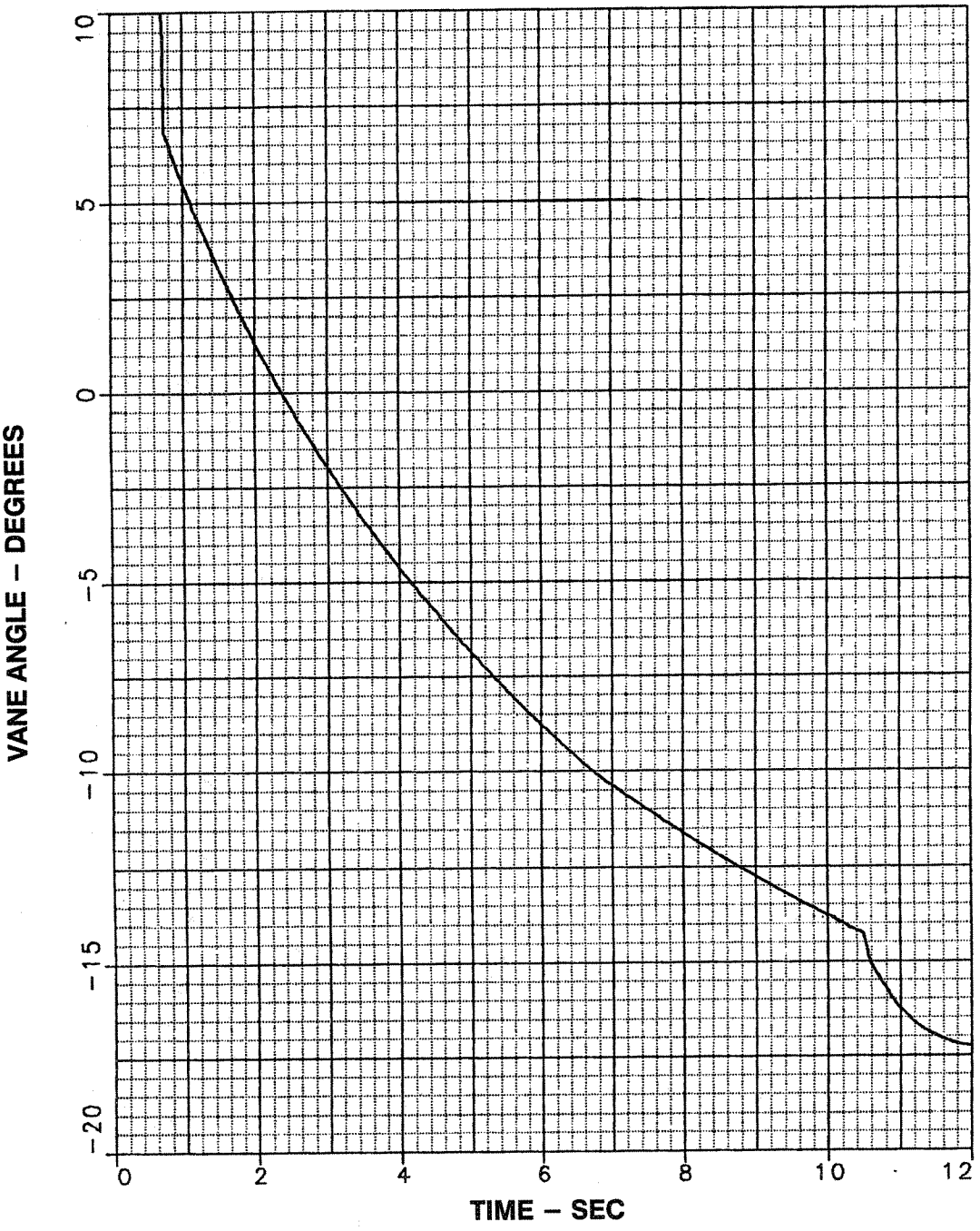

Figure 65. CDFS IGV Angle During Low to High Mode Transition

At the mixing plane immediately downstream of the core driven fan stage, the flow exiting the CDFS OD passes through area (MXD1), while the flow which bypasses the CDFS passes through area (MXD2). A variable area mixer is required to achieve stable operation during the mode transition. Figure 66 and Figure 67 illustrate how these areas are varied. Although the areas have the same values in the low and high modes of operation they must be varied during the transition.

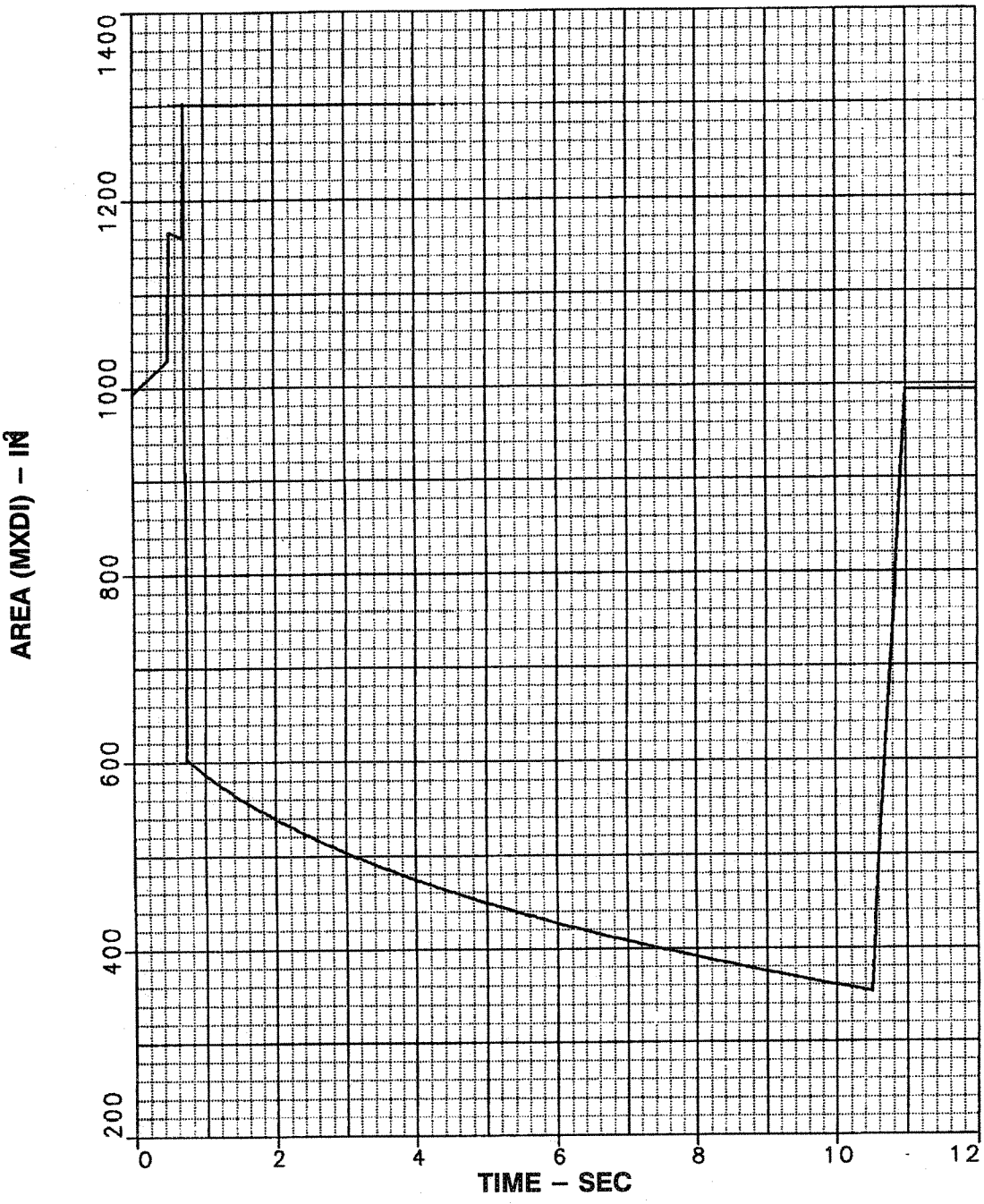

Figure 66. CDF Exit Stream Mixing Plane Area, AREA (MXD1)

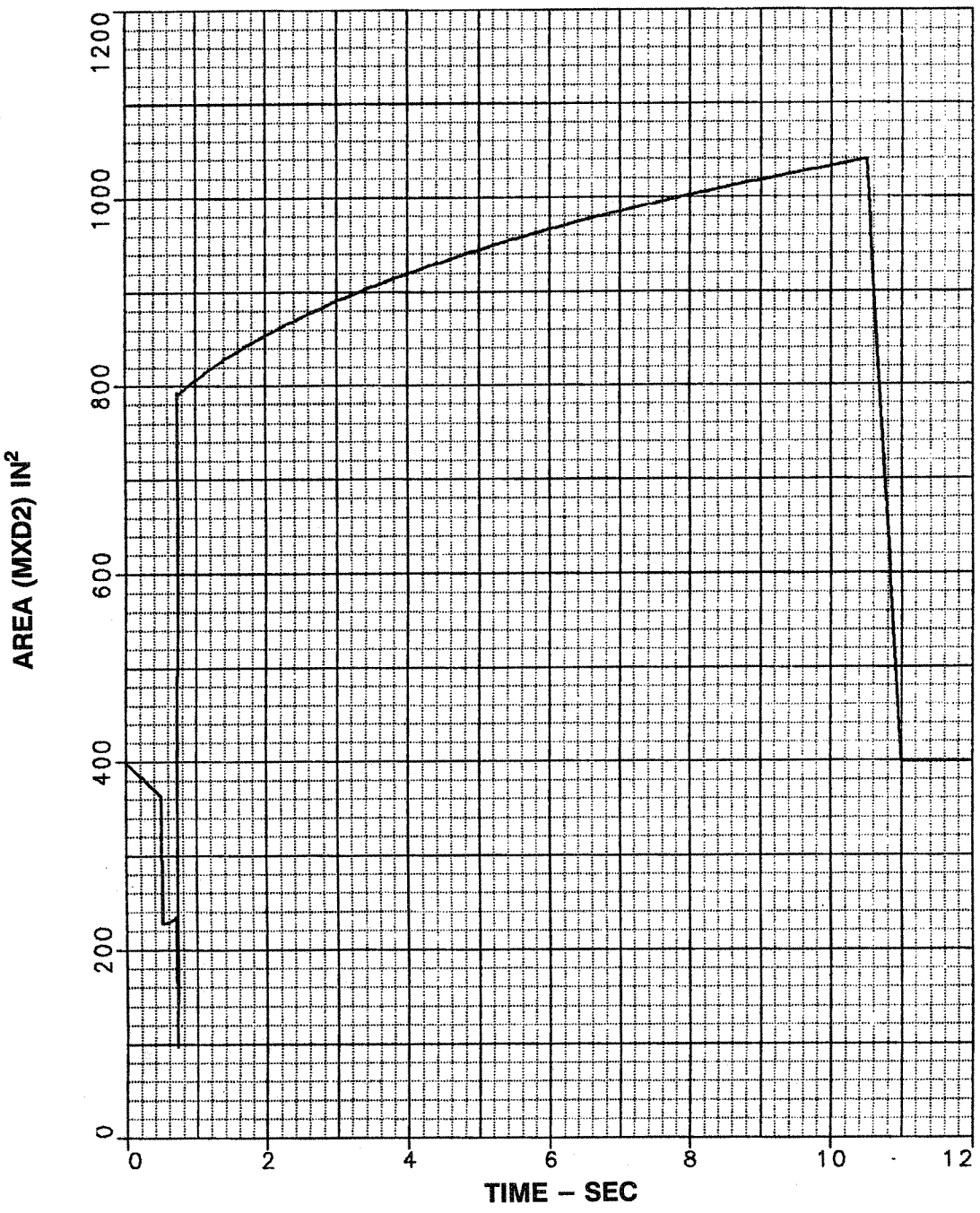

Figure 67. CDF Bypass Stream Mixing Plane Area, AREA (MXD2)

At the rear mixing plane, only the bypass area is variable and it must be increased from 825 in^2 during low mode operation to 2178 in^2 during high mode operation. During the mode transition, a linear variation of this area with time was incorporated, as shown in Figure 68.

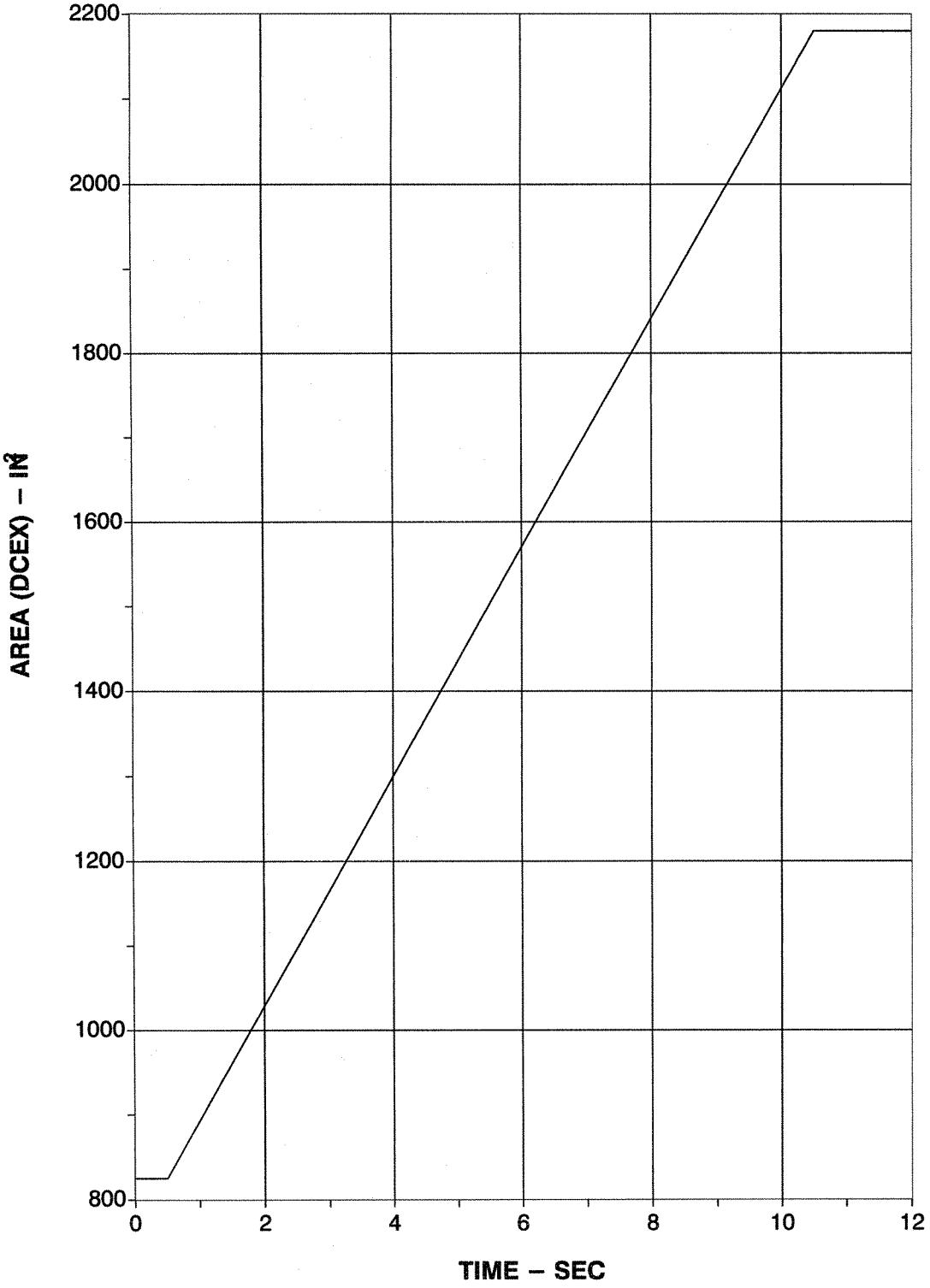

Figure 68. Rear Bypass Mixing Plane Area, AREA (DCEX)

The exhaust nozzle throat area variation during the low to high mode transient is presented in Figure 69. The nozzle area varies from 1735 in^2 to 2400 in^2.

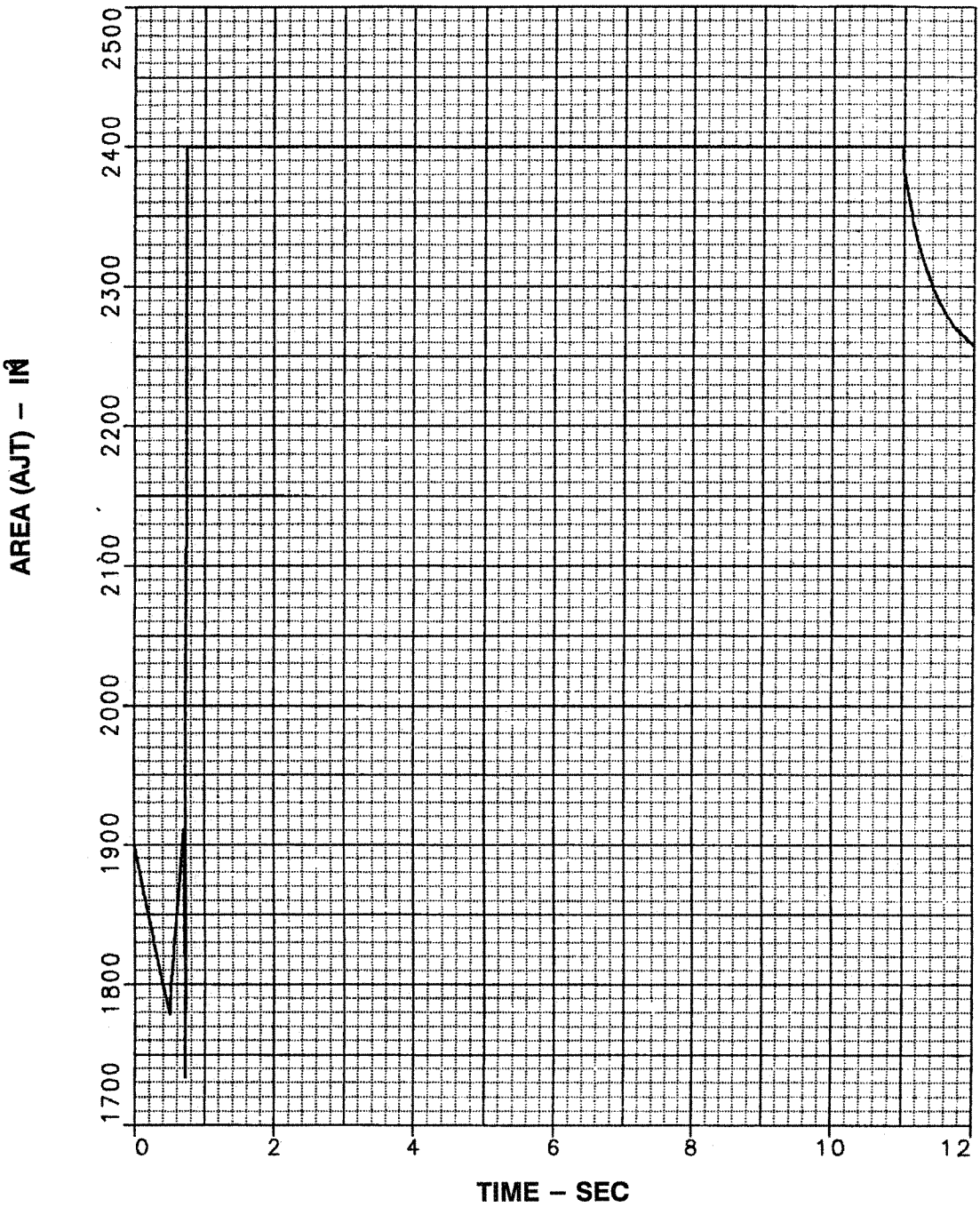

Figure 69. Exhaust Nozzle Throat Area Variation

The variations in fuel flow and combustor exit temperature are presented in Figure 70 and Figure 71. The spike in fuel flow after the valve has reached its high mode position at the 10.5 second point could be eliminated by further study if we were to develop this concept. However, in this transient analysis, we were mainly concerned with achieving stable component operation.

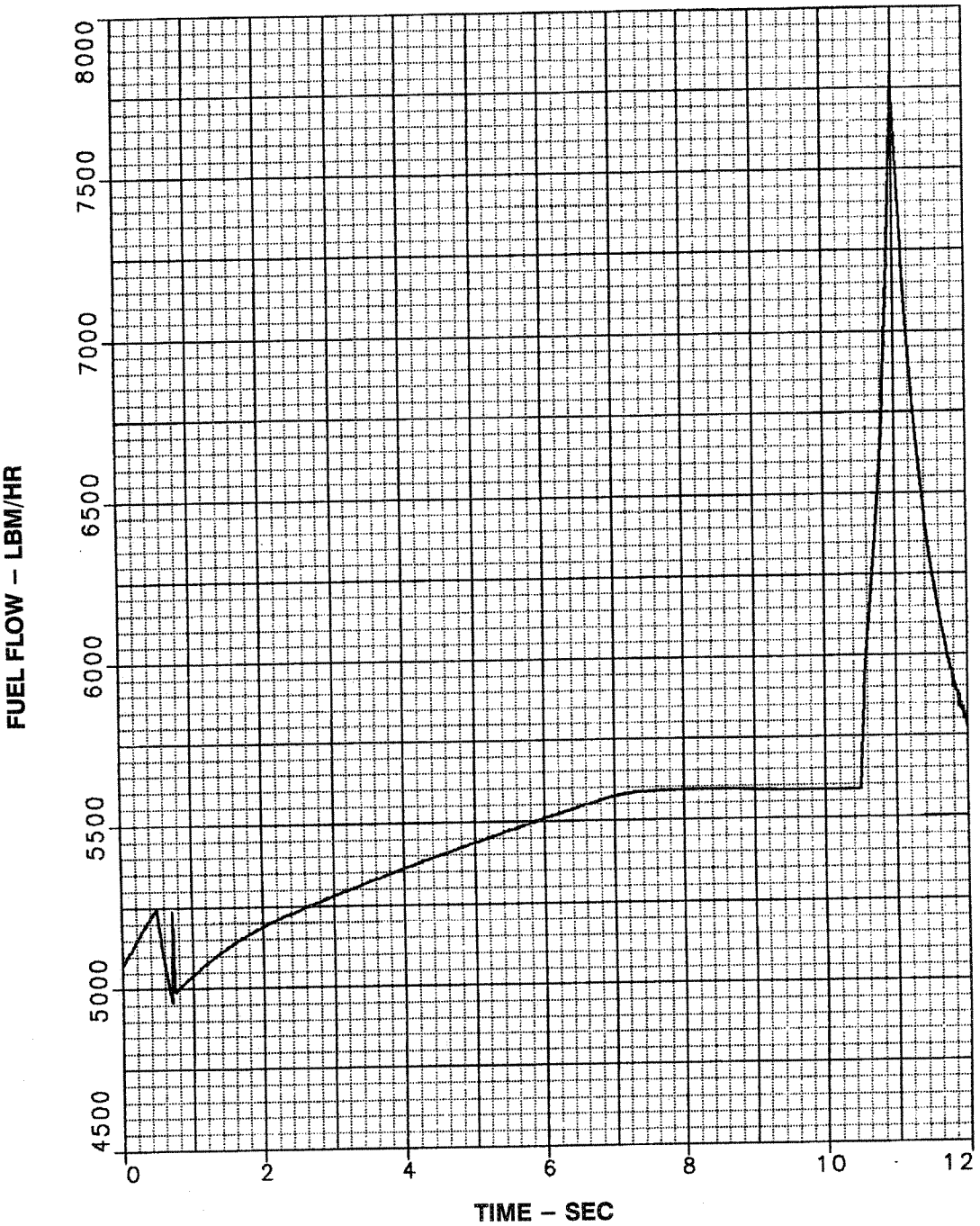

Figure 70. Fuel Flow Variation During Low to High Mode Transition

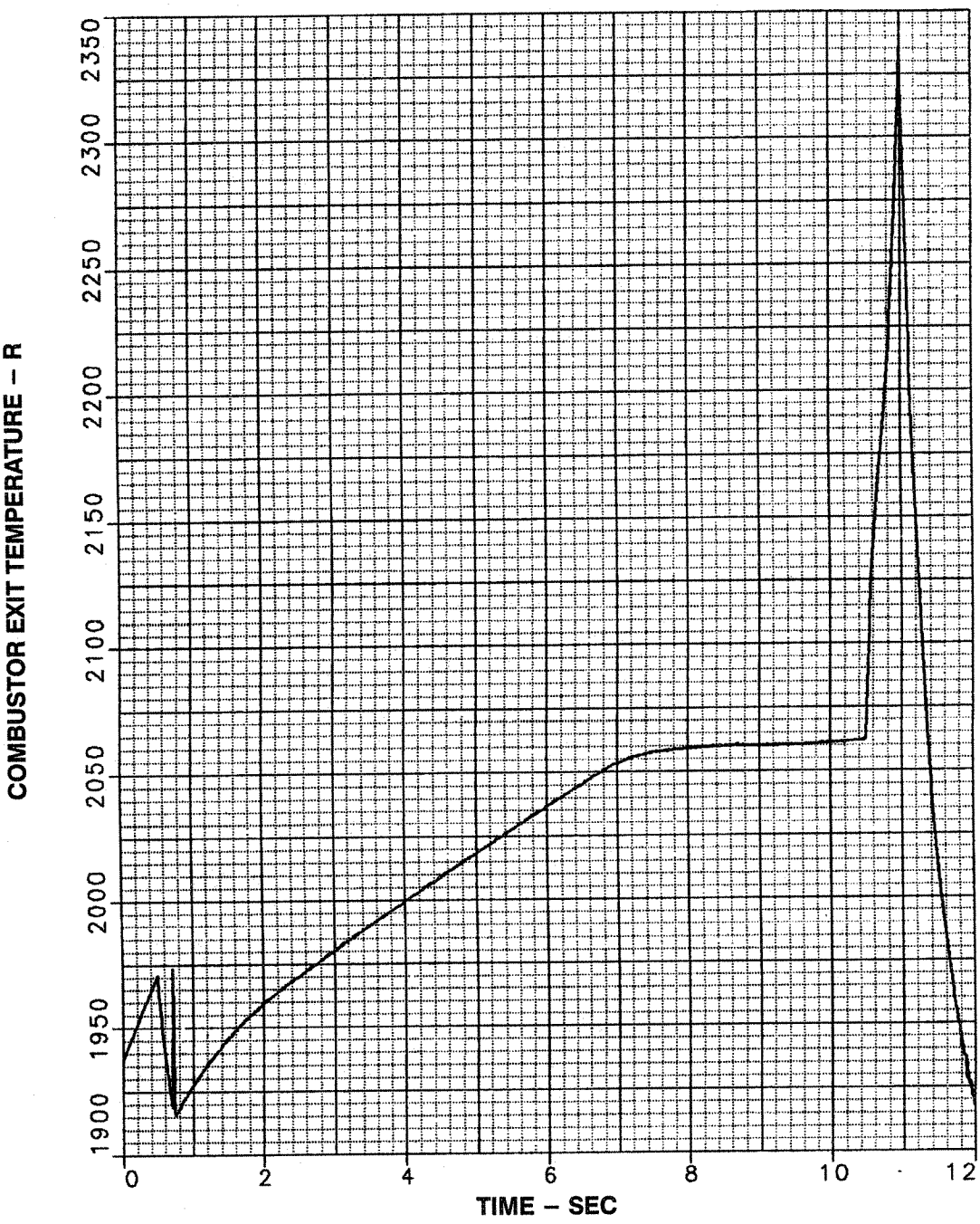

Figure 71. Combustor Exit Temperature Variation During Low to High Mode Transition

The variation in net thrust during the high to low mode transition is presented in Figure 72. If this concept is pursued further, studies would be conducted to reduce the thrust variation during the transition.

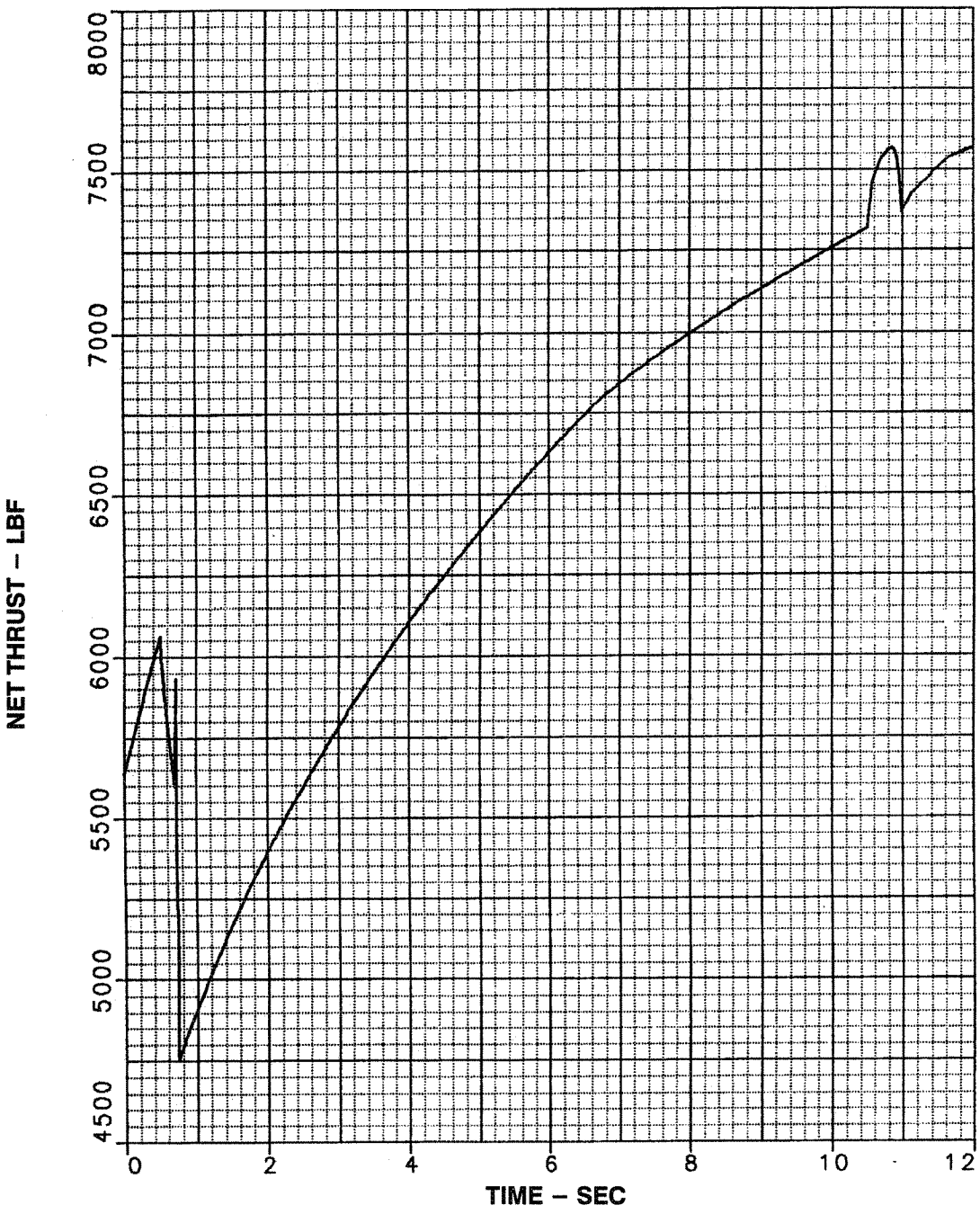

Figure 72. Net Thrust Variation During Low to High Mode Transition

During the low to high mode transition, the front fan rotor speed was held at 4150 rpm, so the fan operating line is along a constant corrected speed line, as shown in Figure 73.

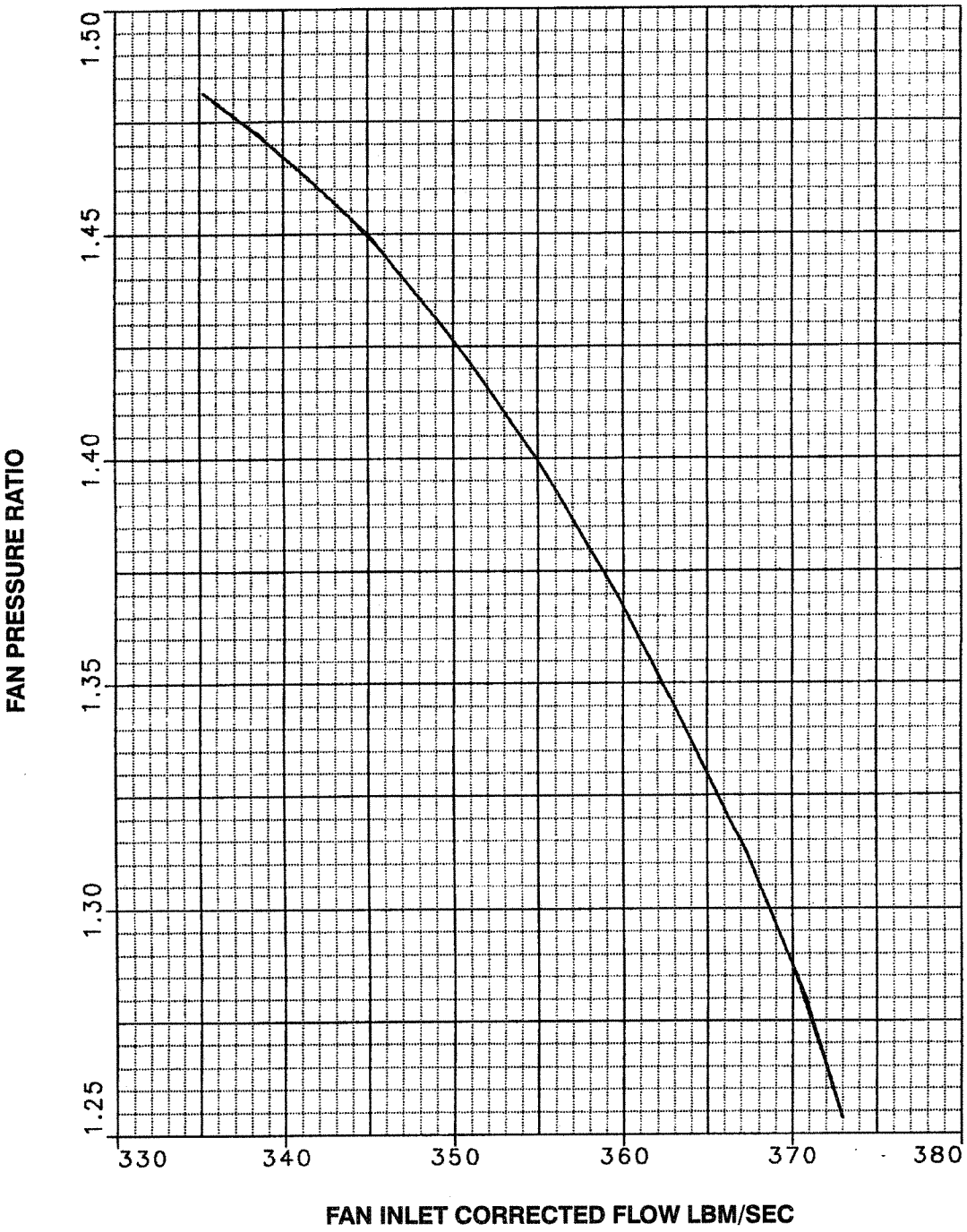

Figure 73. Front Fan Operation During Low to High Mode Transition

The variations in front fan inlet corrected flow, WCFNAA, pressure ratio, PRFNAA, and surge margin are shown in Figure 74, Figure 75 and Figure 76, respectively. The fan surge margin varies from 66% in the low mode to 24% in the high mode. The minimum surge margin of 16.5% occurs at the 11 second point.

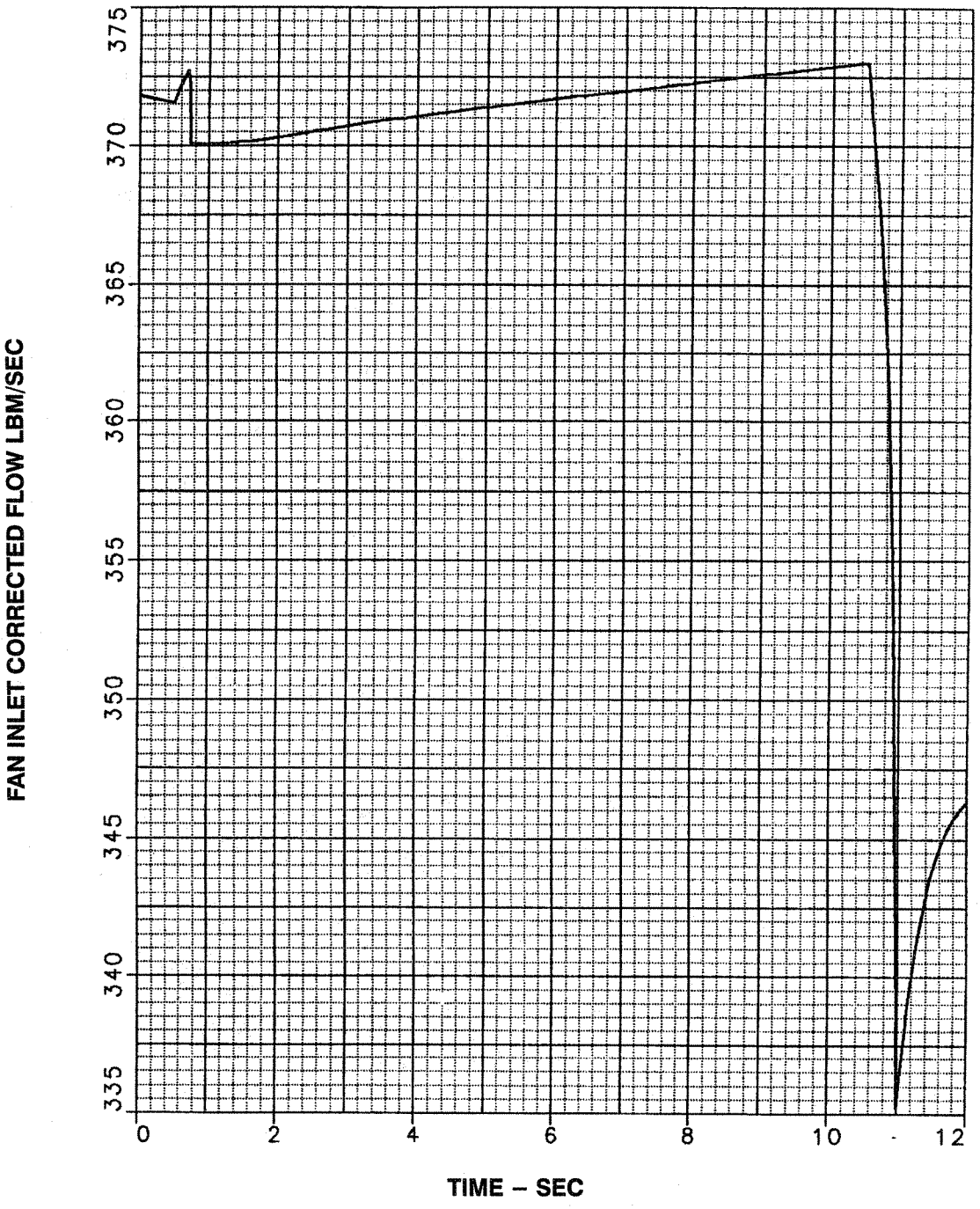

Figure 74. Front Fan Inlet Corrected Flow Variation

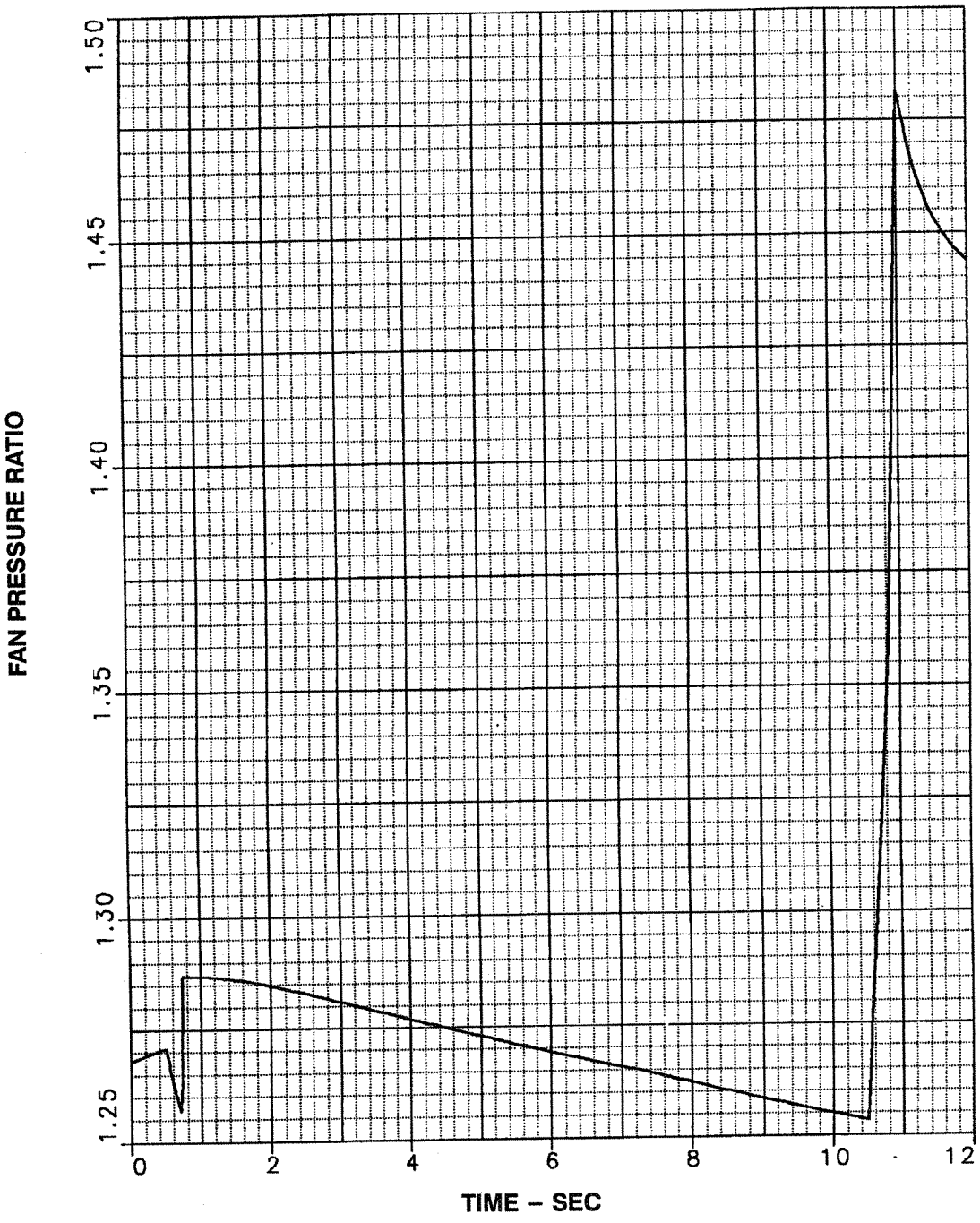

Figure 75. Front Fan Pressure Ratio Variation

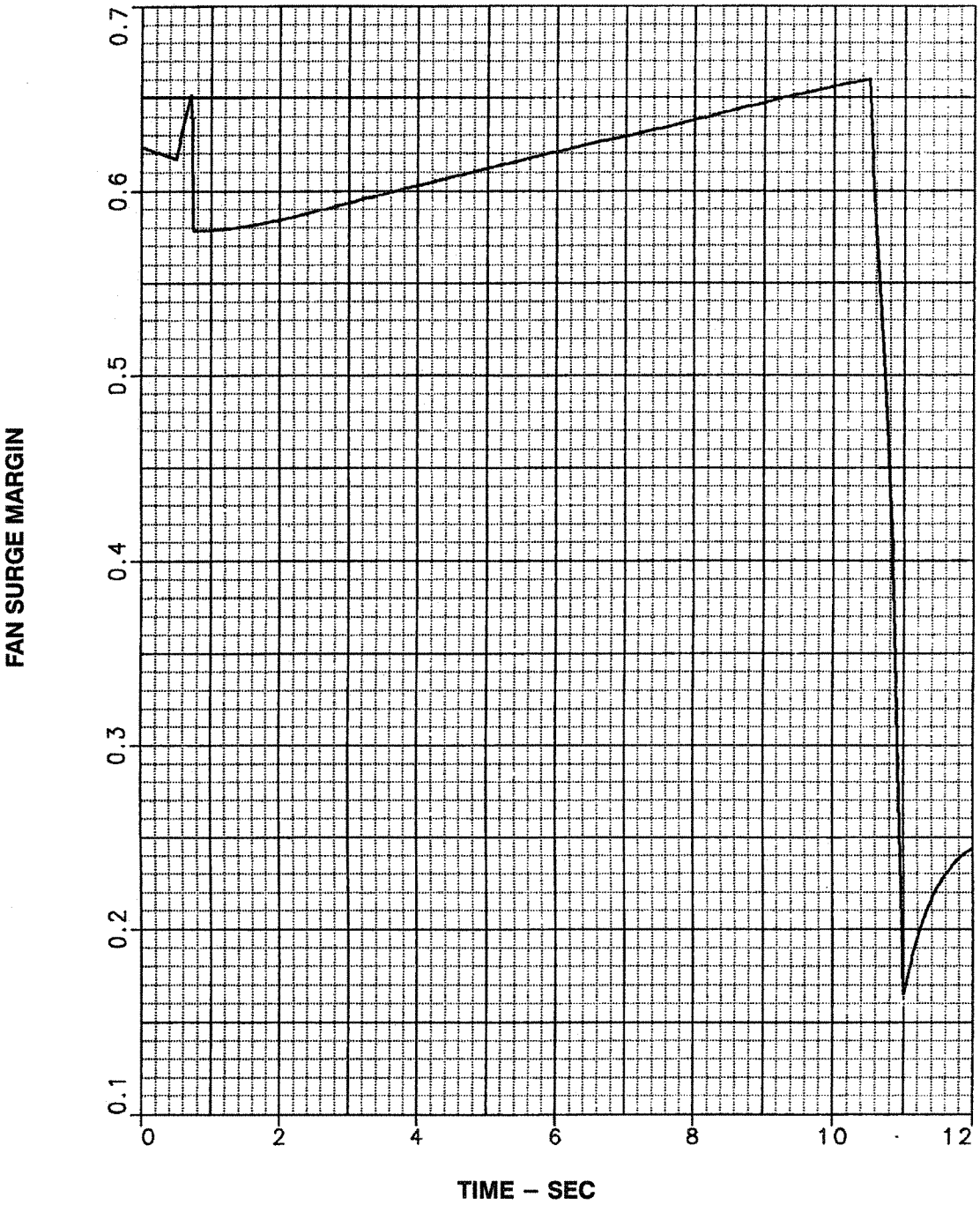

Figure 76. Front Fan Surge Margin Variation

The core driven fan corrected speed, RPMC(CDF2), variation during the low to high mode transition is presented in Figure 77. Although the corrected speed increases during the transition, the corrected flow is reduced, Figure 78, because of the reduction in IGV angle shown in Figure 65.

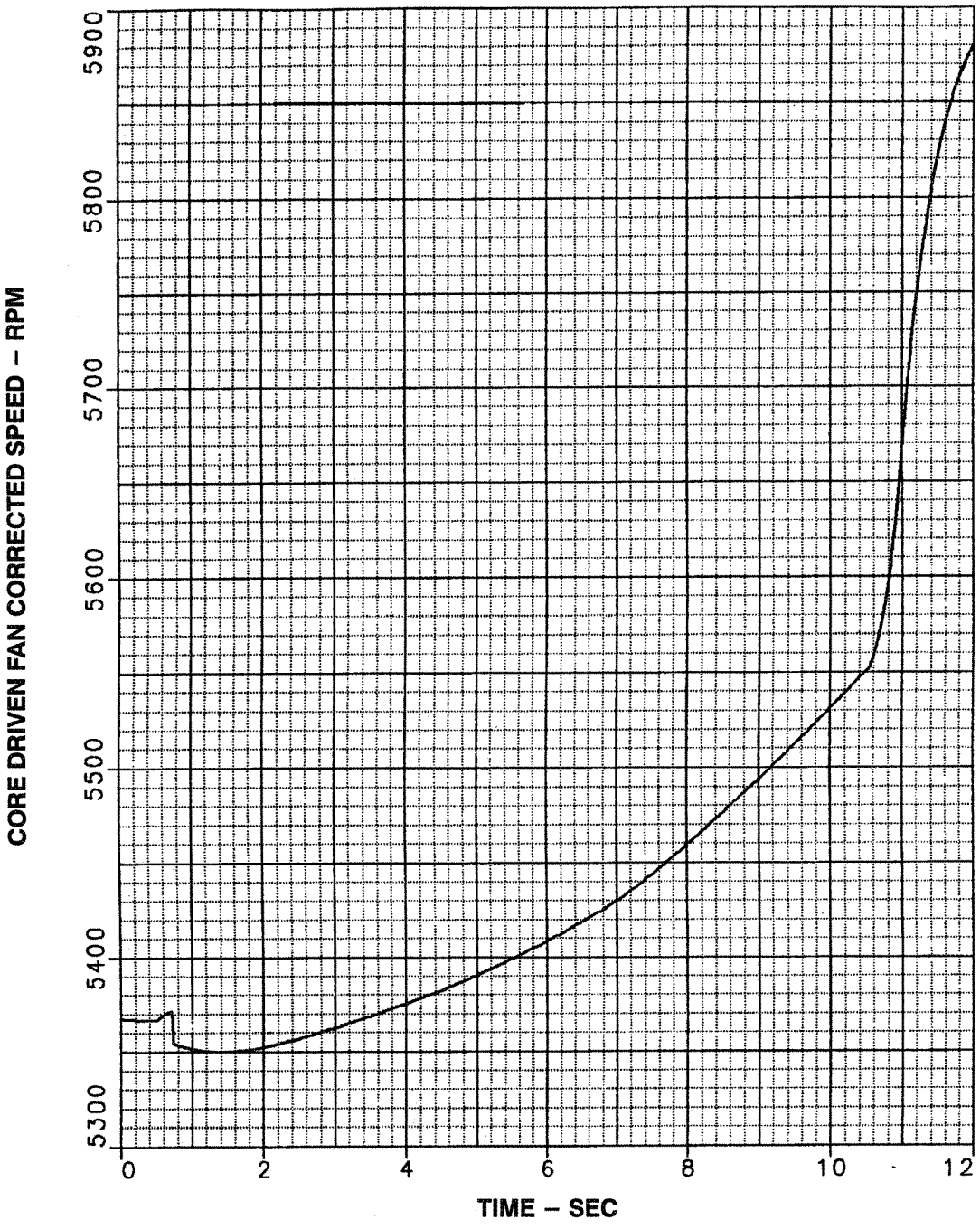

Figure 77. Core Driven Fan Corrected Speed Variation During Low to High Mode Transition

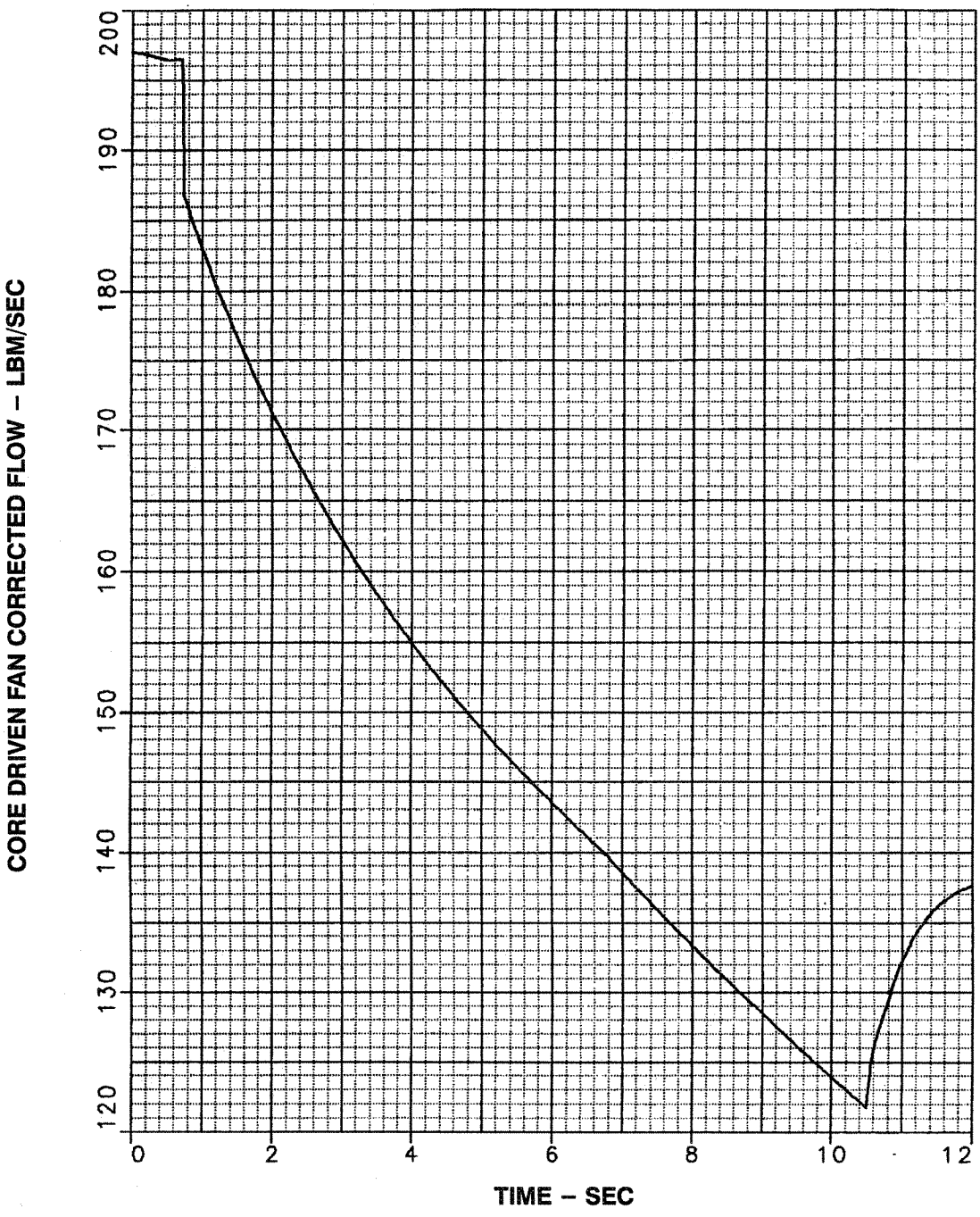

Figure 78. CDF Inlet Corrected Flow During Low to High Mode Transition

Figure 79 presents the variation in CDFS pressure ratio during the transition. The mixing plane area changes were scheduled to keep the CDF surge margin, which is shown in Figure 80, above 20%.

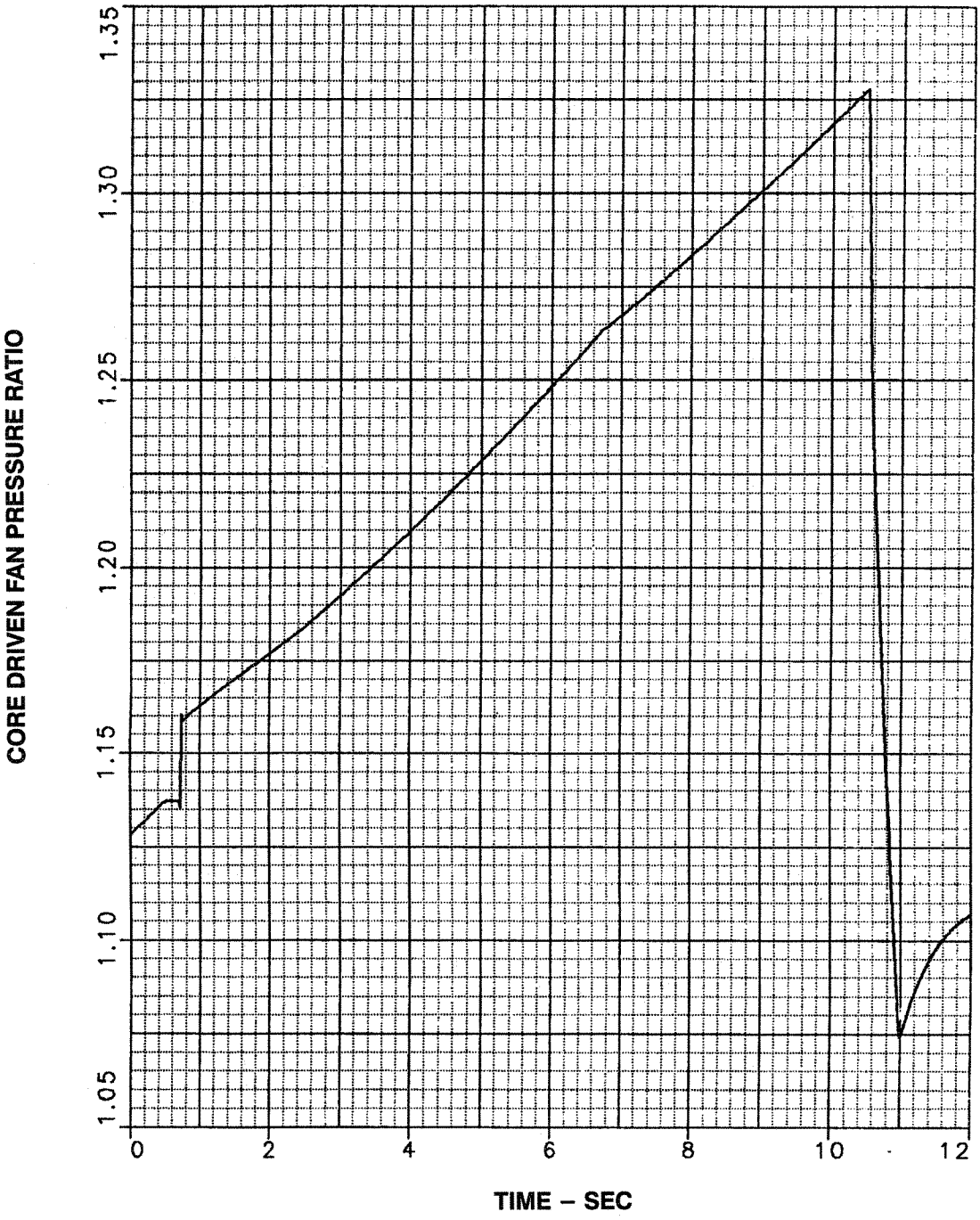

Figure 79. CDFS Pressure Ratio Variation During Low to High Mode Transition

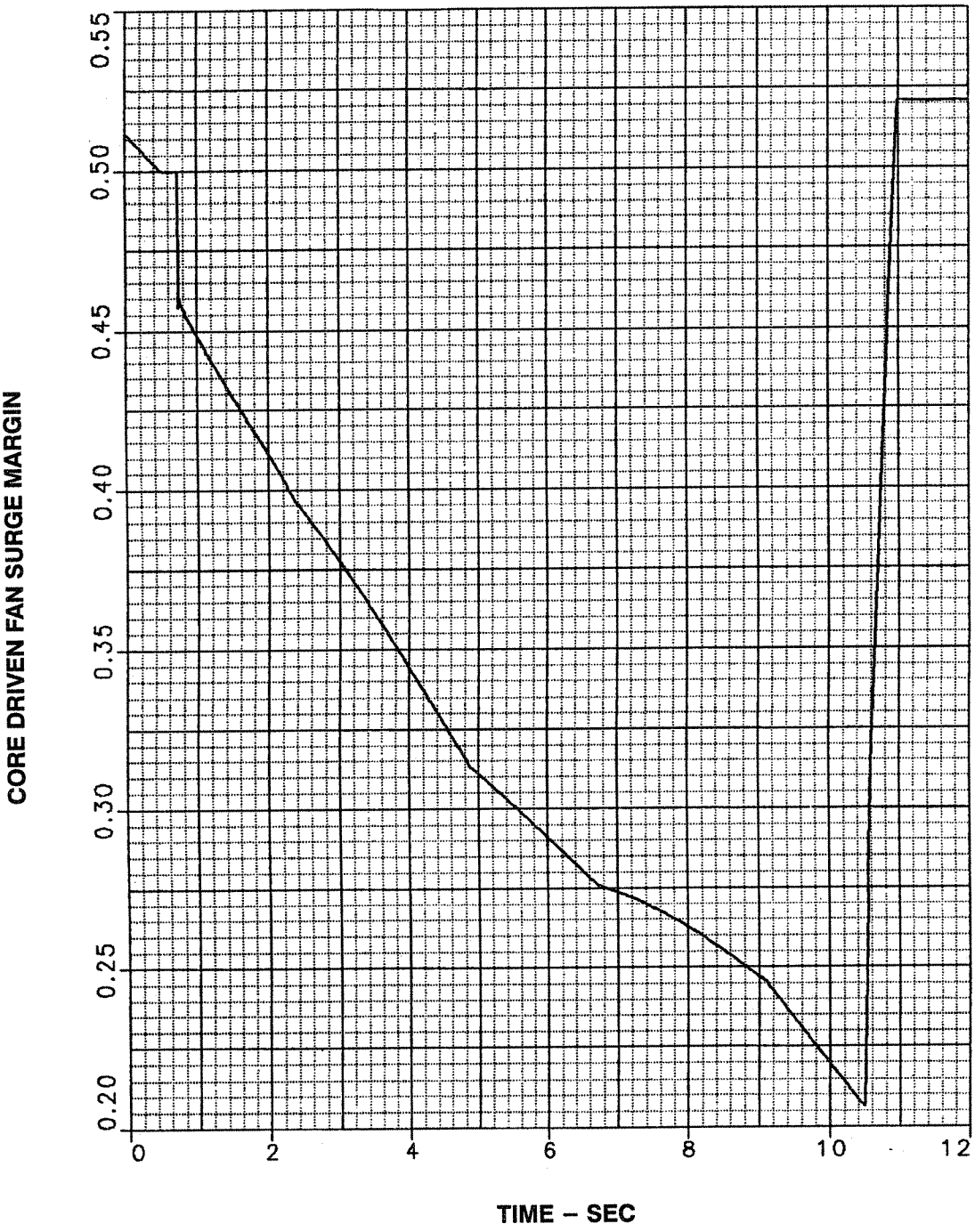

Figure 80. CDFS Surge Margin Variation

Figure 81 presents the CDFS operating line during the transition

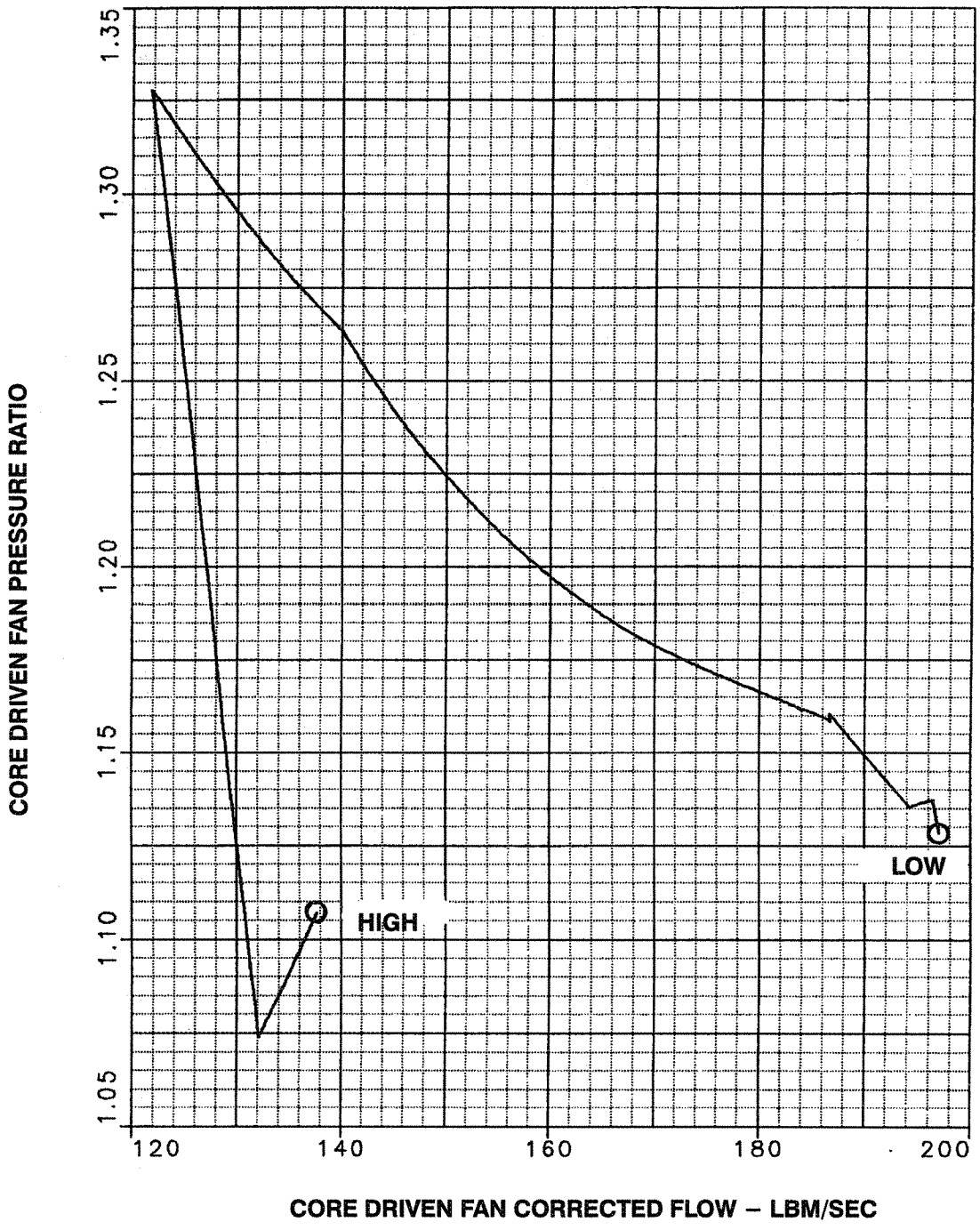

Figure 81. STF 1029 CDFS Operating Line During Low to High Mode Transition

The high compressor (HPC) rotor speed (N2) and operating line during the transition are presented in Figure 82 and Figure 83. The HPC operating line is set to provide a minimum surge margin of 20% during the transition.

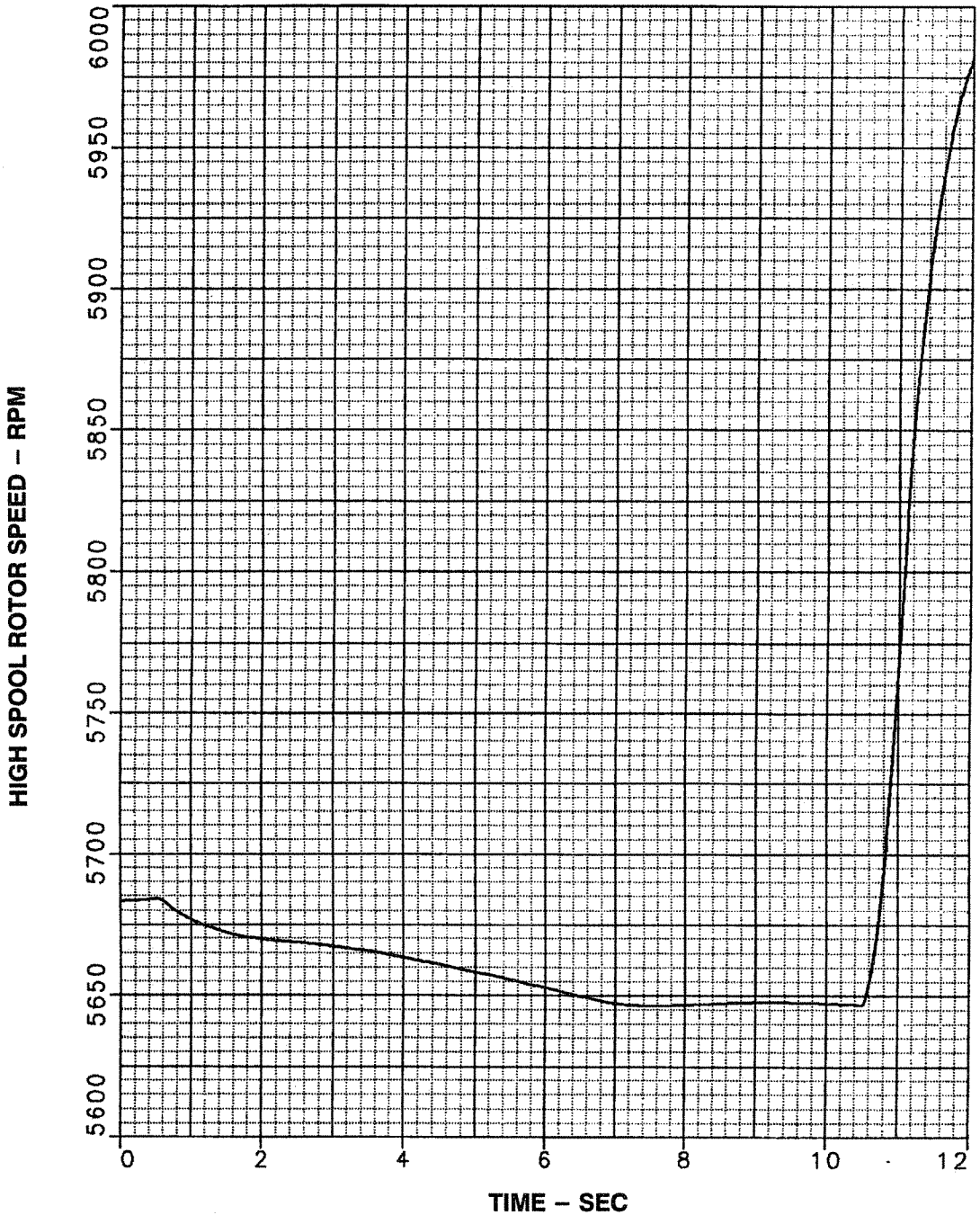

Figure 82. High Spool Rotor Speed

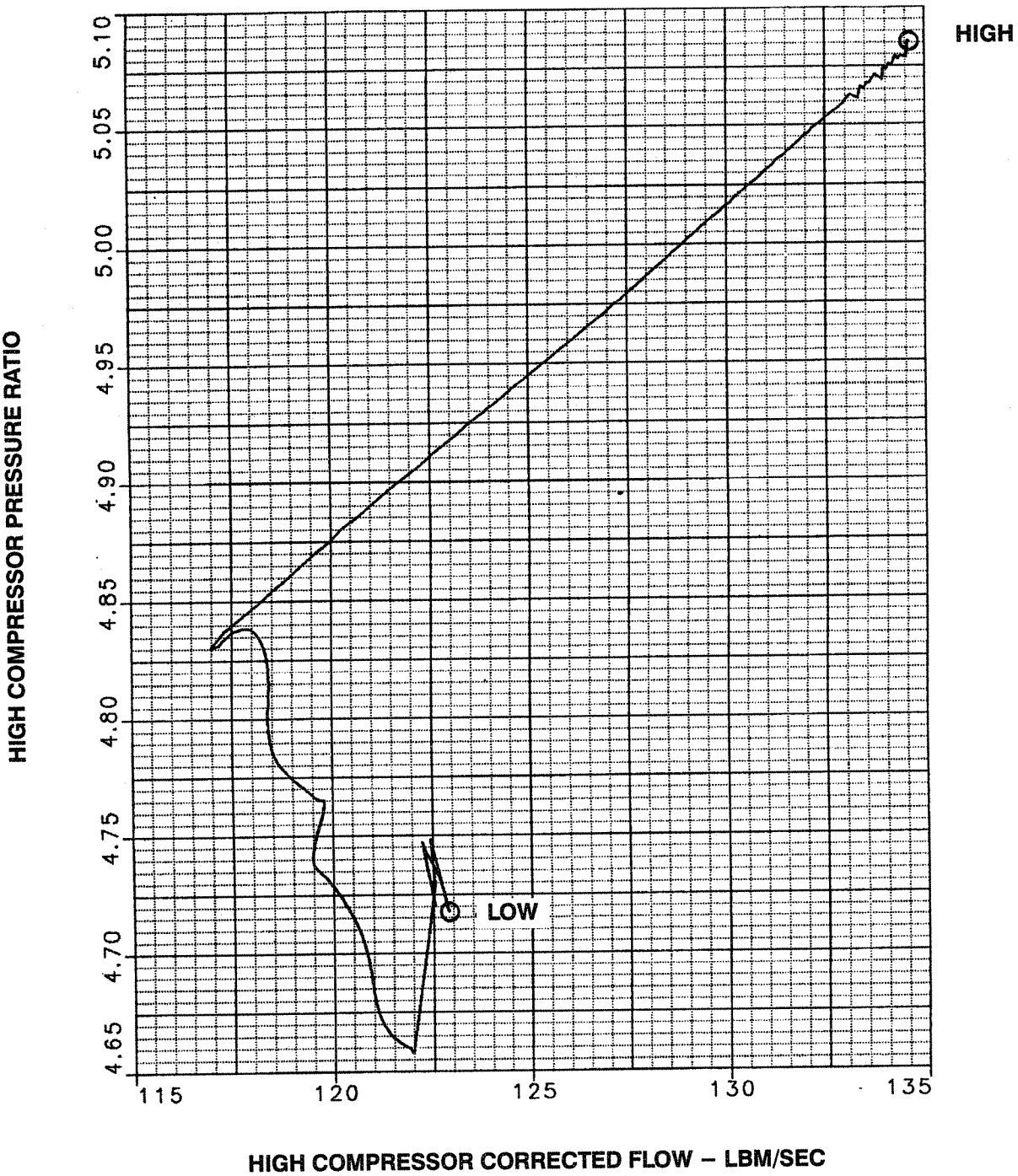

Figure 83. High Compressor Operating Line

Figure 84 and Figure 85 show the variations in HPC inlet corrected flow and pressure ratio during the transition from low to high mode.

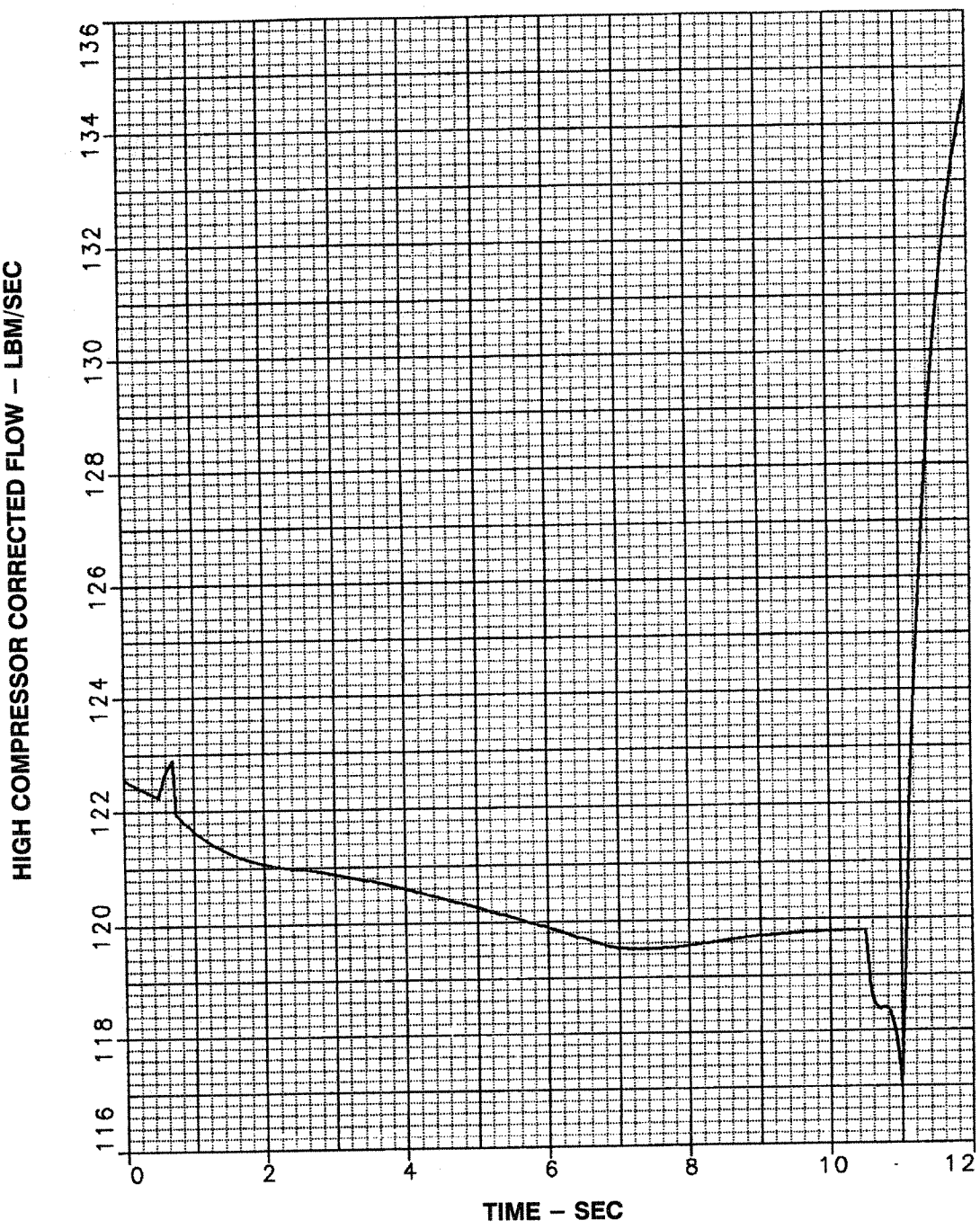

Figure 84. HPC Inlet Corrected Flow

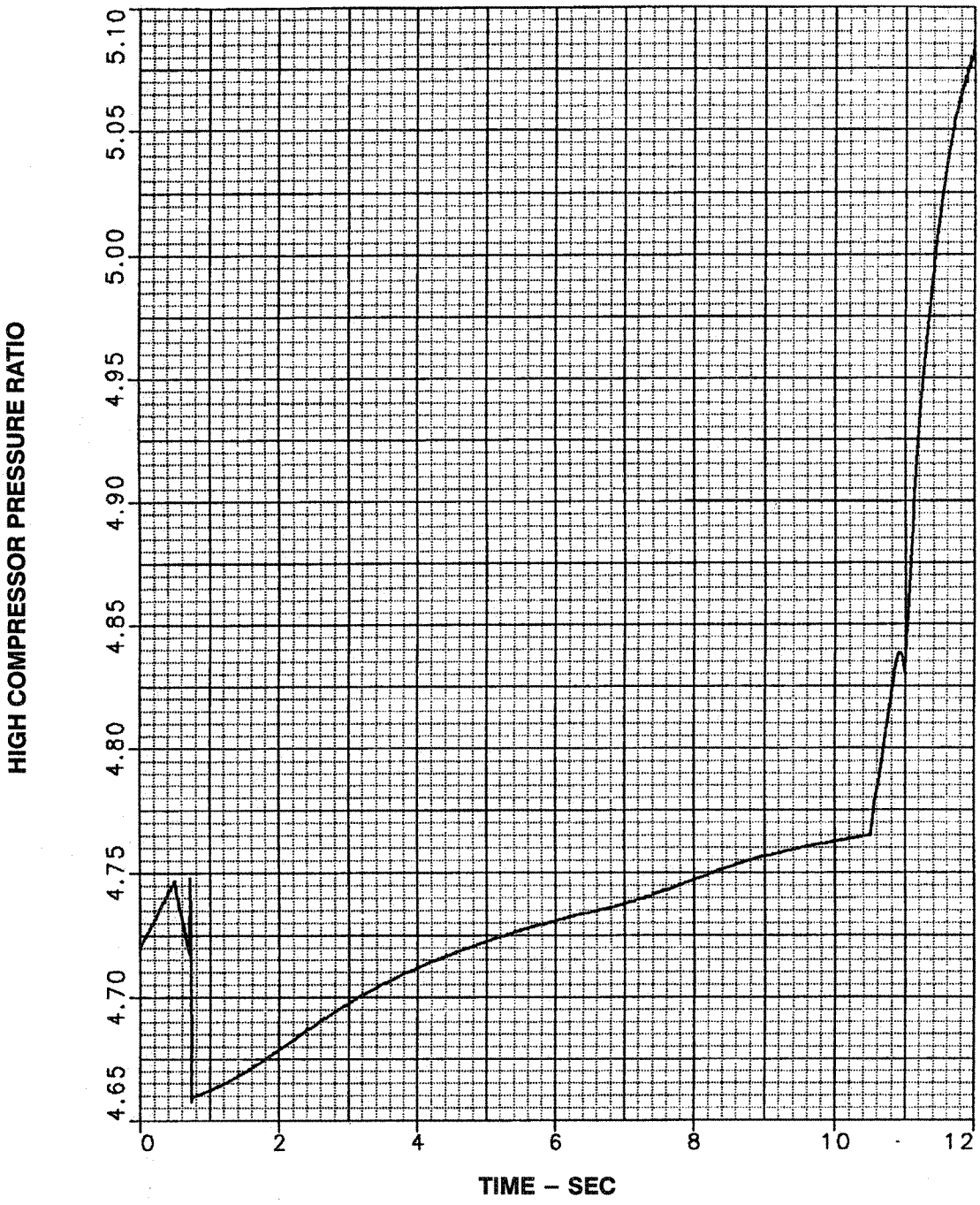

Figure 85. HPC Pressure Ratio

High to Low Mode Transient Analyses:

The partial bypass IFV engine will operate in the high mode during takeoff to reduce jet velocity and noise. The high mode of operation will be continued until the aircraft is beyond a point where low mode operation will not produce noise problems for the community.

For our high mode to low mode transition analysis, an operating flight condition of 14,700 ft – 0.7 Mn was selected. For this dynamic analysis the engine is operated at 50% power in the high mode and the transition to low mode operation was done at a constant fan rotor speed of 5620 rpm.

Table 28 summarizes the high and low mode operating points for this transition.

Table 28. STF1029 High to Low Flow Mode Transition (14,700 ft – 0.7 Mn)

Operating Mode	High Flow	Low Flow
Net Thrust, Lbf	10,000	17,600
Front Fan Speed, rpm	5620	5620
Front Fan Corrected Speed, rpm	5550	5550
Front Fan Corrected Airflow, Lb/sec	545.5	562.3
Front Fan Pressure Ratio	2.005	1.853
Front Fan Surge Margin	25	44
Secondary Flow, Lb/sec	158	0
CDFS (OD) Corrected Airflow, Lb/sec	172.0	163.8
CDFS Pressure Ratio	1.197	1.360
CDFS IGV Setting, °	–20	–10
CDFS Surge Margin, %	64	29
HPC Corrected Flow, Lb/sec	171.8	180.2
HPC Pressure Ratio	6.79	8.18
HPC Rotor Speed, rpm	6871	6952
HPC Corrected Speed, rpm	6077	6227
Combustor Temperature, °R	2270	2910
Front Mixing Plane Outer Area, (MXD2) in^2	399	399
Front Mixing Plane Inner Area, (MXD1) in^2	994	994
Aft Mixing Plane Bypass Stream Area, in^2	2178	825
Aft Mixing Plane Core Stream Area, in^2	1026	1026
Exhaust Nozzle Throat Area in^2	1897	1088

The high to low mode transition was conducted with the valve being transitioned from its high mode to its low mode position between the 0.5 and 10.5 second points shown in the transient plots. Figures 86 and 87 show the linear valve area transitions that were used. In the high flow mode, at time = 0.5 seconds, all the CDFS OD inlet flow is provided by secondary flow. At time = 10.5 seconds all the CDFS OD inlet flow comes from the front fan.

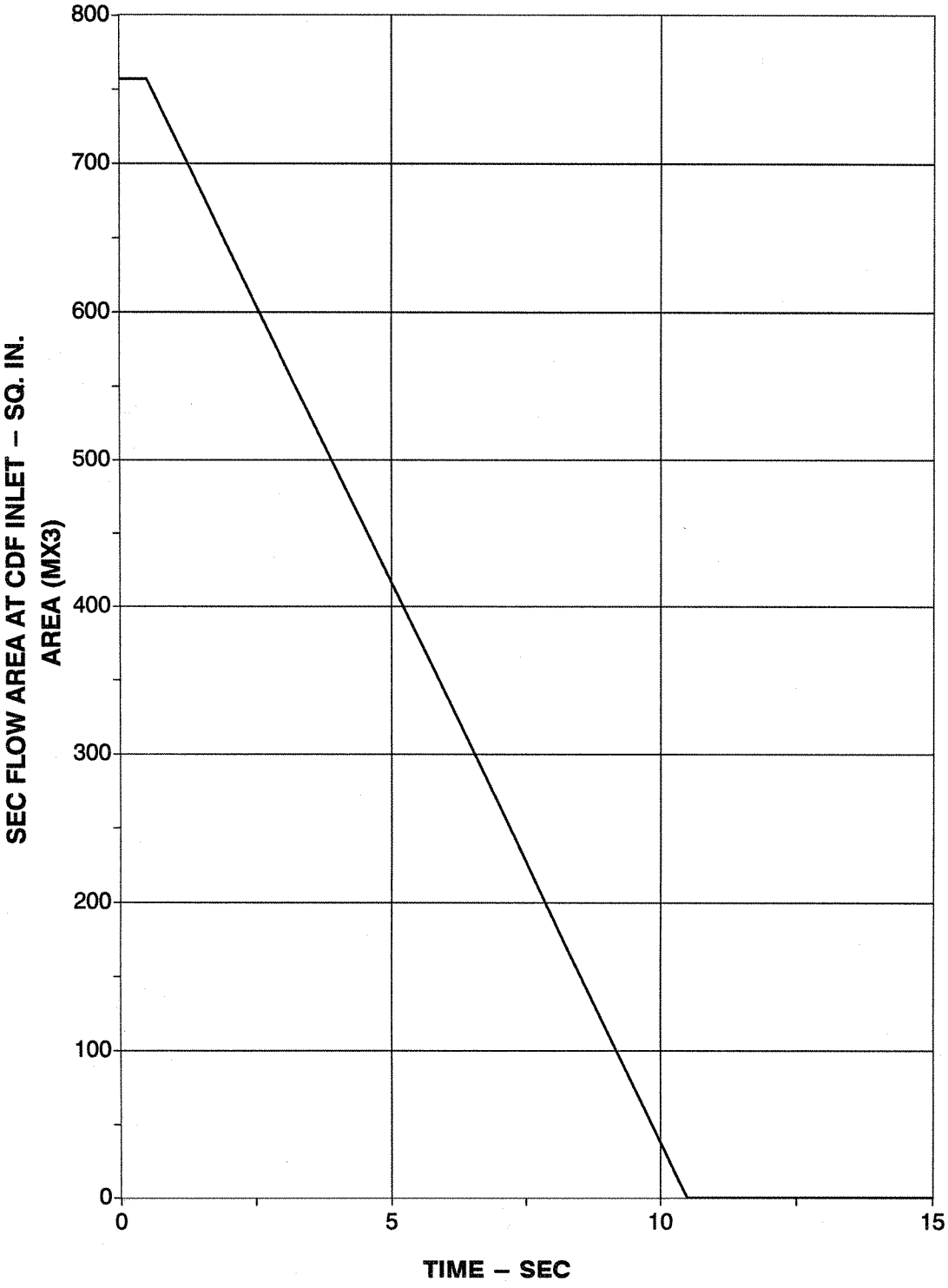

Figure 86. Valve Area of CDFS Inlet Which Feeds Secondary Flow Into the CDFS OD

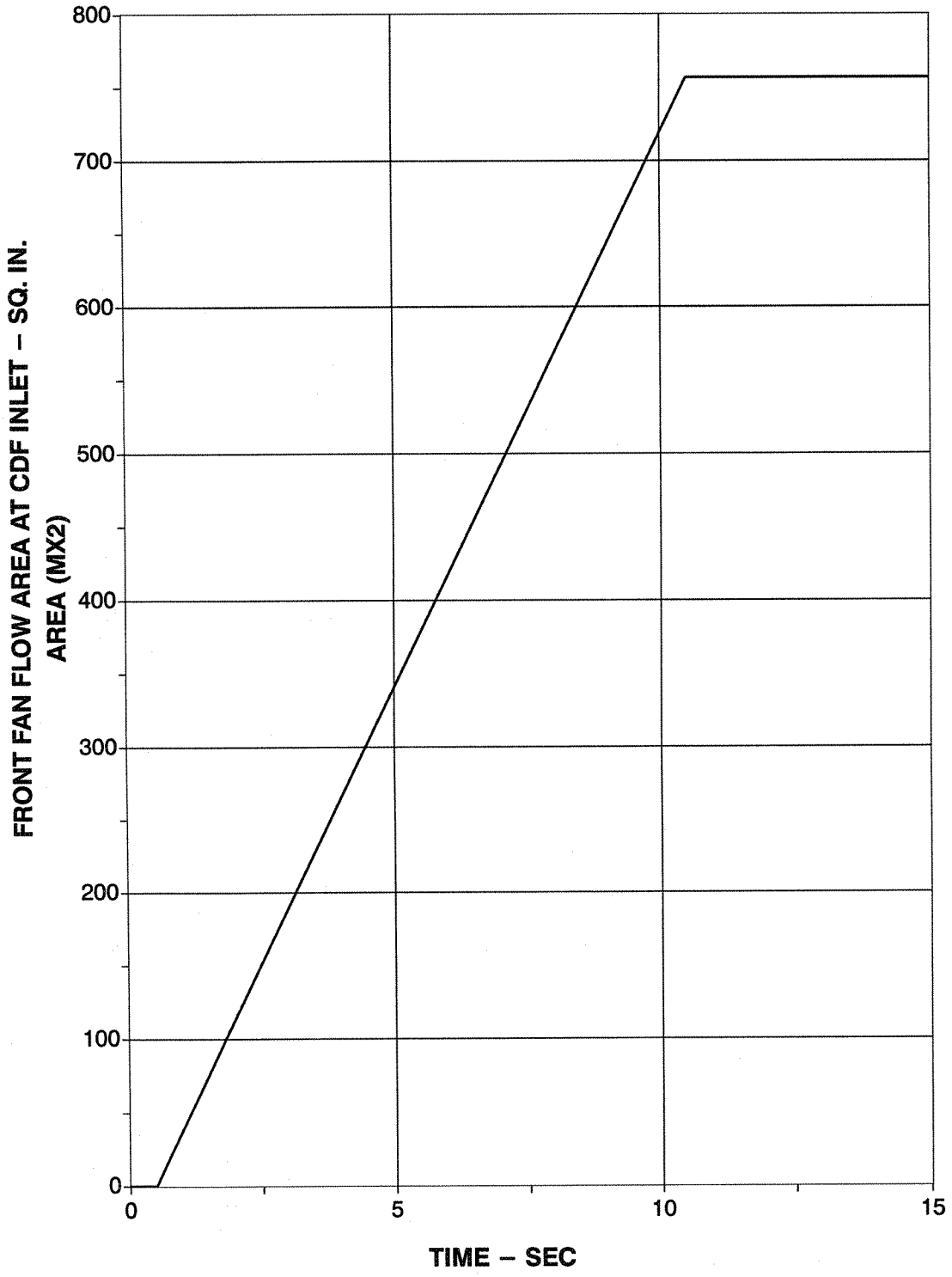

Figure 87. Valve Area at CDFS Inlet Which Feeds Front Fan Flow into the CDFS OD

The amount of secondary flow that is brought into the engine is shown in Figure 88. At the 0.5 second point, all this air is fed into the core driven fan stage. Between 0.5 and 9.0 seconds the valve position, front and rear mixing plane areas, and exhaust nozzle area are varied to reduce the amount of secondary flow into the engine and to ensure stable engine operation.

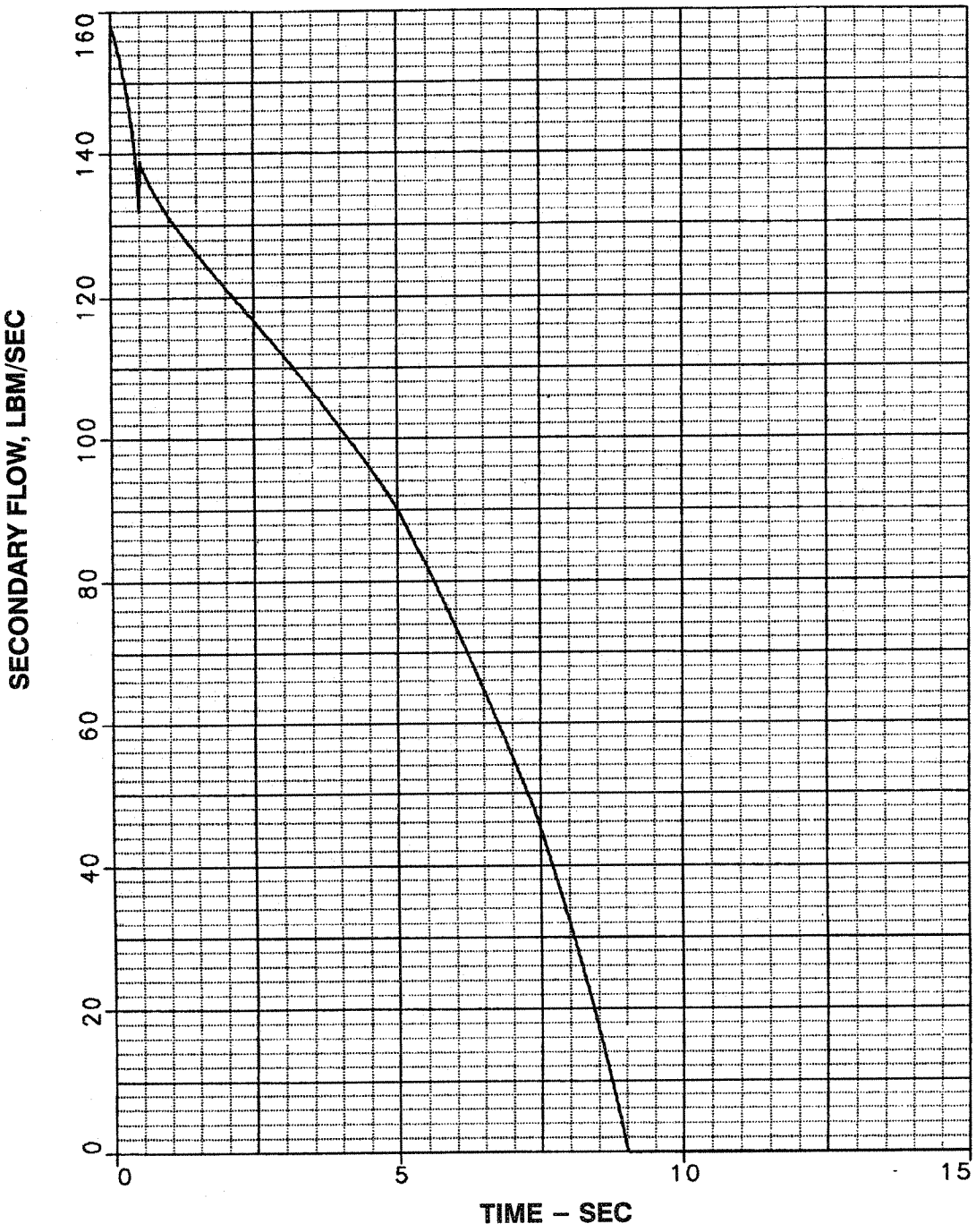

Figure 88. Secondary Airflow Variation
TIME – SEC

Figure 89 and Figure 90 show the variations in the front mixing plane areas, where the CDFS OD exit flow in area MXD1 is mixed with the flow in area MXD2 that comes out of the valve and bypasses the core driven fan stage.

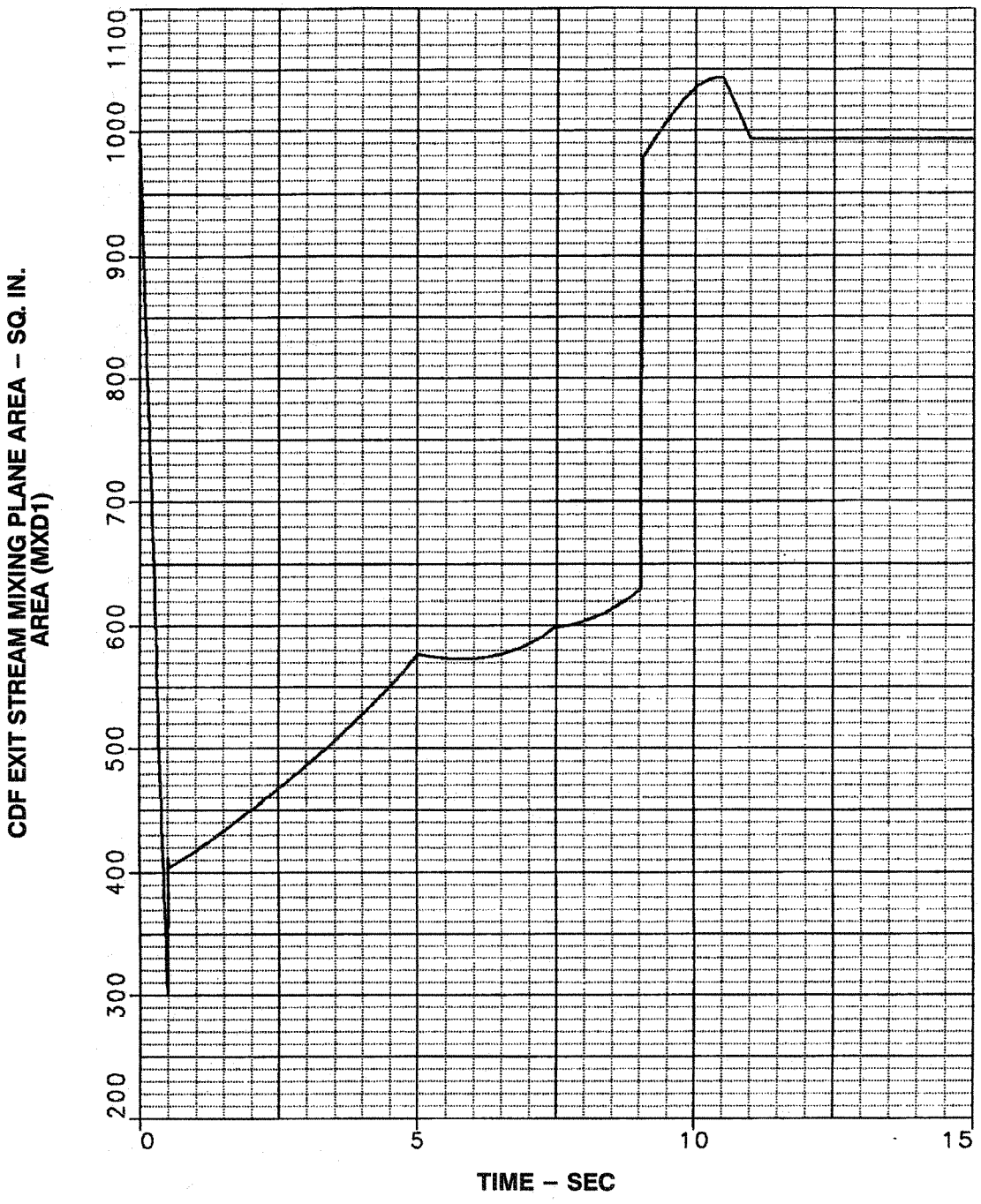

Figure 89. CDF Exit Stream Mixing Plane Area Variation

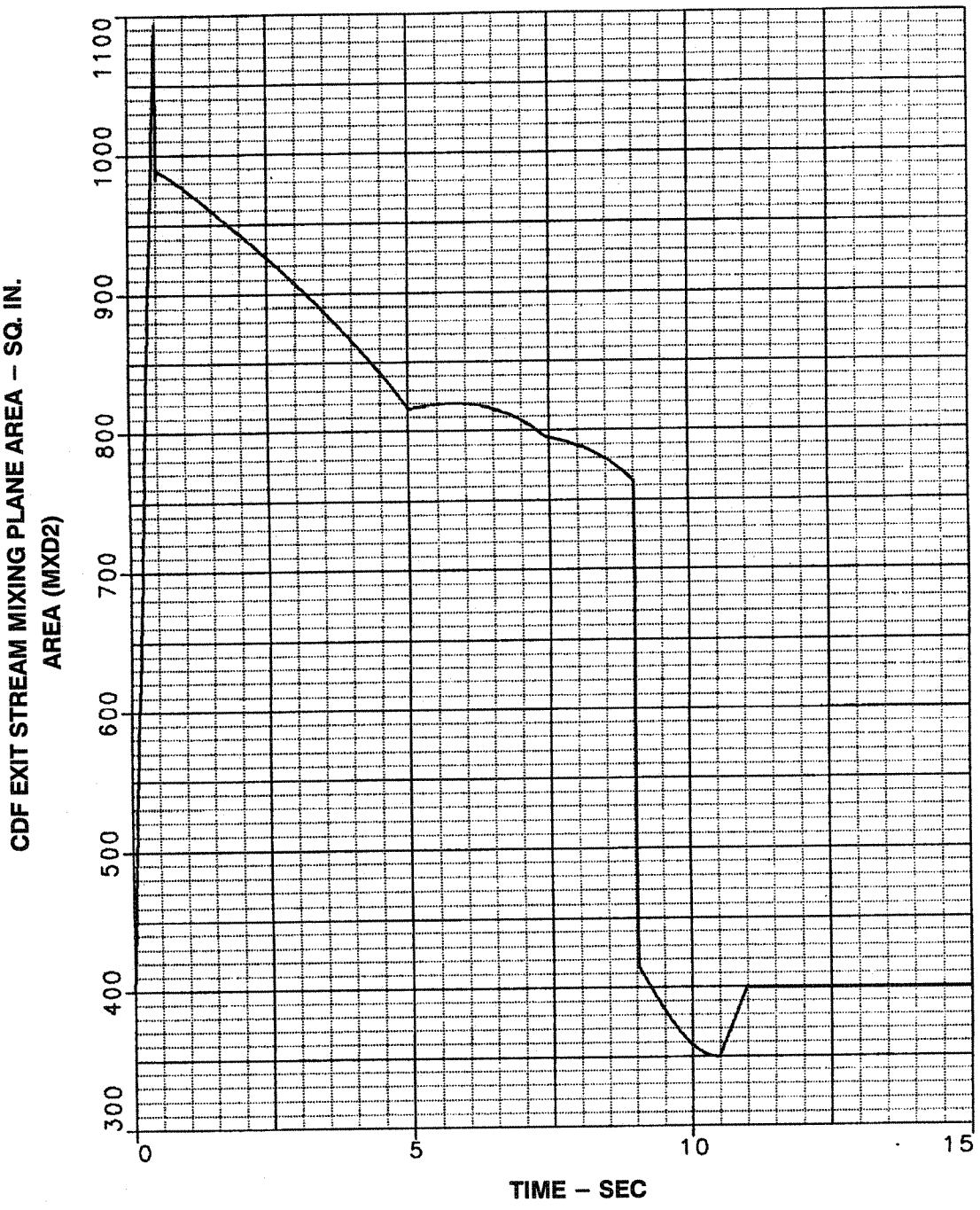

Figure 90. CDF Bypass Stream Mixing Plane Area Variation

The rear mixing plane bypass area (DCEX) variation is shown in Figure 91. This area varies from 2178 in^2 in the high flow mode to 825 in^2 in the low flow mode.

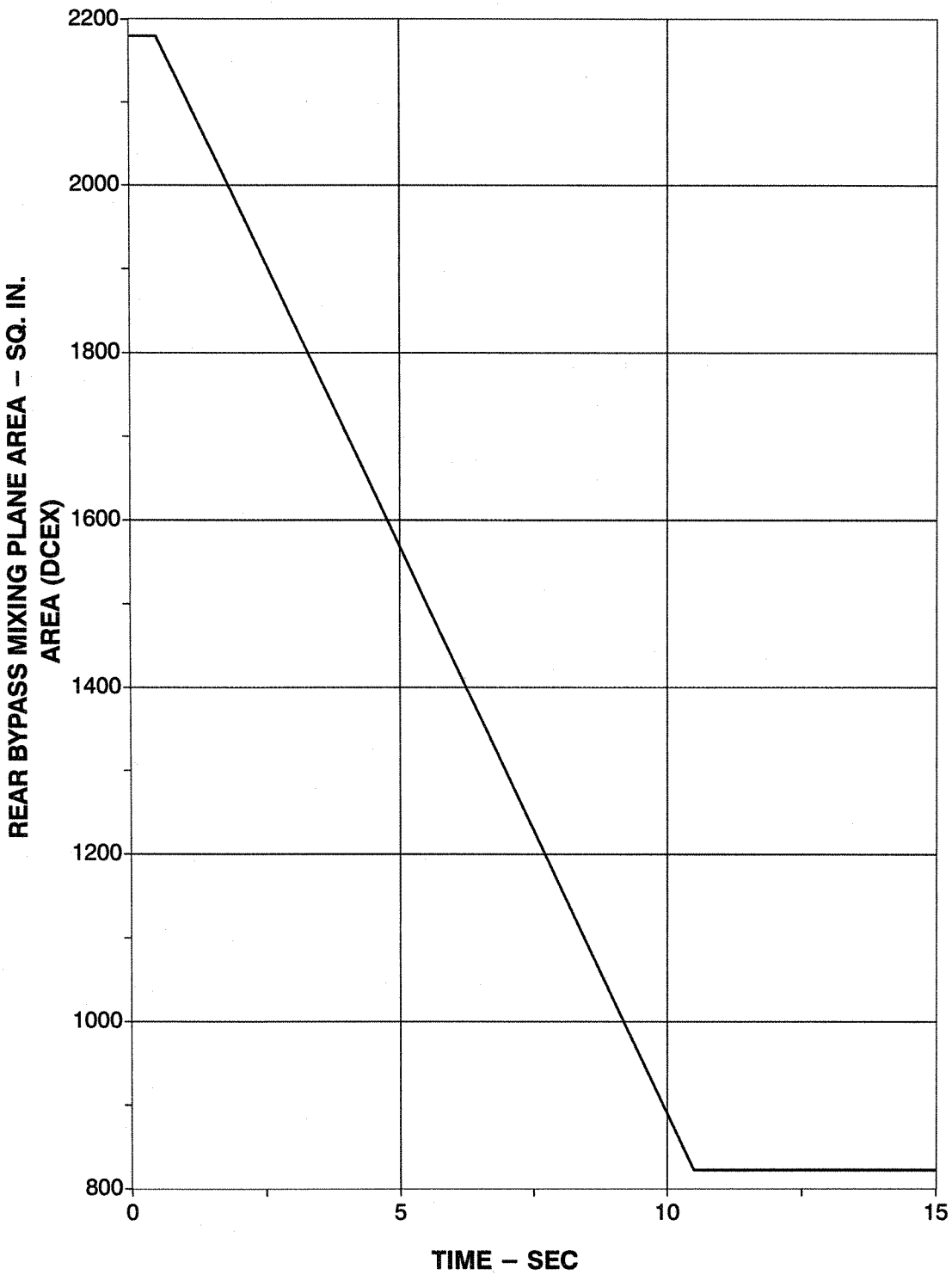

Figure 91. Rear Bypass Mixing Plane Area Variation During High to Low Mode Transition

The exhaust nozzle throat area changed from 1900 in^2 to 1090 in^2 during the high to low mode transition, as shown in Figure 92.

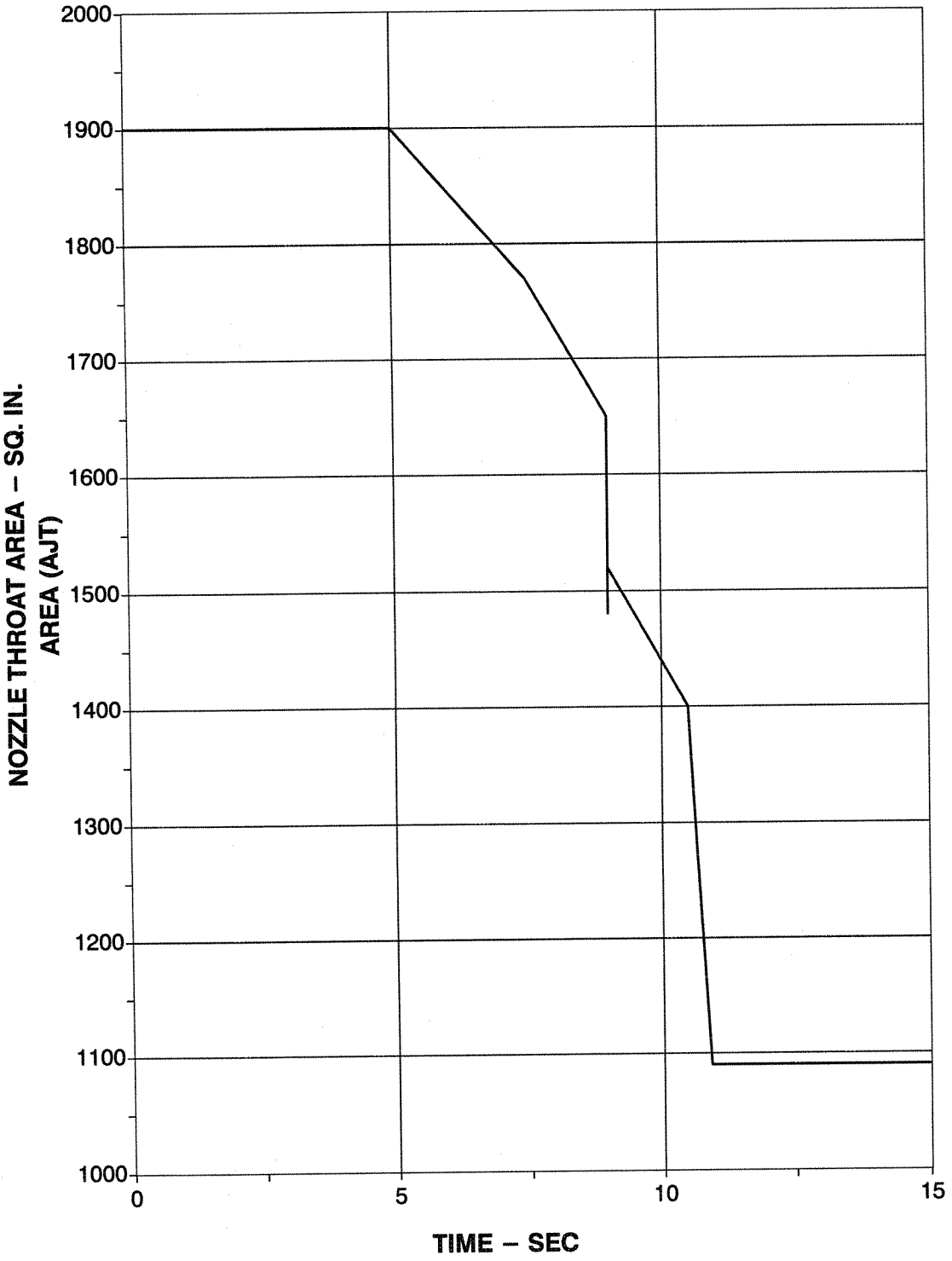

Figure 92. Exhaust Nozzle Throat Area Variation

The variations in net thrust, fuel flow, and combustor exit temperature are presented in Figure 93, Figure 94, and Figure 95, respectively. Holding constant fan rotor speed during this transition results in an increase in net thrust from 10,000 Lb to 17,600 Lb (Figure 107). Once the valve has reached the low mode position at time = 10.5 seconds, there is a significant increase in fuel flow and combustor temperature in order to reach the steady state operating condition at 12 seconds. The combustor temperature was allowed to go to a maximum level of 3360°R.

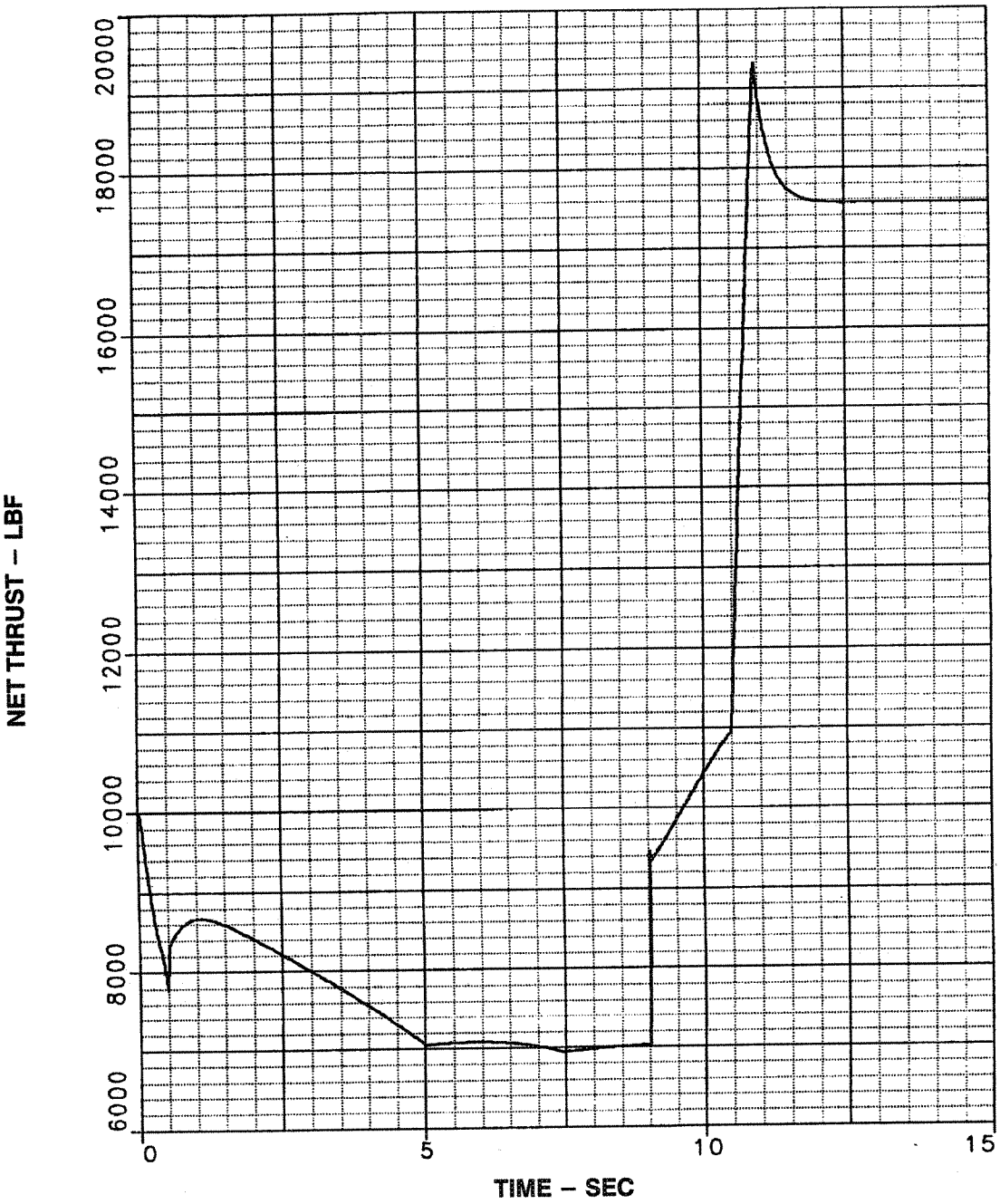

Figure 93. Net Thrust Variation During High to Low Mode

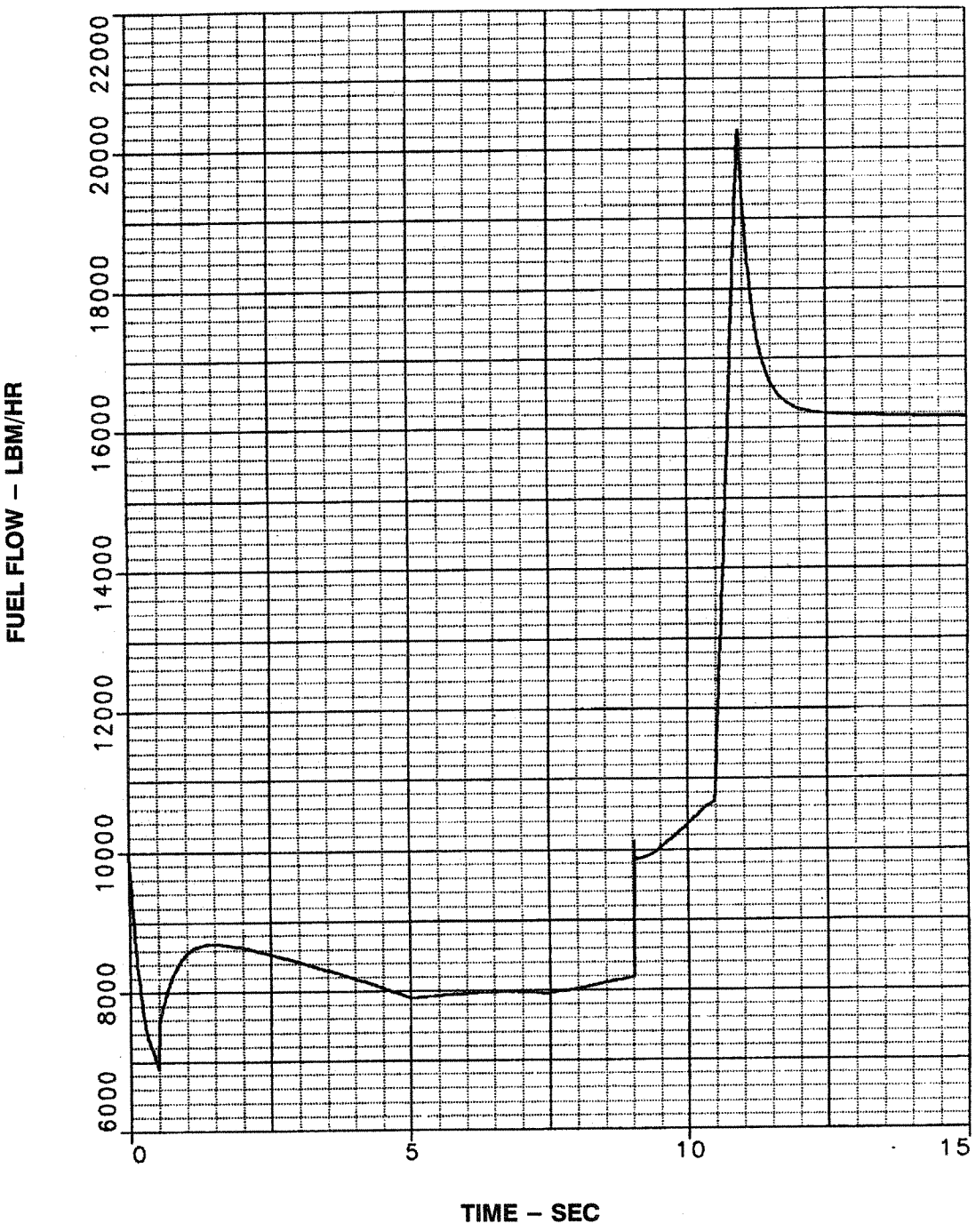

Figure 94. Fuel Flow Variation During Mode Transition

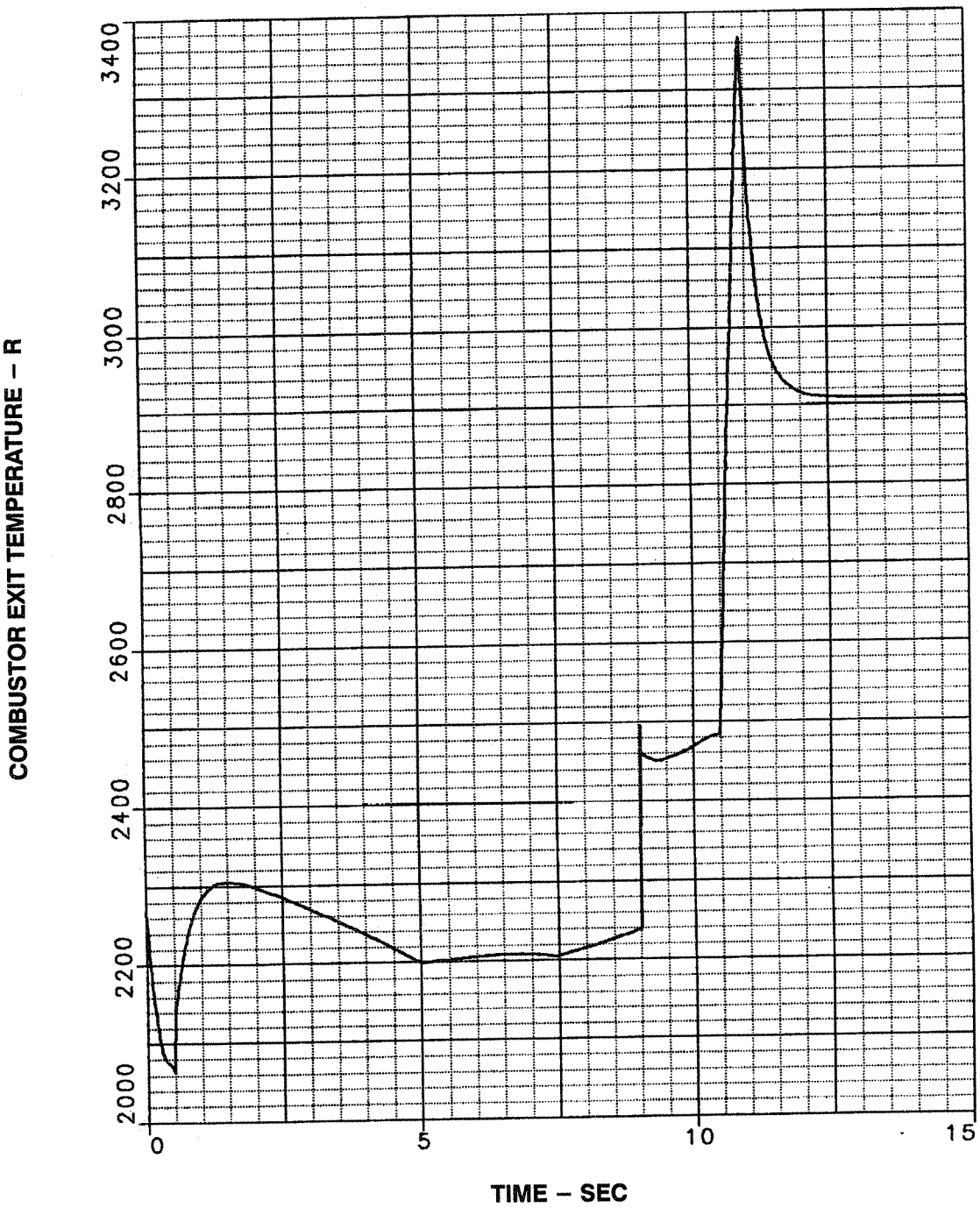

Figure 95. Combustor Temperature Variation

The high to low mode transition was analyzed with the front fan running at a constant speed of 5620 rpm, which at the 14,700 ft – 0.7 Mn condition produces a corrected speed of 5550 rpm. The front fan operating line is shown in Figure 96.

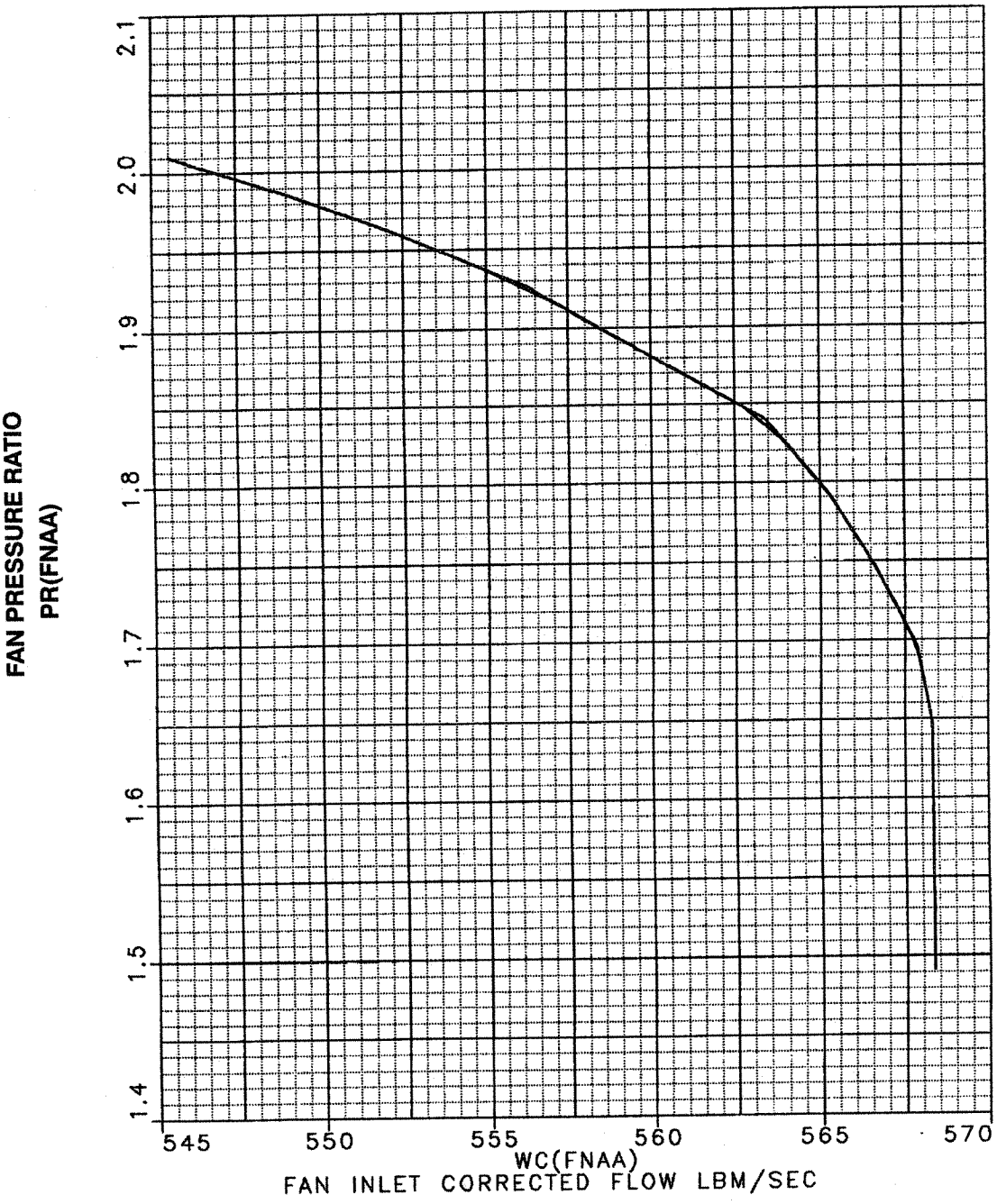

Figure 96. Front Fan Operating Line During High to Low Mode Transition

The variations in front fan inlet corrected flow, pressure ratio and stability margin are presented in Figure 97, Figure 98, and Figure 99. Prior to movement of the valve, the front bypass stream mixing plane area, Figure 90, is increased from 400 in^2 (time = 0 sec) to 1090 in^2 (time = 0.5 sec) in order to drop the front fan pressure ratio and increase its surge margin (Figure 99).

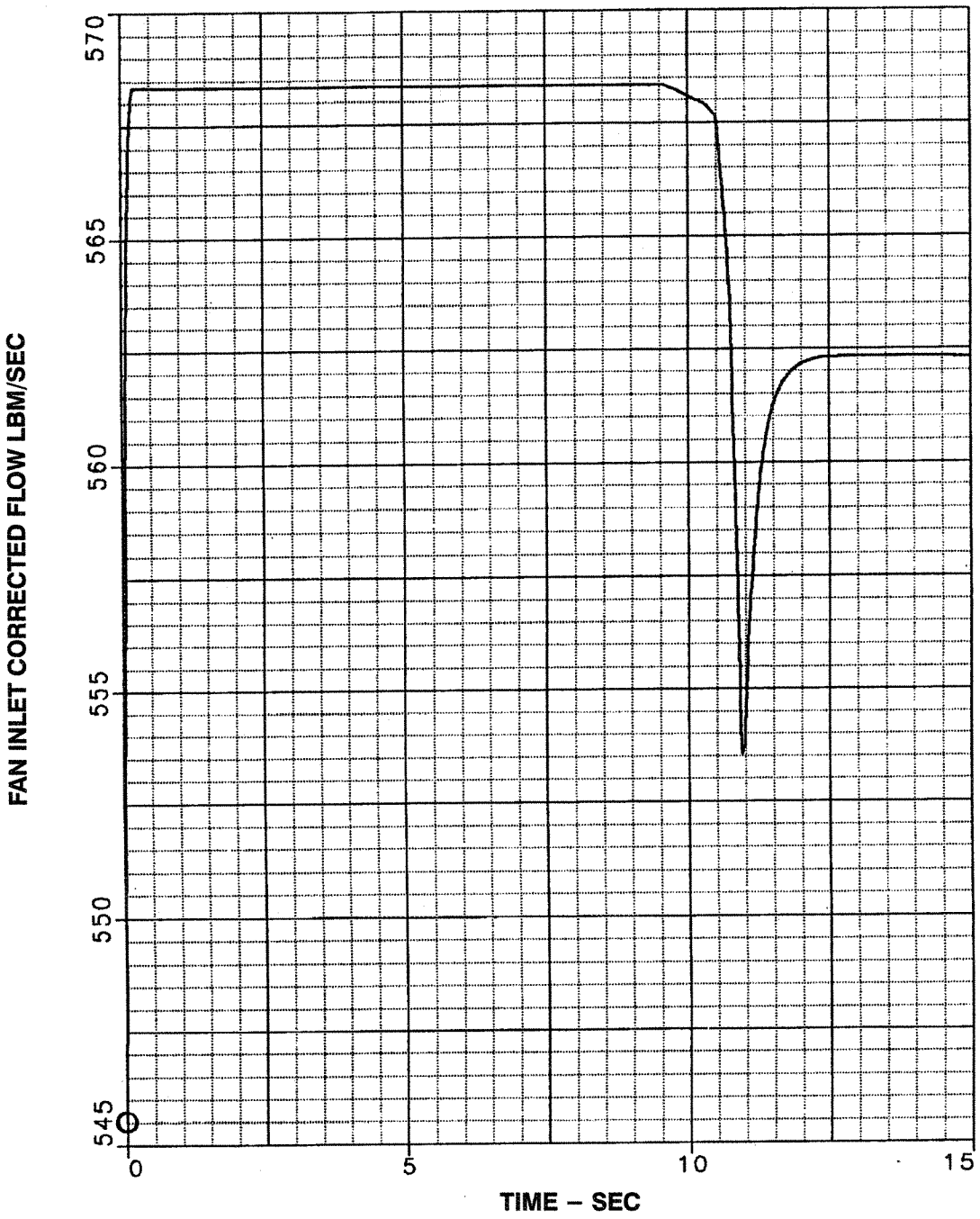

Figure 97. Front Fan Inlet Corrected Flow Variation During High to Low Mode Transition

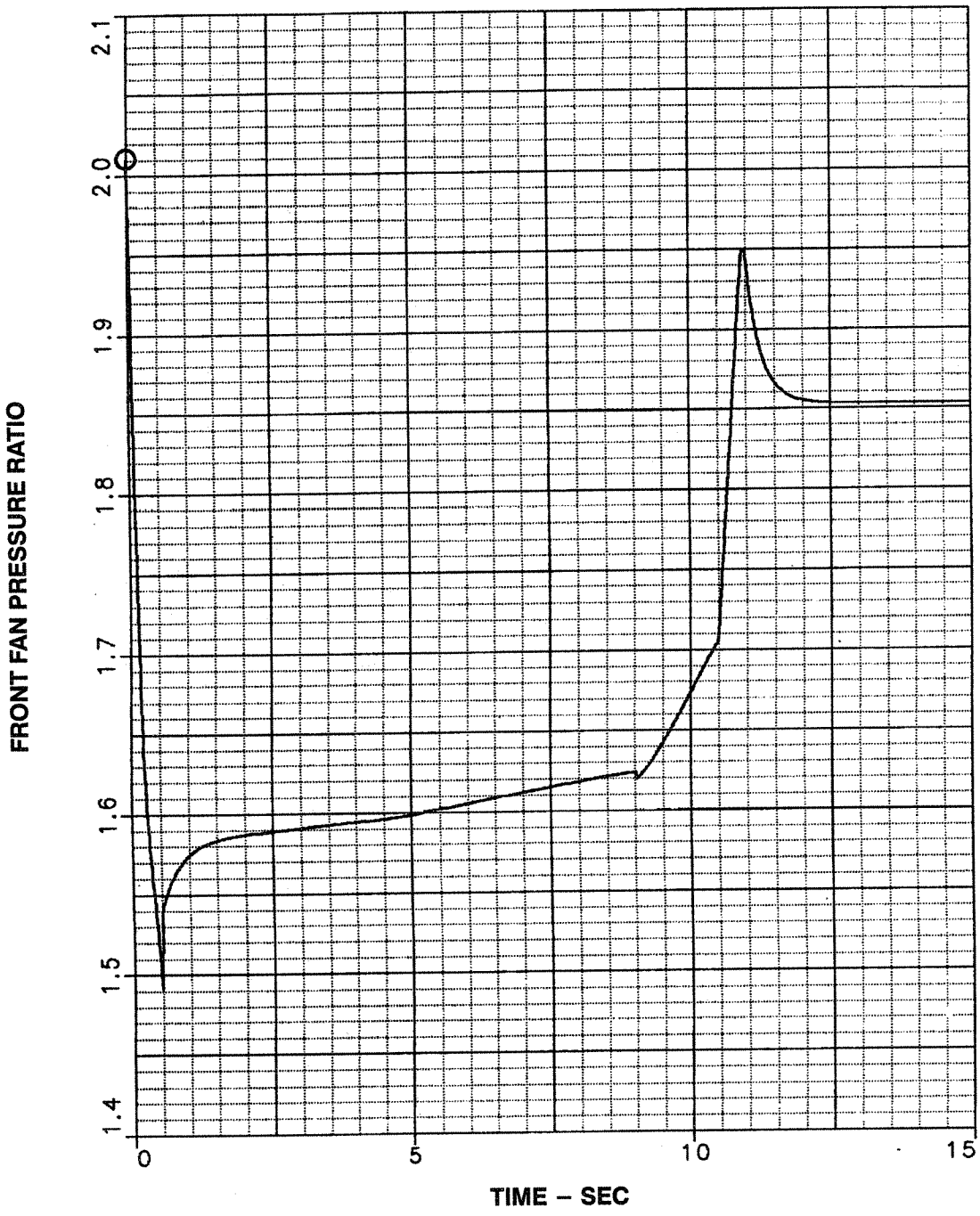

Figure 98. Front Fan Pressure Ratio Variation

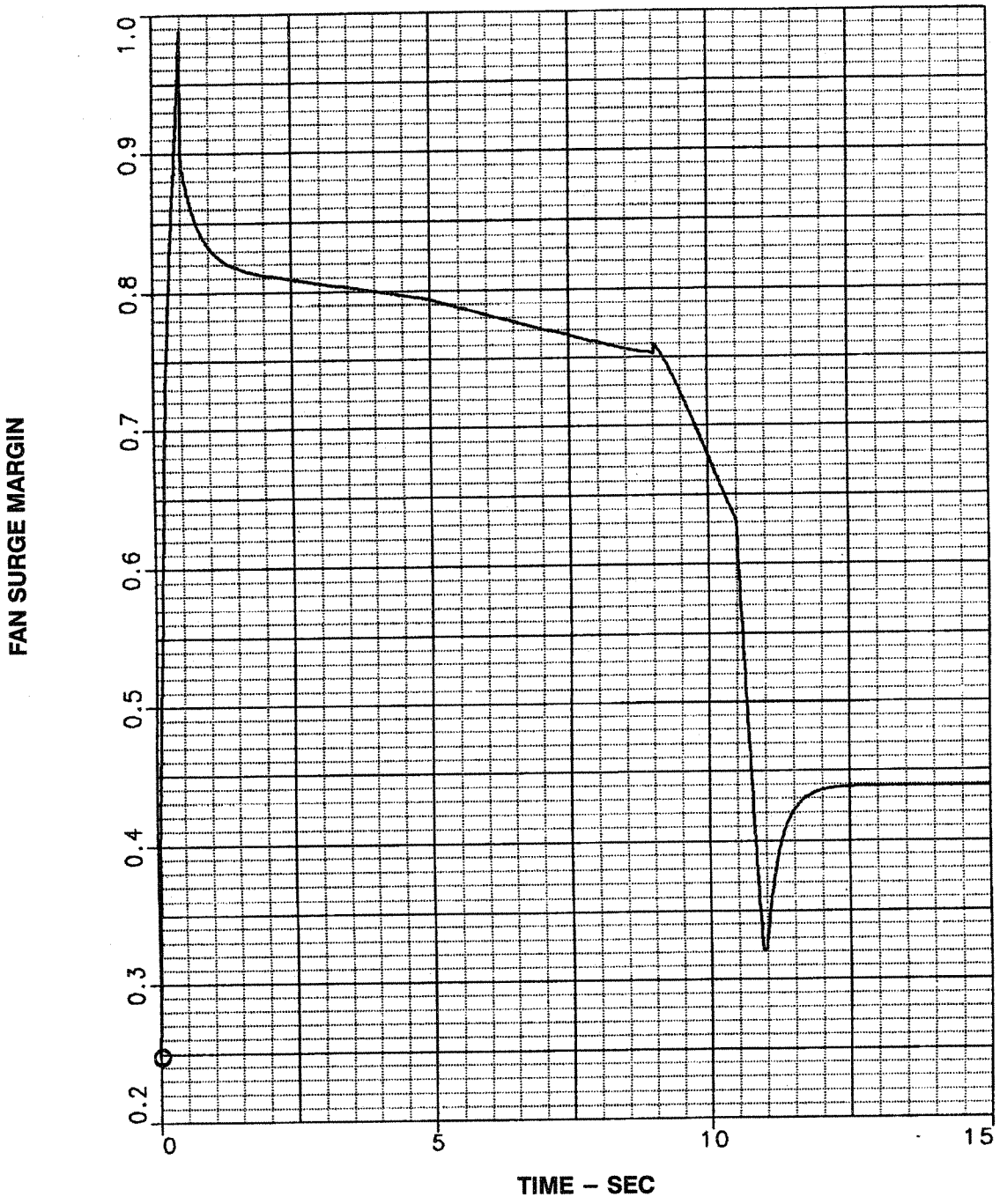

Figure 99. Front Fan Surge Margin During High to Low Mode Transition

The core driven fan stage corrected speed variation is shown in Figure 100. The CDFS inlet guide vane schedule is shown in Figure 101. The IGV is varied from −20° to + 10° during the valve transition in order to provide stable operation. The IGV angle is reduced from +10° to −10° to set the final low mode operating point.

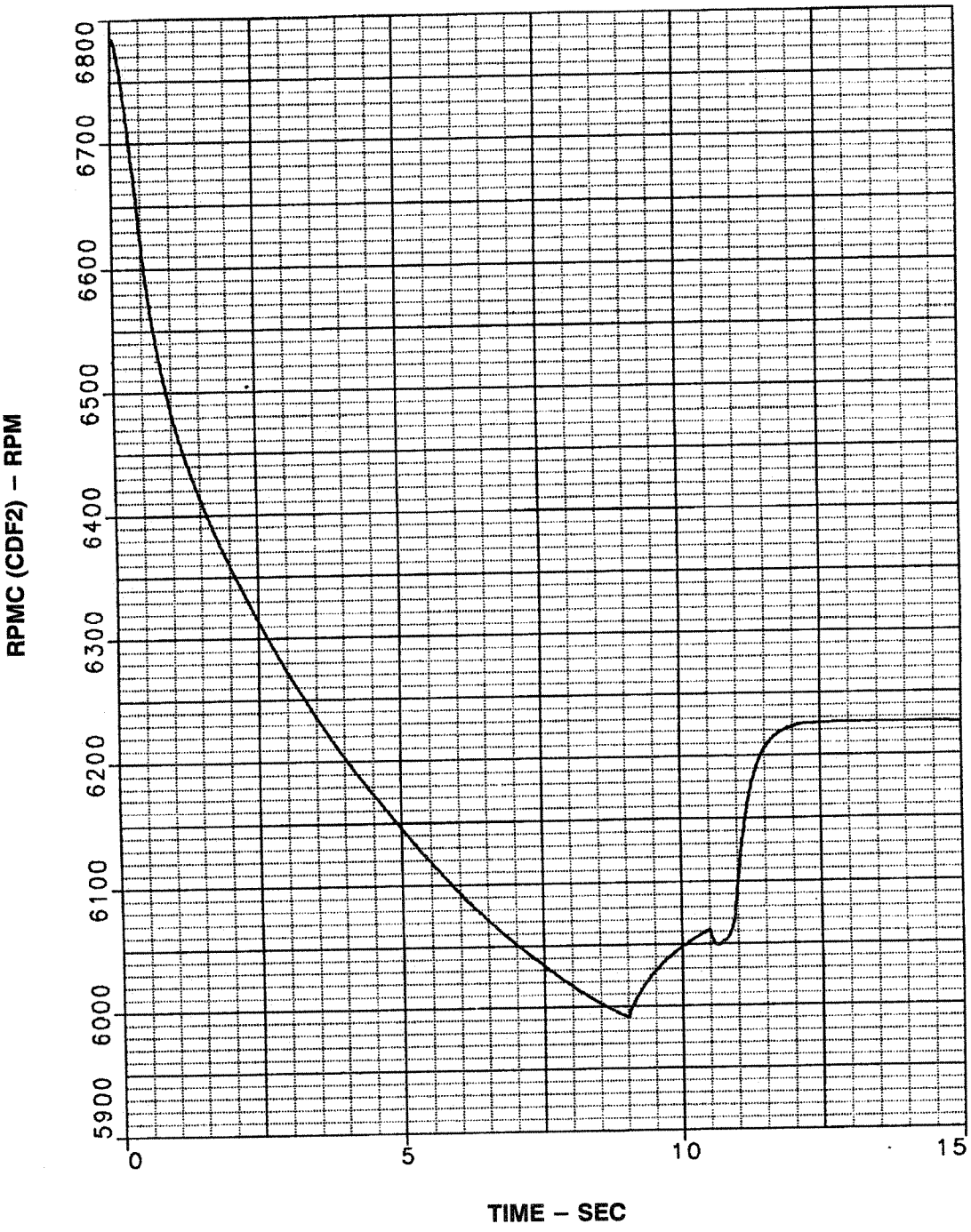

Figure 100. Core Driven Fan Stage Corrected Speed Variation

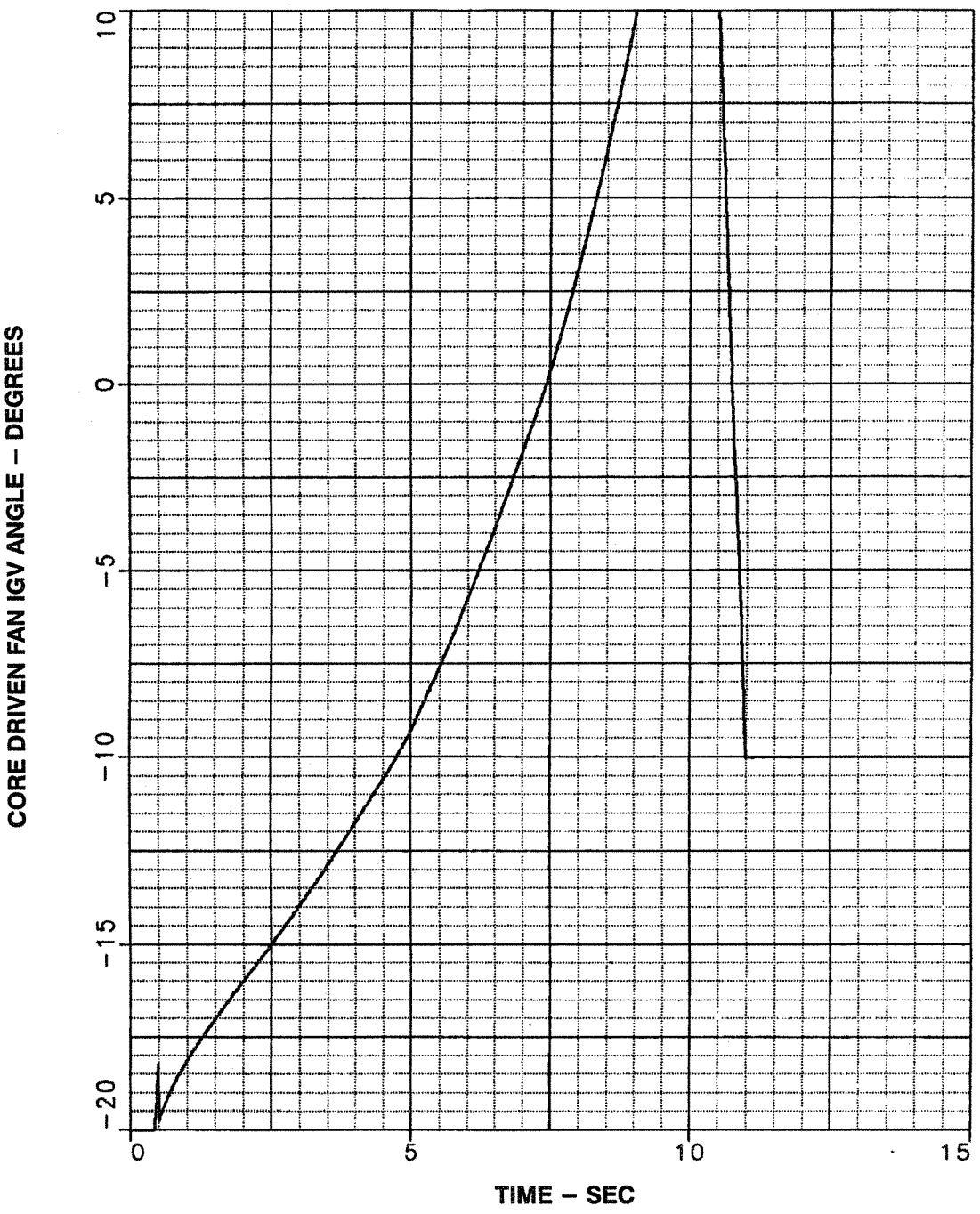

Figure 101. CDFS Inlet Guide Vane Schedule

The variations in CDFS inlet corrected flow, pressure ratio and surge margin are presented in Figure 102, Figure 103, and Figure 104. Although Figure 104 shows that the stability margin is only 10% at the 0.5 second point, it could be increased to 26% by rescheduling the front mixing plane areas, which are shown in Figure 89 and Figure 90.

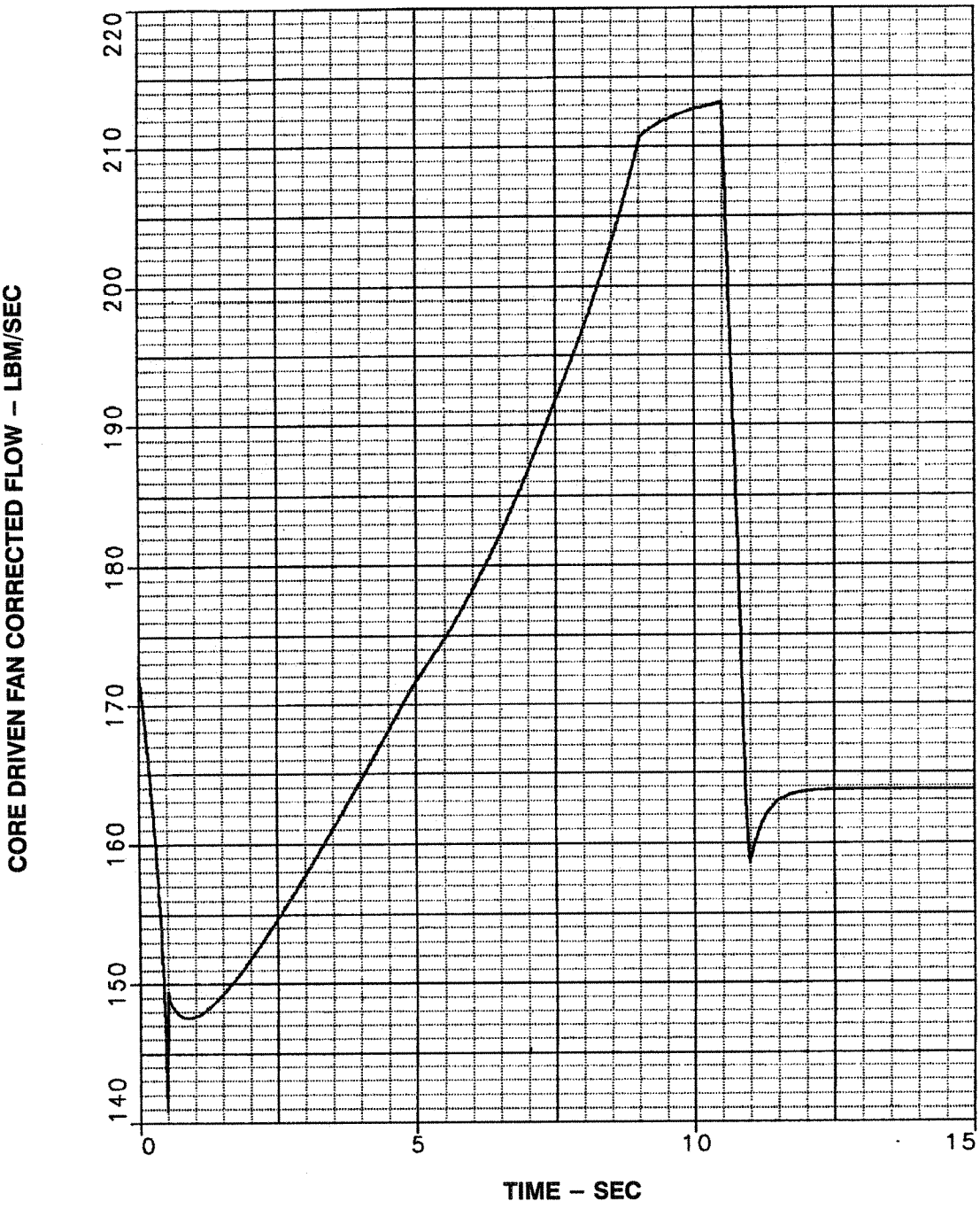

Figure 102. CDFS Inlet Corrected Flow Variation

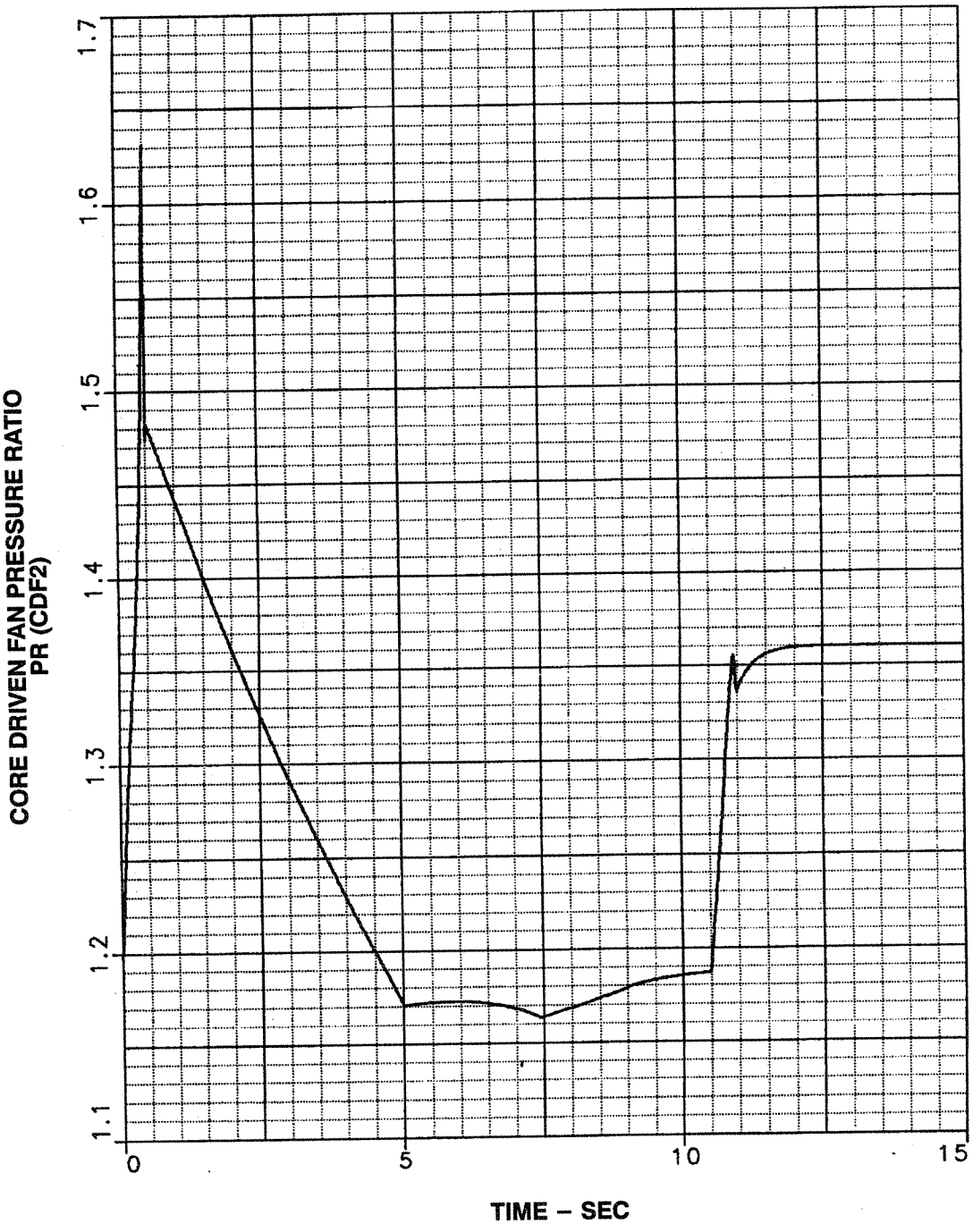

Figure 103. Pressure Ratio Variation

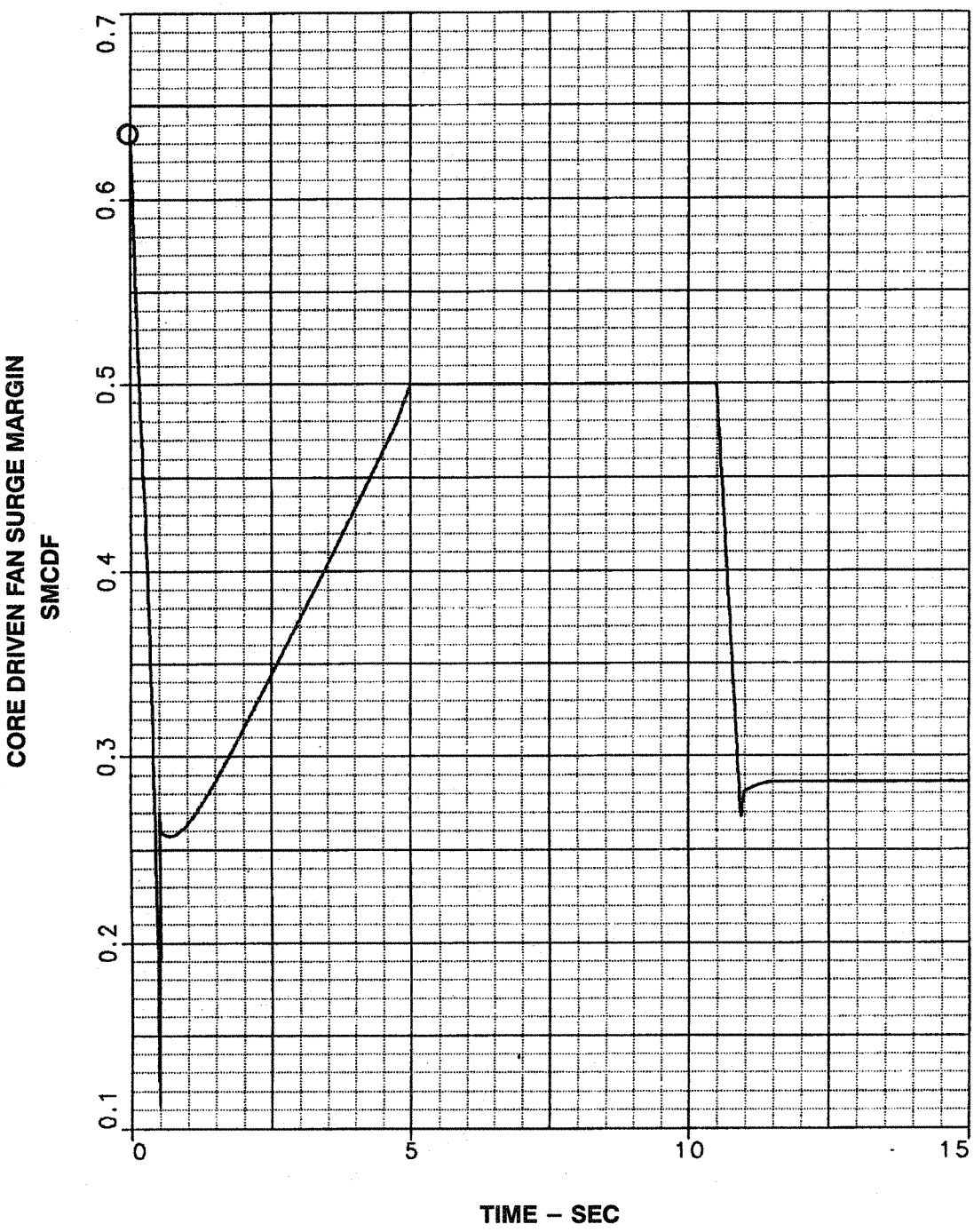

Figure 104. CDFS Stability Margin

The resulting CDFS operation during the high to low mode transition is presented in Figure 105.

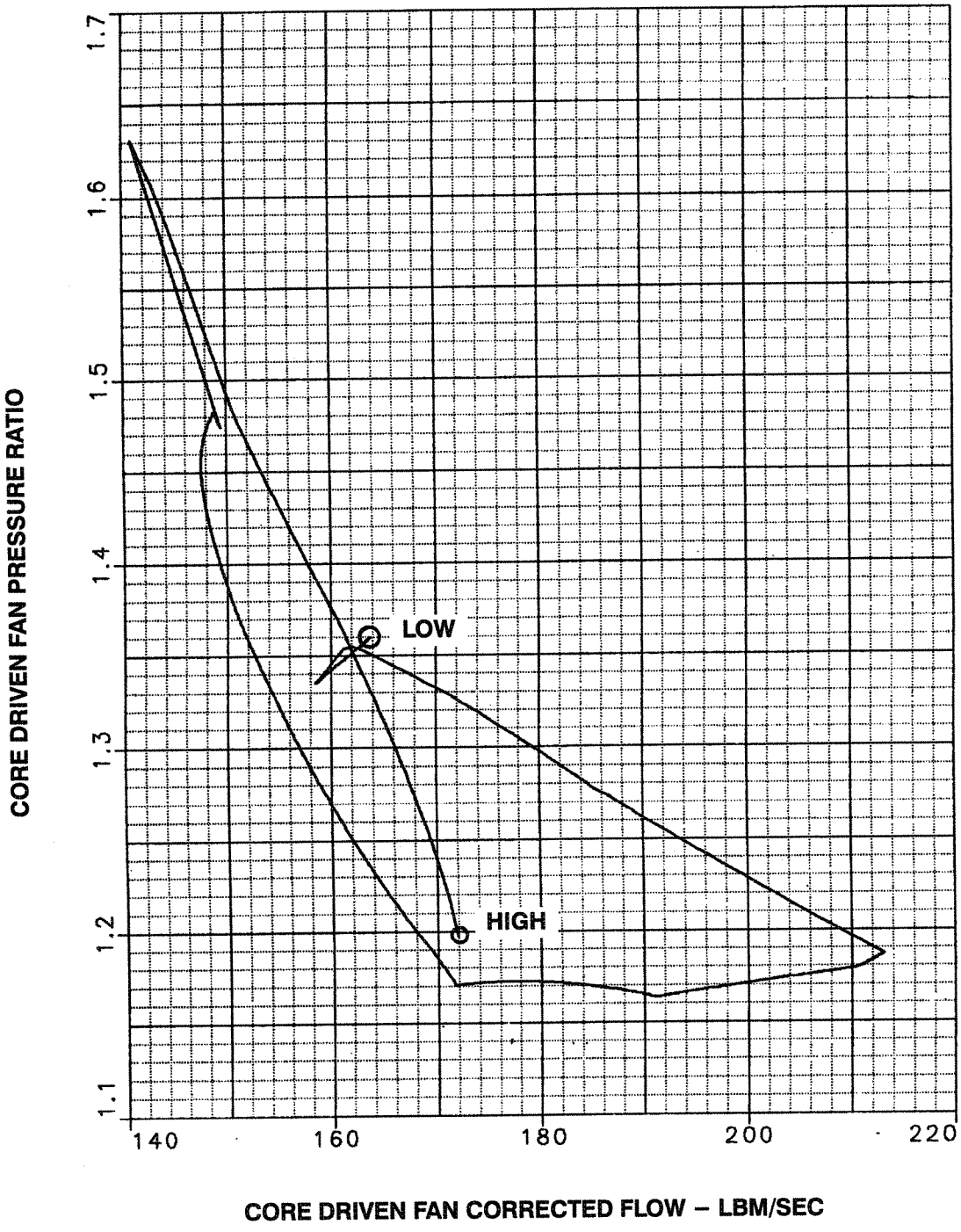

Figure 105. Core Driven Fan Stage Operating Line

The high compressor (HPC) rotor speed and operating line during the high to low mode transition are presented in Figure 106 and Figure 107.

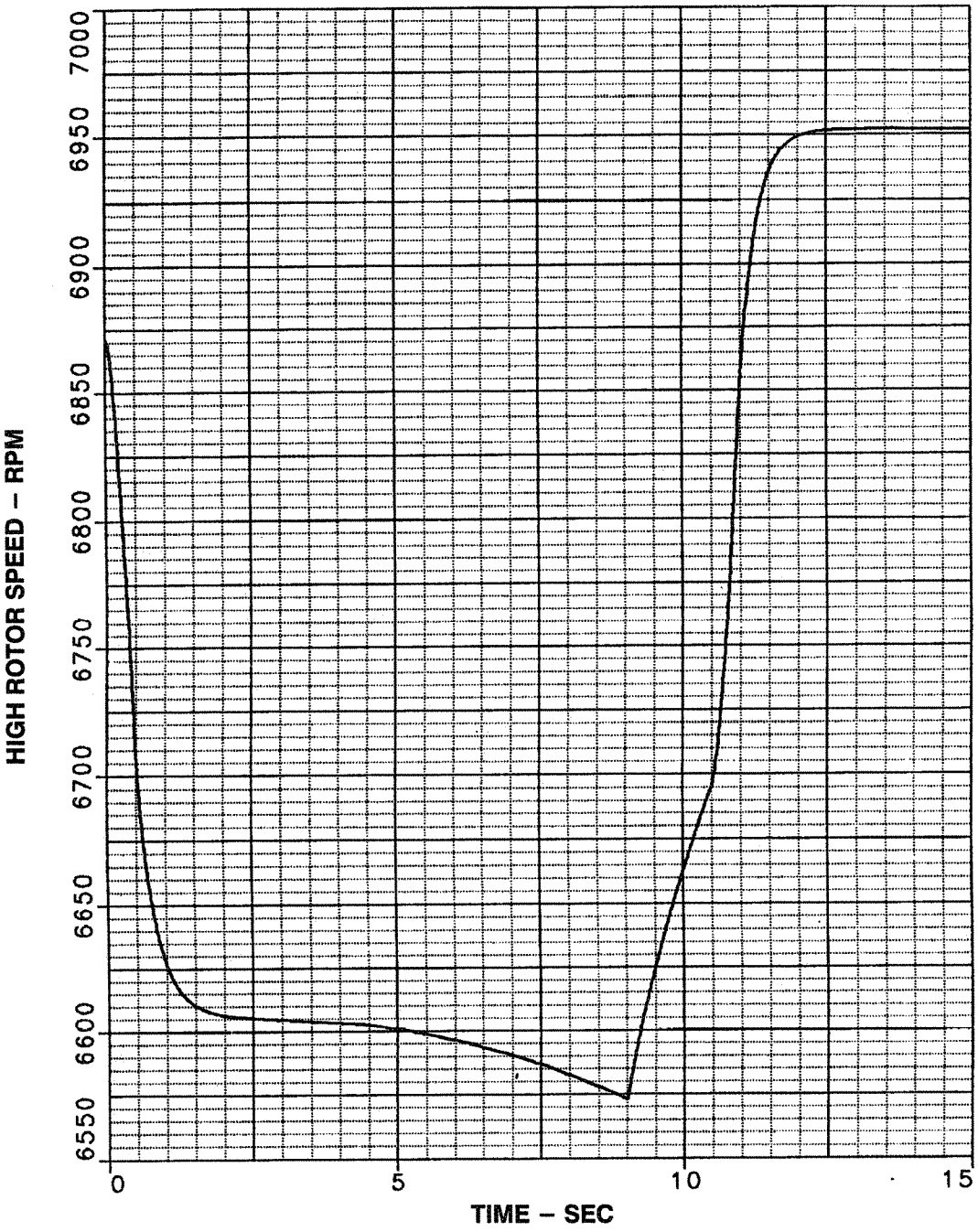

Figure 106. High Spool Rotor Speed

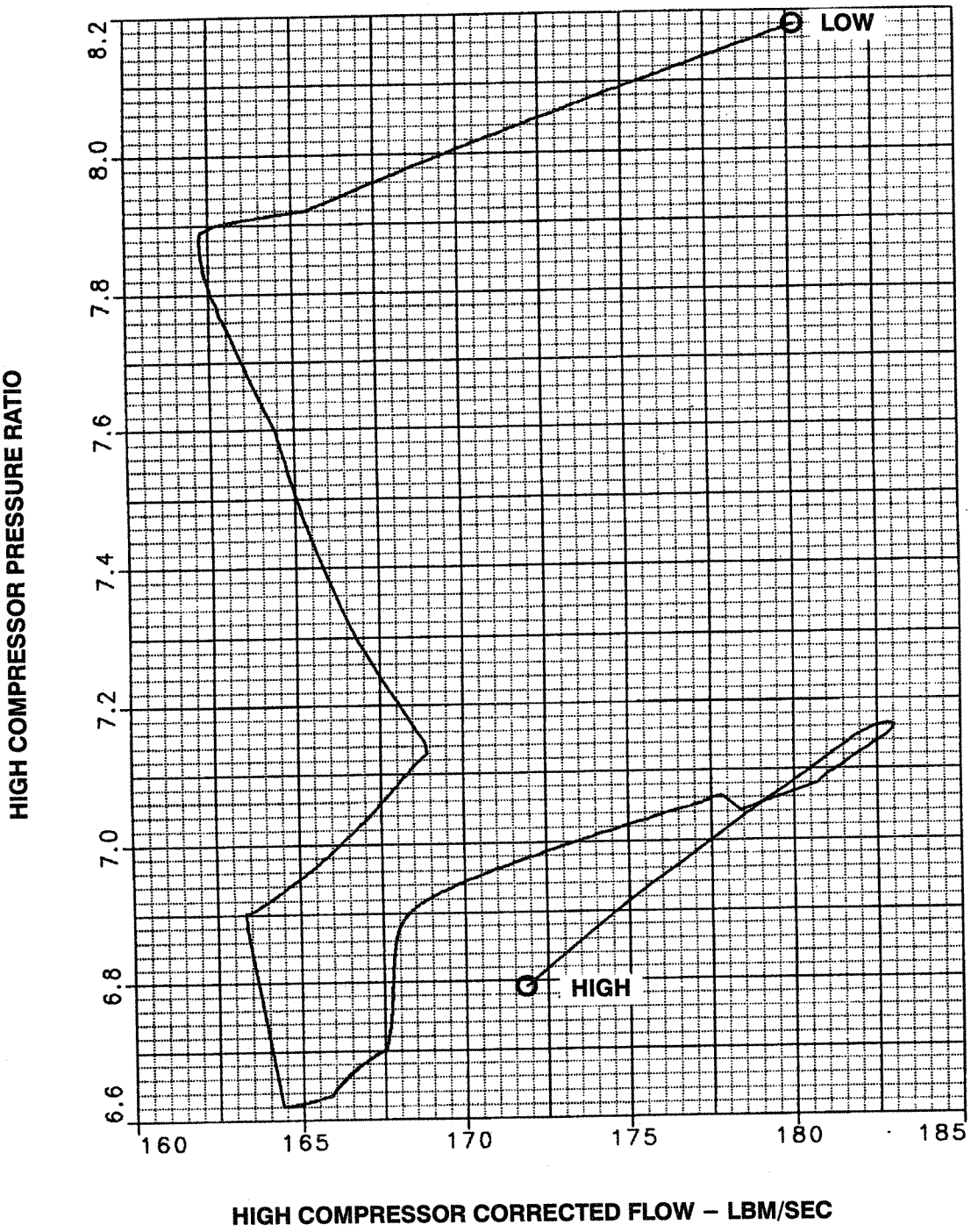

Figure 107. High Compressor Operating Line During Mode Transition

Figure 108 and Figure 109 present the high pressure compressor inlet corrected flow and pressure ratio variations during the high to low mode transition.

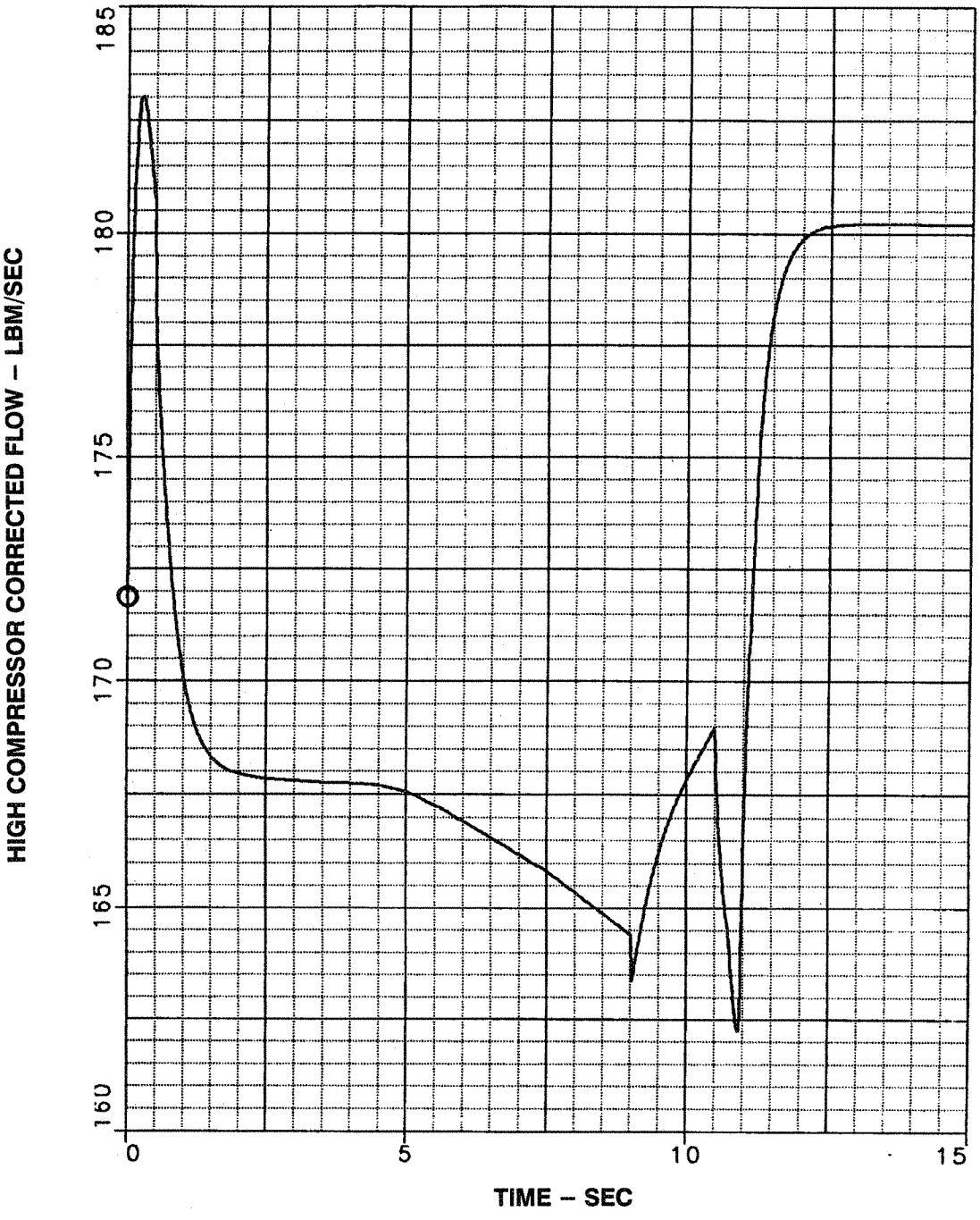

Figure 108. HPC Inlet Corrected Flow Variation

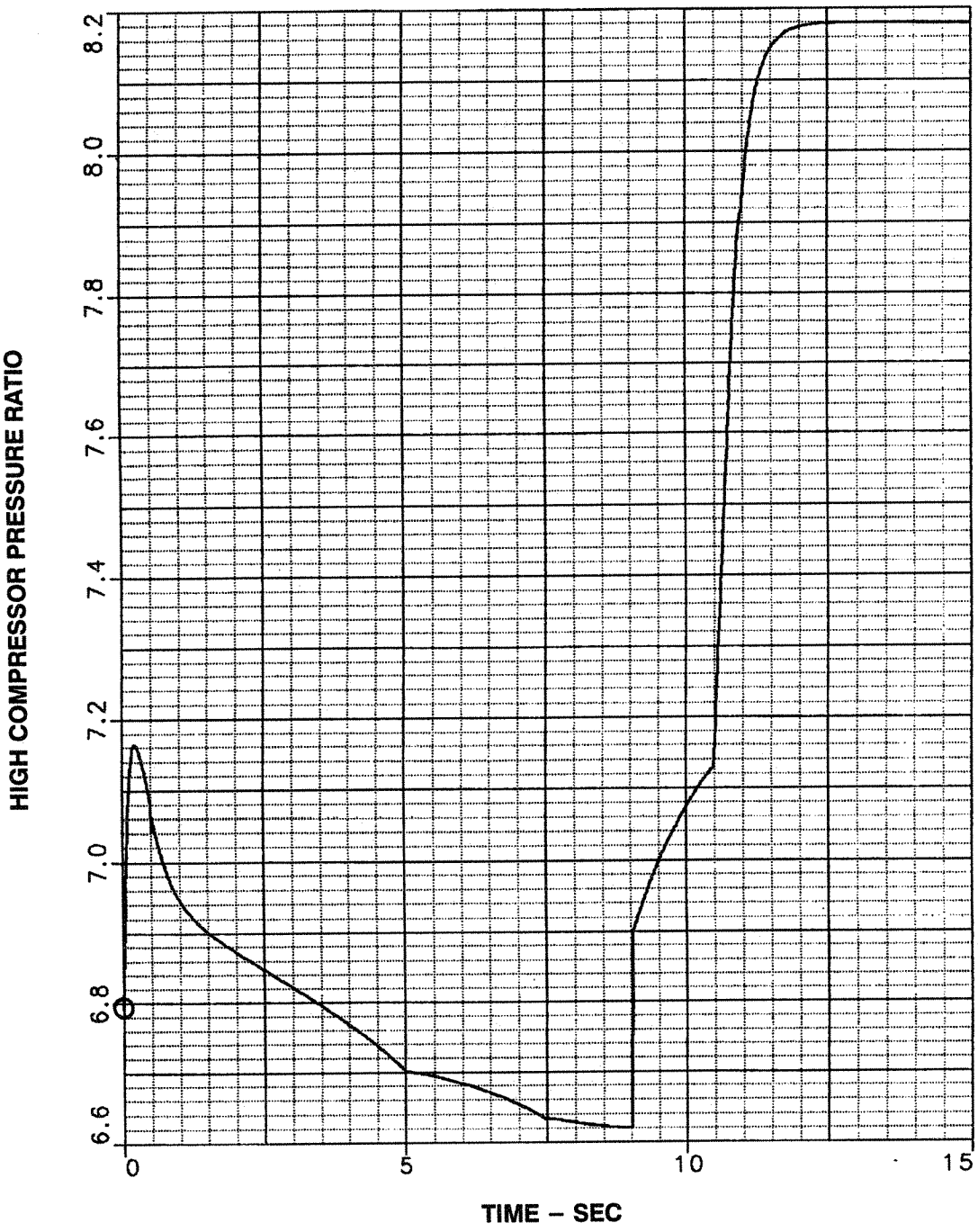

Figure 109. HPC Pressure Ratio Variation

F. MISSION ANALYSIS FOR PARTIAL BYPASS IFV TURBOFAN

Mission analyses were conducted to determine the take off gross weight (TOGW) of a Mach 2.4 high speed civil transport (HSCT) that is powered by the STF 1029 partial bypass IFV turbofan engine. Figure 110 illustrates the Boeing Mach 2.4 planform used in this study. This aircraft is sized to carry 309 passengers over a 5000 nautical mile basic mission with sufficient reserves to cruise subsonically for 260 n. mi. to land at an alternate airport. The mission profile is illustrated in Figure 111.

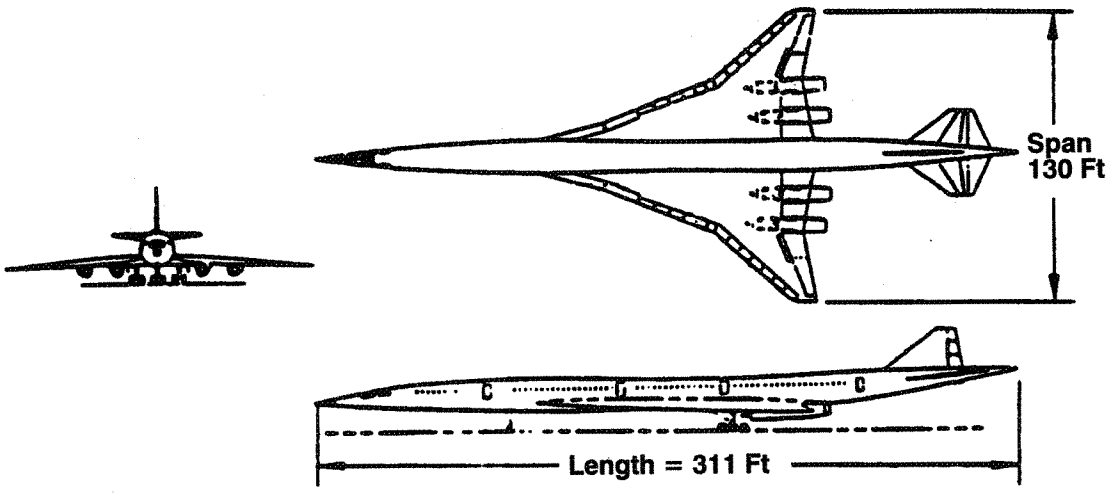

Figure 110. Boeing Mach 2.4 HSCT

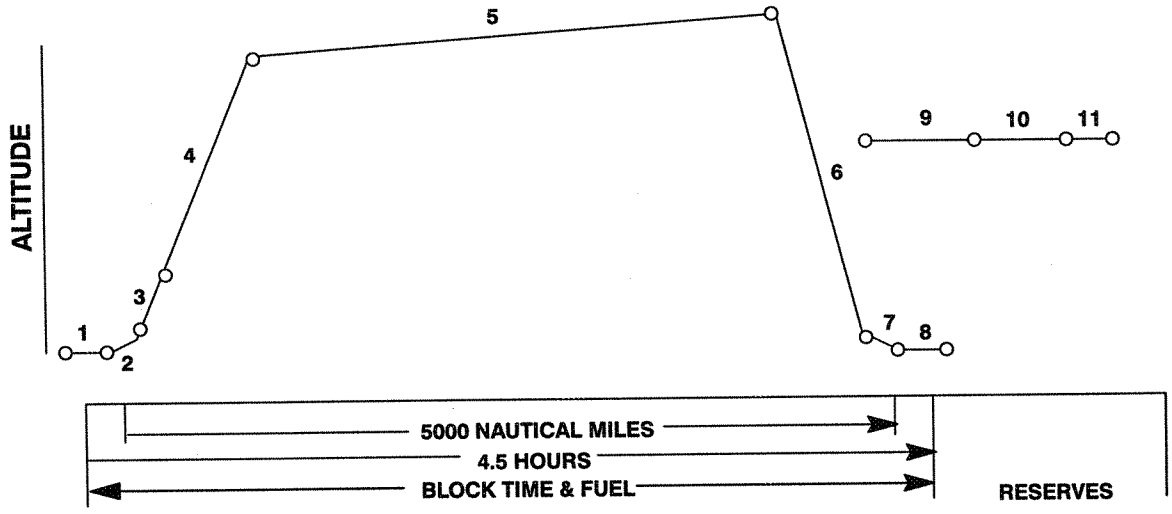

Flight Segment		Beg Alt. (ft)	End Alt. (ft)	Begin Mn	End Mn	Distance (nm)
1	Taxi	0.	0.	0.00	0.00	0.0
2	Takeoff	0.	35.	0.00	0.32	0.0
3	Takeoff Climbout	35.	1000.	0.32	0.37	1.6
4	Climb to Supersonic Cruise	1000.	56489.	0.37	2.40	637.2
5	Supersonic Cruise	56489.	66384.	2.40	2.40	4132.0
6	Descent	66384.	1500.	2.40	0.32	219.3
7	Approach	1500.	0.	0.32	0.22	10.3
8	Land & Taxi	0.	0.	0.22	0.00	0.0
9	Subsonic Cruise to Alternate	37000.	37000.	0.9	0.9	260
10	Hold in Traffic (30 minutes)	15000.	15000.	--	--	0.0
11	6% Enroute Fuel Reserve	--	--	--	--	--

Figure 111. MACH 2.4 HSCT Mission Profile

TOGW analyses were conducted for both the STF 1029 PIFVTF and a conventional mixed flow turbofan (MFTF). The conventional MFTF incorporates a two dimensional (2D) mixer/ ejector exhaust nozzle which entrains 85% secondary airflow during takeoff to reduce the exhaust jet velocity to meet FAR Stage 3 sideline noise regulations. Figure 112 presents a cross–sectional layout of the MFTF propulsion system.

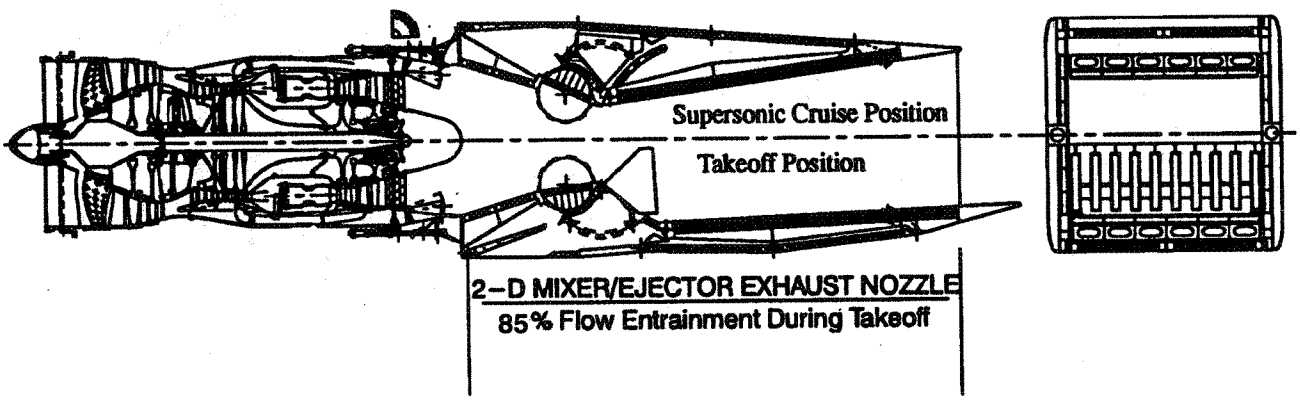

Figure 112. Conventional MFTF With Mixer Ejector Nozzle

Table 29 presents a summary of the cycle characteristics and performance of both engines at Sea Level Static (SLS) and 55,000 feet–Mach 2.4 and a summary of the inlet, engine and nozzle weights in the engine sizes used in the conceptual design studies.

Table 29. Conventional MFTF and STF 1029 PIFVTF Performance and Weight Summaries

Engine	MFTF	PIFVTF
SLS Fan Inlet Corrected Airflow, Lb/sec	650	650
SLS Fan Pressure Ratio	4.30	2.39
SLS Bypass Ratio	0.35	1.12
Secondary Flow Entrainment, %	85	26
SLS Net Thrust, Lbf	46,600	35,000
M=2.4 Fan Inlet Corrected Flow Lb/sec	455	455
M=2.4 Net Thrust, Lbf	19,400	15,300
M=2.4 TSFC, Lbm/hr–lbf	1.30	1.28
Inlet System Weight, Lb	6430	6700
Engine Weight, Lb	7060	8890
Exhaust System Weight, Lb	4385	3250
Total Propulsion Pod Weight, Lb	17,875	18,840

Table 29 shows that the partial bypass IFV turbofan has 31% less takeoff thrust than the conventional MFTF because of its significantly lower fan pressure ratio. At the Mach 2.4 condition, the PIFVTF has 18% less thrust than the conventional MFTF and a 1.5% lower

thrust specific fuel consumption (TSFC) because of its lower fan pressure ratio and higher bypass ratio.

Table 29 shows that the partial IFV turbofan has a total propulsion system weight that is 965 pounds higher than that of its conventional MFTF. The inlet weight is 270 pounds heavier because of the secondary inlet. The engine weight for the PIFVTF is 1830 pounds heavier because of the inlet flow valve, core driven fan stage, associated compression system modifications and the variable bypass mixing plane flaps. The PIFVTF exhaust system is 1135 pounds lighter than the 85% flow entrainment mixer/ejector nozzle required by the conventional MFTF.

Table 30 presents a summary of the mission analysis results for the conventional and partial IFV turbofans. The TOGW of the conventional MFTF powered aircraft is 750,300 Lb and that of the PIFV turbofan powered aircraft is 987,000 Lb.

Table 30. Mission Analysis Summary

Engine	MFTF	PIFVTF
Aircraft Range, N. Mi	5000	5000
Takeoff Gross Weight, Lbm	750,000	987,000
Scaled Engine Size, Lbm/sec	676	1233
Scaled Propulsion Pod Weight, Lbm	18,590	35,580
Mach 2.4 Cruise TSFC, Lbm/hr–lbf	1.29	1.285
Engine Sizing Condition	Climb	Climb
Sideline Noise Level, EPN d B	102.5	106.9

The STF 1029 PIFVTF, because of its lower takeoff and climb thrust, requires an engine of 1233 Lb/sec which results in a scaled propulsion system pod weight of 35,580 Lb. Although the PIFVTF can meet stage 3 sideline noise of 103 EPN d B in its base size of 650 Lb/sec, when it is scaled up to 1233 Lb/sec,. the noise level increases to 106 EPN d B.

The mission analysis results show that the partial bypass IFV turbofan concept is not competitive with a conventional mixed flow turbofan. Since the total takeoff thrust for an IFV engine is directly a function of the total takeoff airflow, a full bypass IFV turbofan, which entrains more flow than the partial bypass concept, should produce a more competitive propulsion system.

The following sections, G through J, describe the studies conducted for a full bypass inlet flow valve concept:

G. FULL BYPASS IFV TURBOFAN CYCLE STUDIES

The full bypass IFV turbofan concept, shown in Figure 113, uses an annular inverter valve between front and rear fan stages to bypass the total front fan exhaust air (stream A and B) around the rear fan and bring in outside ram air (streams C and D) to feed the rear fan during high flow mode of operation. This concept provides more secondary air than the partial bypass concept and thus produces a larger reduction in exhaust jet velocity during takeoff operation.

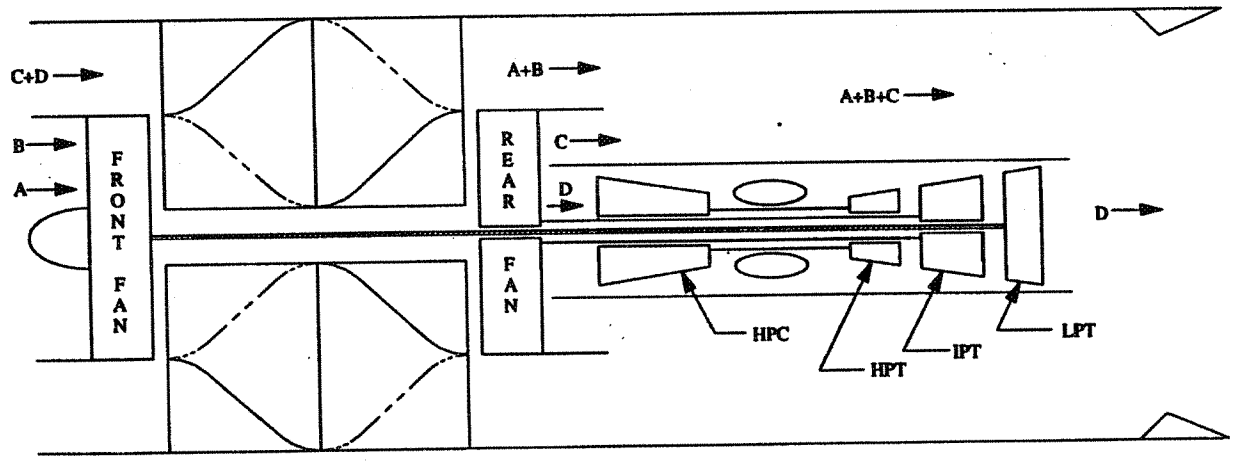

Figure 113. Full Bypass IFV Turbofan – High Flow Operation

During low flow mode operation, streams C and D are shut off and the engine acts as a conventional mixed flow turbofan with stream A going through the core and stream B passing through the rear fan tip section and into the bypass duct, as illustrated in Figure 114.

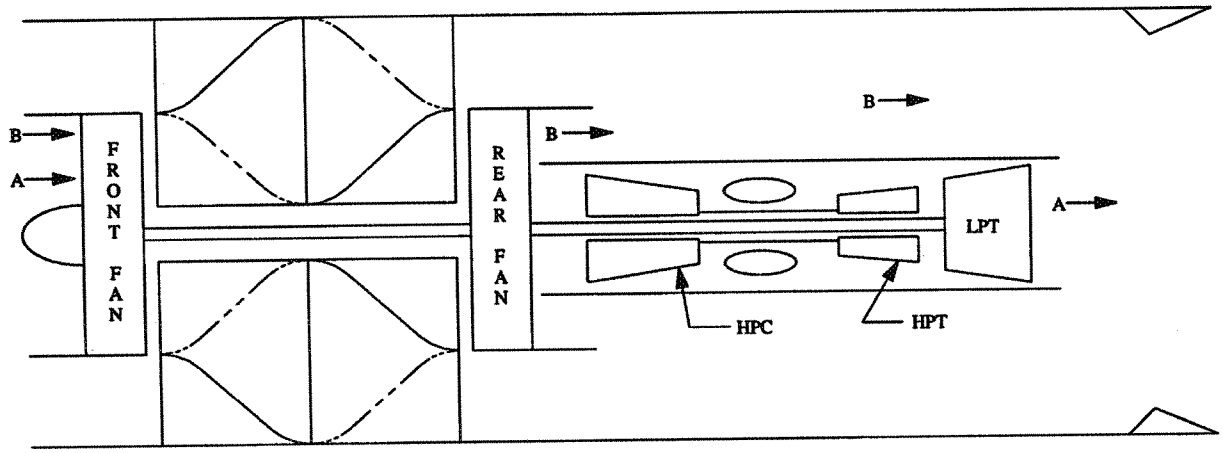

Figure 114. Full Bypass IFV Turbofan–Low Flow Operation

Cycle studies were conducted for the full bypass inlet flow valve (IFV) concept. The front fan pressure ratio was set at 2.1 and the rear fan pressure ratio was originally set at 1.7, as shown in Table 31 (Cycle #1), to achieve an exhaust jet velocity of 1235 ft/sec. in the high mode of operation so that this concept would achieve FAR Stage 3 minus 4 EPNdB sideline jet noise at maximum dry power.. However, when this engine was operated in the low flow mode at the supersonic cruise condition, it produced a Mach 2.4/SLS net thrust ratio of 0.23 which is well below the desired ratio of 0.4 for the Boeing HSCT.

In order to improve supersonic thrust, the rear fan pressure ratio was raised to 2.1 at design and the high turbine rotor inlet temperature was reduced to 2400°F. The two changes reduced the sea level static high mode bypass ratio from 3.52 to 2.40. At the Mach 2.4 condition, the net thrust was increased by 38% with no change in TSFC because of the fan pressure increase and bypass ratio reduction. However, this cycle only produced a Mach 2.4/SLS thrust ratio of 0.29.

In order to further increase the net thrust at Mach 2.4, the front and rear fan pressure ratios at Mach2.4 were increased to the levels shown in Table 31 (Cycle 3). A Mach 2.4 to SLS net thrust ratio of 0.39 was achieved with this cycle.

Table 31. Full Bypass IFV Turbofan Cycle Study Summary

Cycle Number	1	2	3
SLS High Mode:			
Front Fan Inlet Corrected Flow, lb/sec	650	650	650
Front Fan Pressure Ratio	2.1	2.1	2.1
Rear Fan Inlet Corrected Flow, lb/sec	450	450	450
Secondary / Primary flow	0.68	0.68	0.68
Rear Fan Pressure Ratio	1.70	2.10	2.10
Rear Fan Bypass Ratio	0.86	0.40	0.39
Overall Bypass Ratio	3.52	2.40	2.40
Overall Compression Ratio	20.9	20.0	15.5
High Turbine Rotor Inlet Temperature, °F	2600	2400	2400
Jet Velocity (Cv = .985), ft/sec	1235	1354	1360
Net Thrust, lbf	39300	43050	43300
55,000 Ft / 2.4 Mn (Low Mode):			
Front Fan Inlet Corrected Flow, Lb/sec	455	455	455
Front Fan Pressure Ratio	1.28	1.33	1.66
Rear Fan Pressure Ratio	1.15	1.23	1.44
Overall Fan Pressure Ratio	1.45	1.61	2.37
Bypass Ratio	2.42	1.46	0.79
Overall compression Ratio	9.7	10.1	10.7
compressor Exit Temperature, °F	1250	1250	1250
High Turbine Rotor Inlet Temperature, °F	2900	2900	2900
Net Thrust (Cv = .985), lbf	8910	12350	16700
TSFC, lbm / hr–lbf	1.18	1.18	1.19
Mach 2.4/SLS Thrust	0.23	0.29	0.39

Cycle 3, which is designated as the STF 1035, was selected for the conceptual design study. Table 32 summarizes the STF 1035 cycle characteristics for SLS high and low modes of operation and for 55,000 ft – 2.4 Mn operation for the three spool configuration.

Table 32. Full IFV Turbofan Summary (3 Spool)

Mode of Operation	High	Low	Low
Altitude, ft,	0	0	55000
Mach Number	0	0	2.4
Front Fan Inlet Corrected Flow, Lb/sec.	650	650	455
Front Fan Pressure Ratio	2.1	2.26	1.66
Front Fan Inlet Actual Flow, Lb/sec.	606	606	440
Secondary Actual Flow, Lb/sec.	412	--	--
Secondary / Fan Airflow	0.68	--	--
Rear Fan Inlet Corrected Flow, Lb/sec.	450	332	299
Rear Fan Pressure Ratio	2.1	1.75	1.44
High Compressor Pressure Ratio	7.5	5.9	4.5
Overall Compression Ratio	15.5	23.1	10.7
Compressor Exit Temperature, °F	767	925	1250
Turbine Cooling Air, %	28	28	28
Bypass Ratio	2.40	0.43	0.79
HPT Rotor Inlet Temperature, °F	2400	2600	2900
High Turbine Expansion Ratio	2.80	2.71	2.69
Intermediate Turbine Expansion Ratio	1.44	1.39	1.40
Low Turbine Expansion Ratio	1.82	1.55	1.57
Bypass Stream Mixing Plane Area, in^2	2050	300	300
Primary Stream Mixing Plane Area, in^2	1930	1930	1930
Exhaust Nozzle Throat Area, in^2	2210	970	1094
Net Thrust (Cv = .985), Lbf	43300	45500	16700
TSFC, Lbm/hr–Lbf	.51	0.74	1.19

H. Full Bypass IFV Turbofan Component Aerodynamic Designs

The cycles studies for the full bypass IFV concept were conducted with the engine configured as a three spool engine. Use of a three spool concept allows independent control of the rear fan stage which is highly desirable to optimize engine performance and minimize the number of variable geometry vanes required in the rear fan and high pressure compressor. However, Table 32 shows that the intermediate turbine, which drives the rear fan, is lightly loaded and has a turbine expansion ratio of 1.44.

Therefore, component aerodynamic analyses and performance analyses were conducted for three configurations:

a. Three spool engine with the rear fan driven by the intermediate pressure turbine (IPT).

b. Two spool engine with the rear fan and high compressor driven by the high pressure turbine (HPT).

c. Two spool engine with the front and rear fans driven by the low pressure turbine (LPT).

Table 32 summarizes the SLS high mode and 55000 ft−2.4 Mn operating points for the three spool concept (a), while Table 33 summarizes the two spool concepts ((b) and (c) operating points.

Table 33. Two Spool Full IFV Turbofan Summary

Concept	Rear Fan on High Spool		Rear Fan on Low Spool	
Mach Number	0	2.4	0	2.4
Altitude, ft.	0	55000	0	55000
Mode of Operation	High	Low	High	Low
Front Fan Corrected Flow lb/sec	650	455	650	455
Front Fan Pressure Ratio	2.10	1.78	2.10	1.69
Rear Fan Corrected Flow, Lb/sec	450	283	450	295
Rear Fan Pressure Ratio	2.10	1.34	2.10	1.39
Bypass Ratio	2.25	0.68	2.37	0.74
High Compressor Pressure Ratio	7.50	4.65	7.50	4.72
Overall Compression Ratio	15.5	10.95	15.5	10.96
Compressor Exit Temperature, °F	757	1283	753	1253
Turbine Cooling Air, %	28	28	28	28
HPT Rotor Inlet Temperature, °F	2400	2900	2400	2900
High Turbine Expansion Ratio	4.15	3.96	2.80	2.76

Table 33. Two Spool Full IFV Turbofan Summary (Cont'd)				
Concept	**Rear Fan on High Spool**		**Rear Fan on Low Spool**	
Low Turbine Expansion Ratio	1.77	1.63	2.62	2.15
Bypass Stream Mixing Plane Area, in^2	2015	270	2046	300
Primary Stream Mixing Plane Area, in^2	2027	2027	1946	1946
Exhaust Nozzle Throat Area, in^2	2234	1177	2213	1086
Net Thrust, Lbf	43700	17000	43340	17150
TSFC, Lbm 1hr−Lbf	0.53	1.23	0.52	1.20

Tables 32 and 33 show that the Seal Level static cycle characteristics were held the same for all three configurations. The SLS performance differs slightly because of the split in turbine cooling air and turbine efficiencies for the three systems.

At the Mach 2.4 condition, all engines were run to a front fan inlet corrected flow of 455 Lb/sec and a high turbine rotor inlet temperature of 2900°F. All engines produced net thrust and TSFC levels that were within ±1.5 percent.

The following sections describe the component aerodynamic design studies that were conducted for each configuration.

a. Three Spool Engine

Component aerodynamic design studies were conducted for the three spool version of the STF1035 turbofan. Figure 115 shows the flowpath for this full IFV turbofan. This engine incorporates a two stage front fan, a single stage rear fan, a five stage high pressure compressor and single stage high, intermediate and low pressure turbines. The intermediate power turbine (IPT) which drives the rear fan stage is lightly loaded and there is concern that the low blade turning angles may lead to vibrational problems. The IPT was originally configured as counterrotating relative to the HPT and its inlet vane was removed. Relief from the low blade turning can be achieved by putting a vane between the HPT and IPT and making them co−rotating.

The total turbine cooling air for this configuration is estimated at 16% for the HPT, 7% for the IPT and 5% for the LPT.

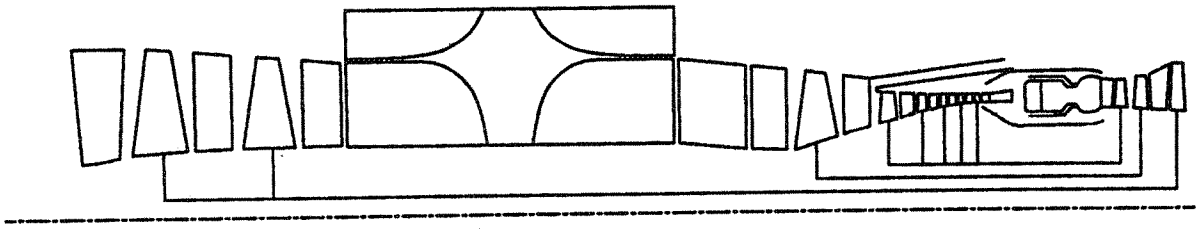

Figure 115. STF 1035 Three Spool Flowpath

The front fan is a two–stage design with a design corrected tip speed of 1585 ft/s. It was decided to use a two–stage design as opposed to a one–stage design, with a slightly lower pressure ratio, because the latter would have a relatively high exit mach number which would lead to significantly higher losses through the IFV. For the given design tip speed, a first pass meanline analysis indicates that a pressure ratio of about 2.2 is achievable with adequate stall margin.

The rear fan is a single–stage design with a maximum inlet specific flow of 41.7 #/sec–ft^2. The flowpath was set by assuming close–coupling with the HPC to avoid the use of a duct between these two components. For a maximum tip speed of about 1800 ft/s, a pressure ratio of about 2.0 is achievable with adequate stall margin.

The high pressure compressor is a five–stage, Constant Outer Diameter (COD) design. It has a pressure ratio of 7.5 and an inlet specific flow of 39.0 #/sec–ft^2.

The combustor for this engine is a lox NO_x combustor which was sized consistently with other HSCT combustors.

The High Pressure Turbine (HPT) is a high–work, high–reaction design for efficient operation, with the vaneless Intermediate Pressure Turbine (IPT). The HPT has a maximum AN^2 of 450×10^8 and a maximum rim speed of 1310 ft/s.

The IPT is a single, counter–rotating stage which is very lightly loaded. This is due to the low work required to drive the rear fan, the rotational speed required by the rear fan, and its rim diameter which is set by the close–coupling constraint with the HPT. As a result of the lightly loaded blade, its turning is a concern as low blade turning angles may lead to vibrational problems. Relief from this low turning blade can be achieved by varying such parameters as reaction of the HPT and rotational direction of the IPT.

The Low Pressure Turbine (LPT) is a single–stage conventional design with a maximum AN^2 of 500×10^8. As with the IPT, the rim diameter was set by a close–coupling constraint with the upstream turbine. With some tweaking of the flowpath and/or reaction level, a turbine exit guide vane should be unnecessary as axial exit flow should be achievable.

b. Two Spool Engine – Rear Fan On High Spool

The aerodynamic analysis of this concept showed that a two–stage high pressure turbine is required. This two–stage HPT will require more turbine cooling air than the two spool engine with the rear fan on the low spool.

Since Table 33 shows that the two spool engine with the rear fan on the high spool has worse performance than the two spool engine with the rear fan on the low spool, it was dropped from further consideration and no engine flowpath was developed.

c. Two Spool Engine – Rear Fan On Low Spool

Component aerodynamic studies were conducted for the two spool configuration with the rear fan on the low spool. This engine incorporates a two–stage front fan, a two–stage rear fan, a six–stage high pressure compressor, a single–stage high pressure turbine, and a two–stage vaneless counter–rotating low pressure turbine. Figure 116 presents the flowpath for this engine.

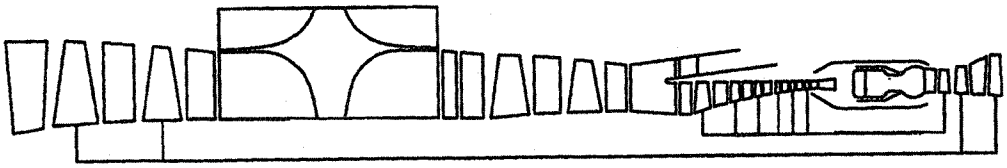

Figure 116. STF1035 Two Spool Engine Flowpath

The front fan for this two spool engine is the same two–stage fan design used in the three spool engine.

Since the rear fan is on the same shaft as the front fan, its first rotor tip diameter is set at 51.5 inches to mate with the inlet flow valve. The tip speed for this rear fan is 1375 ft/sec, which necessitates a two–stage fan to produce a pressure ratio of 2.1.

A six–stage, constant outer diameter high pressure compressor is desired to integrate well with the rear fan.

Table 34 summarizes the compression system characteristics for this engine.

Table 34. Two Spool Compression System Design Characteristics			
SLS Aerodynamic Design Point Take–Off Condition	**Front Fan**	**Rear Fan**	**HPC**
# Stages	2	2	6
Pressure Ratio	2.10	2.10	7.50
W_c/A (#/sec–ft^2)	39.5	40.1	37.5
1st Rotor Inlet Hub–Tip Ratio	0.37	0.47	0.65
Adiabatic Efficiency (%)	86.1	89.1	89.8
Surge Margin (%)	30	28.4	30
Physical Tip Speed (ft/sec)	1585	1375	1305
Corrected Tip Speed (ft/sec)	1585	1375	1160
1st Rotor Tip Diameter (in.)	59.4	51.5	38.4
Rotor Speed (RPM)	6120.0	6120.0	7782.5
Exit Mach Number	0.36	0.40	0.33
Exit Hub–Tip Ratio	0.46	0.57	0.925

The High Pressure Turbine (HPT) is a single–stage design with a maximum AN^2 of 450 x 10^8 (in–RPM)^2. Cooling and leakage air is estimated at 16.0%, consistent with previous HSCT single–stage HPT designs. To integrate with the downstream vaneless, counter–rotating LPT, a high–reaction, high–work HPT design was used. Airfoil aspect ratios are consistent with those used in previous HSCT engines.

The LPT is a two–stage vaneless, counter–rotating design. The total cooling and leakage air requirement is estimated at 7.0% consistent with previous HSCT engines. The maximum AN^2 is 500 x 10^8 (RPM)^2 and the rim velocity ratio is 0.54. Because of the relatively low loading of the LPT, it was possible to design for axial exit flow at the supersonic cruise point and thus no exit guide vane is necessary.

This two spool engine was selected for the mechanical design study because of the high risk associated with the lightly loaded IPT of the three spool design.

Upon completion of the component aerodynamic studies, the performance model was updated. The cycle was also modified to increase the thrust at Mach 2.4 by reducing the turbine temperature at the Sea Level static operating point. Table 35 summarizes the final STF1035 cycle and performance.

Table 35. Final STF1035 Cycle and Performance Summary		
Mach Number	0	2.4
Altitude, ft	0	55000
Mode of Operation	High	Low
ΔT_{amb}, °F	+18	0
Front Fan Corrected Flow, Lb/sec	650	455
Front Fan Pressure Ratio	2.10	1.70
Rear Fan Corrected Flow, Lb/sec	450	294
Rear Fan Pressure Ratio	2.10	1.395
Bypass Ratio	2.38	0.64
High Compressor Corrected Flow, Lb/sec	174	134
High Compressor Pressure Ratio	6.9	4.6
Compressor Exit Temperature, °F	753	1240
Overall Compression Ratio	14.2	10.8
Turbine Cooling Air, %	23.0	23.0
HPT Rotor Inlet Temperature, °F	2360	2900
HPT Expansion Ratio	2.53	2.50
LPT Expansion Ratio	2.67	2.07
Bypass Stream Mixing Plane Area, in^2	1770	300
Primary Stream Mixing Plane Area, in^2	1500	1500
Exhaust Nozzle Throat Area, in^2	2230	1015
Net Thrust, Lbf	43100	19500
TSFC, Lbm/hr−lbf	0.55	1.24

I. FULL BYPASS IFV TURBOFAN MECHANICAL DESIGN

A mechanical design of the STF1035 engine was conducted using materials and structural concepts projected to be available in the year 2000. These concepts and materials are consistent with those used for other propulsion systems being studied for the next generation HSCT. Table 36 provides a summary of the materials used in the STF1035 design.

Table 36. STF1035 Material Summary

Material	Engine Component
PMC	Inlet Case
PMC/Ti	Fan: IGV/Vane
Ti Honeycomb/Kevlar	Blade Containment
ADV. Ti	Fan: Blades, Stage 2 – 4 Disks, IGV Compressor: Blades 1 – 3/Disk 1 – 3/Vanes 1–2–3/Fan Case/Intermediate Case/Bypass Duct Cases
ADV Ni	Compressor: Blades 4 – 6/Disks 4 – 6/Vanes 4 – 6/TEC/Turbine Disks 1 – 3
TiMMC	Fan Stage 1 Disk
SC Ni	Turbine: Blades/Vanes
CMC	TEGV/Combustor Rich Zone Liner
TiAl	Compressor Case/Turbine Outer Case/Diffuser/ Combustor Case
Hastelloy	Combustor lean zone floatwall liner

HSCT propulsion systems operate at near maximum cycle temperatures and component rotational speeds throughout supersonic cruise, resulting in steady–state operation at the worst combination of stress and temperature for the majority of the engine life. Engine design limits are summarized in Table 37. Component material selection and operating temperature were established by the steady–state supersonic cruise flight condition. The engine cold section, defined as the entire compression system, was designed for 18,000 hours of supersonic cruise operation. Based on a typical Mach 2.4 HSCT flight profile, this results in a total life of 35,100 hours with 9,000 Type 1 cycles. The engine hot section, the turbine system, was designed for half the life of the cold section.

Table 37. STF1035 Design Limits

Design Parameter	Design Limit
Engine Inlet Temperature ($TT2_{max}$)	380°F
Compressor Exit Temperature ($TT3_{max}$)	1250°F
HPT Rotor Inlet Temperature ($TT4.1_{max}$)	2900°F
Low Rotor Speed ($N1_{max}$)	6596 rpm
High Rotor Speed ($N2_{max}$)	8700 rpm
HPT AN^2_{max}	$450 \times 10^8 in^2–rpm^2$
LPT AN^2_{max}	$500 \times 10^8 in^2–rpm^2$

Figure 117 shows the mechanical design layout that was developed for the STF1035. The following sections describe the mechanical designs of the individual components.

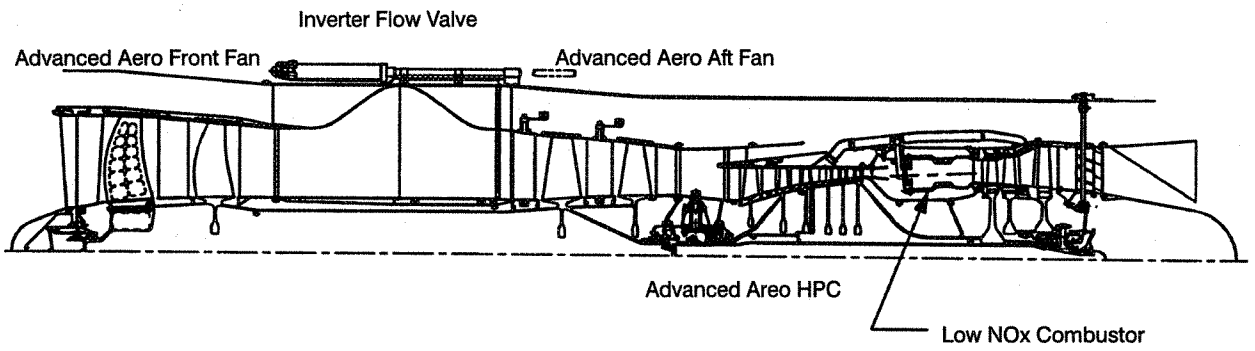

Figure 117. STF1035 Engine Mechanical Design Layout

The compression system is illustrated in Figure 118. The system employs conventionally shaped monolithic disks except for the first fan stage. The first stage utilizes a titanium composite compact bore disk due to space limitations. The second through fourth fan stages and first two stages of the compressor use conventional titanium disks, while the remaining four HPC stages use nickel alloy disks.

For repairability, the first fan stage utilizes a sloped dovetail attachment and may be removed without the need to pull the inlet case and forward bearing compartment. The remaining stages utilize Integrally Bladed Rotor (IBR) construction. A bolted flange is located at the Ti/Ni interface between compressor stages two and three.

The front fan first and second stages employ swept, low aspect ratio airfoils. The aft fan and compressor stages employ conventionally shaped blades. All of the compression stages utilize advanced aero design concepts. The first stage fan blades are large enough and the weight savings significant enough to employ a hollow airfoil design. The blades are manufactured in halves and the inside surfaces are machined before the blade halves are bonded together. The assembled blades are mechanically attached via dovetail attachments. The other fan stages and compressor blades are bonded to their rotors.

Variable geometry is utilized to insure sufficient stability throughout the operating range. All three IGV's, one fan vane, and one compressor vane are variable. The IGV's are those leading to the front fan, the aft fan, and the compressor. The other variable vanes are located aft of fan stage 3 and compressor stage 1. The variable vanes are individually inserted into the split case and held in place by an ID shroud. The fixed vanes are fabricated in segments and circumferentially inserted into the case. A split case design was incorpo-

rated into the compressor because the stages are bonded together and incorporated into the fan for maintenance.

Brush seals provide an interstage seal between static and rotating structure and an abrasive coating is applied to the rotor allowing small clearances to be obtained. Casing treatment is used over the fan blade tips to increase stall margin and a smooth abradable rub strip is incorporated into the double wall case over the six compressor stages.

A kevlar barrier is also located above the fan blades to provide containment in the event of blade loss. There is a mid compressor bleed behind compressor stage three used to cool the compressor rotor cavity.

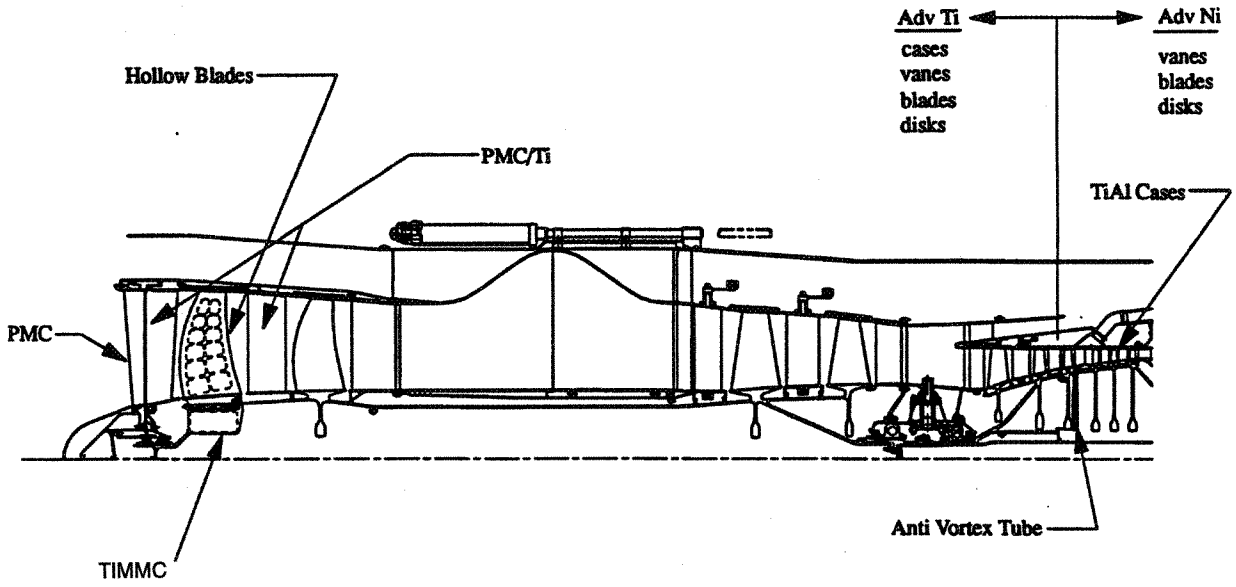

Figure 118. Fan, Inverter Flow Valve, Compressor Designs

The inverter flow valve, Figure 118, is located aft of the forward fan. It consists of two components, a forward, static section and an aft rotating section. The annular inverter valve is designed with eight passages for both the front fan and secondary flows. At the entrance of the valve, these passages are concentric. The passage shapes change in the valve so that at the center of the valve the passages are side by side. The aft rotating section of the valve has the same geometry as the front half. By rotating the aft section 22.5° about the engine centerline, the flow inversion is produced. The aft section of the valve is driven by two redundant actuators via a roller and track arrangement.

The conceptual design of the rich burn–quick quench, lean burn (RLQ) combustor is shown in Figure 119. Variable geometry is required to reduce NOx emissions throughout the flight envelope. Swirler area variation is achieved by a cam and linkage mechanism located aft of the diffusers. Wheeler vortex generators are located inside the diffuser case to reduce diffusion losses.

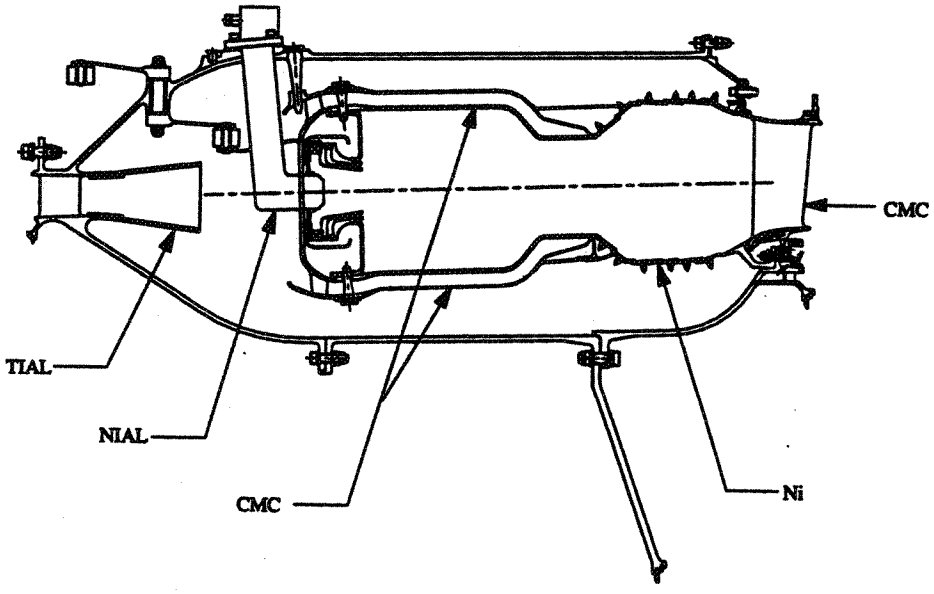

Figure 119. STF1035 RQL Combustor Design

The high (HPT) and low (LPT) designs are shown in Figure 120. The turbine disks are conventionally shaped monolithic advanced nickel alloy. The blades are individually removable and are held by dovetail attachments. The first vane is CMC and is film cooled. The turbine blades and other vanes are an advanced single crystal nickel. The HPT is cooled with compressor discharge air, while the LPT is cooled with compressor interstage bleed air.

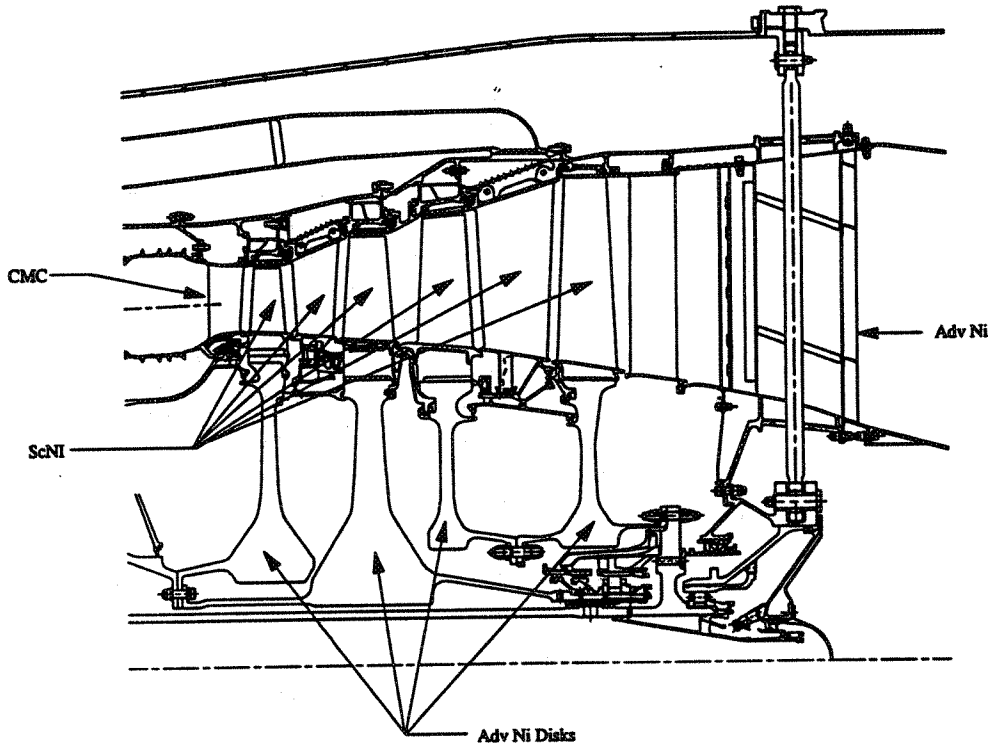

Figure 120. STF1035 Turbine Configuration

Figure 121 presents the mechanical design of the exhaust system for the STF1035.

The STF1035 requires a mixer in the exhaust system to provide 80% mixing effectiveness. the engine also requires that the bypass stream area at the mixing plane be variable in order to produce the desired pressure ratios in the rear fan during the various modes of operation. In order to minimize the complexity and weight of the variable mixing plane area system, it was decided to use a fixed daisy chute mixer and a variable flap to control the bypass stream area. During low flow operation, the flap is positioned as shown in the top portion of Figure 121 to a produce a bypass stream area of 300 in^2. During high flow operation (bottom portion of Figure), the flap is opened to produce an area of 1770 in^2. The area control is provided by a set of articulating flaps similar to those used on afterburning engine nozzles. These flaps are actuated by three actuators using a sync ring and linkages.

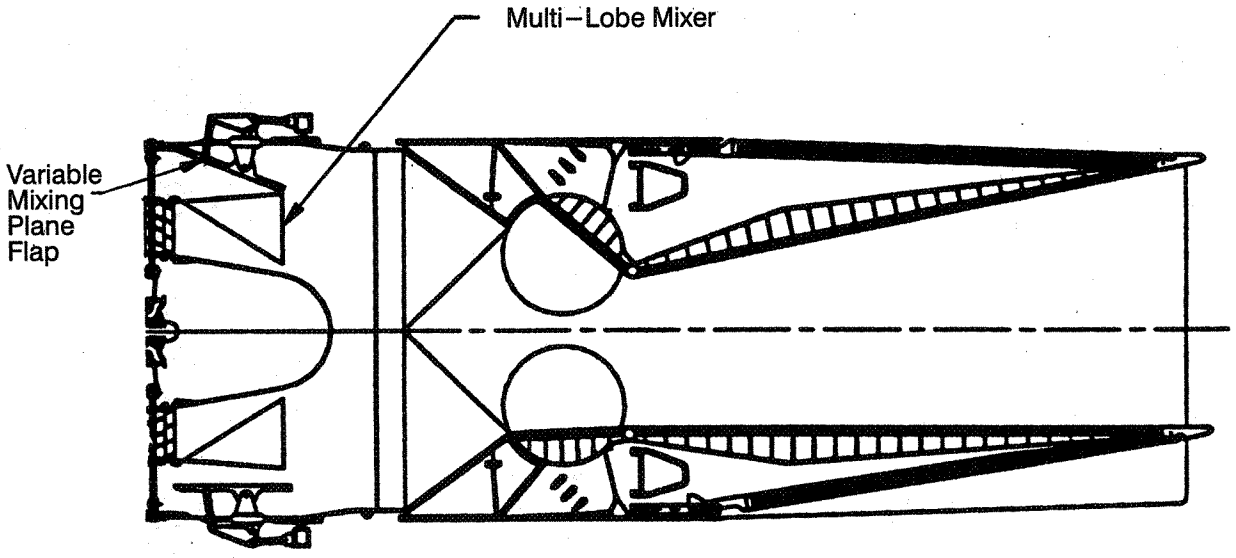

Figure 121. STF1035 Exhaust System

The STF1035 incorporates a conventional 2D–CD nozzle with thrust reversing capability. This nozzle produces an internal gross thrust coefficient of 0.982 at the Mach 2.4 cruise condition. The overall gross thrust coefficient, which includes the effects of a boattail drag, is 0.976.

Figure 122 presents the complete layout of the STF1035 propulsion system.

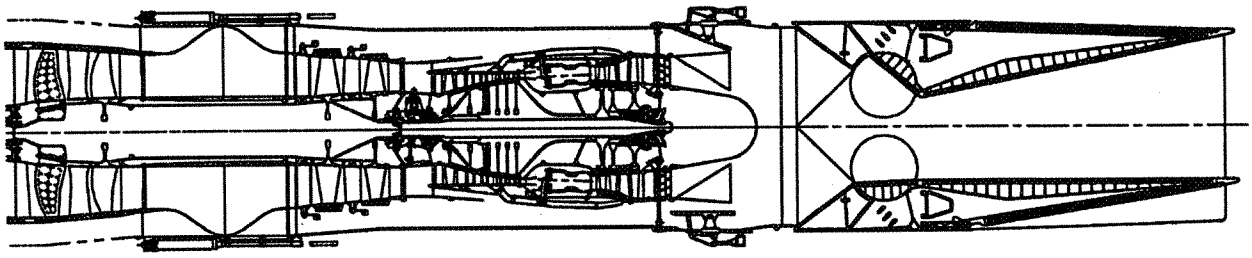

Figure 122. Non Augmented STF1035 Propulsion System

An afterburning version of the STF1035 was also examined. The propulsion system layout is shown in Figure 123. The nozzle length was increased by 19 inches to provide the combustion length required to achieve an afterburning efficiency of 92 percent.

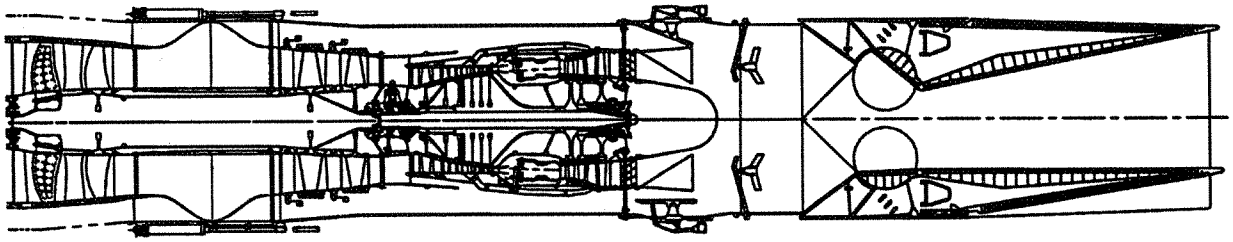

Figure 123. Augmented STF1035 Propulsion System

Table 38 presents the STF1035 component weights.

Table 38. STF1035 Component Weights	
COMPONENT	**WEIGHT, LB**
Front Fan Rotor, Stator, Case	2371
Flow Inverter Valve	445
Intermediate Case, Towershaft	255
Rear Fan Stator and Case	860
HPC Rotor, Stator, Case	1421
Diffuser/Combustor	397
High Turbine Rotor, Stator, Case	569
Low Turbine Rotor, Stator, Case, Shaft	1359
Turbine Exhaust Case, Tailcone	359

Table 38. STF1035 Component Weights (Cont'd)	
COMPONENT	**WEIGHT, LB**
Bearing Compartments	352
Bypass Duct	329
Variable Mixing Plane Flaps/Mixer	466
Controls, Accessories	650
2D–CD Nozzle	2627
Total–Weight–Non Augmented	12,460
Afterburner	266
Total Weight–Augmented	12,726

J. MISSION ANALYSIS FOR FULL BYPASS IFV TURBOFAN

Mission analyses were conducted to determine the TOGW of the Mach 2.4 HSCT that is powered by the STF1035 full bypass IFV turbofan engine. Table 39 summarizes the performance and weight summary for the STF1035 FIFVTF and the conventional mixed flow turbofan (MFTF).

Table 39. Conventional MFTF and STF1035 FIFVTF Performance and Weight Summaries		
ENGINE	**MFTF**	**FIFVTF**
SLS Fan Inlet Corrected Airflow, lb/sec	650	650
SLS Fan Pressure Ratio	4.30	2.10
SLS Bypass Ratio	0.35	2.37
Secondary Flow Entrainment, %	85	67
SLS Net Thrust, Lbf	46,600	44,000
M=2.4 Fan Inlet Corrected Flow, lb/sec	455	455
M=2.4 Net Thrust, Lbf	19,400	18,800
Inlet System Weight, Lbm	6430	7780
Engine Weight, Lbm	7060	9365
Exhaust System Weight, Lbm	4385	3095
Total Propulsion Pod Weight, Lbm	17,875	20,240

Table 39 shows that the FIFVTF propulsion system is 2365 pounds heavier than the MFTF system and has similar supersonic cruise fuel consumption. Takeoff and 55,000 ft–2.4Mn maximum dry power thrust levels for the FIFVTF are 5.5 and 3.1% lower than those of the MFTF, respectively.

The results of the takeoff gross weight (TOGW) analysis are presented in Table 40. The STF1035 FIFVTF powered aircraft weights 859,000 Lbm, which is 109,000 pounds more than the TOGW of the MFTF powered aircraft.

Table 40. FIFVTV Mission Summary

ENGINE	MFTF	FIFVTF
Aircraft Range, N.Mi	5000	5000
takeoff Gross Weight	750,000	859,000
Scaled Engine Size, Lbm/sec	676	901
Scaled Propulsion Pod Weight, Lbm	18,590	27,985
Mach 2.4 Cruise TSFC, Lbm/hr–Lbf	1.29	1.291
Engine Sizing Condition	Climb	Noise
Sideline Noise Level, EPNdB	102.5	103.0

K. COMPARISON OF PARTIAL AND FULL BYPASS IFV ENGINES

Table 41 summarizes the performance and weights of the MFTF, the PIFVTF (STF1029) and FIFVTF (STF1035).

Table 41. Performance and Weight Summary

ENGINE	MFTF	PIFVTF	FIFVTF
SLS Fan Inlet corrected Airflow, Lb/sec	650	650	650
SLS Fan Pressure Ratio	4.3	2.39	2.10
SLS Bypass Ratio	0.35	1.12	2.37
Secondary Flow Entrainment, %	85	26	67
SLS Net Thrust, Lbf	46,600	35,000	44,000
30000 Ft/1.0 Mn Net Thrust, Lbf	19,560	14,130	18,810
M=2.4 Fan Inlet Corrected Flow, Lb/sec	455	455	455
M=2.4 Net Thrust, Lbf	19,400	15,300	18,800
Inlet System Weight, Lbm	6430	6700	7780
Engine Weight, Lbs	7060	8890	9365
Exhaust System Weight, Lbm	4385	3250	3095
Total Propulsion Pod Weight, Lbm	17,875	18,840	20,240

Table 42 summarizes the mission analysis results.

Table 42. Mission Analysis Summary			
ENGINE	**MFTF**	**PIFVTF**	**FIFVTF**
Range, N.Mi	5000	5000	5000
Aircraft TOGW, Lbm	750,000	987,000	859,000
Δ TOGW, %	–	+31.6	+14.5
Sideline Noise Level, EPNdB	102.5	106.9	103.0
Engine Sizing Condition	Climb	Climb	Noise
Scaled Engine Size, Lbm/sec	676	901	1233
Scaled Pod Weight, Lbm	18,590	27,985	35,580
M=2.4 Cruise TSFC, Lbm/hr–lbf	1.29	1.285	1.291

Figure 124 shows the variations in TOGW with engine flow size for all three propulsion systems. The MFTF mixer ejector nozzle flow entrainment of 85% was set to achieve the Stage 3 noise for the 11,000 foot takeoff field length, (TOFL) sized aircraft.

The full IFV turbofan provided a dramatic improvement over the PIFV turbofan because of its large increase in takeoff and transonic thrust, as shown in Table 41. However, the heavier propulsion system weight of the FIFVTF makes it uncompetitive with the MFTF powered aircraft. The TOFL sized TOGW of 825,000 pounds for the STF1035 produces a sideline noise level of 1.3 dB above the FAR stage 3 requirement.

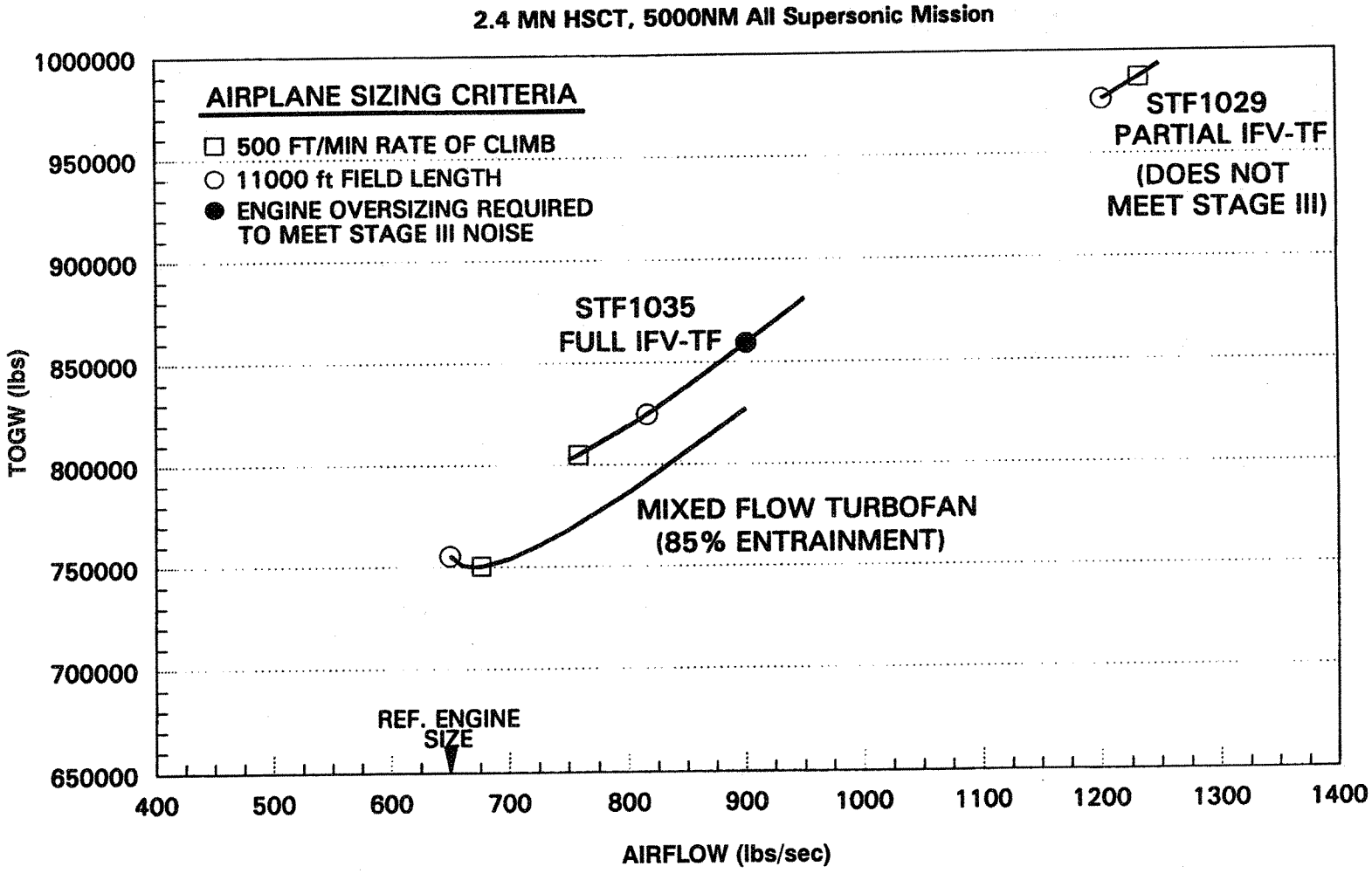

Figure 137. MFTF and IFV Powered HSCT TOGW Results

REPORT DOCUMENTATION PAGE

Form Approved
OMB No. 0704-0188

1. AGENCY USE ONLY (*Leave blank*)	2. REPORT DATE	3. REPORT TYPE AND DATES COVERED
	July 2004	Final Contractor Report

4. TITLE AND SUBTITLE

Inlet Flow Valve Engine Analyses

5. FUNDING NUMBERS

WBS–22–714–09–46
NAS3–26618, Task Order 13

6. AUTHOR(S)

G.A. Champagne

7. PERFORMING ORGANIZATION NAME(S) AND ADDRESS(ES)

United Technologies Corporation
Pratt & Whitney
West Palm Beach, Florida 33410–9600

8. PERFORMING ORGANIZATION REPORT NUMBER

E–14613

9. SPONSORING/MONITORING AGENCY NAME(S) AND ADDRESS(ES)

National Aeronautics and Space Administration
Washington, DC 20546–0001

10. SPONSORING/MONITORING AGENCY REPORT NUMBER

NASA CR—2004-213119

11. SUPPLEMENTARY NOTES

This research was originally published internally as HRS035 in June 1996. Project Manager, Jerry Knip (retired). Responsible person, Diane Chapman, organization code 2100, 216–433–2309.

12a. DISTRIBUTION/AVAILABILITY STATEMENT

Unclassified - Unlimited
Subject Categories: 01 and 07 Distribution: Nonstandard

Available electronically at http://gltrs.grc.nasa.gov

This publication is available from the NASA Center for AeroSpace Information, 301–621–0390.

12b. DISTRIBUTION CODE

13. ABSTRACT ***(Maximum 200 words)***

Pratt &Whitney, under Task Order 13 of the NASA Large Engine Technology (LET) Contract, conducted a study to determine the operating characteristics, performance and weights of Inlet Flow Valve (IFV) propulsion concepts for a Mach 2.4 High Speed Civil Transport (HSCT).

14. SUBJECT TERMS

Inlet flow valve; Propulsion; Aero gas turbine engines

15. NUMBER OF PAGES

158

16. PRICE CODE

17. SECURITY CLASSIFICATION OF REPORT	18. SECURITY CLASSIFICATION OF THIS PAGE	19. SECURITY CLASSIFICATION OF ABSTRACT	20. LIMITATION OF ABSTRACT
Unclassified	Unclassified	Unclassified	